Evaluation of CO$_2$ absorption solvents for post-combustion capture on the basis of pilot plant studies on hard coal-fired power plants

Performed for the purpose of attainment the academic degree of a
Doctor of Engineering Sciences

by

DI Markus Rabensteiner

Submitted at the Graz University of Technology

Faculty of Mechanical Engineering and Economic Sciences

Graz, February 2016

This dissertation has been approved by:

- Univ. Prof. DI Dr.techn. Christoph Hochenauer (Graz University of Technology)
- Ao. Univ. Prof. DI. Dr.techn. Josef Draxler (University of Mining Leoben)

Affidavit

I declare that I have authored this thesis independently, that I have not used other than the declared sources/resources, and that I have explicitly indicated all material which has been quoted either literally or by content from the sources used. The text document uploaded to TUGRAZonline is identical to the present PhD thesis.

_____   _____

Date   Signature

Danksagung

Abstract

The emission of carbon dioxide (CO_2) is mainly responsible for the currently occurring climate change, according to detailed long-term studies. Climate change can be seen in the form of global warming, rising sea levels, the shifting of climate zones, and increase in the frequency and destructive force of extreme weather phenomena. Carbon capture and storage (CCS) enables a massive reduction of CO_2 emissions in the near future. The first full-scale plants are already in operation. To date, post-combustion capture (PCC) technology based on scrubbing with aqueous amines has been the most widespread technology for CO_2 separation.

At this time, PCC technology and the entire CCS chain are unprofitable and unfeasible without subsidies. Many system components have to be made of stainless and high-alloyed steel in order to counteract the corrosivity of several absorption solvents. This results in high investment costs. Shorter absorber and desorber columns reduce the investment costs considerably. The solvent stream determines the size and design of components and the necessary cooling capacity which is often a limited factor in power plant constructions. Additional costs are caused by the removal of harmful components out of the CO_2 cleaned flue gas, resulting from volatility solvents and degradation products. The widespread applicability of PCC technology is also hampered by high operating costs. Operating costs are mainly dependent on the energy required for solvent regeneration. Because of solvent loss by volatility and degradation, fresh solvent has to be continuously refilled. Due to the constant solvent consumption, high running costs can be incurred, which must not be neglected.

All of the factors listed above can be significantly affected by the absorption solvent. The most commonly used amine for CO_2 separation is monoethanolamine (MEA). PCC capture with MEA can be considered a mature technology because this absorption solvent has been used for gas scrubbing for many years. At the same time, there are already extensive studies on CO_2 separation by means of MEA. Major energy savings with MEA are not possible. The trend is towards the testing of attractive new solvents, with a view to energy saving.

A PCC pilot plant, called CO_2SEPPL was put into operation at the hard coal-fired power plant Dürnrohr, in Austria. Realistic measurement conditions were made possible by the use of real power plant flue gas and the almost industrial column heights. This was confirmed by comparing measurement results from some much larger demonstration plants. Closed material and energy balances enable a scientific discussion.

An intensive literature review was carried out in order to find attractive new solvents for PCC. First, extensive laboratory tests for study of the CO_2 absorption capacity, CO_2 absorption rate, and solvent regenerability were done in order to determine the solvent behavior in pilot plant operation in advance. The amines ethylenediamine (EDA), piperazine (PIP) and 2-amino-2-methyl-1-propanol (AMP) were tested on a pilot plant-scale for their suitability as CO_2 absorption solvents.

The CO_2SEPPL pilot plant allows a detailed parametric study of various solvents due to the large number of variable operating parameters. Studies with flue gas of a natural gas-fired boiler are also possible. The effects of the decrease in flue gas CO_2 content can thus be observed.

Piperazine-based solvents show large saving potential in terms of investment and operating costs because of their fast kinetics. For example, the energy requirement for solvent regeneration can be reduced by approximately 15 % compared to operation with the benchmark solvent 30 wt% MEA. Small solvent flow rates and thus significant savings in terms of PCC dimensioning can be achieved by adding AMP to the piperazine solution. Piperazine-based solvents have a high resistance to thermal and oxidative degradation which is demonstrated by low concentrations of volatile components in the purified flue gas and separated CO_2 stream. Certain elements have to be carefully observed for safe operation with these solvents. Additives have to be added and certain concentration ranges and operating areas must be avoided in order to prevent solidification, crystallization, and foaming during operation.

Amino acids and ionic liquids were tested in the pilot plant in addition to amine-based solvents. The main advantage of such solvents is their low or immeasurable vapor pressure. The expected emissions are small. This assumption was refuted in the pilot plant study. Strongly increased concentrations of ammonia, the main degradation product, were measured at the absorber outlet for the studied amino acids. Amino acids and ionic liquids have a huge energy demand in comparison to the tested amine-based solvents. The increase in energy demand may be caused by poor solvent regenerability and the ensuing slow kinetics. Additionally, the high viscosity of ionic liquids complicates mass transfer in the columns. Based on the CO_2SEPPL pilot plant studies in Dürnrohr, it is possible to conclude that amino acids and ionic liquids offer no alternative to amine-based solvents.

Kurzfassung

Der Ausstoß von Kohlendioxid (CO_2), einem Treibhausgas, ist nach detaillierten Langzeitstudien hauptverantwortlich für den derzeitigen Klimawandel, der sich uns durch die globale Erwärmung, den Anstieg des Meeresspiegels, der Verschiebung von Klimazonen und der Zunahme extremer Wetterphänomene zeigt. Carbon Capture and Storage (CCS) ermöglicht es den Ausstoß von CO_2 bereits in naher Zukunft massiv zu senken. Bereits heute sind erste Großanlagen in Betrieb. Bisher war die Post-Combustion Capture (PCC) Technologie basierend auf der Wäsche mit einem wässrigen Amin, die am weitesten verbreitete Anwendung zur CO_2 Abscheidung.

Ohne Subventionen ist ein Betrieb von PCC Anlagen, sowie des gesamten CCS Prozesses aufgrund der hohen Kosten unrentabel und nicht durchführbar. Zum einen wären die hohen Investitionskosten für solche Anlagen zu nennen. Diese entstehen zum Teil durch den Einsatz hochlegierter Edelstähle, bedingt durch die Verwendung korrosiver Medien im Prozess. Der Bau kürzerer Kolonnen für den Absorptions- und Desorptionsprozess könnte die Investitionskosten stark senken. Der im Kreis gepumpte Lösungsmittelstrom bestimmt Größe und Ausführung der Komponenten im Prozess sowie die notwendige, oft in Kraftwerken stark limitierte, Kühlleistung. Zusätzlich entstehen Kosten durch die Entfernung etwaiger flüchtiger Komponenten des Lösungsmittels sowie Degradationsprodukte aus dem CO_2 armen Rauchgas. Neben den Investitionskosten erschweren die hohen Betriebskosten das Betreiben von PCC Großanlagen. Die Betriebskosten hängen dabei im großen Maße von der erforderlichen Regenerationsenergie des Lösungsmittels ab. Der Lösungsmittelverlust aufgrund von Flüchtigkeit und Degradation kann ebenfalls hohe laufende Kosten verursachen und darf daher nicht vernachlässigt werden.

Alle oben genannten Punkte können wesentlich durch den Einsatz verschiedener Lösungsmittel beeinflusst werden. Monoethanolamin (MEA) ist das zurzeit am häufigsten verwendeten Amin zur CO_2 Abscheidung. Da MEA schon seit Jahrzehnten zur Gasreinigung verwendet wird und mittlerweile bereits auch umfangreiche und detaillierte Studien zur CO_2 Abscheidung mit diesem Lösungsmittel vorliegen, kann hier von einer ausgereiften Technologie gesprochen werden. Weitere größere Energieeinsparungspotentiale mit diesem Lösungsmittel können ausgeschlossen werden. Um die Effizienz dieses Prozesses signifikant zu erhöhen geht der Trend daher eher in die Richtung neue, attraktive Lösungsmittel zu finden und zu erproben.

Am Gelände des Steinkohlekraftwerks Dürnrohr in Österreich wurde eine Versuchsanlage namens CO_2SEPPL zur CO_2 Abscheidung in Betrieb genommen. Die realitätsnahen Messbedingungen, die durch die Verwendung von Kraftwerksrauchgas und den nahezu industriellen Kolonnenhöhen gegeben sind, konnten durch den Vergleich von Messergebnissen aus teilweise viel größeren Demonstrationsanlagen bestätigt werden. Durch die geschlossenen Stoff- und Energiebilanzen der Anlage sind wissenschaftliche Diskussionen möglich.

Zur Findung neuartiger, attraktiver Lösungsmittel, wurde eine intensive Literaturrecherche betrieben. Um bereits vorab Schlüsse auf das Betriebsverhalten der Lösungsmittel ziehen zu können, wurden umfangreiche labortechnische Untersuchungen zur CO_2 Aufnahmefähigkeit, CO_2 Absorptionsgeschwindigkeit und Regenerierbarkeit durchgeführt. Basierend auf den

Voruntersuchungen in der CO_2SEPPL Versuchsanlage wurden die Amine Ethylendiamin (EDA), Piperazin (PIP) und 2-Amino-2-Methyl-1-Propanol (AMP) auf ihre Eignung als Lösungsmittel getestet.

Die Versuchsanlage CO_2SEPPL ermöglicht aufgrund ihrer großen Anzahl variabler Betriebsparameter eine detaillierte Untersuchung verschiedenster Lösungsmittel. Versuche mit, aus der Erdgasverbrennung stammenden, Rauchgas und dem damit bedingten geringeren CO_2 Anteil im Rauchgas sind ebenfalls möglich. Auf Piperazin basierende Lösungsmittel zeigen durch ihre schnelle Reaktionsgeschwindigkeit mit CO_2 großes Einsparungspotential hinsichtlich der Investitions- und Betriebskosten. So kann zum Beispiel der Energiebedarf zur Regeneration des Lösungsmittels um rund 15 % im Vergleich zum Betrieb mit dem Standardlösungsmittel 30 m% MEA verringert werden. Sehr kleine Lösungsmittelströme und somit erhebliche Einsparungen in der Auslegung solcher Anlagen können durch das Beimengen von AMP zu Piperazin erreicht werden. Des Weiteren weisen auf Piperazin basierende Lösungsmittel eine große Beständigkeit gegen oxidative und thermische Degradation auf, was in einer sehr geringen Konzentration von flüchtigen Komponenten im gereinigten Rauchgas sowie im abgeschiedenen CO_2 Strom sichtbar wird. Auf den betrieblichen Aspekt muss bei Verwendung solcher Lösungsmittel jedoch größeres Augenmerk gelegt werden. Um eine Erstarrung, Kristallisation sowie ein Schäumen zu verhindern müssen gewisse Additive hinzugefügt, Konzentrationsbereiche eingehalten und Betriebsbereiche vermieden werden.

Neben Aminen wurden auch Aminosäuren sowie ionische Flüssigkeiten in der CO_2SEPPL Versuchsanlage getestet. Großer Vorteil dieser Lösungsmittel ist dabei ihr geringer, bzw. nicht messbarer Dampfdruck, der theoretisch zu geringen Emissionen führen müsste. Doch gerade bei den untersuchten Aminosäuren wurden teilweise stark erhöhte Konzentrationen von Ammoniak, dem Hauptabbauprodukt, am Austritt des Absorbers gemessen. Energetisch betrachtet zeigen Aminosäuren sowie ionische Flüssigkeiten im Vergleich zu Aminen einen stark erhöhten Energiebedarf. Der hohe Energiebedarf ist auf die schlechte Regenierbarkeit im Desorber und der damit verbunden langsamen Kinetik zurückzuführen. Die hohe Viskosität von ionischen Flüssigkeiten erschwert zudem den Stoffaustausch im Absorber. Auf Grundlage, der an der Versuchsanlage CO_2SEPPL durchgeführten Untersuchungen sind Aminosäuren sowie ionische Flüssigkeiten keine Alternativen zu Amine.

Contents

List of Figures

xv

List of Tables

Nomenclature

Abbreviations

Abbreviation	Description
AAS	Amino acid salts
AMP	2-amino-2-methyl-1-propanol
ASP	Air separation plant
CCS	Carbon capture and storage
CCU	Carbon capture and utilization
CESAR	CO_2 enhanced separation and recovery
Ch	Choline
CO_2SEPPL	CO_2 separation plant
conc	Concentration
CSIRO	Commonwealth scientific and industrial research organisation
CYS	Cysteine
ECBM	Enhanced coal bed methane
EDA	Ethylenediamine
EGR	Enhanced gas recovery
EMIM	1-etyhl-3-methylimidazolium
EOR	Enhanced oil recovery
ESA	Electric swing adsorption
EU	European Union
EVN	Energieversorgung Niederösterreich
FID	Flame ionization detector
GC	Gas chromatograph
Gly	Glycine
HETP	Height equivalent to one theoretical plate
HSS	Heat stable salts
IGCC	Integrated gasification combined cycle
IL	Ionic liquid
IUPAC	International union of pure and applied chemistry
KGly	Potassium glycinate
KPr	Potassium prolinate
KSa	Potassium sarcosinate

Abbreviation	Description
L/G	Liquid to gas (ratio)
m	Molal [mol/l$_{solvent}$]
M	Molar [mol/mol$_{H_2O}$]
MEA	Monoethanolamine
NaGly	Sodium glycinate
NaSa	Natrium sarcosinate
PCC	Post combustion capture
PIP	Piperazine
Pr	Proline
PSA	Pressure swing adsorption
PVDF	Polyvinylidene fluoride
Sa	Sarcosine
TBA	Tributylammonium
TCD	Thermal conductivity detector
TEMA	Tris(2-hydroxyethyl)methylammonium
TNO	Nederlandse Organisatie voor toegepast-natuurwetenschappelijk onderzoek (Organization of applied science in the Netherlands)
TOA	Trioctylammonium
TOMA	Trioctylmethylammonium
TSA	Temperature swing adsorption
VLE	Vapor liquid equilibrium
VOC	Volatile organic compounds
VSA	Vacuum swing adsorption

Chemical symbols

Chem. symbol	Species
Ar	Argon
B	Base (in general)
$C_{12}H_{28}N$	Tributylammonium (TBA)
$C_{24}H_{52}N$	Trioctylammonium (TOA)
$C_{25}H_{54}N$	Trioctylmethylammonium (TOMA)
C_2H_4O	Acetaldehyde
$C_2H_5NO_2$	Glycine (Gly)

Chem. symbol	Species
C_2H_7NO	Monoethanolamine (MEA)
$C_2H_8N_2$	Ethylenediamine (EDA)
C_3H_4O	Acrolein
$C_3H_6NO_2S$	Cysteine (CYS)
C_3H_6O	Acetone
C_3H_6O	Propionaldehyde
$C_3H_7NO_2$	Sarcosine (Sar)
$C_3H_7NO_2$	β-alanine
$C_4H_{10}N_2$	Piperazin (PIP)
$C_4H_{11}NO$	2-amino-2-methyl-1-propanol (AMP)
$C_4H_9NO_2$	N,N-dimethylaminoacetic acid
$C_4H_9NO_2$	N-methylalanine
$C_5H_{14}ClNO$	Choline (Ch)
$C_5H_9NO_2$	Proline
$C_6H_{11}N_2$	1-etyhl-3-methylimidazolium (EMIM)
$C_7H_{17}NO_3$	Tris(2-hydroxyethyl)methylammonium (TEMA)
$CaCO_3$	Calcium carbonate
CaO	Calcium oxide
CH_2O	Formaldehyde
CH_3COO^-	Acetate
CH_4	Methane
CN_3H_5	Guanidine
CO	Carbon monoxide
CO_2	Carbon dioxide
CO_3	Carbon trioxide
CO_3^{2-}	Carbonate
Cu	Copper
C_xH_y	Hydrocarbon (in general)
Fe	Iron
$H^+PIPCOO^-·H_2O$	Protonated piperazine carbamate
H_2	Hydrogen
HCO_3^-	Bicarbonate (Hydrogen carbonate)
H_2CO_3	Carbonic acid
H_2O	Water

Chem. symbol	Species
H_2S	Hydrogen sulfide
H_3O^+	Hydronium (Oxonium ion)
HCl	Hydrochloric acid
He	Helium
K	Potassium
K_2CO_3	Potassium carbonate
KOH	Potassium hydroxide
N_2	Nitrogen
N_2O	Nitrous oxide
Na	Sodium
$NaHCO_3$	Sodium bicarbonate
$NaOH$	Sodium hydroxide
$NH_2H^+COO^-$	Zwitterion within ammonium carbamate formation
NH_3	Ammonia
NO_x	Nitrogen oxide (in general)
O_2	Oxygen
OH^-	Hydroxyl ion (Hydroxide)
$PIP \cdot 6H_2O$	Piperazine hexahydrate
R	Placeholder (in general)
R	Side chain (in general)
$R_1R_2NCOO^-$	Carbamate (in general)
$R_1R_2NH^+COO^-$	Zwitterion within carbamate formation (in general)
$R_1R_2NHH^+$	Protonated amine (in general)
SO_2	Sulfur dioxide
SO_3	Sulfur trioxide
SO_x	Sulfur oxide (in general)

Mathematical symbols – Latin

Symbol	Unit	Description
A		Constant in Eq. 3-12 and Eq. 3-16
B		Constant in Eq. 3-12 and Eq. 3-16
c_p	$kJ/(kg \cdot K)$	Specific heat capacity at constant pressure
D_i	m^2/s	Diffusivity coefficient of component i

Symbol	Unit	Description
d_h	m	Hydraulic diameter
E		Enhancement factor
$\dot{E}$	J/s	Separation work
F	$\sqrt{Pa}$	F-factor
f_i	kPa	Fugacity of component i
$\dot{G}_i$	mol/s	Gaseous mole flow of component i
g_i	kPa	Gibbs free enthalpy of component i
h	m	Column height
h	J/kg	Specific enthalpy
h_{abs}	m	Absorber column height
Δh_{abs}	J/mol	Specific molar enthalpy of absorption
$H_{CO_2,i}$	$Pa \cdot m^3/mol$	Henry´s constant of CO_2 in component i
$HETP$	m	Height equivalent to one theoretical plate
Δh_{vap}	J/mol	Specific molar enthalpy of evaporation
$[i]$	mol/m^3	Concentration of component i
k	m/s	Mass transfer coefficient
k_{-1}	$1/s$	Backward first-order reaction rate constant
k_2	$m^3/(mol \cdot s)$	Forward second-order reaction rate constant in zwitterion mechanism
K_a		Acid dissociation constant
k_{app}	$1/s$	Pseudo-first-order rate constant
k_B	$m^3/(mol \cdot s)$	Rate constant for the deprotonation of the zwitterion by a base (amine, water, or hydroxyl ion)
$k_{[CO_2]}$	$1/s$	Rate constant for CO_2
k_g	$mol/(m^2 \cdot Pa \cdot s)$	Gas film mass transfer coefficient
k'_g	$mol/(m^2 \cdot Pa \cdot s)$	Liquid film mass transfer coefficient expressed in gas units
K_G	$mol/(m^2 \cdot Pa \cdot s)$	Overall mass transfer coefficient
k_l^0	m/s	Physical liquid film mass transfer coefficient
k_{OH^-}	$m^3/(mol \cdot s)$	Reaction rate constant for the reaction between CO_2 and OH^-
k_{OV}	$1/s$	Overall pseudo-first-order reaction rate constant
L	m	Length between two points of intersection (plate heat exchanger)
$\dot{m}$	kg/s	Mass flow rate
M	kg/mol	Molar weight
N		Number of theoretical stages
N		Number of components

Symbol	Unit	Description
N_{CO_2}	$mol/(m^2 \cdot s)$	CO_2 flux
Nu		Nusselt number
P	kPa	Total pressure
p_{CO_2}	Pa	CO_2 partial pressure in gas
P_{des}	kW	Power of the heating rod in the desorber sump
p_i	kPa	Partial pressure of component i
pK_a		Base strength value
Pr		Prandtl number
q_{abs,CO_2}	GJ/t_{CO_2}	Heat for reversing reaction related to the separated CO_2
q_{reb}	GJ/t_{CO_2}	Specific energy demand for solvent regeneration
q_{sens}	GJ/t_{CO_2}	Sensible heat for solvent heat up related to the separated CO_2
q_{vap,H_2O}	GJ/t_{CO_2}	Heat for generation of stripping steam related to the separated CO_2
R	$J/(mol \cdot K)$	Universal gas constant
r_{CO_2}	$mol/(s \cdot m^3)$	Reaction rate of CO_2
Re		Reynolds number
R_i	$J/(mol \cdot K)$	Gas constant of component i
s	$J/(kg \cdot K)$	Specific entropy
s	$1/s$	Time constant for surface renewal theory
$\dot{S}$	$J/(s \cdot K)$	Entropy flow
Sc		Sherwood number
Sh		Schmidt number
t	s	Time
T	K	Absolute temperature
t_{equ}	s	Time for reaching equilibrium (Section 4.2.3)
t_{ret}	s	Retention time (Section 8.3)
u	J/kg	Specific internal energy
u	m/s	Superficial velocity
v	m^3/kg	Specific volume
x	m	Position in the film theory
z	m	Axial column coordinate
Z	m	Height of the packed column necessary to obtain a separation equivalent to N theoretical stages

Mathematical symbols – Greek

Symbol	Unit	Description
α	$mol/mol_{eq.\ amine}$ $mol/kg_{solvent}$	CO_2 loading
α	$W/(m^2 \cdot K)$	Heat transfer coefficient
$\Delta\alpha$	$mol/mol_{eq.\ amine}$ $mol/kg_{solvent}$	CO_2 loading difference
δ	m	Film thickness
η	$kg/(m \cdot s)$	Dynamic viscosity
η_{sep}	%	CO_2 separation efficiency
ϑ	$°C$	Temperature
ϑ_{out}	$°C$	Outside temperature in Dürnrohr
λ	$W/(m \cdot K)$	Thermal conductivity
ν	m^3/mol	Molar volume
ξ		Pressure loss coefficient
ρ	kg/m^3	Density
τ	s	Time of exposure
φ_i		Fugacity coefficient of component i
χ	mol_i/mol_M	Mole fraction
Ψ	J/s	Dissipated energy flow

Mathematical symbols – subscript

Symbol	Description
$Bulk$	Bulk solution
c	Critical point
des	Desorber
$feed$	Feed stream
g	Gaseous phase
i	Component number
int	Gas/liquid interface
irr	Irreversible
k	Component number ($1 \leq k \leq N | k \notin i$)
l	Liquid phase

Symbol	Description
lean	Regenerated solvent
reb	Reboiler
ref	Reference
rich	CO_2 enriched solvent
sol	Solvent
T	Total concentration at gas/liquid interface
top	Top position

Mathematical symbols – superscript

Symbol	Description
$*$	Equilibrium
B	Bulk
g	Gaseous phase
l	Liquid phase
s	Saturation

1 Introduction

1.1 Motivation

The warming of the climate system has been unequivocal since the 1950s. Many of the changes observed are unprecedented. The atmosphere and ocean have warmed, amounts of snow and ice have diminished, sea levels have risen, climate zones are shifting, and extreme weather phenomena are becoming more and more frequent. This trend can be attributed in all probability to human-induced emission of greenhouse gases like methane (CH_4), nitrous oxide (N_2O) and, in particular, carbon dioxide (CO_2), as seen in Fig. 1-1 (IPCC, 2014).
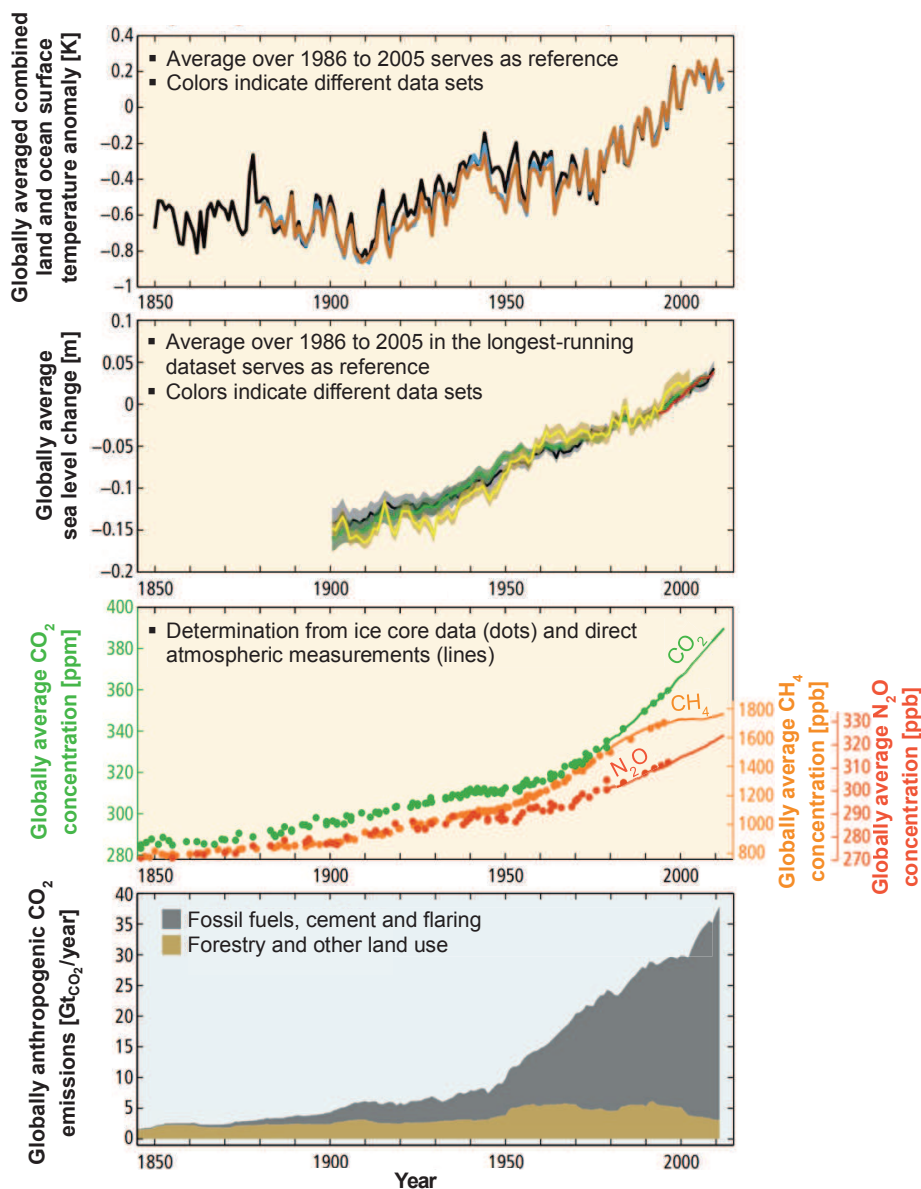
Fig. 1-1:   Impact of climate change caused by human-induced emission of greenhouse gases (IPCC, 2014).

Global CO_2 emissions from fossil fuels have been increasing by 2.7 % annually over the past decade (Le Quéré, et al., 2013) and are now more than 60 % above the level of 1990, the reference year for the Kyoto Protocol. It is estimated that the CO_2 emissions have to be reduced

by at least 50 % to limit the rise of the global average temperature to 2 K by 2050 (IPCC, 2013). A range of different options that could help reach this target for mitigating climate change are being considered worldwide (DECC, 2013; IEA, 2013). These efforts can be divided into energy efficiency enhancements, the integration of renewable energy carriers, the expansion of global nuclear capacity, and, last but not least, the use of fossil fuels including carbon capture and storage (CCS) (IEA, 2011).

CCS faces a number of technical and economic barriers that must be overcome before it can be deployed on a large scale (Cuéllar-Franca & Azapagic, 2015). One of the main economic obstacles is the fact that it is an unprofitable activity that requires large capital investment (Styring, et al., 2011). Development and deployment of CCS are complicated by rarely approved incentives and subsidies.

1.2 Objective of the work

CCS is one of the technologies that would help stop climate change. While comprehensive renewable energy is the long-term objective, CCS can make an import contribution until then. CCS has a major influence on the conventional energy industry. A considerable loss of efficiency has to be accepted for CO_2 capture. The following work addresses the post-combustion capture (PCC) technology which has the highest potential for retrofitting existing power and industrial plants. The method investigated is based on a proven absorption/desorption process with chemical solvents. Since PCC originates from natural gas sweetening, it has to be adapted to the power plant sector and to industrial flue gas cleaning.

The CO_2 content of flue gas from fossil-fired power plants is normally below 15 vol% (dry), depending on the fuel and operating mode of the power plant. The low CO_2 content combined with the nearly atmospheric pressure of flue gases entails a high specific energy demand for CO_2 separation, which makes PCC to a cost intensive option for CO_2 capture.

A pilot plant named CO_2SEPPL was erected at the power plant in Dürnrohr, Austria. Three years of intensive research were carried out on this pilot plant. This project was conducted together with the power plant operator EVN AG and the plant engineering company ANDRITZ Energy & Environment GmbH. The realistic measurement conditions of the CO_2SEPPL pilot plant provide valuable data for the realization of larger plants. This is made possible by using real flue gas from the power plant process. The impact of dust, ash, and residual nitrogen and sulfur oxide out of the power plant process can be directly demonstrated. Due to the strongly fluctuating electricity market, and the attendant change in the power plant´s full and part loads, as well as cold starts, a variety of load cases can be adapted. Realistic measurement conditions are also given by the almost industrial height of the absorber and desorber columns. Slow kinetics of CO_2 absorption lead to widely differing results in laboratory test facilities. The kinetic influence can be significantly reduced in the CO_2SEPPL pilot plant. The separated CO_2 can be compressed and stored in cylinder bundles to demonstrate the full CCS chain. Geological storage was not considered. A substantial utilization of the separated CO_2 for the production of poly-hydroxy-butyric acid, a bioplastic, is currently in operation.

Understanding of the PCC process via chemical absorption and the influence of operating parameters on energy demand are essential objectives of this work. A process optimization can be proposed based on these fundamental principles. Essential factors that influence energy demand are investigated by means of experimental parameter studies. Individual contributions of regeneration energy demand can be identified via the energy balance of the entire system. Consequently, it is possible to obtain approaches for system optimization, which can be used for developing selection criteria for novel solvents.

A reduction of the energy demand for PCC is feasible through the use of novel solvents. First, different criteria of the solvent selection are discussed. CO_2 absorption enthalpy, CO_2 solubility and CO_2 absorption kinetics have a strong influence on the energy demand. The applicability of novel solvents should be examined by detailed parameter studies on the CO_2SEPPL pilot plant. The solvent stability is a decisive factor for solvent loss by means of degradation, upon which the cost of supplying fresh solvent depends. Solvent loss can also be caused by volatility. Harmful components of the solvent and certain degradation products which are released into the atmosphere should be monitored. Solvents with a low vapor pressure are considered in more detail in order to keep the emission of undesirable components low.

2 Carbon capture and storage

2.1 Overview

Carbon capture and storage (CCS) is the process of capturing waste carbon dioxide (CO_2) for large point sources, transporting it to a storage site, and depositing it where it will not enter the atmosphere, normally an underground geological formation (IPCC, 2005). An alternative to CO_2 storage is the use of CO_2 as a raw material in varied processes (Damiani, et al., 2012). An overview of the entire CCS and CO_2 utilization (CCU) process is given in Fig. 2-1.

Power plants, oil refineries, biogas sweetening, as well as the production of ammonia, ethylene oxide, cement, iron and steel are the main industrial sources of CO_2 (Styring, et al., 2011; Markewitz, et al., 2012). For example, over 40 % of the worldwide CO_2 emissions are caused by electrical generation in fossil-fuel power plants (Markewitz, et al., 2012). Therefore, these sources are the main candidates for the potential application of CCS (Cuéllar-Franca & Azapagic, 2015).
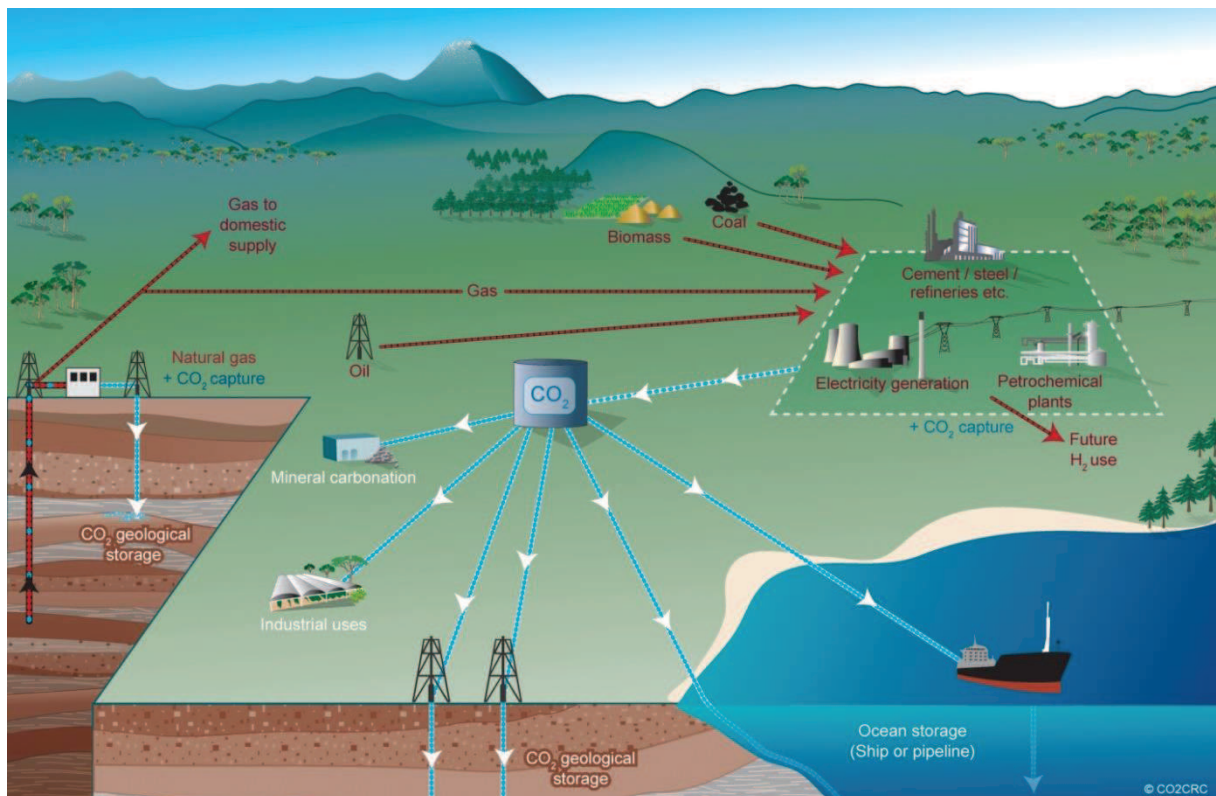
Fig. 2-1:   Schematic overview of CCS and CCU (CO_2CRC, 2015b)

2.2 CO_2 capture technologies

A one-size-fits-all technology for CO_2 capture would not be feasible given the high diversity of industrial processes generating CO_2 emissions. As a consequence, there is a wide variety of CO_2 capture systems, in order to ensure compatibility with the specific industry (Cuéllar-Franca & Azapagic, 2015). The level of maturity among different capturing systems varies across industries. For example, power plants and oil refineries are getting closer to implementing CO_2

4

capturing systems on a large-scale, while the cement, iron, and steel industries still have to overcome the transition from small-scale demonstration plants to industrial deployment (IEA & UNIDO, 2011).

According to Fig. 2-2, CO_2 capture options can be classified as post-conversion[1], pre-conversion[1] and oxyfuel combustion (IEA & UNIDO, 2011; Singh, et al., 2011; Zaimes & Khanna, 2013). Each technology is characterized by the location where the carbon dioxide is captured from the gaseous stream (Kanniche, et al., 2010).
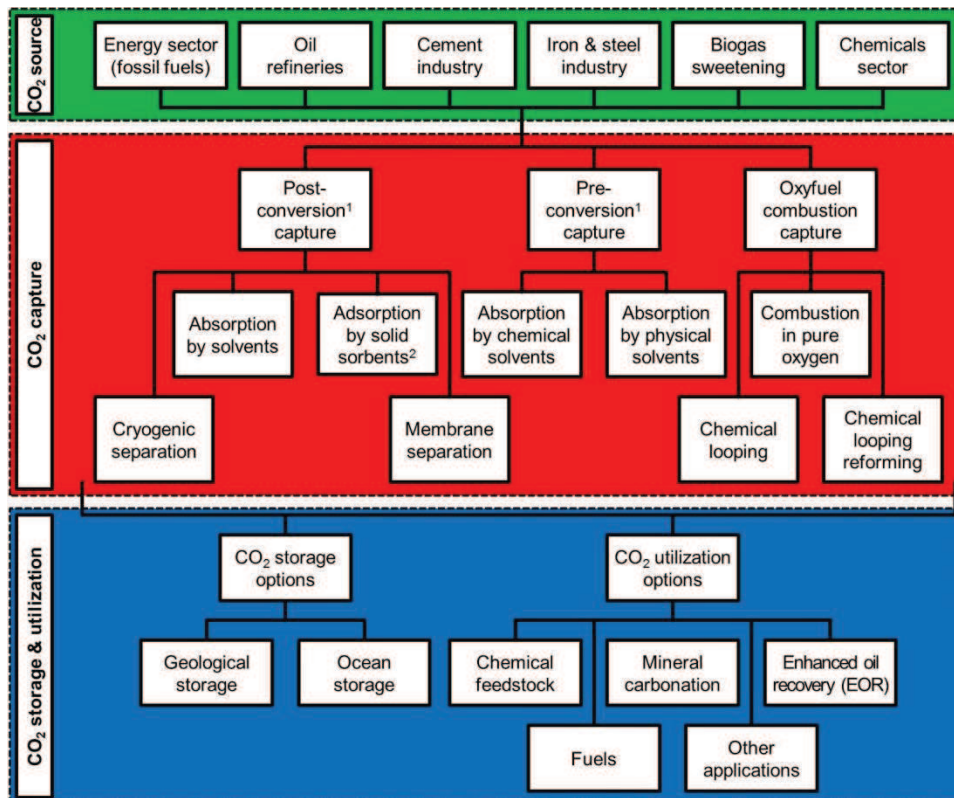
Fig. 2-2:   Summary of CCS and CCU options (Cuéllar-Franca & Azapagic, 2015).

Additional, the technologies are classified in technologies of the first, second and third generation (Aldous, et al., 2013). First generation technologies - like post-combustion capture with chemical solvents – are already in large-scale operation. Efforts regarding these technologies aim towards their further improvement through research and testing. Second generation technologies are new technologies, tested at bench-scale, that offer significant operating cost reductions and performance or environmental benefits. Commercial deployment will be possible in 10 to 15 years. The development of third generation technologies is at an early stage. They comprise potentially game-changing technological concepts. Actual research

---

[1] "Conversion" is written because CO_2 doesn´t have to be generated by combustion. Only combustion processes are discussed in Section 2.2.1 and 2.2.2.

[2] Pressure swing adsorption (PSA) and vacuum swing adsorption (VSA) are considered by Cuéllar-Franca & Azapagic (2015) as its own PCC technology. The present study doesn't make distinctions between these technologies.

is limited on theoretical or laboratory works. Commercial deployment will be possible in 15 to 25 years (Aldous, et al., 2013).

2.2.1 Post-combustion capture

CO_2 is separated from the flue gas out of the power plant process by the post-combustion capture technology (Fig. 2-3). First, the power plant flue gas passes the conventional flue gas cleaning system (not represented), in which dust, sulfur oxides and nitrogen oxides are removed. Thereafter the CO_2 is separated from the flue gas. When retrofitting power plants, the post-combustion technology is characterized by the lowest impact to the power plant process compared to other separation technologies. This is due to the fact that the CO_2 separation takes place only downstream to the conventional power plant process. The mentioned advantages come at the expense of plant efficiency, since the separation of carbon dioxide from flue gases is an energy intense method (Wang, et al., 2011). The CO_2 content of flue gas from fossil-fired power plants is normally below 15 vol% (dry), depending on the fuel and operating mode of the power plant. The low CO_2 content combined with the nearly atmospheric pressure of flue gases entails a high specific energy demand for CO_2 capture, which makes PCC a cost intensive option.
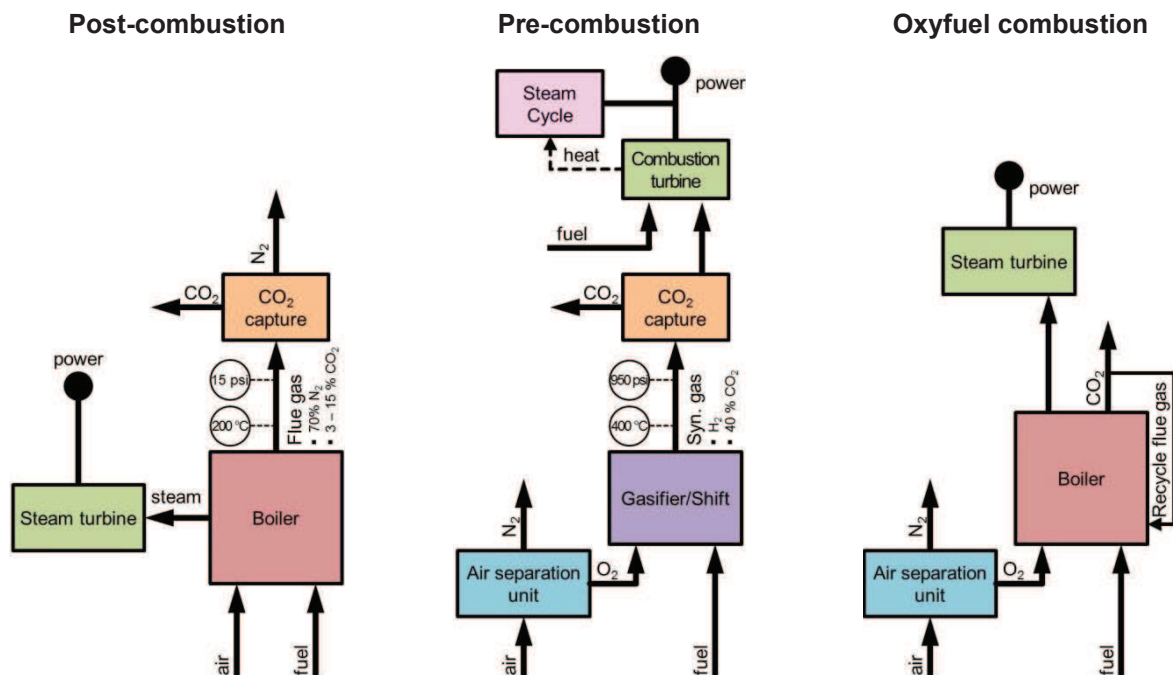
Fig. 2-3:   Schemes of the post-combustion, pre-combustion and oxyfuel combustion technology (Figueroa, et al., 2008).

According to Cuéllar-Franca & Azapagic (2015), CO_2 post-combustion technologies can be divided into absorption by solvents, adsorption by solid sorbents, membrane separation, and cryogenic separation (compare Fig. 2-2). Technologies based on absorption appear to be best adapted to this separation (Kanniche, et al., 2010). Capture technologies based on adsorption, membranes and cryogenics are even less suitable for post-combustion capture than for pre-combustion capture. This is mainly due to the much lower CO_2 partial pressure and the major

influence of dust, impurities (SO_x and NO_x) and incondensable gases (O_2) in post-combustion flue gases than in synthetic gases originating from gasifiers or reformers (Kanniche, et al., 2010).

2.2.1.1 Absorption by solvents

CO_2 is separated in an absorber column by contact with a solvent via selective absorption. Thereafter, the solvent must be regenerated again in a desorber. Solvent regeneration is responsible for 70 to 80 % of the entire energy demand (Aaron & Tsouris, 2005). The difference in CO_2 solubility between absorber and desorber conditions is essential to the efficiency of the process. Absorption can take place by chemical or physical absorption (Notz, 2009).

2.2.1.1.1 Chemical absorption

Chemical absorption of carbon dioxide is associated with the chemical reaction of CO_2 with a solution in an absorber column. The CO_2 loaded (enriched) solvent is regenerated or CO_2 bonds are broken by heat supply in the desorption unit. Subsequent to solvent regeneration, the regenerated solvent is again available for CO_2 absorption in the absorber column. There is a wide range of chemical solvents available that originate mostly from sour gas scrubbing within natural gas purification (Danckwerts & Sharma, 1966). Much research has been done regarding chemical absorption (Kohl & Nielsen, 1997). In more recent times, the development of tailor-made solvents adequate for CO_2 capture from flue gases is the focus of global research (Posch, 2012).

The purity of CO_2, separated by chemical absorption, is above 99 % (Bailey & Feron, 2005). Consequently, the separated CO_2 can be used in the food industry, for example, after undergoing further purification (Notz, 2009). The main challenges of using chemical absorption technologies in power plants are the high energy requirements for solvent regeneration, as well as solvent degradation and corrosion. Idem, et al. (2015) have compiled an actual list of existing PCC pilot plants working with chemical solvents based on the list of Abu-Zahra, et al. (2013).

2.2.1.1.2 Physical absorption

Physical absorption is based on Henry´s law. CO_2 is dissolved in the solvent without chemical reaction (Posch, 2012). The CO_2 uptake occurs in an absorber column, the release in a desorber column, and the same applies for chemical absorption. The solvent can be regenerated by a temperature and/or pressure variation between absorber and desorber. High CO_2 partial pressures are essential for physical absorption because it is driven by concentration gradients. Physical absorption can be neglected in the most cases due to the low CO_2 partial pressures of coal or natural gas-fired power plant flue gases. Physical absorption is economical only for CO_2 contents above 15 vol% (dry) (Chakravarti, et al., 2001). Typical solvent representatives are polyethylene-glycoldimethylether used in the Selexol® process and methanol used in the Rectisol® process (Notz, 2009).

2.2.1.2 Adsorption by solid sorbents

Adsorption by solid sorbents is based on differently strong interactions of flue gas components with a solid surface, e.g. activated carbon, zeolite or calcium oxide. This results in different selectivity towards certain flue gas components (Notz, 2009). Adsorption systems are operated either cyclically, in the form of several parallel and connected fixed bed apparatus, or continually with fluidized beds (Notz, 2009).

2.2.1.2.1 Cyclical adsorption

The flue gas initially passes the unloaded fixed bed, whereby CO_2 is bound to the solid surface. The CO_2 content of the purified gas would rise as the fixed bed reaches equilibrium loading. Before that, the flue gas is switched to an unloaded fixed bed. The fixed bed which is loaded with CO_2 must be regenerated in a second step. Temperature swing adsorption (TSA), pressure swing adsorption (PSA), electric swing adsorption (ESA) and vacuum swing adsorption (VSA) are different methods for regeneration. Cuéllar-Franca & Azapagic (2015) consider PSA and VSA as two distinct PCC technologies. The present study doesn't make distinctions between these technologies.

The regeneration of the fixed bed takes place by increasing the temperature when using TSA. PSA operates with a pressure reduction, usually from an elevated level to near atmospheric pressure. Systems with TSA and PSA are commercially available (Notz, 2009). Desorption of CO_2 is triggered by creating a near-vacuum when using VSA. One advantage of VSA is that this system will operate at near ambient temperature, so it requires less energy. Another advantage is that the energy used is applied only to the CO_2 and so it is thermodynamically more efficient than thermal swing adsorption (CO_2CRC, 2015a). The interactions between the adsorbed molecules and the solid surface are significantly reduced by applying a small electric potential when using ESA. ESA enables a reduction in energy demand in comparison to the other adsorption technologies, but it is still in the development stage (Tlili, et al., 2012).

Cyclically adsorption technologies are used commercially for CO_2 capture in the syngas and hydrogen production, as well as for biogas conditioning. This technology is associated with some disadvantages for CO_2 capture from power plant flue gas, such as a low CO_2 selectivity, CO_2 loading capacity, and adsorption rate, as well as a high pressure drop across the fixed bed and a significant energy demand for regeneration. Therefore, the use of adsorption technics for large-scale CO_2 capture plants is problematic (Thomas, 2005). Novel adsorption materials enable a reduction of the energy demand (Chaffee, et al., 2007).

2.2.1.2.2 Continuous adsorption

Calcium oxide (CaO) can be used for the continuous adsorption of CO_2. CO_2 is separated from the flue gas in a fluidized bed reactor with the formation of calcium carbonate ($CaCO_3$). $CaCO_3$ is regenerated in a second fluidized bed reactor, in which CO_2 is formed in a high concentration. A side product is CaO, which is recycled to the adsorption reactor (Lu, et al., 2006). The advantage of this technology, calling calcium looping, is the energy released during adsorption, obtained at a high temperature level. This heat source can be used for electricity generation (Notz, 2009).

2.2.1.3 Membrane separation

Two different process concepts exist for CO_2 separation by membranes - gas permeation and membrane absorption (IEA, 2002). The flue gas CO_2 content is reduced by selectively captured CO_2 flow through the membrane for both technologies. Selectivity is achieved by different physical effects (IEA, 2002).

2.2.1.3.1 Gas permeation

Selectivity is given by different affinities of flue gas components towards the membrane. The mass transfer is determined by the CO_2 partial pressure difference (Kusakabe, et al., 1999). The CO_2 partial pressure can be increased by a flue gas blower or a vacuum pump, which reduces the permeate pressure. Membranes exhibit only low CO_2 separation efficiencies because of their insufficient selectivity and permeability. Higher CO_2 separation efficiencies can be achieved by multi-stage membrane interconnections. The compression of the whole flue gas stream is necessary to achieve sufficient mass transfer rates and separation efficiencies (IEA, 2002). The energy demand of CO_2 capture with currently available membranes is higher compared to absorption technologies (Norton & Lin, 2014). This technology is currently unsuitable for CO_2 capture from power plant flue gases. In order to increase the usability of gas permeation, further developments in membrane technology are necessary. Tong, et al. (2015) and Norton & Lin (2014) show the current state of development of high-temperature ceramic-carbonate dual-phase membranes for CO_2 capture. CO_2 selective membranes are still at an early stage of development. The use of high-temperature membranes in pre-combustion as well as oxyfuel technology seems favorable (Tong, et al., 2015).

2.2.1.3.2 Membrane absorption

Membranes are most widely used in membrane absorption technology (Notz, 2009). The membrane serves as a contact surface between the flue gas and the solvent. The CO_2 selectivity is only influenced by the solvent. The process is similar to a conventional absorption/desorption process. The advantage of membrane absorption compared to the conventional absorption/desorption process is the prevention of fluid dynamic problems such as flooding, channeling, and foaming, and the reduction of solvent discharge (IPCC, 2005). A larger volume-related mass transfer area can be achieved in comparison with conventional absorption/desorption processes (Notz, 2009). An additional mass transfer resistance through the membrane is installed, whereby the advantage of a larger contact area can be reduced or even eliminated. Membrane absorption does not provide improvements regarding energy requirement for solvent regeneration in comparison to the conventional absorption/desorption process. The CO_2 solubility in the liquid phase is not influenced by the membrane. Other disadvantages of membrane absorption when compared to the conventional absorption/desorption process are the high membrane costs, the poor membrane resistance, the susceptibility of the membrane to contamination, as well as the increased pressure drop of the flue gas stream across the membrane (Notz, 2009).

2.2.1.4 Cryogenic separation

CO_2 is separated from the flue gas by condensation or desublimation at low temperature and high pressure (Aaron & Tsouris, 2005; IEA, 2002). Components such as H_2O, SO_2 and NO_x have to be removed from the flue gas in a pretreatment. The pretreated flue gas is compressed and cooled. Thereby liquid or solid CO_2 occurs, which can be separated. The necessary compression pressure is considerable. Cryogenic separation processes are used commercially for further concentration of streams with a high CO_2 content of 50 to 70 %. An application to low CO_2 concentrated flue gases is uneconomic due to the high energy demand for compression.

The advantage of cryogenic separation is that liquid CO_2 with high purity is generated. The transportation and storage of this medium is technically quite simple. The disadvantage of extremely high energy demand is predominant. Consequently, this process has only a low application potential for large-scale CO_2 capture plants for power stations (Aaron & Tsouris, 2005; IEA, 2002; Thomas, 2005). Potential applications of cryogenic separation are present in pre-combustion and oxyfuel technology (Notz, 2009).

2.2.2 Pre-combustion capture

Pre-combustion capture involves separating carbon dioxide before the fuel is burned, and it may be applied on IGCC (integrated gasification combined cycle) power plants (Padurean, et al., 2012). Pre-combustion CO_2 capture in power generation is based on processes that are used on an industrial-scale to produce hydrogen and chemical commodities. CO_2 is a by-product that is being removed (Fig. 2-3). Pre-combustion CO_2 capture in the chemical industry is mature and has been in use for over 90 years (Jansen, et al., 2015).

Solid fuels are converted in a gasifier into a synthesis gas by the addition of steam and/or pure oxygen at the IGCC process. The subsequent shift reactor increases the H_2 content of the cleaned syngas by the water gas shift reaction ($CO + H_2O \Leftrightarrow CO_2 + H_2$). Thereafter, the syngas consists mainly of H_2 and CO_2. Due to the rather high CO_2 partial pressure in the syngas, CO_2 can be removed via physical absorption as described in Section 2.2.1.1.2. The remaining H_2 can be either used in a subsequent combined cycle power plant process or transported and distributed to customer sites (Baufumé, et al., 2011).

The main advantage of pre-combustion capture is the relatively low energy penalty of the process. The IGCC technology itself consists of a large number of single steps which reduces the plant flexibility and offers no retrofit option for existing power plants. In addition, H_2 turbines are not yet commercially available. H_2 combustion leads to excessive temperatures and flame instabilities in the combustion chamber. In order to reduce the combustion temperature to moderate values, hydrogen can be premixed with N_2 from the air separation plant (ASP) (Posch, 2012).

Combustion of high-hydrogen fuels requires attention to key combustion issues, especially if low emissions are to be achieved using these fuels (McDonell, 2006). Various options can be considered for combustor design and operation (Richards, et al., 2006). Thermal NO_x is formed by oxidation of nitrogen in air and requires sufficient temperature and time to produce. The residence time in typical gas turbine combustors is not long enough to produce significant

thermal NO_x for temperatures below 1700 K. Where temperatures higher than 1700 K cannot be avoided, it is necessary to limit residence time to control NO_x formation, which favors very short combustor designs. Thermal NO_x production also increases with the operating pressure (Richards, et al., 2006).

In general, research activity in pre-combustion decarbonisation has focused more on coal than on natural gas-fired power plants since, in the latter, plant complexity and costs are not competitive with post-combustion CO_2 capture, which is a technology on the verge of commercialization (Jansen, et al., 2015).

2.2.3 Oxyfuel technology

The large N_2 content which has to be separated prior to storage is the main problem of CCS (Notz, 2009). In oxyfuel combustion, the O_2 concentration in the oxidizer is increased from 21 vol% up to 100 vol% by an ASP (Fig. 2-3). The lack of N_2 leads to increasing combustion temperatures compared with conventional air-firing methods and improves the energetic efficiency (Prieler, et al., 2014). The use of oxyfuel increases the CO_2 concentration in the flue gas, making it easier to separate it from the flue gas (Mayr, et al., 2015). The flue gas is purified in a conventional flue gas cleaning system. The steam content is reduced by condensation (Scherer, et al., 2012).

In the glass, steel, and cement industries, oxyfuel or oxygen-enriched combustion is already used (Scheffknecht, et al., 2011). Several publications also deal with the application of oxyfuel combustion in power plants i.e. Scheffknecht, et al. (2011), Chen, et al. (2012) and Wall, et al. (2009). In power plants, the maximum temperature is limited by the high stresses, i.e. for gas turbines 1600 K (Kutne, et al., 2011). The oxidant in power plants using oxyfuel consists of oxygen and recycled flue gas to reduce the maximum temperature. The flue gas in oxyfuel combustion mainly consists of CO_2 and H_2O through the absence of N_2. The total heat transfer characteristic is considerably different to that of air fired conditions. The radiative heat transfer is strongly enhanced by the higher level of CO_2 and H_2O (Mayr, et al., 2015).

2.3 CO_2 compression and transport

A complete CCS system requires safe, reliable and cost-efficient solutions for the transport of CO_2 from the capturing plant to the location of permanent storage. Because of lower pressure drop, pipeline transport of CO_2 over longer distances is most efficient when the CO_2 is in the dense phase i.e. in the liquid or supercritical regime (Fig. 2-4) (Witkowski & Maijkut, 2012).

Compressor discharge pressures in the range of 130 to 200 bar are required when pressure losses and sufficient pipeline distances are taken into account (Witkowski & Maijkut, 2012). CO_2 compression differs from most fluid compression tasks by its high molecular weight, highly compressible behavior, and the presence of a critical point (Fig. 2-4). The CO_2 volume reduction is enormous during the compression process. This results in a large impeller diameter at the first stage and a very small impeller diameter at the last stage. Existing CO_2 compressors are expensive because of the high overall pressure ratio and the partly stainless steel construction (Witkowski & Maijkut, 2012).

The CO_2 compression system has to be integrated with both power and CO_2 capture plants in order to use the high amount of waste heat of the CO_2 compressor (Lukowicz, et al., 2011). The selection of CO_2 compression technology is dependent on the applied CO_2 capture method, among other factors (Lüdtke, 2004).
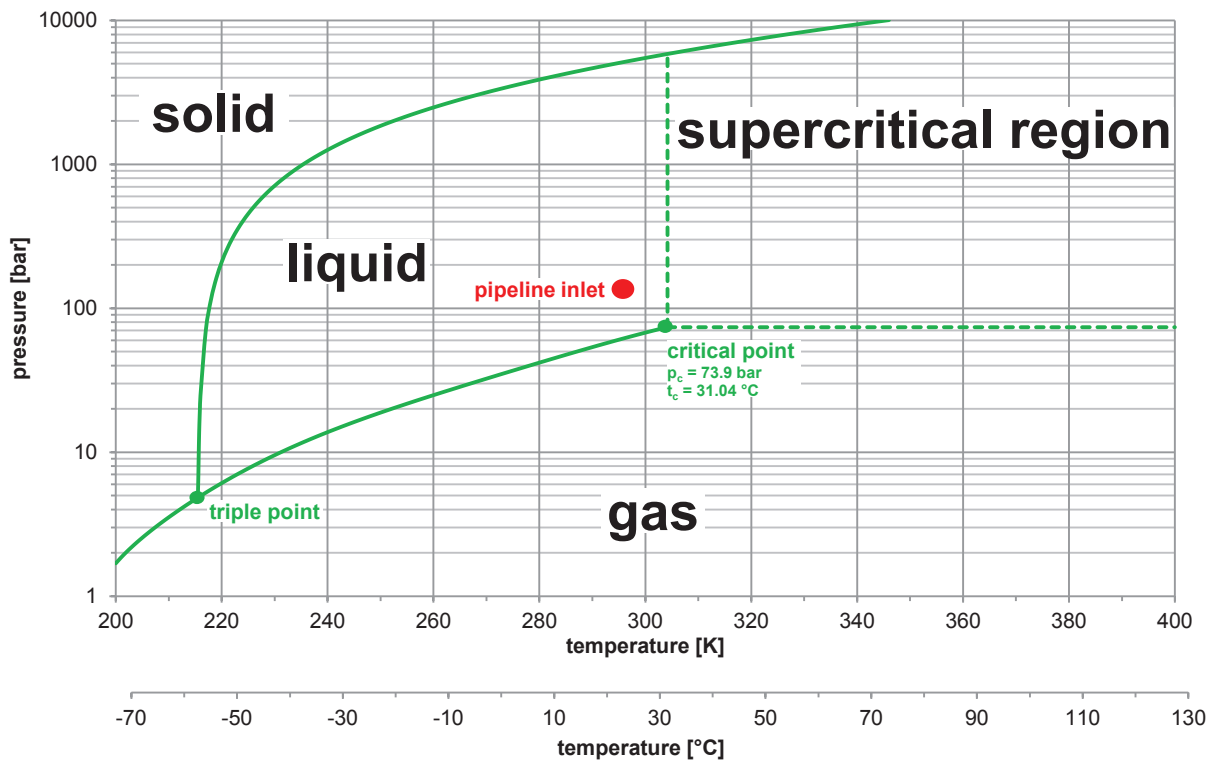
Fig. 2-4. Phase diagram of CO_2 (Witkowski & Maijkut, 2012).

The purified and highly compressed CO_2 is transported by pipelines to a suitable storage facility. Pipelines for CO_2 transport are subject to high security requirements. Because of experience with natural gas pipelines, these requirements should be technically feasible (Witkowski & Maijkut, 2012). Additionally, experience in CO_2 transport has been gained since the 1970s from enhanced oil recovery (EOR) (Chen, 2011). Minimizing water content in the CO_2 stream reduces the corrosion rates of pipelines as well as the costs of pipeline materials significantly (Seiersten, 2001). The removal of other impurities such as N_2, O_2, H_2S and SO_3 avoids over-compression and lowers operational costs (Haszeldine, 2009).

2.4 CO_2 storage and utilization

The secure long-term storage of CO_2 over a period of at least 1000 years must be ensured (IPCC, 2005). In particular, the risk assessment, the guarantee of leakproofness and the acceptance of the general population will be decisive for the applicability of the whole CCS technology. From today´s perspective, the most promising storage sites, are depleted oil/gas reservoirs, deep saline formations, and coal seams, which provide a total capacity that would be adequate for CO_2 storage for many years (IPCC, 2005).

High density CO_2 fluid would be injected into geological formations deeper than 800 m to achieve permanent sequestration (Orr, 2009). CO_2 storage in geological formation has been proved feasible, based on the information and experience gained from CO_2 injection activities in previous EOR and acid gas as well as existing CO_2 storage practices (Melzer, 2012). EOR is defined as injection of CO_2 into an oil reservoir to increase the production. Experience is also available through the decades of use as gas storage for bridging seasonal fluctuations. The disadvantage is the low storage capacity of these reservoirs. The storage capacity of saline aquifers is much higher. Saline aquifers are deep, saltwater-bearing rock layers in which the CO_2 is stored. In these porous rock formations, CO_2 is taken up like water in a sponge. Impermeable rock layers have to be located over this storage reservoir. Due to its expansion, saline aquifers offer the world's largest storage potential for carbon dioxide. Hence, they are considered as most important potential CO_2 storage reservoir (IEA, 2013; IPCC, 2005).

On the technical side, CO_2 leakage rates are uncertain. In some countries, the geological storage capacity is limited, making CCS unfeasible. Partially, there is only offshore storage available, which leads to higher transportation and injection costs (Khoo, et al., 2011; Styring, et al., 2011). The selection, authorization process, and operation of CO_2 storages in the European Union are legally fixed by the directive 2009/31/EG (European Union, 2009). Further sanctions such as the mandatory use of CCS in new power plants, and the retrofitting of existing power plants were discussed, but are not included in this directive (European Parliament, 2008). The EU-directive is not directly applicable to member states. The member states have to convert the directive into national law. While geological CO_2 storage is prohibited by law in Austria (Bundeskanzleramt, 2011), a maximum storage amount of 4 million tons of carbon dioxide per year is legally fixed in Germany (Bundesministerium für Umwelt, Naturschutz, Bau und Reaktorsicherheit, 2012).

To minimize the potential risks to human and ecosystem caused by CO_2 leakage, careful site selection, effective regulatory oversight and appropriate monitoring are required. The cost of CO_2 storage is highly site-specific and generally small compared to current CO_2 capture costs, which comprise 70 % or more of the total cost of CCS (House, et al., 2009).

Carbon capture utilization (CCU) focuses on existing and novel approaches for reducing CO_2 emissions by developing beneficial uses for CO_2. Carbon dioxide can be used in applications that could generate significant benefits. It is possible to develop alternatives that can use captured CO_2 or convert it to useful products such as chemicals, cements, or plastics (Styring, et al., 2011). When evaluating CO_2 utilization processes, the life cycle of the process must be considered, in order to ensure that additional CO_2 is not produced (NETL, 2015). A graphic summary of CO_2 utilization possiblities can be seen in Fig. 2-5.
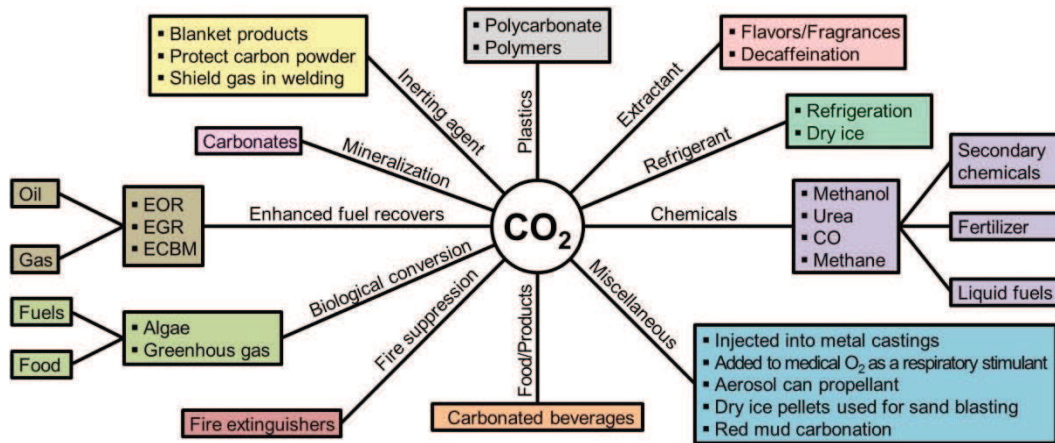
Fig. 2-5. Possibilities of CO_2 utilization (NETL, 2015).

CO_2 separated at the CO_2SEPPL pilot plant in Dürnrohr is used for the production of bioplastic, (poly-hydroxy-butyric acid), which is obtained after a harvest of cyanobacteria. Cyanobacteria are microorganisms and occur in natural bodies of water everywhere. They have particularly good CO_2 binding properties. The cyanobacteria grow due to the constant fertilization with CO_2 (Meixner, et al., 2015).

The current global demand for products made of CO_2 does not have the capacity to sequester enough CO_2 emissions to contribute significantly to meeting the carbon reduction targets (Cuéllar-Franca & Azapagic, 2015).

3 Mass transfer

Theories of mass transfer and kinetics are presented in order to provide background information for the pilot plant results. Physical absorption is studied first in order to introduce and compare different theories on mass transfer. Processes for which the phenomena of mass transfer and of chemical reaction take place simultaneously are described afterwards.

3.1 Mass transfer without reaction

The absorption rate of CO_2 for unit area (CO_2 flux, N_{CO_2}) without any reactive species in the solution depends on the physical solubility of CO_2 in the solution (Henry´s constant[1], H_{CO_2}) and the physical liquid phase mass transfer coefficient (k_l^0) (Chen, 2011; Rochelle, et al., 2001). k_l^0 in Eq. 3-1 is a function of the liquid viscosity and CO_2 diffusivity in the liquid.

$$N_{CO_2} = k_l^0 \cdot \left(\frac{p_{CO_2}}{H_{CO_2}} - [CO_2]^* \right)$$

Eq. 3-1

The following section will briefly review several important mass transfer models that have been developed for description of the absorption mechanism regarding relationship between mass transfer coefficient and the physical properties of the gas and liquid. Although these theories are discussed in the scenario of physical absorption, they can also be applied to mass transfer with chemical reactions (Chen, 2011). The following mass transfer models for physical absorption are available:

- Film theory
- Penetration theory
- Surface renewal theory
- Eddy diffusivity theory

In the following sections, these models are presented with the exception of the last one.

3.1.1 Film theory

A two-film theory is proposed by Lewis & Whitman (1924) to model steady-state mass transfer between gas and liquid. A gas film and liquid film right next to the interface (phase boundary) exists if gas and liquid are in contact with each other (Fig. 3-1). The films are stagnant and of finite thickness of δ_g and δ_l, respectively. A CO_2 balance in the liquid film leads to Eq. 3-2 (Bishnoi, 2000). The concentration of CO_2 in the liquid film is represented as a function of time (t) and position (x) (Eq. 3-2).

$$D_{CO_2} \cdot \frac{\partial^2 [CO_2]}{\partial x^2} - \frac{\partial [CO_2]}{\partial t} + r_{CO_2} = 0$$

Eq. 3-2

---

[1] Henry´s constant of CO_2 H_{CO_2} is defined via the concentration:

$$H_{CO_2} = \frac{p_{CO_2}^*}{[CO_2]^*}$$

Here, $[CO_2]^*$ is the concentration of CO_2 in the liquid phase and $p_{CO_2}^*$ is the partial pressure of CO_2 in the gaseous phase under equilibrium conditions.

D_{CO_2} is the diffusion coefficient[1] of CO_2 in the liquid. The derivative with respect to time for film theory can be delated since it is a steady state theory. No reactions have to be considered at physical absorption ($r_{CO_2} = 0$). Consequently, it can be stated:

$$\frac{\partial^2 [CO_2]}{\partial x^2} = 0$$

Eq. 3-3

The boundary conditions according Fig. 3-1 are:

$[CO_2] = [CO_2]_{int}$ at $x = 0$

$[CO_2] = [CO_2]_{Bulk}$ at $x = \delta_l$

Integration of Eq. 3-3 and evaluation of the boundary conditions leads to the following expressions for the concentration gradient of CO_2 throughout the liquid boundary layer (Bishnoi, 2000):

$$[CO_2] = \frac{[CO_2]_{Bulk} - [CO_2]_{int}}{\delta_l} \cdot x + [CO_2]_{int}$$

Eq. 3-4

The rate of absorption is determined by the diffusion of CO_2 through these two films while the rest of gas and liquid is well mixed and no concentration gradient exists. The gas and liquid are assumed to be in equilibrium at the interface ($[CO_2]_{int} = [CO_2]^*$, $p_{CO_2\,int} = p_{CO_2}^*$) (Chen, 2011). With the setup of the equation of mass balance as well as proper boundary conditions, the concentration profile in the boundary layer can be derived. The CO_2 flux is calculated in Eq. 3-5 with the application of the Fick's law at the interface (Chen, 2011). Eq. 3-6 shows the definition of the physical liquid film mass transfer coefficient as derived from the film theory (Bishnoi, 2000).

$$N_{CO_2} = -D_{CO_2} \cdot \frac{\partial [CO_2]}{\partial x} = \frac{D_{CO_2}}{\delta_l} \cdot ([CO_2]^* - [CO_2]_{Bulk})$$

Eq. 3-5

$$k_l^0 = \frac{D_{CO_2}}{\delta_l}$$

Eq. 3-6

---

[1] Diffusion coefficient D is a proportionality constant between the molar flux due to molecular diffusion and the gradient in the concentration of the species (or the driving force for diffusion). Diffusivity is encountered in Fick's law and numerous other equations of physical chemistry.
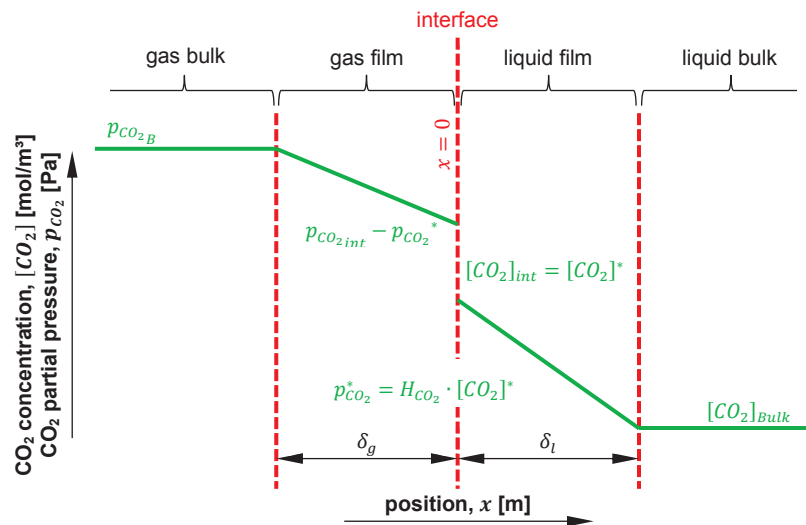
Fig. 3-1. Schematic of the film theory for gas absorption into liquid (Chen, 2011).

The proportional dependence of k_l^0 on diffusivity derived from the film theory is not consistent with most experimental findings. However, the film theory is able to catch the essential feature that "gas must get into the liquid by dissolution and molecular diffusion before it can be transported by convection" (Danckwerts, 1970). The film theory is widely used in modeling of gas-liquid mass transfer because of its simplicity. The films are usually further divided into segments, and mass transfer equations are numerically solved for each segment to improve the accuracy of the calculation for concentration profile within the boundary layers (Chen, 2011).

3.1.2 Penetration theory

The film theory, with its steady flow, is not valid if the penetration period is of the same magnitude as or even longer than the contact time between gas and liquid (Higbie, 1935). Instead Higbie (1935) proposed the penetration theory to describe the real mechanism of absorption. This unsteady-state theory hypothesizes that elements of liquid at the surface are replaced by liquid from the bulk at intervals due to the turbulent motion of the liquid. Absorption only takes place when the elements of liquid are exposed to gas. The time of exposure for each element is of the same length, τ (Chen, 2011).

Analysis of the penetration theory for physical absorption results in elimination of the reactive term in Eq. 3-2. Since the transient term is valid the equation is now a partial differential equation. The expression for the physical liquid mass transfer coefficient in Eq. 3-7 originates after the solution of the partial differential equation and an analysis consistent with film theory (Bishnoi, 2000).

$$k_l^0 = 2 \cdot \sqrt{\frac{D_{CO_2}}{\pi \cdot \tau}}$$

Eq. 3-7

3.1.3 Surface renewal theory

The surface renewal theory is very similar to the penetration theory except for the specification of the length of exposure time, τ. Danckwerts (1951) suggested that the same time of exposure for all the elements of surface is unrealistic. Danckwerts (1951) presented a modification of the penetration theory which suggested a normal distribution of contact times instead of the one used by Higbie (1935). The liquid film mass transfer coefficient is given in Eq. 3-8. s is the mean fractional rate of replacement of any element at the surface (Bishnoi, 2000).

$$k_l^0 = \sqrt{D_{CO_2} \cdot s}$$
Eq. 3-8

3.2 Mass transfer with chemical reaction

In systems with simultaneous reaction, a mass transfer is imperative to ensure the contact of reactants. Normally, it is assumed that the reaction only takes place in the liquid phase. The gas component is transported to the phase boundary. The gas component has to be transported into the liquid phase if no abreaction takes place on the phase boundary in order to react with the liquid molecules. The chemical reaction is closely linked with the mass transfer. There is a phase equilibrium when the rate of mass transfer is larger than that of the chemical reaction. The composition of gas and liquid can be determined by the distribution equilibrium. The absorption process is limited by the kinetics. The mass transfer rate is the imitating factor for the conversion if the rates of chemical reaction and mass transfer are similar. The same applies for a higher reaction rate than mass transfer rate (Kemper, 2012).

3.2.1 Instantaneous reactions

In a limiting case, the reaction between CO_2 and some highly reactive solvents like monoethanolamine and piperazine at high temperature is extremely fast, so equilibrium applies (Chen, 2011). With instantaneous and reversible reactions, the net result of the presence of alkanolamine (chemical compound that contain both hydroxyl and amino functional groups on an alkane backbone) to a first order approximation is the enhancement of CO_2 solubility (Rochelle, et al., 2001). All dissolved forms of the gas, such as bicarbonate or carbamate, are added up to represent the total solubility of CO_2. The mass transfer rate is then given by:

$$N_{CO_2} = k_l^0 \cdot \left([CO_2]_{i,T} - [CO_2]_T^*\right) = k_l^0 \cdot \left(\frac{p_{CO_2}}{H_{CO_2,amine}} - [CO_2]_T^*\right)$$
Eq. 3-9

$H_{CO_2,amine}$ is the Henry's constant of CO_2 in the amine solvent. $[CO_2]_{i,T}$ is the total concentration of the dissolved CO_2 species at the gas-liquid interface that would be in equilibrium with CO_2 partial pressure in the gas phase.

3.2.2 Finite-rate reaction

Fig. 3-2 is a representation of film analysis for CO_2 absorption by bulk liquid with fast chemical reaction. In this case, the reaction rate is not so fast as to be instantaneous while still fast enough for most of the reaction to occur within a thin boundary layer (reaction film) near gas-

liquid interface. This scenario applies to most of CO_2 absorption by amine solvents. The concentration of CO_2 at the interface is now related to the chemical reaction. The rate of absorption is a function of the reaction rate constant as well as thermodynamics (Chen, 2011).
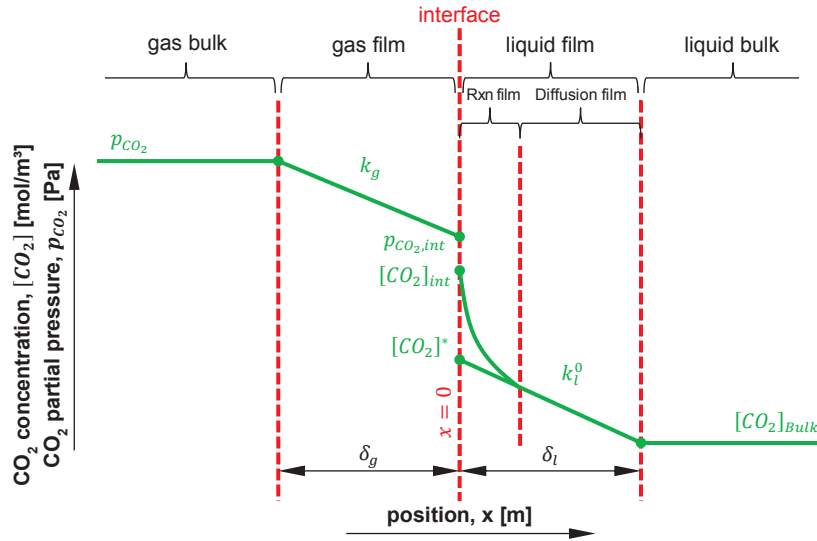
Fig. 3-2.   Mass transfer of CO_2 into bulk liquid with fast chemical reaction (Cullinane, 2005).

The total resistance to mass transfer consists of a series of resistances from gas film, reaction film, and diffusion film, represented by Eq. 3-10 (Chen, 2011).

$$\frac{1}{K_G} = \frac{1}{k_g} + \frac{H_{CO_2}}{E \cdot k_l^0} + \frac{1}{k_{l,PROD}^0} \cdot \frac{\partial p_{CO_2}^*}{\partial [CO_2]_T} = \frac{1}{k_g} + \frac{1}{k_g'} \qquad \textbf{Eq. 3-10}$$

K_G, k_g and k_g' are the overall gas-side and liquid-side mass transfer coefficients with driving force in gas partial pressure unit, respectively (Chen, 2011). $k_{l,PROD}^0$ is the physical liquid phase mass transfer coefficient of reaction product (Ji, et al., 2009). E is the enhancement factor defined as the ratio of CO_2 flux with chemical reaction and CO_2 flux with only physical absorption. $\partial p_{CO_2}^*/\partial [CO_2]_T$ represents the slope of equilibrium curve for CO_2 in amine-CO_2-water (Chen, 2011).

CO_2 flux is usually calculated by solving the steady-state differential equation on CO_2 mass balance in the boundary layer (Eq. 3-2) followed by applying the Fick's law to the CO_2 concentration profile at the interface (Eq. 3-11) (Chen, 2011).

$$N_{CO_2} = -D_{CO_2} \cdot \left. \frac{\partial [CO_2]}{\partial x} \right|_{x=0} \qquad \textbf{Eq. 3-11}$$

Certain simplifications reduce the complexity in solving the differential equation and lead to useful analytical expressions. If the amine concentration is effectively constant across the reactive boundary layer, then the pseudo-first order reaction assumption applies (Chen, 2011).

Since measurements at the gas-liquid interface are extremely difficult, if not impossible, to obtain, the overall mass transfer coefficient, K_G, is obtained during an experiment. The gas film mass transfer coefficient, k_g, is dependent only on the design of the absorption/desorption

equipment and gas properties. Since only the solution properties are of interest in solvent development, the k_g dependence is removed to determine the k_g' which is specific to the solution. The gas film mass transfer coefficient is calculated via gas phase properties. However, each apparatus must be benchmarked with a gas phase controlled system in order to determine the proper gas film resistance of the particular system (Dugas, 2007).

The overall mass transfer coefficient K_G, can be obtained from CO_2 absorption and desorption experiments in a wetted-wall column. The gas film mass transfer coefficient, k_g, can be determined by the analytical correlation proposed by Hobler (1966) for short columns (Eq. 3-12) (Ji, et al., 2009).

$$Sh = A \cdot \left(Re \cdot Sc \cdot \frac{d_h}{h} \right)^B$$ **Eq. 3-12**

The Sherwood number, Sh, Reynolds number, Re and Schmidt number, Sc are defined as:

$$Sh = \frac{R \cdot T \cdot d_h \cdot k_g}{D_{CO_2}}$$ **Eq. 3-13**

$$Re = \frac{d_h \cdot u \cdot \rho}{\eta}$$ **Eq. 3-14**

$$Sc = \frac{\eta}{\rho \cdot D_{CO_2}}$$ **Eq. 3-15**

Where R is the gas constant of the component, T is the temperature, d_h is the hydraulic diameter of the annulus, h is the height of the wetted-wall column, D_{CO_2} is the diffusion coefficient of CO_2 in the gas phase, u is the gas velocity, ρ is the gas density, and η is the dynamic gas viscosity. These dimensionless numbers can be calculated under specific experiment conditions and the constants A and B can be regressed according to Eq. 3-12. k_g can be calculated according to Eq. 3-16 (Ji, et al., 2009).

$$k_g = A \cdot \frac{D_{CO_2}}{R \cdot T \cdot d_h} \cdot \left(\frac{u \cdot d_h^2}{h \cdot D_{CO_2}} \right)^B$$ **Eq. 3-16**

The liquid film mass transfer coefficient, k_g', can be calculated by transforming Eq. 3-10.

3.3 The impact of mass transfer and kinetics on pilot plant studies

The CO_2 absorption in an absorber column can be limited by the mass transfer or reaction kinetics. In a limiting case the reaction between CO_2 and some highly reactive solvents like monoethanolamine and piperazine at high temperature is fast (Chen, 2011). The mass transfer is the limiting factor in this case. The kinetics are the limiting factor when using amino acids (NaGly, KGly). The examined ionic liquid ($[Ch_2][CO_3]$) has a very high viscosity. A high viscosity reduces the mass transfer. Kinetic data of the ionic liquid are not available. At this point, no statement can be made whether the CO_2 absorption of the ionic liquid is limited by the mass transfer or kinetics.

4 Preselection of CO$_2$ absorption solvents

Chemical absorption of carbon dioxide is associated with the chemical reaction of CO$_2$ with an absorption solvent in an absorber column. The CO$_2$ loaded (enriched) solvent is regenerated or CO$_2$ bonds are broken by heat supply in the desorption unit. Subsequent to solvent regeneration, the regenerated solvent is again available for CO$_2$ absorption in the absorber column. In general, chemical solvents purposed for any kind of absorption should possess the following properties (Sattler, 1988):

- High absorption capacity and reactivity
- High selectivity (with respect to CO$_2$)
- Good regenerability
- Low vapor pressure and intermediate boiling point
- Low melting point
- Low viscosity
- Chemical and thermal stability
- Low cost and high availability
- Low corrosivity
- Low environmental impact

A number of absorption solvents are eligible for post-combustion CO2 capture per chemical absorption. All commercially used solvents are aqueous solutions (Posch, 2012). In general, the solvent concentration used originates from a trade-off between high CO$_2$ absorption capacity on one side and high viscosity and corrosivity on the other side (Posch, 2012).

4.1 Amine-based solvents

First and foremost, aqueous amine solutions are the most popular group of solvents for CO$_2$ separation. They have a long history in gas sweetening applications (Posch, 2012). Amines are derivatives of ammonia (NH$_3$) and can be subdivided into primary, secondary and tertiary amines, depending on the number of hydrogen atoms of the former ammonia molecule, which are replaced by functional organic compounds.

4.1.1 Reaction systems

The high CO$_2$ absorption capacity of aqueous amines is mainly affected by chemical reactions. The reversibility of all reactions is essential for the regenerability of the solvent. CO$_2$ reacts in aqueous amine systems to form either bicarbonate (also known as hydrogen carbonate, HCO_3^-) or carbamate ($R_1R_2NCOO^-$) (da Silva & Svendsen, 2007). These species are shown in Fig. 4-1. The placeholder R_1 and R_2 of the carbamate can be a proton or any form substituted group (da Silva & Svendsen, 2007).
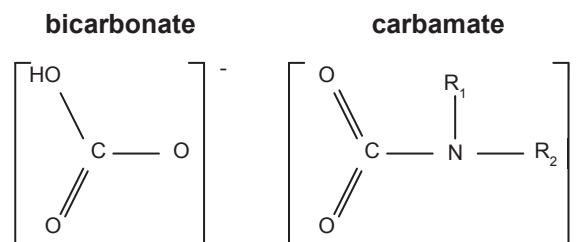
Fig. 4-1. Molecular structure of bicarbonate and carbamate (da Silva & Svendsen, 2007).

4.1.1.1 Bicarbonate formation

The formation of bicarbonate from CO_2 and water is a well-known reaction in chemistry. There are three related mechanisms for this reaction - the formation of carbonic acid (H_2CO_3) (R 4-1), the bicarbonate formation out of molecular CO_2 and a hydroxyl ion (OH^-) (R 4-2) and the bicarbonate formation out of carbonic acid and a hydroxyl ion (R 4-3). The hydroxyl ion in R 4-2 and R 4-3 is formed by the dissociation of water ($2H_2O \rightleftharpoons H_3O^+ + OH^-$). Bicarbonate is the salt of the carbonic acid (da Silva & Svendsen, 2007).

$$CO_2 + H_2O \Leftrightarrow H_2CO_3 \qquad\qquad \textbf{R 4-1}$$

$$CO_2 + OH^- \Leftrightarrow HCO_3^- \qquad\qquad \textbf{R 4-2}$$

$$H_2CO_3 + OH^- \Leftrightarrow HCO_3^- + H_2O \qquad\qquad \textbf{R 4-3}$$

Primary, secondary and tertiary amines have a free electron pair on the nitrogen atom. In aqueous solutions, the nitrogen atom can be protonated analog R 4-4, resulting in the formation of a hydroxyl ion. This leads to the basic character of aqueous amines (Notz, 2009).

$$R_1R_2N + H_2O \Leftrightarrow R_1R_2NH^+ + OH^- \qquad\qquad \textbf{R 4-4}$$

The bicarbonate formation (R 4-2) is a rather slow reaction. Bicarbonate can again be deprotonated by a base molecule (B) (R 4-5). The base molecule is usually an amine molecule or a hydroxyl ion (from R 4-4) (da Silva & Svendsen, 2007). By itself bicarbonate formation is, however, a rather slow reaction. It has been observed that this reaction proceeds more quickly in the presence of amine molecules, an effect beside the direct effect of the amines as bases (Donaldsen & Nguyen, 1980).

$$HCO_3^- + B \Leftrightarrow CO_3^{2-} + BH^+ \qquad\qquad \textbf{R 4-5}$$

4.1.1.2 Carbamate formation

At least one free hydrogen atom exists on the nitrogen atom at primary and secondary amines. In this way, molecular CO_2 formed carbamate with the amine molecule. Tertiary amines have no hydrogen atom. Consequently, the reaction cannot take place (Notz, 2009).

The reaction of CO_2 with amines can either be described by the zwitterion mechanism or by a termolecular mechanism (Aboundheir, et al., 2003). The formulation of the zwitterion reaction mechanism is based on two steps (Blauwhoff, et al., 1983; Kucka, 2003). A zwitterion ($R_1R_2NH^+CCO^-$) is formed in the first step (R 4-6). Thereafter, the zwitterion is converted to

carbamate (R$_1$R$_2$NCOO$^-$) by a base (R 4-7). The net reaction is given in R 4-8. Water, the hydroxide and in particular all present amines can react as base in the considered reaction system (Aboundheir, et al., 2003).

$$CO_2 + R_1R_2NH \Leftrightarrow R_1R_2NH^+COO^-$$ **R 4-6**

$$R_1R_2NH^+COO^- + B \Leftrightarrow R_1R_2NCOO^- + BH^+$$ **R 4-7**

$$CO_2 + R_1R_2NH + B \Leftrightarrow R_1R_2NCOO^- + BH^+$$ **R 4-8**

The reaction conversion rate of the reaction system of R 4-1 to R 4-7 in equilibrium is dependent on the equilibrium constants for each reaction. Thereby, the distribution of the molecular and ionic components in the liquid phase, in particular the relation between CO$_2$, HCO$_3^-$, CO$_3^{2-}$, R$_1$R$_2$NH$^+$CCO$^-$ and R$_1$R$_2$NCOO$^-$ is determined (Notz, 2009).

Two moles of the amine are necessary to bond one mole of carbon dioxide when using a primary amine. This is responsible for limiting the maximum stoichiometric carbon dioxide loading to 0.5 mol CO$_2$ per mol of amine (Jamal, et al., 2006). Higher loadings can be obtained due to the hydrolysis of carbamate at high CO$_2$ partial pressures. The free amine generated can further react with CO$_2$ (Jamal, et al., 2006). The carbamate formation is responsible for the high CO$_2$ absorption rate in aqueous solutions of primary and secondary amines (Aroua & Salleh, 2004).

Tertiary amines react with CO$_2$ following a base-catalyzed hydration mechanism, which is different from the zwitterion mechanism, to form hydrogen carbonate instead of carbamate. Tertiary amines are characterized by a high CO$_2$ loading capacity of 1 mol$_{CO_2}$/mol$_{amine}$ because no carbamate species are formed (Chowdhury, et al., 2013). The reactivity of tertiary amines with respect to CO$_2$ is lower than that of primary and secondary amines. The corresponding enthalpy of reaction for hydrogen carbonate formation is lower than that for the carbamate formation (Tan, 2014).

4.1.2 Selection of amine-based solvents
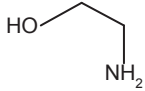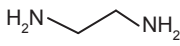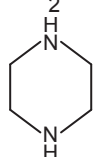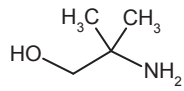
When choosing an amine for CO$_2$ capture, a trade-off between reactivity and CO$_2$ loading capacity has to be taken into account. Primary amines are characterized by high reaction rates but a small CO$_2$ loading capacity. Tertiary amines have a high CO$_2$ loading capacity. However, the slow kinetics of tertiary amines lead to the construction of higher absorber columns (Posch, 2012).

Both primary amines as well as secondary amines have a considerable heat of CO$_2$ absorption. The heat of CO$_2$ absorption is a part of the energy required for solvent regeneration (compare Section 6.3.1). A high heat of absorption seems to be unfavorable with respect to the energy demand. The overall heat demand for solvent regeneration can be minimized though when using solvents with high heat of absorption by consideration of process parameters, in particular the desorber pressure (Oexmann & Kather, 2010).

In recent times, solvents based on secondary and tertiary amines, polyamines as well as sterically hindered amines, have gained in importance. The mixing of amines is another way to

reduce the energy demand of CO$_2$ capture with amines. Table 4-1 provides an overview of amines used in the CO$_2$SEPPL pilot plant in Dürnrohr.

Table 4-1:   Properties of tested amines.

	monoethanolamine	ethylenediamine	piperazine	2-amino-2-methyl-1-propanol
Abbreviation	MEA	EDA	PIP	AMP
Chem. symbol	C$_2$H$_7$NO	C$_2$H$_8$N$_2$	C$_4$H$_{10}$N$_2$	C$_4$H$_{11}$NO
Amine type	primary	primary	secondary/cyclic	primary
Amine groups	1	2	2	1
Molecular structure				
Molecular weight [g/mol]	61.08	60.10	86.14	89.14
Melting point [°C]	10.3	8	106	30
Boiling point [°C]	170	116	146	165

4.1.3 Monoethanolamine – benchmark solvent

Monoethanolamine (MEA) has been used in gas cleaning for decades. Because of vast experience in gas sweetening processes coupled with good availability and low prices, MEA serves as the benchmark solvent for CO$_2$ separation. MEA is a primary amine; therefore, it has a high reactivity with respect to CO$_2$. The CO$_2$ loading capacity is limited to 0.5 mol$_{CO_2}$/mol$_{equ.\ amine}$[1].

Besides the limited loading capacity, MEA is characterized by some other disadvantages with respect to CO$_2$ separation. First and foremost, the regeneration energy duty is in the range between 3.5 and 4.0 GJ/t$_{CO_2}$, which entails a drastic reduction of power plant efficiency for full-scale CCS implementation (Posch & Haider, 2011).

MEA shows significant tendencies towards degradation and foaming. Degradation of MEA occurs through oxidative reactions, salt formations, carbamate polymerization and thermal influences (Epp, et al., 2011). Oxidative degradation leads to the formation of ammonia and various degradation products (organic acids, aldehydes and CO$_2$) (Schmidt & Moser, 2013). Organic acids in the solvent promote the irreversible formation of ions which are known in literature as heat stable salts (HSS) (Epp, et al., 2011). Higher concentrations of SO$_x$ and NO$_x$ (> 20 ppm) in the flue gas lead to the formation of amine salts in the solution (Epp, et al., 2011). Amine salt formation can be reversed in a reclaimer.

Thermal degradation of monoethanolamine is twofold. First, at temperatures higher than 200 °C thermal degradation of MEA starts (Epp, et al., 2011). For CCS applications, low pressure steam is provided for solvent regeneration, which limits the maximum reboiler temperature to 135 °C (Posch, 2012). For small-scale pilot plants, electric heating rods are preferred for solvent regeneration, such as in Dürnrohr, where surface temperatures may lie beyond the 200 °C threshold (Posch, 2012). Second, thermal degradation of MEA occurs at elevated temperatures,

---

[1] The CO$_2$ loading in the present work is indicated in mole per mole equivalent amine (mol$_{CO_2}$/mol$_{equ.\ amine}$) in order to make the CO$_2$ loadings comparable. The exception is the indication of CO$_2$ loading of the blend 28/17 wt% AMP/PIP.

where irreversible reactions with carbon dioxide are promoted. The formation of carbamate polymers is also enhanced at higher temperatures (Epp, et al., 2011).

The standard concentration of 30 wt% MEA (7 m MEA) was tested in the CO$_2$SEPPL pilot plant operation in Dürnrohr.

4.1.4 Ethylenediamine[1]

CO$_2$ absorption in aqueous ethylenediamine (EDA) has been studied by several authors since 1955. Early studies about CO$_2$ absorption with EDA were carried out by Hikita, et al. (1977), Jensen & Christensen (1955), Sada, et al. (1977), Sharma (1965), Trass & Weiland (1971) and Weiland & Trass (1971).

EDA is a primary diamine. Because of that, the EDA molecule has two amine groups and can bind twice as much CO$_2$ per molecule as MEA. EDA has a smaller equivalent weight and a higher concentration of alkali at a given amine weight concentration than MEA and piperazine. It potentially has a greater CO$_2$ capacity (Zhou, 2009).

EDA reacts rapidly with CO$_2$ at low CO$_2$ loadings (Zhou, 2009). The majority of the works that cover the kinetics of CO$_2$ absorption in aqueous EDA solutions focus on unloaded solutions. Sharma (1965) used the same experimental method for EDA and MEA and realized that the second-order reaction rate constant (k$_2$) for EDA is higher than for MEA[2].

No significant thermal degradation can be observed up to 120 °C (Zhou, et al., 2010). With an inhibitor, oxidative degradation in the presence of the catalyst Fe^{2+} can be reduced even further (Sexton, 2008a; Zhou, 2009). Next to MEA, EDA is the only amine that produces significant amounts of ammonia by oxidative degradation (Voice, 2009). The production of ammonia increases in the presence of Fe^{2+}. A reduction of the ammonia rate is possible with the addition of the same inhibitor.

The volatility of the amine is important for the design of the washing section in real plants. Measurement data for EDA is provided by Nguyen, et al. (2010) and Zhou, et al. (2010). With increasing CO$_2$ loading, the partial pressure of amine decreases. This becomes especially apparent at 32 wt% EDA. At higher CO$_2$ loadings (from about 0.13 mol$_{CO_2}$/mol$_{equ.\ amine}$ for 40 °C), 32 wt% EDA is more volatile than 30 wt% MEA (Zhou, et al., 2010). The biodegradability

---

[1] Segments of this section have already been published in Rabensteiner, et al. (2014c).

[2] The reaction of CO$_2$ with primary and secondary amines is generally explained with the zwitterion mechanism, whereas the reaction with tertiary amines is interpreted using the base-catalyzed hydration of CO$_2$ (Kadiwala, et al., 2012). The zwitterion mechanism was suggested by Caplow (1968) based on the suggestion that the reaction between CO$_2$ and the amine follows the two-step mechanism. Initially, a formation of an intermediate zwitterion occurs (R 4-6).

$$CO_2 + R_1R_2NH \underset{}{\overset{k_2\ (k_{-1})}{\rightleftharpoons}} R_1R_2NH^+COO^- \qquad \text{R 4-6}$$
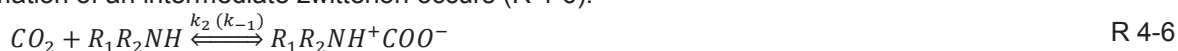
Thereafter the zwitterion undergoes a deprotonation by bases resulting in carbamate formation (R 4-7).

$$R_1R_2NH^+COO^- + B \overset{k_B}{\Leftrightarrow} R_1R_2NCOO^- + BH^+ \qquad \text{R 4-7}$$
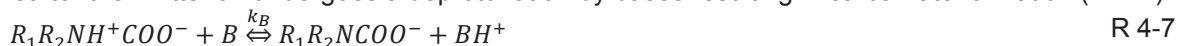
The zwitterion formation is a second-order reaction because the reaction rate it is dependent on the CO$_2$ and amine concentration. k_2 is the forward second-order reaction rate constant in zwitterion mechanism and will be used for comparison of kinetic data of different primary and secondary amines in the present work.

of EDA, for example, is similar to MEA, but shows lower toxicity with respect to algae growth (Eide-Haugmo, et al., 2011; 2009).

Pilot plant tests with aqueous EDA were carried out in the course of the EU-project CESAR on test facilities at the coal-fired power plant in Esbjerg (Denmark) and in the Laboratory of Engineering Thermodynamics at the University of Kaiserslautern (Germany). These test facilities are described in Section 5.3.4 and 5.3.5. In addition, important technical data are listed in Table 5-1. In the CESAR-project, a 32 wt% EDA solution (7.9 m EDA), called CESAR2 or CESAR3, was used. The same concentration was tested in the present work.

4.1.5 Piperazine[1]

Extensive laboratory based research by Prof. Rochelle and his research staff from the University of Texas at Austin has indicated that aqueous piperazine (PIP) solutions possess the following benefits under laboratory conditions (Freeman, et al., 2010; 2009; Rochelle, et al., 2011):

- Double CO$_2$ absorption rate in comparison to MEA
- Nearly double CO$_2$ absorption capacity compared to MEA
- Thermal stability up to a temperature of 150 °C
- Much lower oxidative degradation than MEA
- Low solvent vapor pressure

Pilot plant tests with aqueous piperazine were carried out on the J.J. Pickle pilot plant in Austin (USA) and on the Tarong pilot plant in Nanango (Australia). These test facilities are described in Section 5.3.2 and 5.3.3. In addition, important technical data are listed in Table 5-1. 40.8 wt% PIP (8 m PIP) was used in these studies. In contrast, 37.6 wt% PIP (7 m PIP) was used in the present pilot plant study.

4.1.5.1 Physical and chemical properties of aqueous piperazine

Piperazine is a secondary polycyclic amine and can be used in a concentrated form or as a reaction rate promoter for other solvents (compare the blend with 2-amino-2-methyl-1-propanol in Section 4.1.6). A detailed description of the chemical structure of piperazine and its speciation can be found in Freeman (2011). Initial work focused on the use of piperazine promoted potassium carbonate (K$_2$CO$_3$) (Behr, et al., 2011; Chen, et al., 2006; Cullinane, 2005; Cullinane & Rochelle, 2006; 2005; 2004; Oexmann & Kather, 2009a; Oexmann, et al., 2008). Such a blend was also investigated in the pilot plant in Dürnrohr (Posch, 2012). Since the 2010s, the focus has been on concentrated aqueous piperazine. The University of Texas at Austin, in particular, has done intensive research on the use of this absorption solvent.

At low CO$_2$ loading, the dominant reaction products are piperazine carbamate and protonated piperazine. The dominant reaction product is protonated piperazine carbamate at higher CO$_2$ loadings. Although piperazine dicarbamate is present, it is never the dominant reaction product (Bishnoi & Rochelle, 2000).

---

[1] Segments of this section have already been published in Rabensteiner, et al. (2015a).

Compared to MEA, piperazine has nearly double the loading capacity of CO_2 at double reaction rate (Freeman, et al., 2010). The majority of the increased CO_2 capacity is due to the fact that each mol of piperazine has two functional nitrogen groups (Table 4-1). This allows piperazine to react twice in the CO_2 reaction, whereas MEA can only react once (Dugas, 2009). The fast kinetics of piperazine demonstrate why it is an effective promoter of carbon dioxide absorption. The rate constant is an order of magnitude higher than that from primary amines such as MEA, while the first carbamate stability constant is comparable (Bishnoi & Rochelle, 2000). The heat of CO_2 absorption at mid-loading (Fig. 6-16) is lower than those of aqueous MEA solutions (Xu & Rochelle, 2011). The investigation of Svensson, et al. (2013) shows similar absorption heats and weak temperature dependence.

In earlier literature (Aroua & Salleh, 2004; Bishnoi & Rochelle, 2000; Derks, et al., 2005; Ermatchkov, et al., 2006; Kamps, et al., 2003), the CO_2 solubility of only low concentrated piperazine solutions (up to 26 wt% PIP) was investigated. Hilliard (2008) showed that the CO_2 solubility in the range of 19.7 wt% to 30.1 wt% PIP (0.9 to 5 m PIP) changes only slightly with piperazine concentration. The investigations of Dugas & Rochelle (2009) and Freeman, et al. (2010; 2009) could extend this assertion up to piperazine concentrations of 50.4 wt% (12 m PIP).

Understanding solvent stability and robustness is an important feature to understand when scaling up a PCC process. Solvent degradation can increase plant operating costs through solvent make-up costs and reduced capture capacity (Freeman, et al., 2010). Piperazine does not have an alcohol group that could promote thermal degradation. Consequently, it can be regenerated at higher temperature and pressure than MEA, resulting in a decreasing CO_2 compression rate (Cottrell, et al., 2013). The oxidative degradation is also lower than those of MEA (Freeman, et al., 2010). The volatility of piperazine in aqueous solution is less than that of MEA, despite the lower boiling point of piperazine (Table 4-1) (Rochelle, et al., 2011). Piperazine can react slowly with NO_x in the presence of O_2 to form nitrosamine derivatives (Fine, et al., 2014; Jackson & Attalla, 2011).

The fast kinetics of piperazine under absorber conditions were able to be demonstrated with the experiments according to Section 4.2.3.1. The investigation results in a similar CO_2 absorption capacity of the fresh solvent as the benchmark solvent, 30 wt% MEA. The measured CO_2 absorption capacity of the regenerated solvent is higher.

4.1.5.2 Production of the solvent

Piperazine is commercially available as a solid flake or as 68 wt% aqueous solution (the latter was used in Dürnrohr). In either case, the solvent has a solid component at ambient conditions and therefore requires additional preparation before it can be added to the pilot plant. Low piperazine concentrations are advantageous for the handling of piperazine solutions at low temperatures. Preparing solid piperazine flake into a 10 wt% solution enables easy handling as excess water in the pilot plant is a drawback (Cottrell, et al., 2013).

4.1.5.3 The risk of solidification and precipitation

The attractive properties of aqueous piperazine as a solvent for CO_2 capture have been known for some time. It is used as an absorption rate promoter in solvent blends. However, in these applications, only piperazine concentrations less than 2 m PIP (~ 10 wt% PIP) were examined (Cottrell, et al., 2013). One challenge with aqueous piperazine solutions is the high melting point of pure piperazine (Table 4-1). When diluting piperazine with water, the melting point can be significantly reduced. Unloaded 37.6 wt% PIP (7 m PIP) is only in solution at temperatures above 40 °C (Fig. 4-2). The data from Bishnoi (2000), Hilliard (2008), Merck Corporation (2009), Muhammad, et al. (2009) and the DOW Chemical Company (2001) show a eutectic point at around 60 wt% PIP. The data from the DOW Chemical Company (2001) show the evidence of a metastable freezing point in the region of 20 wt% PIP.
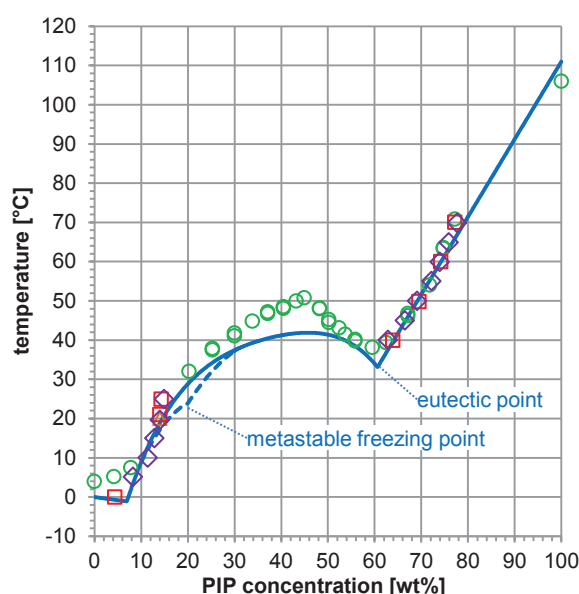
Fig. 4-2:   Freezing point (atmospheric pressure) of aqueous piperazine as a function of the piperazine concentration (Data from Bishnoi (2000) (□), Hilliard (2008) (○), Merck Corporation (2009) (△), Muhammad, et al. (2009) (◇) and DOW Chemical Company (2001) (—)).

The solid solubility of 8 and 10 m PIP (about 40.8 and 46.3 wt% PIP respectively) over a range of CO_2 loadings and temperatures were studied by Freeman, et al. (2010) (Fig. 4-3). The transition temperature is the temperature at which a liquid solution will first precipitate when cooled slowly. The transition temperature of 8 and 10 m PIP is similar. Therefore, the measurement results of 8 m PIP from Freeman, et al. (2010) were used for approximation for 37.6 wt% PIP (7 m PIP). At low CO_2 loadings, piperazine hexahydrate (PIP·6H_2O(s)) is known to precipitate from solution. In this case, the regenerated solvent is in danger of solidification. With increasing CO_2 loading, the temperature at which piperazine hydrate is formed can be greatly reduced. In addition, at high CO_2 loadings, protonated piperazine carbamate (H^+PIPCOO$^-$·H_2O(s)) is thought to precipitate out of solution. The CO_2 loading, at which the carbamate is formed, is almost independent of the temperature. CO_2 loadings should be maintained between 0.1 and 0.4 $mol_{CO_2}/mol_{equ.\ amine}$ at typical operating temperatures (e.g. 40 – 150 °C). When the temperature drops below 40 °C, CO_2 loadings need to be restricted to a

narrower range to avoid precipitation issues (0.32 to 0.37 $mol_{CO_2}/mol_{equ.\ amine}$). Fig. 4-3 shows the operating ranges of the measurement series performed on the test facilities considered. A detailed discussion about the different CO_2 loading ranges of the considered pilot plants can be found in Section 6.3.4.1.
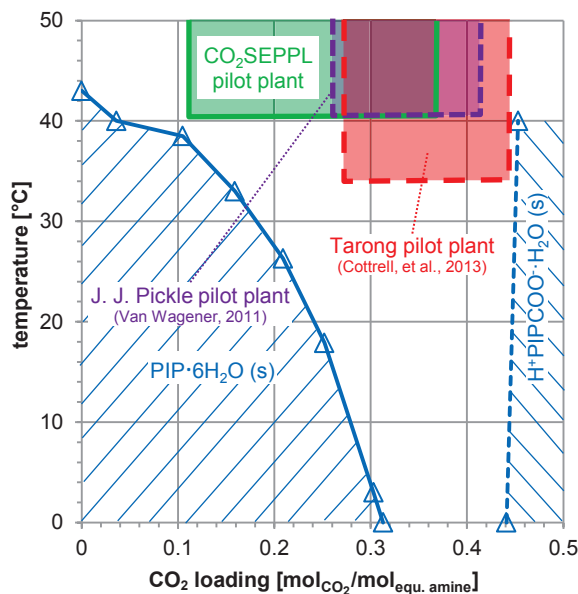
Fig. 4-3:   Solid-liquid transition temperature (atmospheric pressure) for 8 m PIP (40.8 wt% PIP) (Freeman, et al., 2010).

4.1.5.4 Foaming

Concentrated aqueous piperazine for CO_2 capture has a high foaming tendency. In general, foaming is promoted when fine particles, condensed liquid hydrocarbons, amine degradation products, or chemical additives like corrosion inhibitors are present in the solution (Chen, et al., 2011). After one week of operation, foaming was observed at the pilot plant (Fig. 4-4). The entire absorber column was filled with foam, which lowers the absorption capacity, reduces mass transfer coefficients and tremendously increases column pressure drop (Posch, 2012). The foam was able to be broken within a short time by adding small amounts of a silicon anti-foaming agent (MERCK, catalogue number 107743) (Posch, 2012).

Fig. 4-4:   Escape of foam from the absorber (Posch, 2012).

4.1.6 2-amino-2-methyl-1-propanol

2-amino-2-methyl-1-propanol (AMP) is a sterically hindered amine (Hartono, et al., 2013). A sterically hindered amine was originally defined by Sartori & Savage (1983) as an amine belonging to one of the following categories:

- a primary amine in which the amine group is attached to a tertiary carbon;
- a secondary amine in which the amine group is attached to at least one secondary or tertiary carbon.

AMP is the hindered form of MEA obtained by substituting two hydrogen atoms attached to the α-carbon atom to the amine group in MEA by two methyl groups (Bougie & Iliuta, 2012). This results in fundamentally changed properties, such as CO$_2$ absorption capacity (Yoon & Lee, 2003). The CO$_2$ absorption capacity of AMP is high and in the same magnitude as for tertiary amines (Adeosum, et al., 2013). The carbamate stability of AMP has been studied by Ciftja, et al. (2011) and Chakraborty, et al. (1986). Low carbamate stability can be associated with the formation of predominantly carbonate/bicarbonate and thereby a reduction in regeneration energy requirement may be possible.

The use of AMP is associated with the use of high absorber columns because of its slow kinetics. Piperazine as a cyclic diamine enables faster mass transfer compared to most alkanolamines (Derks, et al., 2006; Sun, et al., 2005) and has to be considered as a promoter for AMP. Brúder, et al. (2011) reported that an aqueous blend of 3 M AMP and 1.5 M PIP (26.1/12.8 wt% AMP/PIP) can be a very strong contender for the benchmark solvent, currently 30 wt% MEA, due to its large cyclic capacity, comparable heat of absorption, and good equilibrium temperature sensitivity.

An aqueous AMP solution promoted with piperazine was investigated on pilot plant-scale over the course of the CESAR project which was co-funded by the 7th Framework Program of the European Commission. The concentration of the solvent, which was named CESAR1, was set to 28 wt% AMP and 17 wt% PIP (Mangalapally & Hasse, 2011a). By using CESAR1, the energy demand for solvent regeneration on the pilot plant is Esbjerg could be reduced to 2.6 GJ/t$_{CO_2}$ with lean vapor compression and absorber intercooling (CESAR, 2011b). The same concentration was set in the present work. A slightly modified concentration of 29/18 wt% AMP/PIP is indicated in Tönnis, et al. (2011), which is also apparent from the CESAR project.

4.2 Amino acids[1]

For some years, there has been growing interest in the use of amino acids for CO$_2$ capture. Amino acids are nonvolatile due to their ionic structure which leads to less solvent loss. Furthermore they have better resistance to oxygen rich flue gas streams (Hook, 1997). Many amino acids occur naturally and have favorable biodegradation properties; these factors make their disposal easier and lower their environmental impact (Yan, et al., 2015). There are already

---

[1] Segments of this section have already been published in Rabensteiner, et al. (2014b; 2015c; 2015d).

many publications available which discuss the use of amino acids for CO$_2$ capture, but as of yet no detailed and meaningful results of pilot plant operation with amino acids exist.

Amino acid salts (AAS) have been used for acid gas removal since the 1930s. The Alkazid$^®$ process developed by BASF SE uses the potassium salts of N,N-dimethylaminoacetic acid (C$_4$H$_9$NO$_2$) and N-methylalanine (C$_4$H$_9$NO$_2$). This process is widely used throughout Europe, especially in Germany (Weiland, et al., 2010a; 2010b).

The earliest experiments using amino acids for CO$_2$ capture were based on the Giammarco-Vetrocoke process using an alkali carbonate solution activated with glycine (Kohl & Nielsen, 1997). In the recent past, sodium glycinate in glycerol within an immobilized liquid membrane, was used for the removal of carbon dioxide from the atmosphere in closed-loop life support systems, like in spacecraft or space suits (Chen, et al., 2000; Murdoch, et al., 2001; 2002). Siemens AG has developed a proprietary PCC technology (PostCap™) based on an aqueous solution of potassium salt of undisclosed amino acid (Schneider & Schramm, 2011). TNO proposed three CO$_2$ separation processes using aqueous alkaline salts of amino acids (Feron & Adbroek, 2004; Fernandez & Goetheer, 2011; Sanchez Fernandez, et al., 2013). The membrane gas absorption process is based on the use of a polypropylene hollow fibre membrane. In contrast to alkanolamines, potassium salts of certain amino acids enable stable operation with the considered membrane modules. The DECAB and the recently developed DECAB Plus process take advantage of the fact that when absorbing CO$_2$ in alkaline salts of amino acids, at some point a precipitate will be formed, resulting in higher achievable CO$_2$ loadings. The influence of precipitation can result in an increase in the mass transfer coefficient due to interfacial turbulence (Westerterp, et al., 1984). The CASPER process by the iCAP consortium applies precipitation in the CO$_2$ saturated amino acid salt solution (β-alanine, C$_3$H$_7$NO$_2$) for a simultaneous separation of CO$_2$ and SO$_2$ from flue gas (Misiak, et al., 2013). Aqueous potassium glycinate (KGly) was used as a solvent for CO$_2$ removal with gas-liquid PVDF hollow fiber membrane contactors in Ghasem, et al. (2014; 2013).

4.2.1 Chemical composition

Amino acids are a group of amines. Each amino acid has a central carbon, called the α-carbon, to which four different groups are attached – a basic amine group, an acidic carboxyl group, a hydrogen atom and a distinctive side chain (Fig. 4-5). The properties of each amino acid are dependent on its side chain (—R) (Nagai & Taniguchi, 2014).
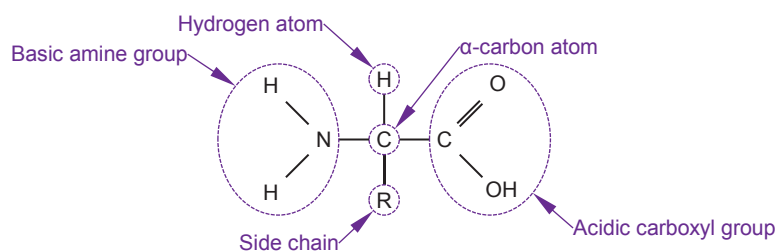
Fig. 4-5:   Structure of an amino acid (Nagai & Taniguchi, 2014).

Amino acids are amphoteric electrolytes; they are thus capable of exhibiting both acidic and basic functions. In water, amino acids exist as molecules carrying a positive charge at one end

and a negative charge at the other. This molecule is called zwitterion. R 4-9 shows the glycine, the simplest primary amino acid in an aqueous solution as zwitterion.

$$^-COO - CH_2 - NH_3^+$$ **R 4-9**

The amine group of the zwitterion is protonated, meaning it is completely non-reactive toward CO$_2$. The amine group deprotonates if a strong acid such as sodium or potassium hydroxide (NaOH, KOH) is added to the zwitterionic amino acid solution. The deprotonation of the glycine zwitterion due to NaOH can be seen in R 4-10.

$$NaOH + {}^-COO - CH_2 - NH_3^+ \Rightarrow Na^+OOC - CH_2 - NH_2 + H_2O$$ **R 4-10**
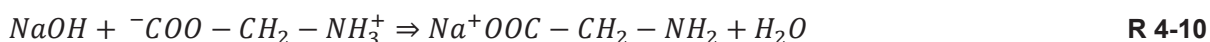
The formed amine group can further react with CO$_2$ (Majchrowicz, 2014; Weiland, et al., 2010a). Amino acids with a deprotonated amine group react with CO$_2$ in a similar way as alkanolamines (Kumar, et al., 2003a; van Holst, et al., 2009). As with alkanolamines, the distinction must be made between primary, secondary and tertiary amino acids, depending on the number of compounds of the deprotonated amine group with carbon-nitrogen bonds. The further reaction scheme can be seen in R 4-1 to R 4-8.

4.2.2 Selection of amino acids to be used

A high reaction rate is generally important to reduce the size and hence the capital costs of an absorber. During CO$_2$ absorption, chemical reactions occur partly simultaneously and successively. Amine concentration, CO$_2$ loading and the question of whether it is a primary, secondary or tertiary amino acid determine if certain reactions can be neglected. In order to draw inferences about reaction rates, many reaction rate constants can be found in literature. For example, van Holst, et al. (2009) have used the overall pseudo-first-order rate constant, k_{OV}[1], for the comparison of several potassium salts of amino acids.

---

[1] The overall pseudo-first-order reaction rate constant k_{OV} can be expressed as
$$k_{OV} = k_{app} + k_{OH^-}[OH^-].$$
$[OH^-]$ is the concentration of hydroxyl ion in the liquid phase (van Holst, et al., 2009). The reaction rate constant k_{OH^-} for the reaction between CO$_2$ and the hydroxyl ion

$$CO_2 + OH^- \overset{k_{OH^-}}{\rightleftharpoons} HCO_3^-$$ R 4-2
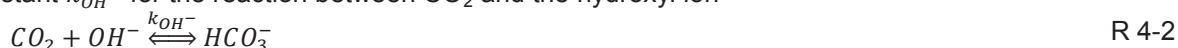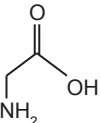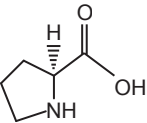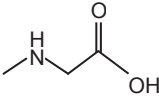
is dependent on the hydroxyl ion concentration, ionic strength and counterions in the solutions (K$^+$, Na$^+$) (Haubrock, et al., 2007; Pohorecki & Moniuk, 1988). Based on these studies, it is very likely that k_{OH^-} will vary with the type and concentration of the amino acid solution used and the cation, however this dependence is not known (van Holst, et al., 2009). The pseudo-first-order rate constant k_{app} is defined by:

$$k_{app} = \frac{k_2 \cdot [R_1R_2NH]}{1 + \sum k_B[B]}$$

$\sum k_B[B]$ is the contribution of all the bases present in the solution for the removal of proton. In lean aqueous solutions, the species amine, water and hydroxyl ion can act as bases as shown by Blauwhoff, et al. (1983). Because the hydroxyl concentration is typically low in the reaction of CO$_2$ with amines, its contribution to the deprotonation of the zwitterions is generally assumed to be negligible (Blauwhoff, et al., 1983; Versteeg & Oyevaar, 1989; Xu, et al., 1996). However, in some of the concentrated amino acid salt solutions, the pH can rise up to considerable values so its contribution to the deprotonation of the zwitterion might not be negligible in these cases (van Holst, et al., 2009).

A low pK_a[1] (base strength value) is of importance to minimize the energy requirement in the desorber (Kohl & Nielsen, 1997). According to van Holst, et al. (2009), salts of L-proline, sarcosine and glycine, which combine a relatively high k_{OV} with a relatively low pK_a, are the most promising amino acids for CO$_2$ capture. Based on the findings of Van Holst, et al. (2009), these amino acids were used for further investigation. Table 4-2 lists the amino acids investigated.

Table 4-2: List of used amino acids.

	Glycine	L-proline[2]	Sarcosine
Abbreviation	Gly	Pr	Sa
Chem. symbol	C$_2$H$_5$NO$_2$	C$_5$H$_9$NO$_2$	C$_3$H$_7$NO$_2$
Amine type	primary	secondary	secondary
Amine groups	1	1	1
Molecular structure			

As is also the case for alkanolamines, the reaction rate of primary amino acids is higher than that of secondary amino acids. The same is true for the CO$_2$ absorption capacity. Secondary amino acids can include more CO$_2$ than primary amino acids. Through the preparation of a blend, the high CO$_2$ absorption capacity of secondary amino acids and the fast kinetics of primary amino acids can be combined, resulting in attractive solvents. Siemens AG has developed a proprietary PCC technology (PostCap™) based on an aqueous solution of potassium salt of undisclosed amino acid (Schneider & Schramm, 2011). According of the patent application of Siemens AG (2011), what is involved here is a blend composed of a secondary amino acid as the active scrubbing substance, and a primary amino acid as an additive. The most advantageous ratio between secondary and primary amino acid is in the weight-related range of 90/10 to 95/5. Further additives cannot be excluded according to Siemens AG (2011). Siemens AG has built a pilot plant at the power plant Staudinger for advancement of the PCC process. This pilot plant is characterized by the total absorber height of 35 m (Siemens AG, 2009). According to Schneider & Schramm (2011), PostCap™ enables a reduction of energy requirements of down to 2.7 GJ/t$_{CO_2}$. But it is not explicitly stated whether this value was measured at the abovementioned pilot plant. Investigations are carried out in the present study to confirm the performance of these highly praised blends.

---

[1] In an aqueous solution, the equilibrium of acid dissociation can be written symbolically as:
$$HA + H_2O \Leftrightarrow A^- + H_3O^+$$
HA is a generic acid that dissociates into A$^-$, known as the conjugate base of the acid and a hydrogen ion which combines with a water molecule to make a hydronium ion (Miessler, et al., 2013). The acid dissociation constant K_a is defined by:
$$K_a = \frac{[A^-][H_3O^+]}{[HA][H_2O]}$$
The pK_a value is the negative decadic logarithm of K_a (Miessler, et al., 2013).
$$pK_a = \log_{10} K_a$$
A linear relationship between the pK_a of an acid or base with its catalytic effect on reaction rate was reported by Brønsted & Guggenheim (1927).
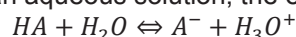
[2] Except for glycine, all amino acids contain at least one asymmetric carbon atom, giving two or more isomers. Such isomers are non-superimposable mirror images and are analogous to left and right hands. The L in L-proline means a left configuration (Nagai & Taniguchi, 2014).

4.2.3 Preliminary studies on laboratory-scale

Two quick laboratory tests were carried out to examine solvents for their suitability as CO$_2$ absorption solvents. The first experiment provides qualitative results about the CO$_2$ absorption rate, whereas the second experiment draws inferences about the CO$_2$ absorption capacity and solvent regenerability. These values are of great importance for CO$_2$ absorption solvents. Pilot plant tests were carried out with the most promising solvents based on these preliminary investigations (Rabensteiner, et al., 2015d).

4.2.3.1 Investigation of CO$_2$ absorption rate

These measurements were described in more detail by Wappel, et al. (2010) and Wappel (2010). The absorption experiment was carried out in a 20 ml glass flask (Fig. 4-6), equipped with a magnetic stirrer. The flask was flushed for five minutes with pure CO$_2$ and was sealed afterwards with a gas-tight septum. Two needles were inserted into the septum, with one needle reaching to the ground and with the tip of the other needle slightly above. CO$_2$ was inserted through the longer needle, while the other needle removed excess CO$_2$. This process took three minutes. Both needles were removed, the upper needle followed immediately by the lower needle. Subsequently, the glass flask was immersed in a bath. The temperature of the bath was set to 25 °C in the first case. A further measurement campaign was carried out with a higher bath temperature of 60 °C. The magnetic stirrer was set at a constant 120 rpm. In order to reduce excess pressure in the flask caused by thermal expansion of the gas, a needle was briefly introduced into the septum. To measure internal pressure, a needle was inserted into the septum which was connected to a pressure gauge. 1 ml of the test solvent was injected into the flask by using a hypo-dermic syringe (Rabensteiner, et al., 2014b; 2015d).
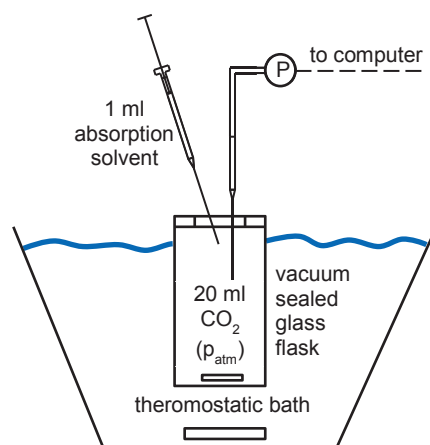
Fig. 4-6.   Screening apparatus for investigation of the CO$_2$ absorption rate (Rabensteiner, et al., 2014b).

The CO$_2$ is absorbed by the solvent. This resulted in a pressure drop in the glass flask. The pressure over time is an approximation of the CO$_2$ absorption rate. The time required equilibrium, recognizable by the consistent pressure, can be used for a qualitative comparison (Fig. 4-7) (Rabensteiner, et al., 2014b; 2015d). This experiment provides only a qualitative estimation of the CO$_2$ absorption rate. Only the CO$_2$ absorption rate of the unloaded or slightly loaded solvent can be studied with this experiment because of the low final CO$_2$ loading of

about 0.1 mol$_{CO_2}$/mol$_{equ. amine}$ (Rabensteiner, et al., 2014b). The kinetics of CO$_2$ absorption are slower with increasing CO$_2$ loading (Chen, 2011). Consequently, the regenerability of the solvent has to be considered.
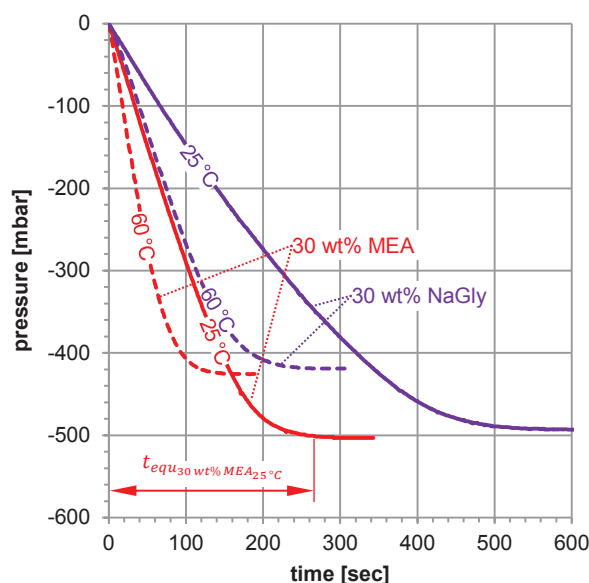
Fig. 4-7. Examples of pressure records (30 wt% MEA, 30 wt% NaGly) (Rabensteiner, et al., 2014b).

The objective of these screening tests was to establish a quick and straightforward procedure for the qualitative evaluation of the CO$_2$ absorption rate. The tests at a temperature of 25 °C are particularly important for the basic evaluation of the CO$_2$ absorption rate. This is because the water vapor partial pressure can be neglected at 25 °C. The more water in the test sample, the higher the water vapor partial pressure in the glass flask. The water vapor partial pressure strongly affects the results of the screening tests at 60 °C. The water vapor partial pressure indicates the additional pressure which is associated with the amount of water at certain temperature. The water vapor pressure influences the final pressure in the closed system. The water vapor pressure counteracts the vacuum which results from CO$_2$ absorption. Solvents having higher molar water content have a higher equilibrium pressure (Wappel, 2010).

The water content of the tested aqueous solutions of amino acids is between 0.926 and 0.952 mol$_{H_2O}$/mol$_{solvent}$ (Table 4-3). Only the water content of 30 wt% MEA is significantly lower (0.888 mol$_{H_2O}$/mol$_{solvent}$). Consequently, the measurement results for 60 °C cannot be directly compared with the data of 30 wt% MEA. The measurement results of the test campaign with a temperature of 60 °C are not presented in the current study. The measurement values for 25 °C were used for comparison.

Table 4-3: Molar water content of the used aqueous solvent based on amino acid salts.

	molar water content [mol$_{H_2O}$/mol$_{solvent}$]
30 wt% MEA	0.888
30 wt% NaGly	0.926
30 wt% KGly	0.936
30 wt% NaSa	0.935
30 wt% KSa	0.943
30 wt% KPr	0.952
30 wt% KSa/KGly 85/15	0.942
30 wt% KSa/KGly 90/10	0.942
30 wt% KSa/KGly 95/5	0.942

4.2.3.2 Investigation of the regenerability and CO$_2$ absorption capacity

Absorption experiments in a small packed column were carried out (Fig. 4-8) to determine the CO$_2$ absorption capacity. The absorber column was filled with ceramic packings (Raschig random packing Ø6 mm, dumping height 320 mm, column diameter 40 mm). The column was fed with a constant flow rate of 1 l/min CORGON$^®$ 18-gas (18 % CO$_2$ and 72 % Ar). The gas flow rate was controlled by a rotameter to obtain reproducible results. The test solvent (200 g) was pumped from a gas-tight bottle to the top of the column and forced downwards through the column in order to absorb CO$_2$ from the gas stream. A gear pump (Heidolph, PUMPdrive PD 5230) pumped the solvent at a flow rate of 50 ml/min. The gas exited the column at the top, where it was dried with silicagel. The CO$_2$ concentration of the purified gas stream was recorded by infrared analysis. The experiment was completed when the CO$_2$ capacity of the solvent was reached and CO$_2$ concentrations of the input and output gas stream matched (Fig. 4-9).
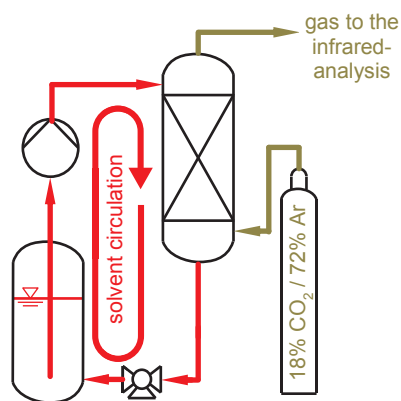
Fig. 4-8. Experiment setup of the small packed column for investigation of the regenerability and CO$_2$ capacity (Rabensteiner, et al., 2014b).

After loading the absorption solvent with carbon dioxide, bounded CO$_2$ was dissolved again through heating. The regeneration was carried out by reflux boiling. The solvent was placed in a flask with a water cooled reflux condenser while boiling chips prevented superheating. To accelerate desorption, the solvent was still stripped with N$_2$. The experiment described above was performed again using the regenerated solvent.
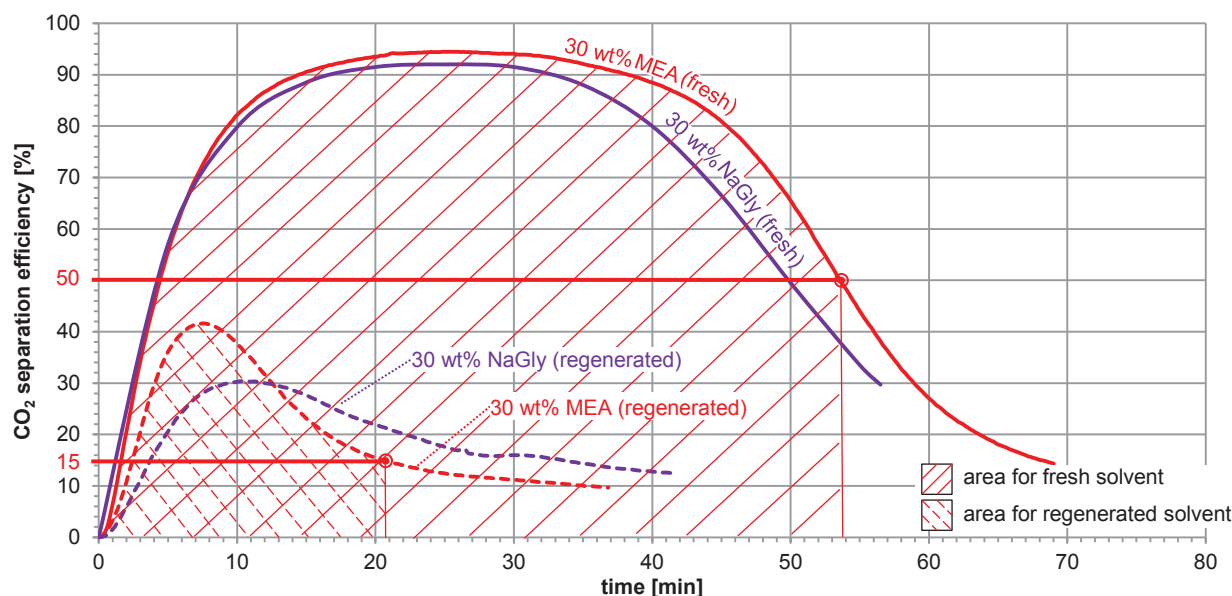
Fig. 4-9.   Exemplary results for 30 wt% MEA and 30 wt% NaGly of the pre-investigations with the small packed column.

The CO$_2$ separation efficiency increases quickly at the beginning of the experiment, independent of the solvent that is used (Fig. 4-9). The fresh solvents reach the highest CO$_2$ separation efficiency after about 15 minutes. Thereafter, the CO$_2$ separation efficiency remains relatively constant for a certain time. The CO$_2$ separation efficiency drops a few minutes later, depending on the absorption solvent used. The reaction rate of CO$_2$ absorption decreases with increasing CO$_2$ loading (Chen, 2011). This results in an asymptotic approximation to the zero line at the end of the experiment. The experiments were terminated prematurely. A sharp decrease in CO$_2$ loading capacity can be seen for all regenerated solvents.

4.2.3.3 Results of preliminary studies

The first experiment (Section 4.2.3.1) provides qualitative results about the CO$_2$ absorption rate, whereas the second experiment (Section 4.2.3.2) draws inferences about the CO$_2$ absorption capacity and solvent regenerability. Based on these preliminary investigations, pilot plant tests were carried out with the most promising solvents (Rabensteiner, et al., 2015d).

The benchmark solvent 30 wt% MEA reached the equilibrium (25 °C) in the first experiment in just under 300 seconds (Fig. 4-7 and Fig. 4-10). All tested aqueous amino acids needed more time to reach equilibrium in the glass flask. The primary amino acid glycine (30 wt% KGly and 30 wt% NaGly) shows a significantly faster CO$_2$ absorption rate in comparison to the secondary amino acids L-proline (30 wt% KPr) and sarcosine (30 wt% KSa and 30 wt% NaSa). This indicates the faster kinetics of primary amines. A significant acceleration of the reaction is evident by adding small amounts of KGly to KSa. A weight-related ratio between secondary and primary amino acid of 90/10 appears to be most advantageous (Rabensteiner, et al., 2015d).
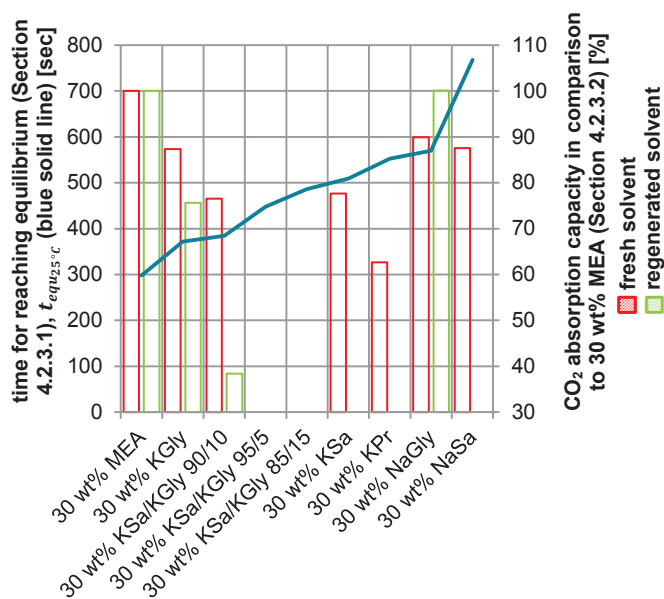
Fig. 4-10: Measurement results of the pre-investigations with aqueous amino acids (Rabensteiner, et al., 2015d).

The kinetic rate constant of the reaction between CO_2 and hydroxyl ions in electrolyte solutions depends not only on the reactants concentration, but also on the type of ions present in a solution (Pohorecki & Moniuk, 1988). The kinetic rate constant was found to vary significantly with the ionic strength assuming first order in the hydroxyl ion and CO_2. The data indicate that the reaction in potassium hydroxide is faster compared to the reaction with sodium hydroxide at similar molar concentrations. The overall reaction rate in the present study for glycine and sarcosine salts (compare 30 wt% KGly with 30 wt% NaGly and 30 wt% KSa with 30 wt% NaSa) shows the same dependency.

Fig. 4-10 shows also the summary of the measurements for determining CO_2 absorption capacity and solvent regenerability (Section 4.2.3.2). Since the experiments had to be terminated prematurely, the area under the curve up to a CO_2 separation efficiency of 50 % was calculated for the fresh solvents. The area for 30 wt% MEA serves as reference (Fig. 4-9). The CO_2 separation efficiency is significantly lower when using regenerated solvents. Consequently, the area under the curve up to separation efficiency to 15 % was used as reference for the regenerated solvents. The measured area of 30 wt% MEA also serves as reference. 30 wt% MEA has the highest CO_2 absorption capacity in both the unloaded and regenerated state. The CO_2 absorption capacity in unloaded state for 30 wt% NaGly and 30 wt% KGly is similar. In the regenerated state, 30 wt% NaGly shows a similarly high CO_2 absorption capacity such as the benchmark solvent 30 wt% MEA. The CO_2 absorption capacity of regenerated 30 wt% KGly is significantly lower. Other solvents examined exhibit lower CO_2 capacities (Rabensteiner, et al., 2015d).

Because of the fast CO_2 absorption rate of 30 wt% KGly and high CO_2 absorption capacity of 30 wt% NaGly, these solvents are investigated in detail in the CO_2SEPPL pilot plant. The remaining aqueous amino acids were discarded from further study because of their lack of performance.

4.2.4 Physical and chemical properties

The material properties database for aqueous NaGly is more complete than that of aqueous KGly. In the subsequent discussion in Section 6, reference is made to data from aqueous NaGly, if substance data for aqueous KGly are not available.

Physical properties of aqueous NaGly have been investigated by Lee, et al. (2005), Park, et al. (2006) and Harris, et al. (2009). Lee, et al. (2005) discussed CO_2 unloaded solutions for different NaGly concentrations (10 to 50 wt%) and temperatures (30 to 80 °C), and subsequently offered values for density, viscosity, surface tension, alkalinity and hydrogen ion activity (pH). Harris, et al. (2009) investigated the density of aqueous NaGly before and after CO_2 absorption for a concentration range of 1 to 30 wt% within a temperature range of 25 to 80 °C.

4.2.4.1 The risk of solidification and precipitation

For temperatures above 0 °C there is no risk of solidification of aqueous KGly and NaGly (Fig. 4-11). The solidification temperature decreases even further at higher amino acid concentrations. Aqueous KGly and NaGly have the same solidification temperature. The solidification temperature in the unloaded state is about -14 °C for solvents with an amino acid concentration of 25 wt%. The solidification temperature increases only slightly with rising CO_2 loading. The solidification temperature of low concentrated amino acid solvents (< 10 wt%) is independent of the CO_2 loading. This dependence rises with increasing amino acid concentrations. The maximal expected CO_2 loading in the process is about 0.50 $mol_{CO_2}/mol_{equ.\ amine}$ (compare CO_2 solubility data from Fig. 4-12), when assuming equilibrium loading in the bottom of the absorber column. The solidification temperature of 25 wt% KGly and 25 wt% NaGly with a CO_2 loading of 0.5 $mol_{CO_2}/mol_{equ.\ amine}$ is about -11 °C. Consequently, there are no problems with solidification expected, even for higher CO_2 loadings.

Precipitation during CO_2 absorption can occur at temperatures above 0 °C and with high amino acid concentrations (> 30 wt%) (Fig. 4-11). The precipitate of KGly most likely corresponds to the zwitterionic form of the amino acid (RNH_3^+) (Kumar, et al., 2003b). The CO_2SEPPL pilot plant in Dürnrohr is not designed for precipitation, in contrast to the DECAB, DECAB Plus and CASPER processes. Consequently, precipitation must be prevented. The risk of precipitation increases with increasing amino acid concentration and CO_2 loading. For 40 wt% KGly, which was filled into the CO_2SEPPL pilot plant, a maximal CO_2 loading of less than 0.5 $mol_{CO_2}/mol_{equ.\ amine}$ is measured in pilot plant operation. That means that the temperature should not be lower than 18 °C in order to avoid precipitation. The precipitation temperature for 40 wt% NaGly, which was also filled into the CO_2SEPPL pilot plant, seems to be even higher (~ 25 °C) for the same CO_2 loading.

In pilot plant operation, the line between absorber and main heat exchanger is particularly affected by precipitation. The temperature of the CO_2 enriched solvent in this line is usually higher than 40 °C so that precipitation can be mostly avoided. In the case of a system failure and low outside temperatures solidifications are still expected. To avoid solidification, exposed areas have to be trace-heated. A shutdown without damage is ensured by prior regeneration of the solvent. Here the opposite of the operation with aqueous piperazine is true, in which the

solvent should be loaded as high as possible before the plant is turned off (Rabensteiner, et al., 2015a).

The risk of precipitation when using aqueous NaGly is generally slightly higher in comparison to aqueous KGly. For unloaded and low loaded NaGly solutions, there is a particularly higher risk of system failure.
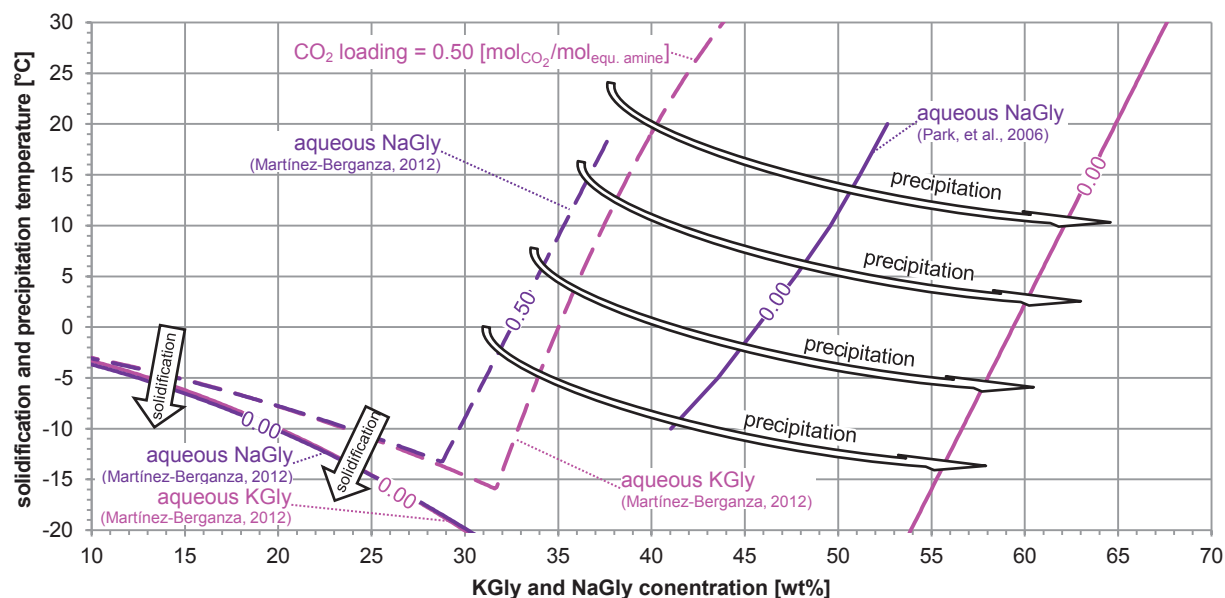
Fig. 4-11:   Solidification and precipitation of aqueous KGly and NaGly.

4.2.4.2 CO₂ solubility

Portugal, et al. (2009) investigated the CO_2 solubility of KGly concentrations of 0.1 M (1.13 wt%), 1 M (10.78 wt%) and 3 M (29.14 wt% KGly (referred to hereinafter as 30 wt% KGly)) and temperatures between 20 °C and 78 °C (Fig. 4-12).

The solubility of carbon dioxide in an aqueous NaGly solution was studied by Song, et al. (2008; 2006) and Harris, et al. (2009). Song, et al. (2006) provided VLE data for 10, 20 and 30 wt% NaGly for temperatures of 30, 40 and 50 °C. Harris, et al. (2009) investigated mainly CO_2 partial pressures in the excess pressure range. The data of these studies vary widely within the range of overlap. Song, et al. (2008) investigated the solubility of CO_2 in 30 wt% NaGly over a wider temperature range. Several large deviations exist between the VLE data from Song, et al. (2006) and Song, et al. (2008). The data of Song, et al. (2008) were determined later and those are comparable with the measured CO_2 loadings of the present work. Therefore, the data from Song, et al. (2008) are used as a reference in the present work.

The measured CO_2 solubility in 10.78 wt% KGly does not differ significantly from the data obtained by Song, et al. (2006; 2008) for 10 wt% NaGly (Portugal, et al., 2009). Contrary to the results for low concentrate solutions, the CO_2 solubility of 30 wt% KGly is not in line with the results published by Song, et al. (2008) for 30 wt% NaGly. This could be due to the difference in the salt cation. Although the glycinate anion reacts with CO_2, the salt cation may start playing a significant role in the process at solution concentrations as high as 30 wt% by modifying the ionic character of the solution. According to the Guggenheim equation, differences between

short-range interactions of K^+ (from KGly) and Na^+ (from NaGly) and the other ions present in the solution would become more noticeable at higher concentrations (Portugal, et al., 2009).

The CO_2 partial equilibrium pressure when using 30 wt% KGly is higher than for 30 wt% NaGly for low CO_2 loading and temperature (40 °C) because of the higher molar concentration of active substance in 30 wt% NaGly. The temperature in the desorber bottom is about 120 °C. The CO_2 solubility in 30 wt% NaGly for 120 °C is characterized by the low CO_2 partial pressure in comparison to that of 30 wt% MEA. The low CO_2 partial pressure at 120 °C leads to a high amount of generated steam in order to reach the desired CO_2 loading of the regenerated solvent. The CO_2 loading of the regenerated solvent would be higher if the same amount of steam is generated as in the process with MEA. This results in a rising CO_2 loading level leading to slower absorption kinetics (Chen, 2011). No statements about the KGly performance in pilot plant operation can be made since no data are available for this temperature range for aqueous KGly (Rabensteiner, et al., 2015c).
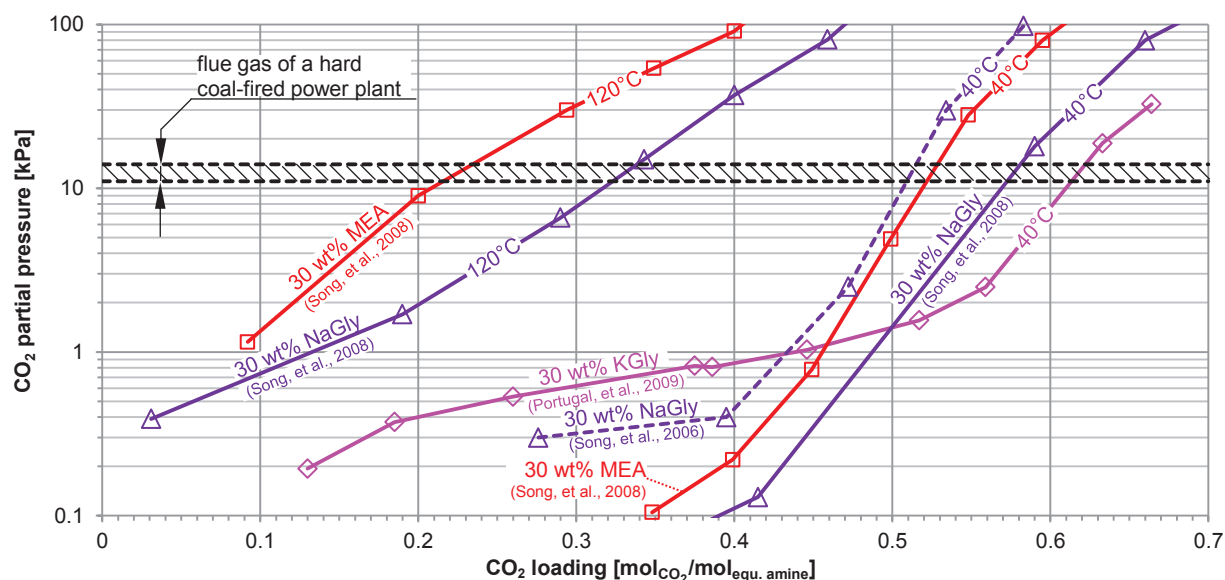
Fig. 4-12: CO_2 solubility data for 30 wt% KGly, 30 wt% NaGly and 30 wt% MEA.

4.2.4.3 Kinetics

The reaction with potassium glycinate was studied earlier by Jensen, et al. (1952), Caplow (1968), Penny & Ritter (1983) and recently, by Kumar, et al. (2003b), Portugal, et al. (2007) and Vaidya, et al. (2010). Lee, et al. (2007), Park, et al. (2008) and Weiland, et al. (2010a) investigated the kinetics of CO_2 absorption in aqueous sodium glycinate.

Because of their similar functional groups, it can be assumed that the alkaline salt of amino acid reacts by a zwitterionic mechanism such as primary and secondary amines do (Kumar, et al., 2003b). Bases such as water, amine, or hydroxyl ion can contribute to the deprotonation during deprotonation of zwitterions to carbamate in an aqueous solution (Lee, et al., 2007). The initial CO_2 absorption rate increases, but the regeneration efficiency decreases with the rise in the basicity of amino acid salts (Yan, et al., 2015). Contrary to primary aqueous alkanolamines, the partial reaction order in amino acid salt changes with the molar salt concentration. The reaction

order changes from 1 at low concentration to 1.5 at salt concentrations approaching 3 M (29.14 wt% KGly, 25.44 wt% NaGly) (Kumar, et al., 2003b). This indicates that the deprotonation step in the zwitterion mechanism is not much faster than the zwitterion formation step, a behavior typically exhibited by the secondary aqueous alkanolamines. Also, it indicates that the zwitterion of the amino acid is less stable compared to primary alkanolamines (Kumar, et al., 2003b). Since the reaction order is under 2, the zwitterion formation is rate-determining (Kemper, 2012). The zwitterion mechanism can be conveniently used to describe the experimental kinetic data (Kumar, et al., 2003b). Therefore, the second-order rate constant (k_2) can be used as reference value for the absorption rate. The reaction order of CO₂ absorption in aqueous MEA is under 2 (Aboundheir, et al., 2003), meaning that the zwitterion formation is also rate-determining (Kemper, 2012).

k_2 rises generally with increasing temperature. The k_2 of NaGly is much lower than that of MEA within the temperature range investigated (Fig. 4-13). Weiland, et al. (2010a) indicated a much higher value of k_2 for aqueous KGly than proposed by Lee, et al. (2007), but do not state, how this high value is determined. There are also some discrepancies in reported results on potassium glycinate. k_2 is far higher than the values to be expected, based on the Brønsted plot for aqueous amines reported in Versteeg, et al. (1996) and Penny & Ritter (1983). This indicates that the Brønsted plot of amino acids might be different from that of aqueous alkanolamines (Kumar, et al., 2003b). The k_2 of aqueous KGly is on average higher than that of aqueous NaGly.

The data in Fig. 4-13 fit well with the measurement results of the laboratory experiment (Section 4.2.3.3), carried out in the present work. The CO₂ absorption measurements in the glass flask also show that the reaction in potassium salts is faster than in sodium salts.
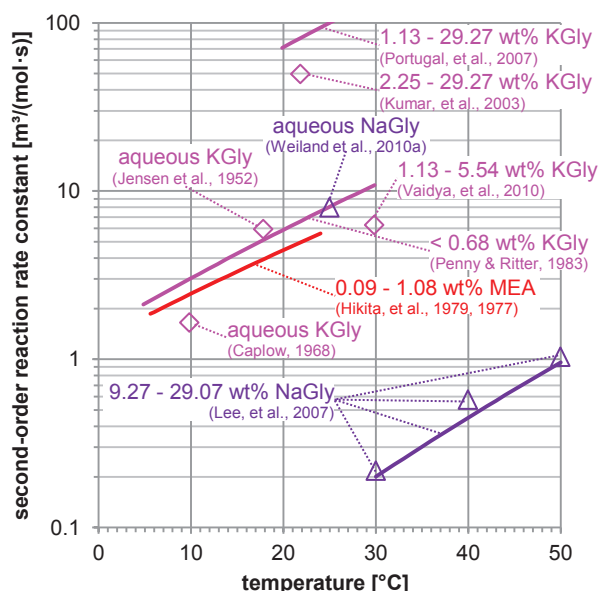
Fig. 4-13: Second order reaction rate constant dependent on the temperature for aqueous KGly, NaGly and MEA.

The mass transfer is also influenced by the solvent viscosity (compare Section 3.2.2). 30 wt% KGly (Portugal, et al., 2007), 30 wt% NaGly (Lee, et al., 2005) and 30 wt% MEA (Amundsen, et al., 2009) have similar viscosity values, so that this effect is neutralized.

4.2.4.4 CO_2 absorption enthalpy and sensible heat

CO_2 absorption kinetics and solubility of the solvent in particular determine the required heat of evaporation for generating stripping steam. Further energy must be provided to reverse reaction (CO_2 absorption enthalpy) and solvent heat up (sensible heat).

The enthalpy of CO_2 absorption of NaGly has been investigated by Salazar, et al. (2010), Song, et al. (2008) and Weiland, et al. (2010a). A smaller absorption enthalpy of NaGly is obvious, despite the varying areas of investigation of these research works. For example, the CO_2 absorption enthalpy of 30 wt% NaGly (0.4 $mol_{CO_2}/mol_{equ.\ amine}$) is 69 kJ/kmol. Thus, the CO_2 absorption enthalpy is almost 13 % lower than that of 30 wt% MEA (Song, et al., 2008). Absolute values for CO_2 absorption enthalpy for aqueous KGly are not available in literature. Yan, et al. (2015) recorded the solvent temperature during CO_2 absorption. It may be deduced from these results that KGly has a lower CO_2 absorption enthalpy then MEA. Consequently, less heat is required to break the CO_2-NaGly and CO_2-KGly solution complex.

The specific heat capacity of 30 wt% NaGly is about 3.5 kJ/(kg·K) and exhibits only a slight dependence on the temperature (Fig. 4-14). Thus, the specific heat capacity is significantly lower than that of 30 wt% MEA, which furthermore rises sharply with increasing temperature. At desorber temperatures, the specific heat capacity of 30 wt% MEA is about 15 % higher than that of 30 wt% NaGly (Song, et al., 2008). Therefore, less sensible heat is required to raise the temperature of the CO_2 enriched NaGly solvent. The specific heat capacity of 4 M KGly (~ 40 wt% KGly) is 3.35 kJ/(kg·K) (Erga, et al., 1995). The temperature for this study is unknown. It may be deduced from these results that the specific heat capacity of KGly is also significantly lower than for MEA. In contrast to CO_2 absorption enthalpy, inferences cannot be drawn from solvent properties about this share of energy demand because the sensible heat is also significantly affected by the solvent flow rate and solvent temperature difference in the desorber.
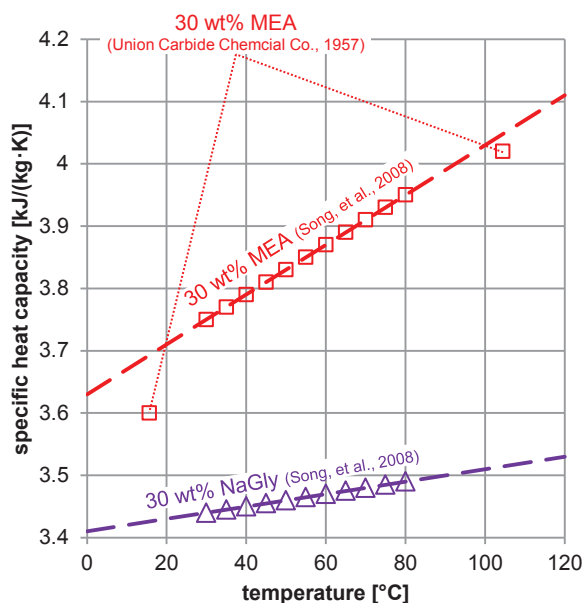
Fig. 4-14: Specific heat capacity dependent on the temperature for 30 wt% NaGly and 30 wt% MEA.

4.2.4.5 Degradation

Aqueous solutions of amino acids are known to be corrosive and require stainless steels (Weiland, et al., 2010a). According to Huang, et al, (2013), the thermal degradation rate of NaGly is higher than that of MEA.

4.2.5 Laboratory studies with 30 wt% NaGly and 30 wt% KGly

Various studies were performed in order to test the suitability of the solvents. Previous works investigated the properties of 30 wt% NaGly. The same concentration was tested in order to compare measured data in the present work. The same concentration was used for aqueous KGly. Density, pH-value, concentration, and CO_2 loading of different loaded solvents were investigated.

4.2.5.1 Solvent preparation

Preparation of 30 wt% NaGly can be done in two ways. First, through the dissolution of sodium glycinate hydrate (from Sigma-Aldrich Chemical Co. with a mass purity of higher than 99 %) in deionate (Fluid 1), and secondly through the mixture of glycine, sodium hydroxide solution (50 wt%) and deionate (Fluid 2). The production method of 30 wt% KGly is the same. For the first method of production, potassium glycinate hydrate is used instead of sodium glycinate hydrate. But suppliers of potassium glycinate hydrate could not be found. Potassium hydroxide thus had to be used instead of sodium hydroxide solution for the production of aqueous potassium glycinate through the second method.

In order to determine the influence of the CO_2 loading on the solvent properties, solutions were prepared with different CO_2 loadings. For the production of semi-loaded (50 % loaded) solvent, unloaded solvent (0 % loaded) was mixed in equal mass amount with equilibrium-loaded

(100 % loaded) solvent, loaded with pure CO_2 at atmospheric pressure and 20 °C. For production of the quarter-loaded solvent (25 % loaded), mass equal amounts of unloaded and semi-loaded solvent were mixed. For the three-quarter-loaded solvent (75 % loaded) the semi- and equilibrium-loaded solvent were mixed. This process was carried out with both Fluid 1 and Fluid 2. Table 4-4 lists all measured and calculated values of Fluid 1 and Fluid 2.

Table 4-4: Summary of the physical properties of Fluid 1 and Fluid 2.

	CO_2 loading			Concentration of active substance			density			pH-value	
	$mol_{CO_2}/mol_{equ.\ amine}$			[wt%]			[kg/m³]			[-]	
	30 wt% NaGly		30 wt% KGly	30 wt% NaGly		30 wt% KGly	30 wt% NaGly		30 wt% KGly	30 wt% NaGly	
	Fluid 1	Fluid 2	Fluid 2	Fluid 1	Fluid 2	Fluid 2	Fluid 1	Fluid 2	Fluid 2	Fluid 1	Fluid 2
unloaded	0.017	0.002	0.008	24.10	30.15	31.78	1127.5	1164.0	1155.6	12.38	12.11
25 % loaded	0.152	0.146	0.086	23.26	29.43	30.80	1147.5	1190.0	1179.8	11.00	10.84
50 % loaded	0.319	0.307	0.251	22.90	29.14	30.15	1165.2	1210.0	1199.0	10.39	10.34
75 % loaded	0.474	0.480	0.459	22.39	28.92	29.58	1177.4	1222.0	1215.7	9.40	9.66
100 % loaded	0.673	0.639	0.638	21.17	27.28	29.12	1184.1	1248.0	1228.7	7.77	8.07

4.2.5.2 Measurement results

Determination of the CO_2 loading was performed by titration with hydrochloric acid. The measurement setup for determination of the CO_2 loading can be seen in Fraubaum (Fraubaum, 2013). The equilibrium loading (100 % loaded) with pure CO_2 (100 kPa) fits with the measured values of Song, et al. (2008) (compare Fig. 4-12) (Rabensteiner, et al., 2014b). The measurement results of the CO_2 loading are listed in Table 4-4.

The concentration of active substance was determined by titration with hydrochloric acid (Fig. 4-15a). The measured density of Fig. 4-15b was used for the calculation of the active substance concentration. The measurement deviation increases with increasing CO_2 loading. The deviation of Fluid 1 for 30 wt% NaGly is much larger in comparison to Fluid 2. The reason for the low NaGly concentration of Fluid 1 is an undetermined amount of crystal water in the sodium glycinate hydrate. The true NaGly concentration of Fluid 1 is in the range of 24 wt% (Rabensteiner, et al., 2014b).

The density was measured with a 10 ml Gay-Lussac pycnometer at a temperature of 25 °C. Fig. 4-15b shows the density of Fluid 1 and Fluid 2 as a function of the CO_2 loading. The density of Fluid 2 is higher than that of Fluid 1 in consideration of the measurement results for aqueous NaGly. This results from the higher NaGly concentration of Fluid 2. The density values of unloaded 30 wt% NaGly published by Lee, et al. (2005) and Harris, et al. (2009) fit well with the measured values of Fluid 1 (Rabensteiner, et al., 2014b).

It is possible that the stated NaGly concentration doesn´t match the real NaGly concentration in previous literature, including Lee, et al. (2005) and Harris, et al. (2009). This is apparent from the density data. The real NaGly concentration of the solvents used in previous literature is about 24 wt% (Rabensteiner, et al., 2014b).
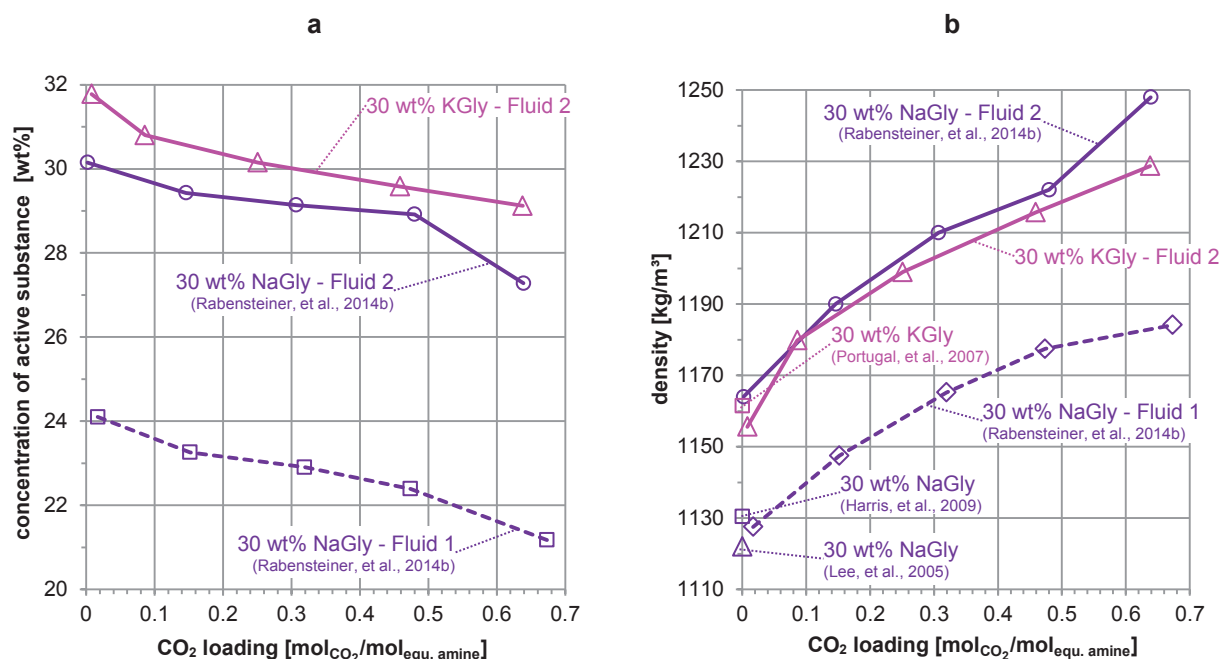
Fig. 4-15: Measured concentration of active substance **(a)** and density (at 25 °C) **(b)** of Fluid 1 and Fluid 2 as a function of the CO_2 loading.

The pH-value of dilute solutions is approximately the negative decadic logarithm of the molar oxonium ion concentration in mol per liter ($pH = -\log_{10}([H_3O^+] \cdot l/mol)$). An oxonium ion is produced during the carbamate formation according to R 4-8, if the base (B) is water. The oxonium ion concentration rises during CO_2 absorption. Consequently, the pH-value decreases with rising CO_2 loading.

The pH-values of Fluid 1 and Fluid 2 for aqueous NaGly are similar. The measured pH-value from Lee, et al. (2005) for an unloaded solvent shows a good correlation. For each measuring point of the pilot plant study, a sample of the loaded (rich) and regenerated (lean) solvent was taken (Fluid 2). It is clear that a linear relationship exists between the measured pH-value and the CO_2 loading of the solvent. Rich and lean solvents are considered independently of each other. Consequently, the CO_2 loading of the solvent can be calculated by measuring the pH-value in operation.

4.2.6 Numerical investigations with aqueous sodium glycinate

A variety of simulations with aqueous NaGly as CO_2 absorption solvent had been carried out prior to this study; however, only few operating parameters are known for some simulations. A scientific discussion is therefore difficult to carry out. NaGly concentrations between 30 and 47.5 wt% were investigated. Most simulations yielded better results than with 30 wt% MEA. Only the work of Song, et al. (2008) showed above-average specific regeneration energies for aqueous NaGly. The optimal solvent flow rate (L/G-ratio) for reaching the minimal energy demand for solvent regeneration is also predominantly low. A summary of the parameters and results are shown in Table 4-5. Numerical studies with aqueous KGly were not conducted.

Table 4-5. Summary of simulation studies of aqueous NaGly as CO_2 absorption solvent.

	Weiland, et al. (2010a)	Weiland, et al. (2010b)	Optimized Gas Treating (2010)	Lee, et al. (2008)	Ogawa (2013)	Song, et al. (2008)
NaGly concentration [wt%]	45	45 / 30	47 (47.5)	30	45	30
Simulation tool	ProTreat®	ProTreat®	ProTreat®	Pro/II	ProTreat®	-
General information						
Flue gas flow rate [m³/h]	~ 700.000	~ 700.000	~ 700.000	~ 900	-	-
└ F-factor [√Pa]	└ ~ 1.5	-	-	-	~ 1.5	-
Desorber pressure [bar$_{rel}$]	-	0.5 - 1.5	-	0.75	1	-
Flue gas CO_2 content [vol% (dry)]	13	-	13	10.2	4.72	-
Main heat exchanger pinch temperature [K]	5.5	-	-	-	4	-
Absorber						
Total height of packing [m]	20	10	15.24	-		-
Type of packing	Mellapak™ 250.X	FLEXIPAC® 3Y	Mellapak™-Plus 252.Y	-	Mellapak™ 250.X	-
Regenerated solvent temperature [°C]	43	-	-	-	40	-
Flue gas temperature [°C]	43	-	-	-	40	-
Pressure drop [mbar]	20	-	-	-	-	-
Bottom pressure [mbar]	70		85	1.000 – 9.000	-	-
Optimal operating point						-
Specific energy for solvent regeneration [GJ/t$_{CO_2}$]	3.0	2.8 / 4.0	2.23	3	3.3	5.7
L/G-ratio [l/m³]	~ 1.8	~ 2.4 / ~ 3.6	~ 0.54	-	~ 1.1	-
CO_2 separation efficiency [%]	90	90	90	-	80	-

4.3 Ionic liquids

4.3.1 Chemical composition

Ionic liquids are salts with a melting temperature below the boiling point of water (Wasserscheid & Welton, 2008). This means that ionic liquids are molten salts at room temperature. Ionic liquids consist only of ions. In contrast to solutions, ionic liquids do not need a solvent, as the ions are present in dissociated form (Wappel, 2010).

Emissions are an important criterion to evaluate absorption solvents. In this field, ionic liquids have an advantage over the commonly used amines. Since ionic liquids have no measurable vapor pressure, no emissions due to the volatility occur (Mahurin, et al., 2010). Furthermore, ionic liquids have a very distinct liquid range and high thermal stability. Since ionic liquids consist only of ions, any combination of anion and cation are possible, resulting in an extremely wide range of variation (Anderson, et al., 2007).

The naming of ionic liquids in this research work is based on the rules of the IUPAC (International Union of Pure and Applied Chemistry). First, the naming of the cation takes place. The abbreviations of cation and anion are written in square brackets.

Wappel (2010) investigated some ionic liquids in his research work ([TOMA][acetate], [TOMA][acetate] + 10 wt% TOA, [TEMA][acetate], 25 wt% [EMIM][CYS] + H_2O, 42 wt% [EMIM$_2$][CO$_3$] + H_2O, 28 wt% [Guanidine][CO$_3$] + H_2O, 43 wt% [TBA$_2$][CO$_3$] + H_2O, 48 wt% [Ch$_2$][CO$_3$] + H_2O) for their suitability as CO_2 absorption solvents using screening experiments. The ionic liquid [Ch$_2$][CO$_3$] was determined to be the most suitable.

[Ch$_2$][CO$_3$] consists of two ions choline, a primary alcohol with a quaternary ammonium compound, and a carbonate ion. Fig. 4-16 shows the chemical structure of the ionic liquid [Ch$_2$][CO$_3$] (Wappel, 2010).
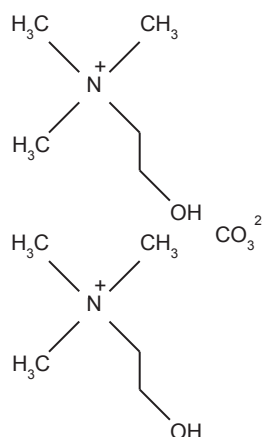
Fig. 4-16. Molecular structure of $[Ch_2][CO_3]$ (Wappel, 2010).

4.3.2 Reaction rate

Kinetic data of CO_2 absorption with $[Ch_2][CO_3]$ are not available in literature. The CO_2 absorption rate of $[Ch_2][CO_3]$ was investigated using a screening apparatus, explained in Section 4.2.3.1. 30 wt% MEA was used as reference solvent. MEA has relatively fast CO_2 absorption kinetics. A low concentration of 48 wt% $[Ch_2][CO_3]$ was selected in order to lower the viscosity and reduce the influence of the limiting mass transfer (Wappel, 2010).

Only the kinetics of the unloaded or slightly loaded solvent can be studied because of the low achievable CO_2 loading in this experiment (~ 0.1 $mol_{CO_2}/mol_{equ. amine}$). The expected CO_2 loading is especially high for aqueous $[Ch_2][CO_3]$ when considering the equilibrium data in Fig. 4-19. The expected CO_2 loading of the regenerated solvent is up to 0.4 $mol_{CO_2}/mol_{equ. amine}$ higher in comparison with 30 wt% MEA. This is only an estimate because Fig. 4-19 is valid for 60 wt% $[Ch_2][CO_3]$. In pilot plant operation, the kinetics will therefore be much slower (Aboundheir, et al., 2003). The measured pressure curves can still be used as an indication.

Experimental results for 48 wt% $[Ch_2][CO_3]$ and 30 wt% MEA are presented in Fig. 4-17 as pressure decrease as a function of time. The time required to achieve the equilibrium pressure for 48 wt% $[Ch_2][CO_3]$ is longer than for 30 wt% MEA. This implies slower CO_2 absorption reaction kinetics. Although the absorption rate of the selected ionic blend liquid was slower than that of 30 wt% MEA, it was much faster than the K_2CO_3 solution. The slow kinetics of not-promoted K_2CO_3 solutions prevent the pilot plant operation from using this solvent. Consequently, a pilot plant operation with aqueous $[Ch_2][CO_3]$ in view of the kinetics seems to be possible in principle (Wappel, 2010).

The comparative difference with MEA solution decreases with increasing temperature, leading to a relatively small difference at 80 °C. The high viscosity of the ionic liquid is critical to this effect. The viscosity appears to be the determining factor in this experiment. By increasing the temperature, the viscosity of the ionic liquid can be significantly reduced (Fig. 4-18). Accordingly, the pressure decrease in this experiment is faster. The viscosity change of 30 wt% MEA, however, is relatively small (Wappel, 2010).
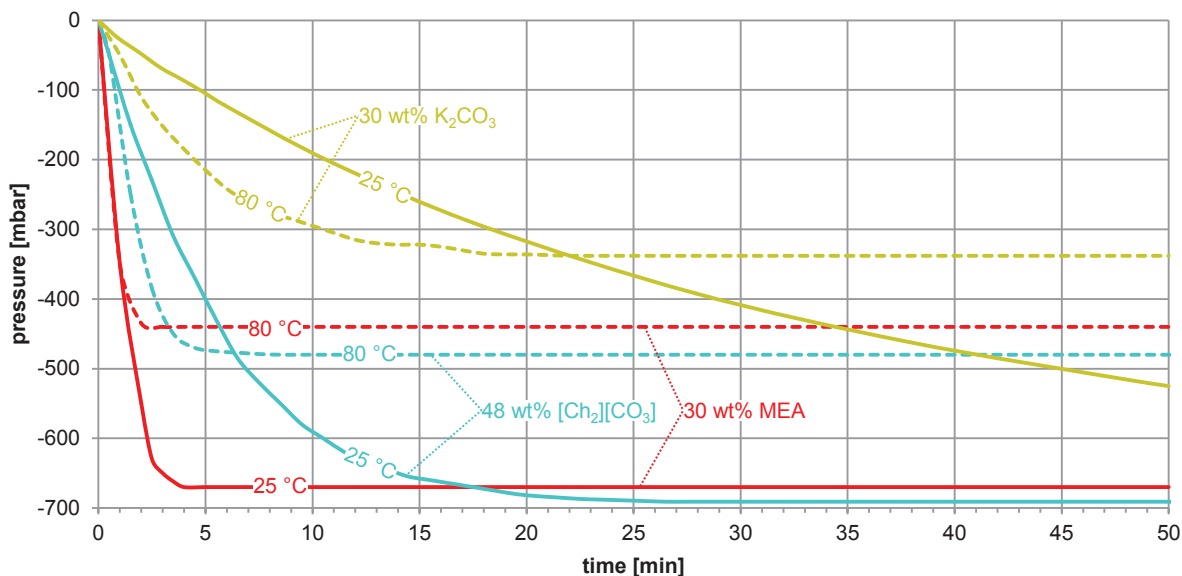
Fig. 4-17. Results of the screening experiment with 48 wt% [Ch$_2$][CO$_3$], 30 wt% K$_2$CO$_3$ and 30 wt% MEA (Wappel, 2010; Wappel, et al., 2010).

The water vapor partial pressure affects the result of measurement. The pressure due to the resulting water vapor increases negligibly at a low temperature (25 °C). The influence of the water pressure rises with increasing temperature. Solvents having higher molar water content have a higher water vapor equilibrium pressure (Wappel, 2010). The water content of the aqueous solution ionic liquid is 0.942 $mol_{H_2O}/mol_{solvent}$ (Table 4-6). The water content of 30 wt% MEA is significantly lower (0.888 $mol_{H_2O}/mol_{solvent}$). Consequently, the measurement results for 80 °C cannot be directly compared with the data of 30 wt% MEA.

Table 4-6: Molar water content of the investigated solvents.

	molar water content [$mol_{H_2O}/mol_{solvent}$]
30 wt% MEA	0.888
48 wt% [Ch$_2$][CO$_3$]	0.942
30 wt% K$_2$CO$_3$	0.947

4.3.3 Viscosity

Many ionic liquids cannot be used for CO_2 absorption because their viscosity (dependent on the combination of anion and cation) is much higher than the technical application criteria. Viscosities up to 1000 mPas at ambient temperature are not unusual. When using [Ch$_2$][CO$_3$] as an absorption solvent, the viscosity is also critical. [Ch$_2$][CO$_3$] is too viscous for use as an undiluted solvent. Therefore, it is necessary to add water to reduce the viscosity. A certain amount of water can be used for strip steam in the desorption unit. Basically it is beneficial to keep the water content as low as possible since the water has to be heated and evaporated in the desorber. This affects both operation and capital costs (Wappel, 2010). Wappel (2010) measured the dynamic viscosity of various water contents at 25 °C and 50 °C in order to select the right blend of active ionic liquid and water (Fig. 4-18).
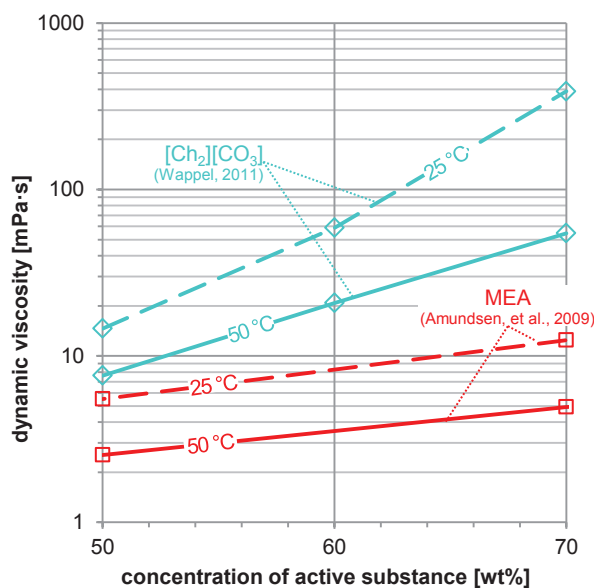
Fig. 4-18. Dynamic viscosity of aqueous [Ch$_2$][CO$_3$] and MEA in the CO$_2$ unloaded state as a function of the concentration of active substance.

The dynamic viscosity of aqueous MEA is almost independent of the MEA concentration (Fig. 4-18). In contrast, the dynamic viscosity is highly dependent on the concentration for aqueous [Ch$_2$][CO$_3$] solvents. The concentration range of 50 to 70 wt% was investigated. An increasing concentration leads to a disproportionate increase in dynamic viscosity. Based on these viscosity measurements, the [Ch$_2$][CO$_3$] content for the VLE measurements was defined as 60 wt%. This results in the fact that 60 wt% [Ch$_2$][CO$_3$] has twice the concentration of active substance compared to 30 wt% MEA. The high molecular mass of [Ch$_2$][CO$_3$] (268.34 g/mol) leads to a significant reduction of the molar concentration. For 30 wt% MEA (61.08 g/mol), the molar concentration of active substance is 4.91 mol$_{MEA}$/kg$_{solvent}$ or 0.112 mol$_{MEA}$/mol$_{solvent}$. For 60 wt% [Ch$_2$][CO$_3$], the molar concentration is only 2.23 mol$_{[Ch_2][CO_3]}$/kg$_{solvent}$ or 0.091 mol$_{[Ch_2][CO_3]}$/mol$_{solvent}$.

4.3.4 CO$_2$ solubility

The equilibrium data for the solubility of CO$_2$ in 60 wt% [Ch$_2$][CO$_3$] (shown in Fig. 4-19) for temperatures between 40 °C and 110 °C was determined by Wappel (2010). An apparatus based on the works of Austgen, et al. (1991) and Ma´mun, et al. (2007; 2005) was used. This apparatus was designed for measurements below the boiling temperature of the absorption solvent. Due to the low water content of the examined ionic liquid and the resulting high boiling temperature, equilibrium measurements up to 110 °C were carried out (Wappel, 2010).
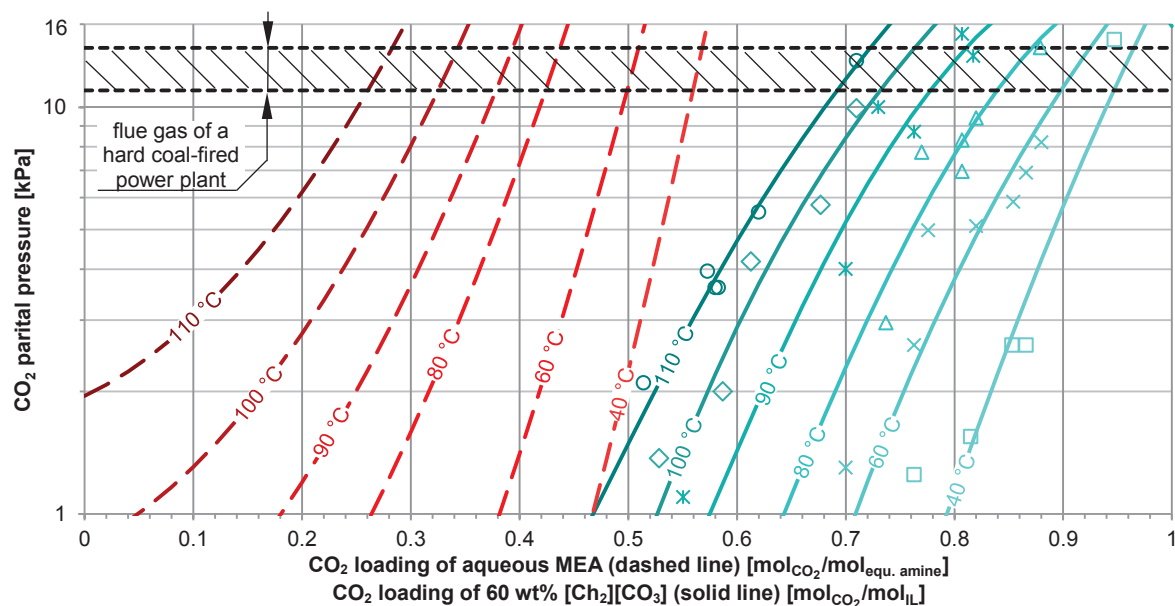
Fig. 4-19. CO_2 solubility data for 60 wt% $[Ch_2][CO_3]$ (solid line) (Wappel, 2010) and aqueous MEA (dashed line) (Xu & Rochelle, 2011). Data regressed by Xu & Rochelle (2011) hold true for 17.6 to 44.3 wt% MEA.

The equilibrium data of 60 wt% $[Ch_2][CO_3]$ and 30 wt% MEA are very different. Based on the data of Xu & Rochelle (2011), the CO_2 loading of 30 wt% MEA varies between 0.25 and 0.56 $mol_{CO_2}/mol_{equ.\ amine}$ in the temperature range of 40 and 110 °C and a CO_2 partial pressure of 10 kPa. In contrast, the CO_2 loading of 60 wt% $[Ch_2][CO_3]$ varies in the same temperature range and at the same CO_2 partial pressure between 0.65 and 0.92 mol_{CO_2}/mol_{IL}. The high CO_2 loading has no direct influence on energy consumption; however, high CO_2 loadings lead to slower absorption kinetics (Wappel, 2010).

The high molecular mass of $[Ch_2][CO_3]$ (268.34 g/mol) leads to a significant reduction of the difference of CO_2 amount within the abovementioned CO_2 loading range of 0.65 and 0.92 mol_{CO_2}/mol_{IL}. The CO_2 amount difference is only 0.6 $mol_{CO_2}/kg_{solvent}$. The CO_2 loading range for 30 wt% MEA is between 0.56 and 0.25 $mol_{CO_2}/mol_{equ.\ amine}$. The CO_2 amount difference is significantly higher (1.5 $mol_{CO_2}/kg_{solvent}$) because of the low molecular mass (61.08 g/mol) of MEA. Consequently, the solvent flow rate tends to be higher in pilot plant operation when using the ionic liquid.

Measurements of the CO_2 absorption capacity with the experimental setup as shown in Fig. 4-8 confirm the low CO_2 absorption capacity (Wappel, 2010). The absorber column was filled with ceramic packings. The column was fed with a constant flow rate of a gas with 18°% CO_2 and 72 % Ar. The gas flow rate was controlled to obtain reproducible results. The test solvent was pumped from a gas-tight bottle to the top of the column and forced downwards through the column in order to absorb CO_2 from the gas stream. The CO_2 concentration of the purified gas stream was recorded. The experiment was completed when the CO_2 capacity of the solvent was reached and CO_2 concentrations of the input and output gas stream matched.

Maximum CO_2 separation efficiency occurs when using 54 wt% $[Ch_2][CO_3]$ (used in the pilot plant studies) very quickly, similar to 30 wt% MEA (Fig. 4-20). The maximum CO_2 separation efficiency is not 100 % but only 50 % when using the ionic liquid. The CO_2 separation efficiency

drops immediately after reaching the maximal CO$_2$ separation efficiency with 54 wt% [Ch$_2$][CO$_3$]. Thereafter, the CO$_2$ separation efficiency drops continuously over the test period. The linear decrease shows that the kinetic properties are the determining factor in this experiment. The reaction rate decreases with increasing CO$_2$ loading (Aboundheir, et al., 2003), resulting in reduced CO$_2$ separation efficiency.
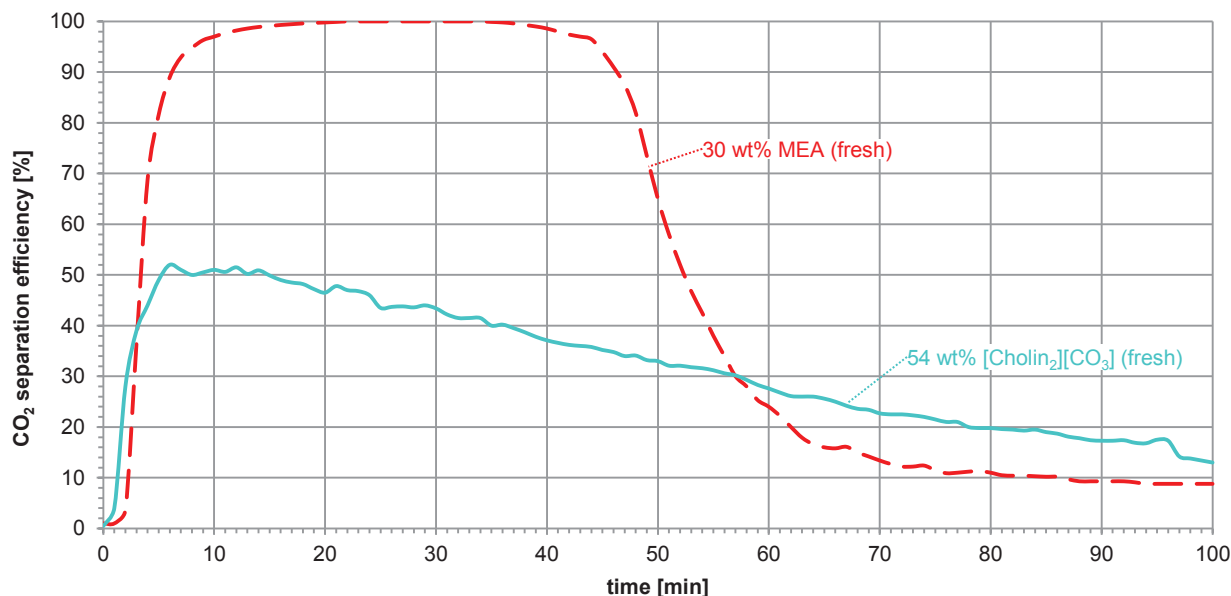
Fig. 4-20. Results of the absorption experiment with 54 wt% [Ch$_2$][CO$_3$] (solid line) and 30 wt% MEA (dashed line) (Wappel, 2010).

4.3.5 Heat of CO$_2$ absorption

The heat of CO$_2$ absorption of 60 wt% [Ch$_2$][CO$_3$] is -41.1 ±3.2 kJ/mol (Wappel, 2010). Consequently, the reaction enthalpy is half as small as that of 30 wt% MEA (-82 to -84 kJ/mol) (investigated by Carson, et al. (2000) and Kim & Svendsen (2007)).

5   Pilot plant study of CO_2 post combustion

5.1   Coal-fired power plant Dürnrohr

Because of the plebiscite results of November 5, 1978, the start-up of Austria's first nuclear power plant in Zwentendorf an der Donau was prevented. A hard coal-fired power plant was erected in the nearby village Dürnrohr in order to use the already completed power supply lines and switchgears in the transformer station. The commissioning of the power plant Dürnrohr took place in 1987. The entire plant consists of two units. The first unit (on the right side in Fig. 5-1) is operated by EVN AG and has an output of 352 MW_{el}. The second unit (on the left side in Fig. 5-1), which was operated by VERBUND Thermal Power GmbH & Co KG has been out of operation since April 2015. The electrical output of this unit was 405 MW_{el} (Smolak, 2011). Besides electrical power generation, the EVN unit of the power plant also supplies district heating for the municipal areas of St. Pölten, Zwentendorf an der Donau and Pischelsdorf (Stöger, 2011).

Fig. 5-1.   Power plant Dürnrohr.

The main fuel of the power plant is imported hard coal. The flue gas CO_2 content varied between 11.3 and 13.3 vol% (dry) for the whole measurement campaign of the present work. This wide variation can be attributed to the power plant´s various operation modes (e.g. part or full load) and different hard coal charges, which differ widely in their chemical composition, depending on the mining area. Natural gas is used as the main fuel during the start-up and shutdown procedure at the annual power plant revision, resulting in a significant drop of flue gas CO_2 content. Flue gas CO_2 contents between 6.0 and 7.3 vol% (dry) were measured during natural gas firing.

5.2 CO$_2$SEPPL pilot plant[1]

The commissioning of the pilot plant CO$_2$SEPPL, which is an acronym for CO$_2$ SEParation PLant, took place in May 2010. CO$_2$SEPPL was designed by EVN AG, ANDRITZ Energy & Environment GmbH and the Institute of Energy Systems of the Technical University Vienna. The pilot plant dimensioning is based on the operating results of the predecessor pilot plant (Section 5.3.1), which was previously in operation at the power plant site. The main difference from the predecessor pilot plant is an increase in absorber height, flue gas flow rate, and measurement instrumentation (Posch, 2012). The significant increase in absorber height enables a comparison of different solvents with widely varying physical and chemical properties. A CO$_2$ compressor unit was designed and erected for the extension of the CCS process. A list of the technical data of the CO$_2$SEPPL pilot plant is shown in Table 5-1.

The following description refers to Fig. 5-2. A detailed flow scheme of the CO$_2$SEPPL pilot plant can be seen in Appendix A.1. A slipstream of the flue gas is branched off to the pilot plant downstream to the flue gas cleaning line and the draught fan of the power plant. The flue gas, with a dust content of 10 to 15 mg/m³$_{STP}$ (dry) (Rabensteiner, et al., 2014a), passes a dust filter, where fine dust is separated. The dust content has to be reduced to 5 to 10 mg/m³$_{STP}$ (dry) for undisturbed operation over the long term (Lerche & Dreuscher, 2011). The amount of dust in the flue gas is small and the CO$_2$SEPPL pilot plant doesn´t operate continuously. Consequently, the remaining dust on the surface of the baghouse filter can be removed by pressured air. The filter was removed and cleaned during the annual power plant revision.

A downstream radial type flue gas blower increases the pressure and supplies flue gas flow rates up to 100 m³$_{STP}$/h. This corresponds to an F-factor[2] of about 2 √Pa in the absorber column. A frequency converter defines the rotational speed of the blower and the actual flue gas flow rate. The temperature of the flue gas at the absorber entry can be set through a plate heat exchanger, which is connected downstream of the blower. Cooling water, electric power, and pressurized air for the operation of the CO$_2$ capture and compression plant is supplied by the power plant. The condensate generated in the heat exchanger is separated in a phase separator next to to the flue gas cooler. A siphon at the outlet of the condensate prevents an uncontrolled discharge of flue gas at this point.

A pre-scrubber decreases the amount of sulphur oxides (SO$_x$) in order to reduce the degradation rates of chemical solvents. Pre-scrubbing is carried out with an aqueous solution of NaOH which is pumped in circuit. In order to investigate the influence of dust and sulphur oxides, the dust filter and pre-scrubber are bypassed. All measurements in the present study

---

[1] Segments of this section have already been published in Rabensteiner, et al. (2014a; 2014b; 2014c; 2014d, 2015a; 2015b; 2015d).

[2] The F-factor (F) is a parameter used to describe the gas load (gas amount) in a thermal separation apparatus, such as columns for rectification, stripping or absorption. The F-factor is dependent on the gas velocity relating to the empty cross section (u_g) and the gas density (ρ_g).

$$F = u_g \cdot \sqrt{\rho_g}$$

The gas velocity rises with increasing gas rates. Consequently, the F-factor and gas load also rise with the increasing amount of gas passed through the apparatus. The F-factor is especially relevant for the fluid-dynamic design of columns.

were performed with an upstream dust filter and pre-scrubber. The pH-value of the NaOH solution is kept in the range between 5 and 8 by the discontinuous manual addition of an aqueous solution of sodium hydroxide (50 wt%). Elevated pH-values lead to the formation of carbonate and consequently to pre-scrubber blocking (Posch, 2012). Unstructured packings in the pre-scrubber column intensify the mass transfer for SO_x absorption. The SO_2 concentration upstream of the pre-scrubber is 50 to 65 mg/m³$_{STP}$ (dry) during full load and 30 mg/m³$_{STP}$ (dry) during part load (Rabensteiner, et al., 2014a). In the pre-scrubber, the SO_x content in the flue gas is reduced to values smaller than 10 ppm (Posch, 2012). Due to the marginal amounts of sulfur oxides presented in the flue gas, regeneration of the NaOH solution is not necessary. The sump of the pre-scrubber column is equipped with a heating rod in order to prevent freezing at low ambient temperatures.
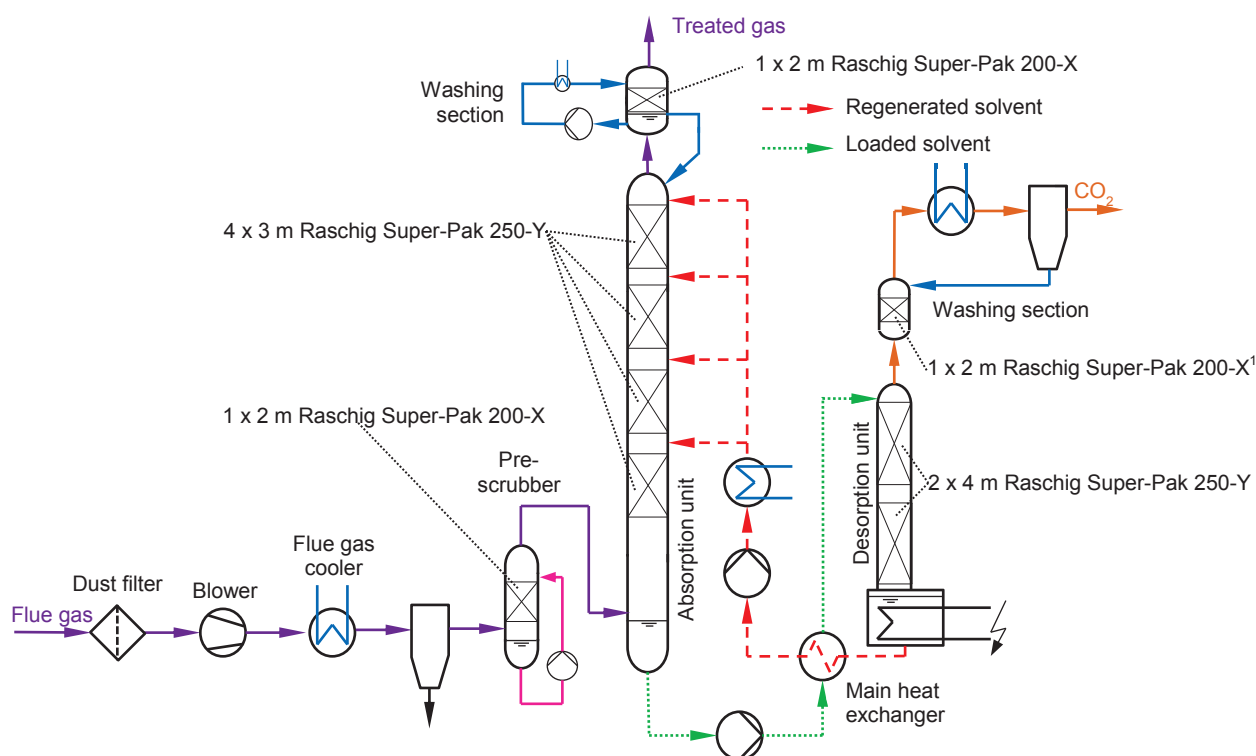
Fig. 5-2. Flow scheme of the CO₂SEPPL pilot plant (Rabensteiner, et al., 2015d).[1]

Subsequent to the pre-scrubbing unit, the saturated flue gas enters the bottom of the absorber column, where the chemical absorption of carbon dioxide takes place. An absorption solvent flows from the top of the absorber column to the bottom, counter current to the flue gas stream. The absorber consists of four sections and is equipped with structured packings in order to maximize the mass transfer by increasing the interfacial area between gaseous and liquid phase. Each section of the absorber column is 3 m high, resulting in a total packing height of 12 m. The diameter of the absorber is 0.15 m. The packings are equipped with deflectors in order to prevent an accumulation of absorption solvent at the boundary of the column (direction

---

[1] Pall rings (15 x 0.3) were used in the desorber water washing section for the tests with 30 wt% MEA, 32 wt% EDA and aqueous NaGly.

of solvent onto the packing). The effective absorber height can vary between 3, 6, 9 and 12 m by manually opening and closing the ball valves.

A number of temperature sensors are installed over the entire absorber column resulting in a high-resolution temperature profile. The temperature of the treated flue gas is measured at a height of 12 m. The lowest temperature sensor is located in the sump of the absorber column and measures the temperature of the enriched solvent (assuming that the absorber sump level is above the temperature sensor). The eleven intermediate temperature sensors measure a combination of the solvent and flue gas temperature, which is denoted as absorption temperature in the present work.

The top of the absorption unit is equipped with a water washing section. This washing section includes a demister unit, too. The water washing section prevents solvent slip, which can occur due to moderate to high vapor pressures of the used solvent. Degradation products in the treated flue gas are also trapped in this unit by means of deionized water which is pumped in circuit. The column of the water washing section is filled with unstructured packings. The treated flue gas leaving from the top of the absorber column has to be re-cooled because of the exothermic process of CO_2 absorption. Consequently, a part of the water vapor in the treated flue gas condenses and the water balance is kept closed. The water washing water circuit is equipped with a water re-cooler in order to control the flue gas temperature at the outlet of the water washing section. Excess washing water flows back to the absorber column. A deflector located at the flue gas exit prevents water entering from the atmosphere.

The CO_2 enriched solvent is collected in the absorber sump. The absorber sump is equipped with an electric heating rod in order to prevent freezing at low ambient temperatures. Overheating of the heating rod is prevented by a level indicator. The CO_2 enriched solvent is pumped through a piston driven membrane pump to the desorber column. The volume flow rate of the CO_2 enriched solvent stream is regulated by the absorber sump level. The CO_2 enriched solvent passes the main heat exchanger, where a temperature increase of the enriched solvent occurs. The regeneration of the solvent is carried out within the desorption unit. Heat must be supplied in the sump of the desorption unit to release the captured CO_2. This is realized by the electric heating rod. Overheating of the desorber heating rod is prevented by the installation of a level indicator and a bimetal switch.

The generated gaseous CO_2/H_2O mixture passes the desorption unit countercurrent to the enriched solvent from the bottom to the top. An intensive interaction between the gaseous and the liquid phase is provided by structured packings in the desorber column. The captured CO_2 is released from the enriched solvent and leaves at the top of the desorber column with the gas stream. The top of the desorber column is equipped with a washing section and a demister, similar to the absorption unit. The gaseous CO_2/H_2O mixture is re-cooled in the overhead condenser subsequent to the demister outlet of the desorption unit. The condensate produced is trapped in the phase separator. The total water balance is closed by recirculating condensate to the desorber column. A pressure retention valve keeps the pressure in the desorption unit at a constant value. The separated carbon dioxide can either be released to the atmosphere or piped to the CO_2 compression unit of the CO_2SEPPL pilot plant. The atmosphere outlet of CO_2

is erected at the very top position of the plant, in order to prevent a high carbon dioxide concentration at positions where human work is necessary.

An overview of the test facility is shown in Fig. 5-3. The CO$_2$SEPPL pilot plant is located in the large tower in the middle of the picture. The 20 m tower consists of seven levels (the first two levels are enclosed). The CO$_2$ compression unit is situated on the left side of the CO$_2$ separation plant. A description of the CO$_2$ compression unit can be found in Posch (2012).

Fig. 5-3.   Overview of the CO$_2$SEPPL pilot plant.

Pilot plant components in contact with either the absorption solvent, the flue gas, or the captured CO$_2$ stream are all made of stainless steel.

5.3 Other pilot plants[1]

Several PCC pilot are in operation at the present day. The pilot plants include test facilities on a laboratory-scale, such as the test facility in Kaiserslautern, and realistic demonstration plants, such as in Esbjerg and Niederaußem. The sections below will present pilot plants in which the same or similar solvents were tested as at the CO$_2$SEPPL pilot plant. The subsequent Section 6 will refer to the results of these studies.

The benchmark solvent 30 wt% MEA was tested in each of the following pilot plants. The investigation of novel solvents is the focus of the present research work. The measurement results with 30 wt% MEA are used as reference for these solvents. The 30 wt% MEA measurement results are also used in order to demonstrate realistic measurement conditions on the CO$_2$SEPPL pilot plant. The pilot plants on the power plants in Esbjerg and Niederaußem are also operated with real power plant flue gas. The absorber columns of these pilot plants are industrial-scale. The processed quantities of power plant flue gas are some orders of magnitudes larger than in the CO$_2$SEPPL pilot plant. Consequently, these two pilot plants are used for the comparison of the 30 wt% MEA measurement results.

---

[1] Segments of this section have already been published in Rabensteiner, et al. (2014a; 2014c; 2015a).

5.3.1 Predecessor pilot plant Dürnrohr

A minor predecessor pilot plant was operated at the Dürnrohr power plant site prior to the construction of the CO_2SEPPL pilot plant. The design of the pilot plant and measurements were carried out by a consortium of EVN AG, Austrian Energy & Environment AG (now ANDRITZ Energy & Environment GmbH) and the University of Leoben. An adapted chemical scrubber was used, which was originally designed for CO_2 removal from biogenic sources. The pilot plant was developed for the characterization of ionic liquids (Wappel, 2010). During the measurement campaign, it became apparent that the absorber column was too low for industry related measurements. The time for CO_2 absorption in the absorber column is very short. Absorption kinetics have a high influence on the measurement results. Furthermore, the repeatability of measuring points was hard to achieve due to geometric limitations (Wappel, 2010). The predecessor pilot plant was in operation from 2009 to 2010.

The following description of the predecessor pilot plant refers to Fig. 5-4. The flue gas is passed through a cartridge filter for the substantial removal of residual dust and other impurities (aerosols, salts). The pre-scrubber operates with sodium bicarbonate ($NaHCO_3$). The temperature of the flue gas at the absorber entry can be set by a heat exchanger which is integrated in the pre-scrubber. The absorber consists of two sections which are filled with random packings. The absorber is not equipped with a water washing section. Both sections of the desorber column are filled with random packings. The solvent is heated by an electrical heating rod in the desorber sump which produces the stripping steam. The water vapor of the CO_2 stream is condensed in a downstream condenser. The condensate is drained into the desorber sump. The regenerated solvent is intermediately stored in a buffer vessel for decoupling the absorption and desorption process (Wappel, 2010).

The entire facility is provided with thermal insulation to keep heat loss low and allow an energy balance. All components of the pilot plant are made of stainless steel. The pilot plant has been described in detail by Maierhofer (2010) and Ratz (2010). The technical data of the pilot plant are shown in Table 5-1.
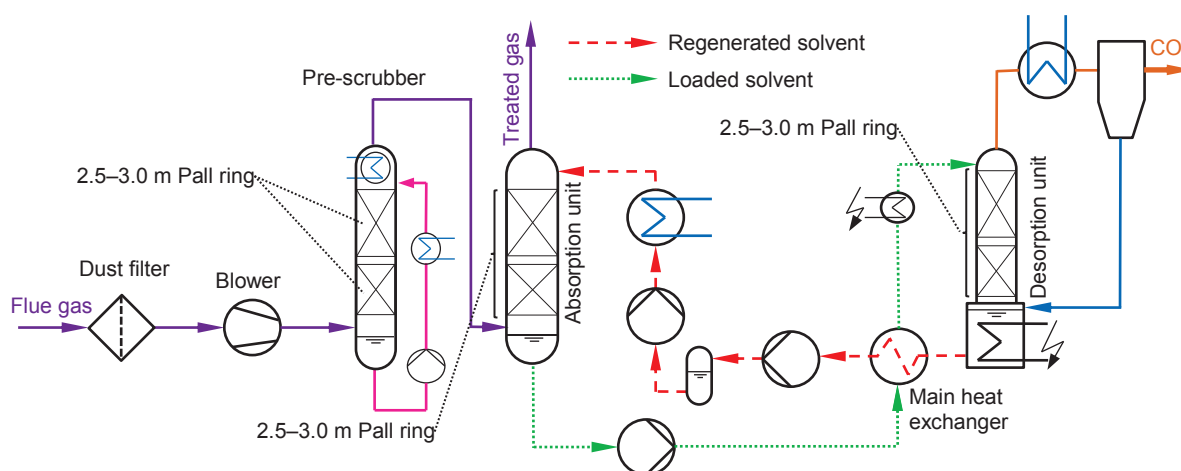
Fig. 5-4.   Flow scheme of the predecessor model (Wappel, 2010).

5.3.2 J.J. Pickle pilot plant

The University of Texas at Austin operates a PCC pilot plant in order to demonstrate the practicality of novel solvents and configurations. The pilot plant is located at the J.J. Pickle Research Center in North Austin (USA). The flue gas is artificially produced by mixing ambient air and CO_2. The separated CO_2 stream is recycled. The dimensions of the pilot plant are described precisely in Dugas (2006). The maximum flue gas flow rate is approximately 1060 m^3_{STP}/h. Consequently, this pilot plant can process about ten times higher flue gas flow rate than the CO_2SEPPL pilot plant in Dürnrohr. Table 5-1 lists the technical data of the J.J. Pickle pilot plant.

Three measurement series were carried out with 8 m PIP (40.8 wt% PIP) (Plaza, 2011; Van Wagener, 2009). The absorber of the pilot plant was equipped with an intercooler after the first measurement series. The desorber was replaced by a two-stage flash in the second stage of expansion. The measurement results of the first measurement series can be compared with the results of the test campaign on the CO_2SEPPL pilot plant. 14 measurement points were recorded in this measurement series. Closing the mass and energy balance was impossible at this early stage of investigation (Van Wagener, 2009). The heat loss to the environment of the desorber is enormous (Table 5-1). The high desorber energy loss is deducted by the calculation of the specific energy for solvent regeneration in Fig. 6-8. The energy demand for solvent regeneration increases by an average of 0.9 GJ/t_{CO_2} if the desorber energy loss is not considered. A comparison of the measurement results is only partially possible based on these facts.

5.3.3 Tarong pilot plant

Hard coal is used as fuel in the Tarong power plant in Nanango, Australia, resulting in similar flue gas CO_2 contents as in the CO_2SEPPL power plant in Dürnrohr. The pilot plant separated approximately 100 kg of carbon dioxide per hour, resulting in a flue gas flow rate of about 580 m^3_{STP}/h (Cottrell, et al., 2013). Important technical data are listed in Table 5-1.

CSIRO (Commonwealth Scientific and Industrial Research Organisation) investigated 8 m PIP (40.8 wt% PIP) in this pilot plant. The tests with aqueous piperazine were carried out after an investigation of the benchmark solvent, 30 wt% MEA. The pilot plant components were reconstructed for experiments with aqueous piperazine. The packings in the columns have been replaced because of the higher viscosity of piperazine-based solutions. The gasket materials were exchanged due to the higher temperatures of the process when carried out with concentrated piperazine. The absorber was equipped with an intercooler in order to achieve higher CO$_2$ loadings of the enriched solvent. A larger main heat exchanger was installed due to the lower heat transfer coefficients (α)[1] of the more viscous piperazine-based solvents (Cottrell, et al., 2013).

5.3.4 Esbjerg pilot plant

The Esbjerg power plant used hard coal as main fuel for electric power generation. The CO$_2$ content of the flue gas is in the same order of magnitude as at the CO$_2$SEPPL pilot plant. The pilot plant separates 1 ton of CO$_2$ per hour. The absorber is operated at a pressure slightly below atmospheric pressure because the fan is placed downstream from the absorber. The pilot plant has no pre-scrubber or dust filter (Knudsen, et al., 2009; 2007). Important technical data are listed in Table 5-1.

Results for 32 wt% EDA and 28/17 wt% AMP/PIP on the Esbjerg pilot plant were published by Tönnis, et al. (2011) and Knudsen, et al. (2011). Extended measurements with an inter-stage cooling system in the absorber and a lean vapor re-compression cycle have also been carried out. The impact of such modifications have been discussed in general in literature (Plaza, et al., 2009; Reddy, et al., 2008). This pilot plant is used as a reference plant for the comparison of measurement results of the benchmark solvent 30 wt% MEA because of the industrial dimensions and the use of real power plant flue gas.

5.3.5 Kaiserslautern pilot plant

The pilot plant at the University of Kaiserslautern operates with flue gas produced by a natural gas burner. The CO$_2$ content of the flue gas can be set between 3 and 14 vol% (dry) by recirculating the separated CO$_2$. The time available to absorb the CO$_2$ is significantly limited because of the small height of the absorber column of 4.25 m. CO$_2$ absorption kinetics heavily

---

[1] The dependence the heat transfer coefficient (α) on the solvent viscosity will be explained briefly in the following section. The heat transfer coefficient yields to

$$\alpha = \frac{\lambda \cdot Nu}{d_h}.$$

The Nusselt number (Nu) is a function of the Reynold (Re) and Prandtl number (Pr). Nu rises with increasing Re or Pr. Empirical formulas for calculating Nu and the hydraulic diameter of the main heat exchanger (d_h) can be found in corresponding literature. Both, Re and Pr are dependent on the viscosity. Re decreases with increasing viscosity η. The opposite is true for Pr.

$$Re = \frac{\rho \cdot u \cdot d_h}{\eta}$$

$$Pr = \frac{\eta \cdot c_p}{\lambda}$$

With increasing viscosity η the Nusselt number drops because Nu is higher order influenced by Re.

influence the performance of the pilot plant. Only solvents with similar CO_2 absorption kinetics may be compared in order to neglect this influence (Mangalapally & Hasse, 2011a; 2011b). A comparison of the technical data with the other test facilities is shown in Table 5-1.

The influence of mass transfer and absorption kinetics on the results can be studied directly in the pilot plant. The flue gas flow rate was varied while the other parameters were kept constant for this purpose. A low flue gas flow rate leads to a low mass flow rate of captured CO_2. The amount of CO_2, which has to be transferred per time through the interfacial area decreases. Consequently, a lowering of the flue gas flow rate has similar effects to an increase in the column height at a constant flue gas flow rate (Mangalapally & Hasse, 2011b).

The Kaiserslautern pilot plant is operated in the same way as the pilot plant in Esbjerg within the scope of the EU-project CESAR. Preliminary studies in Kaiserslautern for pilot plant tests in Esbjerg were conducted with 32 wt% EDA and 28/17 wt% AMP/PIP (Mangalapally & Hasse, 2011a; 2011b; Tönnis, et al., 2011).

5.3.6 Staudinger pilot plant

In 2009, Siemens AG and E.ON SE erected a PCC pilot plant at the hard coal-fired power plant Staudinger, near Großkrotzenburg, in the federal state Hessen. This pilot plant is characterized by an enormous absorber column height (Siemens AG, 2009). The pilot plant has no pre-scrubber. Flue gas cooling takes place by circulating water. The flue gas cooler can also be operated with potassium hydroxide for SO_x reduction. A small slipstream of the regenerated solvent is taken for reclaiming (Horn, et al., 2014). The pilot plant operates without an absorber or desorber washing section. The water balance of the entire system is kept closed by adding water. Table 5-1 lists the most important technical data of the pilot plant.

An aqueous solution of potassium salt of undisclosed amino acid enables a reduction of energy requirements of up to 2.7 GJ/t_{CO_2} according to Schneider & Schramm (2011). Further additives cannot be excluded according to Siemens AG (2011). However, it is not explicitly stated whether the value was measured at the Staudinger pilot plant.

5.3.7 Niederaußem pilot plant

The commissioning of this pilot plant at the lignite-fired power plant in Niederaußem took place in 2009. The plant was developed by RWE Power AG, BASF SE and Linde AG. The flue gas slipstream out of the power plant process amounts to 1550 m^3_{STP}/h. The absorber column is equipped with 24 m structured packings. This corresponds to a commercial plant (Schmidt & Moser, 2013). The absorber is equipped with an intercooler. The intercooler can be operated at different absorber heights. This means that the solvent can be extracted, cooled, and recycled at several levels. Table 5-1 lists the most important technical data of the pilot plant.

This pilot plant is used as a reference plant for the comparison of measurement results of the benchmark solvent 30 wt% MEA because of its industrial dimensions and the use of real power plant flue gas.

5.4 Listing of technical data

The pilot plants have to be compared in order to draw scientific inferences from the measurement results. Table 5-1 lists the most important technical data of all pilot plants considered.

Table 5-1a: Comparison of PCC pilot plants.

	CO$_2$ SEPPL pilot plant Dürnrohr/AUT	Predecessor pilot plant Dürnrohr Dürnrohr/AUT	J.J. Pickle pilot plant Austin/USA	Tarong pilot plant Nanango/AUS
		(Maierhofer, 2010; Ratz, 2010; Wappel, 2010)	(Dugas, 2006; Plaza, 2011; Van Wagener, 2009)	(Cottrell, et al., 2013; Cousins, et al., 2012; 2010; Saimpert, et al., 2013)
			Image source: (Plaza, 2011)	Image source: (Cottrell, 2012)
Initial operation	2010	2009	2006	2010
Tested absorption solvents		▪ 30 wt% MEA ▪ 48 wt% [Ch$_2$][CO$_3$]	▪ 30 wt% MEA ▪ 40.8 wt% PIP	▪ 30 wt% MEA ▪ 40.8 wt% PIP
General information				
Main fuel/flue gas source	Hard coal (natural gas)	Hard coal (natural gas)	Air/CO$_2$ + recycled CO$_2$	Hard coal
Flue gas CO$_2$ content [vol% (dry)]	11.3 - 13.3 (6.0 - 7.3)	11.3 - 13.3 (6.0 - 7.3)	12.0[1]	9.8 – 13.0[2]
Maximal flue gas flow rate [m³$_{STP}$/h]	100	42	1060[3]	~ 580[4]
└ Maximal F-factor [√Pa]	└ 2.00	└ 0.80	└ 2.59	└ 2.12
Heat loss of the pilot plant [kW]	0.9 (absorber) 1.2 (desorber)	-	12.1 - 32.3 (desorber)	-
Heat loss with respect to the maximal flue gas flow rate [kJ/m³$_{STP}$]	32 (absorber) 43 (desorber)	-	41 - 110 (desorber)	-
Main heat exchanger pinch temp.[5] [K]	5 - 6	-	-	-
Absorber				
Inner diameter [mm]	150	150	427	350
Total height of packing [m]	12.00	2.50 - 3.00	6.10	7.00
Type of packing	Raschig Super-Pak 250-Y	Pall rings	Sulzer Mellapak™ 2X[6]	Sulzer Mellapak™ 250.X
Desorber				
Maximal pressure [bar$_{abs}$]	3.0	-	-	-
Inner diameter [mm]	100	100	427	250
Total height of packing [m]	8.00	2.50 - 3.00	6.10	7.00
Type of packing	Raschig Super-Pak 250-Y	Pall rings	-	Sulzer Mellapak™ 350.X
Pre-scrubber		unavailable		
Total height of packing [m]	2.00	2.50 - 3.00	-	2.70
Type of packing	Raschig Super-Pak 200-X	Pall rings	-	25 mm pall rings
Washing section absorber		unavailable	unavailable	
Total height of packing [m]	2.00	-	-	1.56
Type of packing	Raschig Super-Pak 200-X	-	-	Sulzer Mellapak™ 250.X
Washing section desorber		unavailable	unavailable	
Total height of packing [m]	2.00	-	-	1.12
Type of packing	Raschig Super-Pak 200-X[1]	-	-	Sulzer Mellapak™ 350.X

---

[1] No information exists whether the water content is considered.
[2] Measured in previous MEA-experiments (Cousins, et al., 2012).
[3] Highest measured flue gas flow rate of Plaza (2011).
[4] No information available → Calculation by the captured CO$_2$ stream.
[5] Measured for 30 wt% MEA.
[6] The absorber column is equipped with 6.1 m of Sulzer Mellapak™ 250.Y according to Van Wagener (2009). The present work used the data from Plaza (2011) because of the explicit specification of the used packings for the PIP-tests.

Table 5-1b: Comparison of PCC pilot plants.

	Esbjerg pilot plant	Kaiserslautern pilot plant	Staudinger pilot plant	Niederaußem pilot plant
	Esbjerg/DK	Kaiserslautern/DE	Großkrotzenburg/DE	Niederaußem/DE
	(Knudsen, et al., 2011; 2009; 2007)	(Notz, et al., 2011; Mangalapally & Hasse, 2011a; 2011b)	(Horn, et al., 2014; Schneider & Schramm, 2011; Siemens AG, 2009)	(Schmidt, 2014; Schmidt & Moser, 2013)
	Image source: (Knudsen & Jensen, 2009)	Image source: (Mangalapally & Hasse, 2011a)	Image source: (Siemens AG, 2014)	Image source: (Schmidt, 2014)
Initial operation	2005	2010	2009	2009
Tested absorption solvents	▪ 30 wt% MEA ▪ 32 wt% EDA ▪ 28/17 wt% AMP/PIP	▪ 30 wt% MEA ▪ 32 wt% EDA ▪ 28/17 wt% AMP/PIP	▪ potassium salt of undisclosed amino acid	▪ 30 wt% MEA
General information				
Main fuel/flue gas source	Hard coal	Natural gas + recycled CO_2	Hard coal	Lignite coal
Flue gas CO_2 content [vol% (dry)]	12.4[2]	3.0 – 14.0	11.6 - 14.3	13.5 - 15.5
Maximal flue gas flow rate [m³$_{STP}$/h]	5000	65[3]	230	1550
└ Maximal F-factor [√Pa]	└ 1.75	└ 2.10	└ 2.58	└ 1.74
Heat loss of the pilot plant [kW]	60[2]	1.3 - 1.5	2.4	-
Heat loss with respect to the maximal flue gas flow rate [kJ/m³$_{STP}$]	43	72 - 83	38	-
Main heat exchanger pinch temp.[4] [K]	7 - 8	3 - 6	-	-
Absorber				
Inner diameter [mm]	1100	125	200	610
Total height of packing [m]	17.00	4.25	25.00[5]	24.00
Type of packing	Sulzer Mellapak™ 250.X	Sulzer BX 500	unkn. structured packing	Sulzer Mellapak™ 250.Y
Desorber				
Maximal pressure [bar$_{abs}$]	3.0	2.5	3.0	-
Inner diameter [mm]	1100	125	150	457
Total height of packing [m]	10	2.55	15	-
Type of packing	Koch-Glitsch IMTP® #50	Sulzer BX 500	unkn. structured packing	Sulzer IR #40
Pre-scrubber	unavailable			
Total height of packing [m]	-	0.84	2.60[6]	-
Type of packing	-	Sulzer Mellapak™ 250.Y	unkn. structured packing	-
Washing section absorber			unavailable	
Total height of packing [m]	3.00	0.42	-	
Type of packing	Sulzer Mellapak™ 250.Y	Sulzer Mellapak™ 250.Y	-	Sulzer Mellapak™ 250.Y
Washing section desorber			unavailable	unavailable[7]
Total height of packing [m]	3.00	0.42	-	-
Type of packing	Koch-Glitsch IMTP® #50	Sulzer Mellapak™ 250.Y	-	-

[1] Pall rings (15 x 0.3) were used for the tests with 30 wt% MEA, 32 wt% EDA and aqueous NaGly.
[2] Average value of a 550 h-test (min: 9.3 vol% (dry), max: 13.9 vol% (dry)).
[3] Conversion in the present work.
[4] Measured for 30 wt% MEA.
[5] An absorber column height of 35 m is stated in Siemens AG (2009).
[6] The flue gas cooler can operate as pre-scrubber with an aqueous potassium hydroxide solution.
[7] A backwash tray is installed.

Heat losses of the entire system must be considered in order to compare the measurement results from the various test facilities. The heat loss of the CO$_2$SEPPL pilot plant is about 2.1 kW. This corresponds to about 20 % of the power which is supplied in the desorber sump by the electrical heating rod. The heat loss of the entire CO$_2$SEPPL pilot plant with respect to the maximal flue gas flow rate is about 75 kJ/m$^3_{STP}$. The Kaiserslautern pilot plant has a similar heat loss with respect to the maximal flue gas flow rate. The entire heat loss of the Esbjerg and Staudinger pilot plants can be reduced to 43 or 38 kJ/m$^3_{STP}$ due the magnitude effect of these highly insulated larger pilot plants. The heat losses of the remaining pilot plants are unknown.

The achievable pinch temperature of the main heat exchanger strongly influences system performance. An increase in efficiency is possible, especially at a high solvent flow rate through better heat transfer in the main heat exchanger[1] (Knudsen, et al., 2007). The pinch temperature of the main heat exchanger is also dependent on the solvent used. The heat transfer coefficient is dependent on the thermal conductivity λ and the dynamic viscosity η of the solvent as can be seen in the footnote on page 60. The indicated pinch temperatures of the main heat exchangers in Table 5-1 are measured during operation with 30 wt% MEA. The pinch temperature can rise when using more viscous solvents, such as aqueous piperazine. The main heat exchangers of the CO$_2$SEPPL and Kaiserslautern pilot plants have similar pinch temperatures. The pinch temperature of the main heat exchanger at the Esbjerg pilot plant is slightly higher (compare Table 5-1). Pinch temperatures of the remaining pilot plants are unknown.

5.5 Comparison of the absorber columns

The design of the absorber column is very important for the performance of the entire pilot plant. Mass transfer efficiency is related to intimate contact and rate transfer between liquid and vapor phase in packed columns. The $HETP$-value (height equivalent to one theoretical plate) is widely used concept to evaluate the height of a packed column (Mendes, 2011), defined by Eq. 5-1.

$$Z = HETP \cdot N$$ **Eq. 5-1**

Z is the height of the packed column necessary to obtain a separation equivalent to N theoretical separation plates (Caldas & Lacerda, 1988). The $HETP$-value represents the real height of one theoretical stage. A strong practical background is required to convert from

---

[1] The dependence of the heat transfer coefficient (α) on the solvent flow rate will be explained briefly in the following section. The heat transfer coefficient yields to

$$\alpha = \frac{\lambda \cdot Nu}{d_h}.$$

The main heat exchanger in the CO$_2$SEPPL pilot plant is a plate heat exchanger. The Nusselt number (Nu) for calculating the heat transfer coefficient on each side of the plate can be obtained approximately from (Lévêque, 1928; VDI, 2006)

$$Nu = 1.615 \cdot \left(\frac{\xi \cdot Re}{64} \cdot Re \cdot Pr \cdot \frac{d_h}{L} \right)^{1/3}.$$

Empirical formulae for the calculation of the pressure loss coefficient ξ of the plate heat exchangers can be found in VDI (2006). L is the length between two points of intersection (VDI, 2006). The Reynolds number Re is dependent on the solvent velocity.

$$Re = \frac{\rho \cdot u \cdot d_h}{\eta}$$

Consequently, α rises with increasing solvent flow rate.

theoretical stages to real dimensions for packed columns. Unfortunately, there are only a few generalized methods available in the open literature for estimating the $HETP$-value. These methods are empirical and supported by the packing vendors (Mendes, 2011).

Table 5-2 lists all relevant data for the comparison of absorber columns. Data about the packings were taken from Sulzer AG (2015) and Raschig GmbH (2015). Although the $HETP$-value is dependent on various operation parameters such as column pressure and reflux ratio[1], it can be used as reference value. The maximal flue gas flow rate of the CO$_2$SEPPL pilot plant is 120 m³/h, which corresponds to an F-factor of 2 √Pa. The HETP value of the Raschig Super-Pak 250-Y used is about 0.25 m at this point. Consequently, there are 35.3 theoretical separation plates in the 12 m high absorber column. A comparison with the other absorber columns considered indicates that the CO$_2$SEPPL pilot plant is one of the plants with the highest separation efficiency (Table 5-2).

Table 5-2. Comparison of the absorber columns.

	Total height of absorber column packing [m]	Type of packing[2]	Max. F-factor [√Pa]	$HETP$ at the max. F-factor [m]	Pressure loss per height at the max. F-factor [mbar/m]	Number of theoretical separation plates at the max. F-factor [-]	Pressure loss across the entire absorber column at the max. F-factor [mbar]
CO$_2$SEPPL pilot plant	12.00	Raschig Super-Pak 250-Y	2.00	0.34	1.20	35.3	14.4
Predecessor pilot plant Dümrohr	2.50 - 3.00	Pall rings	0.80	-	-	-	-
J.J. Pickle pilot plant	6.10	Sulzer Mellapak™ 2X[3]	2.59	0.66	0.85	9.4	5.0
Tarong pilot plant	7.00	Sulzer Mellapak™ 250.X	2.12	0.49	0.60	14.3	4.2
Esbjerg pilot plant	17.00	Sulzer Mellapak™ 250.X	1.75	0.49	0.38	34.7	6.5
Kaiserslautern pilot plant	4.25	Sulzer BX 500	2.10	0.25	1.90	17.0	8.1
Staudinger pilot plant	25.00	unkn. structured packing	2.58	-	-	-	-
Niederaußem pilot plant	24.00	Sulzer Mellapak™ 250.Y	1.74	0.38	1.00	63.2	24.0

The calculated pressure loss of 14.4 mbar across the entire absorber column is lower than the pressure loss measured on the CO$_2$SEPPL pilot plant. The reason for this is, inter alia, the higher operating volume flow rate in the absorber column. The operating volume flow rate, which was used for calculation of the F-factor in Table 5-2, is measured at the entrance of the absorber column. The flue gas at this point has a temperature of around 40 °C in the standard case. The temperature of the flue gas rises in the absorber column through the released CO$_2$ absorption heat. Consequently, the real actual flue gas flow rate is significantly higher. A higher F-factor leads to an increase in pressure loss. The reflux flow from the top to the bottom of the absorber column and the solvent used also influence pressure loss.

---

[1] Structure packings produced by Sulzer AG: 960 mbar head pressure (Sulzer AG, 2015)
Structured packings produced by Raschig GmbH: 330 mbar head pressure, cyclohexane/n-Heptane-system, 0.43 m SRP column, 3.05 m bed (Raschig GmbH, 2015).
[2] Structured packings, which have included "Y" in their names, have a nominal inclination angle of 45°. They are the most widely used in new installations. Structured packings, indicated with "X", have a nominal inclination angle of 60° from horizontal and are used where high capacity and low pressure drop are the foremost requirements for a specific application. The "X" packings provide a lower pressure drop per theoretical stage compared to the same size "Y" packing (Koch-Glitsch, 2015).
[3] The absorber column is equipped with 6.1 m of Sulzer Mellapak™ 250.Y according to Van Wagener (2009). The present work used the data from Plaza (2011) because of the explicit specification of the used packings for the PIP-tests.

The absorber column height of the Kaiserslautern pilot plant is only 4.25 m. Structured packings with a high separation efficiency (small $HETP$-value) are used in order to obtain a corresponding number of theoretical separation plates. Consequently, the absorber column of the Kaiserslautern pilot plant has 17 theoretical separation plates. A low $HETP$-value inevitably leads to a high pressure loss across the absorber column. The pressure loss across the absorber column of the Kaiserslautern pilot plant is thus comparatively high. The absorber columns of the J.J. Pickle and Tarong pilot plant have also a smaller number of theoretical separation plates than the CO$_2$SEPPL pilot plant. The Esbjerg pilot plant has a similar number of theoretical separation plates than the CO$_2$SEPPL pilot plant. The absorber column of the Niederaußem pilot plant has by far the highest number of theoretical separation plates. A comparison of the absorber columns of the predecessor pilot plant in Dürnrohr and the Staudinger pilot plant is impossible because their structured or random packings are unknown.

6 Parameter study

6.1 Measurement matrix[1]

CO_2SEPPL is a highly flexible pilot plant, which makes it possible to adjust many of the operating parameters. A measurement matrix was developed to determine the optimum operating point of the solvent and to investigate process behavior under varying operating conditions. The varying operating parameters are:

- Solvent flow rate, or in other words, liquid to gas ratio (L/G-ratio)
- Flue gas flow rate
- Desorber pressure
- Flue gas CO_2 content[2]
- Absorber height
- Regenerated solvent temperature
- Flue gas temperature
- CO_2 separation efficiency

A detailed parameter study was applied to the measurement matrix. One operating parameter is changed while the others are kept constant. A reference case has to be established in order to carry out the measurement campaign. The operating parameters of the reference case are listed in Table 6-1. The reference absorber height is set to 12 m in order to match industry-related conditions. The reference flue gas carbon dioxide content is determined by the combustion of hard coal. Other values are default values from literature.

Table 6-1:   Reference parameters of the test campaigns.

Process variable	Reference value
Desorber pressure [bar$_{abs}$]	2
Flue gas carbon dioxide content [vol% (dry)]	11.3 - 13.3[3]
Absorber height [m]	12
Regenerated solvent temperature [°C]	40
Flue gas temperature [°C]	40
CO_2 separation efficiency [%]	90

The flue gas and solvent flow rate have to be determined for the completion of the reference case. Two series of measurements were carried out before the pre-investigation was completed. In order to determine the approximate location of the optimal L/G-ratio, the reference values (Table 6-1) were set, with the exception of the CO_2 separation efficiency. System-specific values were set for the flue gas flow rate and the desorber heating rod power. The CO_2 separation efficiency was recorded by varying solvent flow rate. The location of the optimal operating point is recognizable by the highest CO_2 separation efficiency. The highest concentration of measurement points will be carried out in the parameter study (compare Section 6.3) in the range of the optimal L/G-ratio.

---

[1] Segments of this section have already been published in Rabensteiner, et al. (2014b).
[2] Operation with flue gas from a hard coal-fired boiler is the reference case. Experiments with flue gas from a natural gas-fired boiler are limited in time.
[3] Determined by the operating mode of the hard coal-fired power plant.

This first measurement series will be explained with an example using 25 wt% NaGly. A high flue gas flow rate of 90 m³/h was set. The desorber heating rod power is 15 kW (Fig. 6-1a). There was a steady increase in the CO_2 separation efficiency up to the maximum L/G-ratio of 5 l/m³. Setting a higher L/G-ratio has not been possible because the L/G-ratio is limited by the performance of the pump. The flue gas flow rate was reduced to 70 m³/h in order to increase the L/G-ratio up to 7 l/m³. The CO_2 separation efficiency continued to increase due to the increased L/G-ratio. A further reduction of the volume flow rate, to 50 m³/h, resulted in full CO_2 separation (100 % CO_2 separation efficiency, not indicated in Fig. 6-1a). This makes detection of the optimum L/G-ratio impossible. The heating power of the heating rod was consequently reduced to 11.25 kW. An optimum L/G-ratio of about 7 l/m³ is visible with these settings.

The previously optimum L/G-ratio of 7 l/m³ was set for the second fast test series (Fig. 6-1b) to determine the optimal flue gas flow rate. The heating power of the desorber heating rod was set to 11.25 kW. The optimum flue gas flow rate was determined by varying the flue gas flow rate and recording the specific energy necessary for solvent regeneration. An increase of the flue gas flow rate from 30 to 50 m³/h leads to a strong decrease in energy demand. Only small energy savings are apparent at higher flue gas flow rates. In order to carry out experiments with L/G-ratios larger than 7 l/m³, the reference case was set to 50 m³/h.
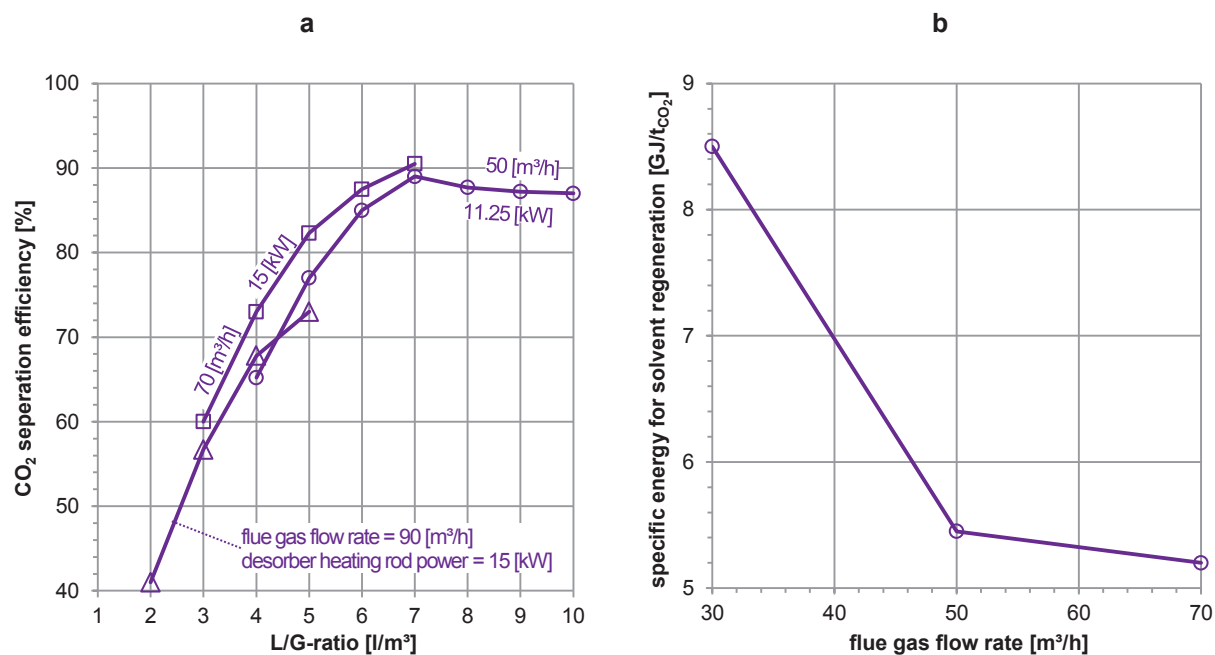
Fig. 6-1:   Fast test series for localization of the optimal L/G-ratio **(a)** and flue gas flow rate **(b)** (example for 25 wt NaGly).

Table 6-2 lists all reference values of L/G-ratios and flue gas flow rates of the measurement campaigns for all solvents investigated. Amine-based solvents and aqueous solutions of amino acids were tested in the CO_2SEPPL pilot plant. Table 6-2 also indicates the concentration of the solvents tested. The flue gas flow rate is significantly higher when using amine-based solvents. The flue gas flow rate of the process with amino acids had to be reduced to 50 m³/h because of the high specific energy for solvent regeneration.

Table 6-2:   Reference values of L/G-ratio and flue gas flow rate.

	Amine-based solvents				Amino acids			
	MEA	**EDA**	**PIP**	**AMP/PIP**	**NaGly**			**KGly**
	(Rabensteiner, et al., 2015a)	(Rabensteiner, et al., 2014c)	(Rabensteiner, et al., 2015a)		(Rabensteiner, et al., 2014b)			(Rabensteiner, et al., 2015c)
Concentration of active substance [wt%]	30	32	37.6	28/17	15	25	40	40
└ [molal]	└ 7.0	└ 7.8	└ 7.0	└ 4.4/2.4	└ 1.8	└ 3.4	└ 6.9	└ 5.9
L/G-ratio[1] [l/m³]	3.20	2.50	2.50	2.25	-[2]	8.00	8.00	9.00
Flue gas flow rate [m³/h]	90	90[3]	100	100	50	50	50	50
└ F-factor [√Pa]	└ 1.50	└ 1.50	└ 1.65	└ 1.65	└ 0.84	└ 0.84	└ 0.84	└ 0.84

6.2 Evidence of realistic measurement conditions

The CO_2SEPPL pilot plant is not a laboratory test facility. The step to full-scale plants is still extremely large. Such systems are much more complicated in their construction and operation. Moreover, the integration into the power plant process is extremely important. Producing realistic measurement results can contribute greatly to the design of full-scale plants.

6.2.1 Realistic measurement conditions at the CO_2SEPPL pilot plant

Realistic measurement conditions on the CO_2SEPPL pilot plant are ensured by the:

- Use of real flue gas out of the power plant process
- Nearly industrial heights of the absorber and desorber columns
- Closed CO_2 balance
- Closed energy balance.

Flue gas is taken directly from the hard coal-fired power plant in Dürnrohr. The influence of typical by-products of coal combustion on the PCC process can be observed. The content of dust, soot and other particles in the flue gas can be reduced by an upstream dust filter. A pre-scrubber for SO_x reduction enables a further application of the CO_2SEPPL pilot plant.

The influence of kinetics and mass transfer on the PCC process can be reduced by the almost industrial-scale of the absorber column. The height of the absorber column determines the contact time of the gaseous and liquid phase. The CO_2SEPPL absorber column is 12 m high. This is an above average absorber column height in comparison to other PCC pilot plants. Pilot plants with shorter absorber columns (i.e. Kaiserslautern pilot plant) produce measurement results which can lead to misunderstandings regarding the process performance. The absorber column of the CO_2SEPPL pilot plant has 35 theoretical separation plates when setting maximal flue gas flow rate (120 m³/h). This value is also higher than average in comparison to other pilot plants (compare Table 5-2). High quality steel must be used for column construction in order to counteract the corrosive effect of several solvents. High absorber columns are therefore

---

[1] The L/G-ratio values of this table were taken from the test series, carried out in Section 6.3, where the minimum specific energy for solvent regeneration occurs. The preliminary studies serve only to find the approximate location of the optimum L/G-ratio.

[2] The excessive solvent flow rate for reaching the optimal operating point could not be provided.

[3] 110 m³/h (F-factor = 1.84 √Pa) was used for the investigation with flue gas of a natural gas-fired boiler.

associated with enormous investment costs. Whether or not extremely high absorber columns (as the Staudinger and Niederaußem pilot plant) are economically viable is an urgent question in the pursuit of making the operation of solvents with low kinetics feasible.

Determining the separated CO_2 stream is essential for the calculation of the specific energy for solvent regeneration. The balancing by CO_2 concentration and the volume flow rate measurement of incoming and exiting flue gas streams can be carried out during pilot plant operation. Balancing above the solvent stream occurs through CO_2 loading measurement of the CO_2 enriched and regenerated solvent in the laboratory. The separated amount of CO_2 can be thus determined by measuring solvent flow rate and CO_2 loading difference. The calculations via the solvent and flue gas stream provided the same results.

The specific energy for solvent regeneration used in the present work refers to the separated amount of carbon dioxide and regeneration energy (GJ/t_{CO_2}). The regeneration energy is supplied by an electrical heating rod in the desorber sump. Heat losses are small and known by energy balancing due to the complete thermal insulation of pilot plant components. Unlike pilot plants with high heat losses, as for instance the J.J. Pickle pilot plant, heat losses are not deducted when calculating the specific energy for solvent regeneration.

6.2.2 Comparison of measurement results with 30 wt% MEA[1]

The evidence of realistic measurement conditions on the CO_2SEPPL pilot plant is made possible by the comparison of measurement results with the benchmark solvent 30 wt% MEA. The much larger demonstration plants in Esbjerg and Niederaußem are used as reference. These pilot plants also take the flue gas out of the power plant process. Descriptions of these pilot plants can be found in Sections 5.3.4 and 5.3.7, respectively. Important technical data from these pilot plants are listed in Table 5-1. These pilot plants are much larger than the CO_2SEPPL pilot plant and can handle several thousand cubic meters of flue gas per hour. The operating parameters of these two pilot plants are listed in Table 6-3. The specific energy for solvent regeneration is recorded as a function of the L/G-ratio which is the most decisive operating parameter. Basic considerations about this measurement series can be found in Section 6.3.1.

Table 6-3:   Operating parameters of the 30 wt% MEA tests.

	CO_2SEPPL pilot plant (Rabensteiner, et al., 2014a)	Esbjerg pilot plant (Knudsen, et al., 2007)	Niederaußem pilot plant (Schmidt & Moser, 2013)
Flue gas flow rate [m³/h$_{STP}$]	84	5000	1550
└ F-factor [√Pa]	└ 1.50	└ 1.75	└ 1.40
Desorber pressure [bar$_{abs}$]	2.00	1.85	1.75
Flue gas CO_2 content [vol% (dry)]	11.8 - 12.7	12.4	13.5 - 15.5
Regenerated solvent temperature [°C]	40	-	40
Flue gas temperature [°C]	40	47	40
CO_2 separation efficiency [%]	90	90	90

Similar measurement results were obtained (Fig. 6-2a) despite the fact that the CO_2SEPPL pilot plant is much smaller than the other two pilot plants. A state near equilibrium can be achieved at the absorber bottom (as compared with VLE-data from Hilliard (2008)) through the industry-related absorber height of the CO_2SEPPL pilot plant. It can be assumed that a CO_2 loading near

---

[1] Segments of this section have already been published in Rabensteiner, et al. (2014a).

equilibrium state is achieved at the other two pilot plants because of their even higher absorber columns and the number of theoretical separation plates (compare Table 5-2). The minimal specific energy for solvent regeneration measured in Dürnrohr is in the range of 3.68 GJ per ton of separated CO_2 (GJ/t_{CO_2}) at an L/G-ratio of 3.2 l/m³ (Fig. 6-2a).
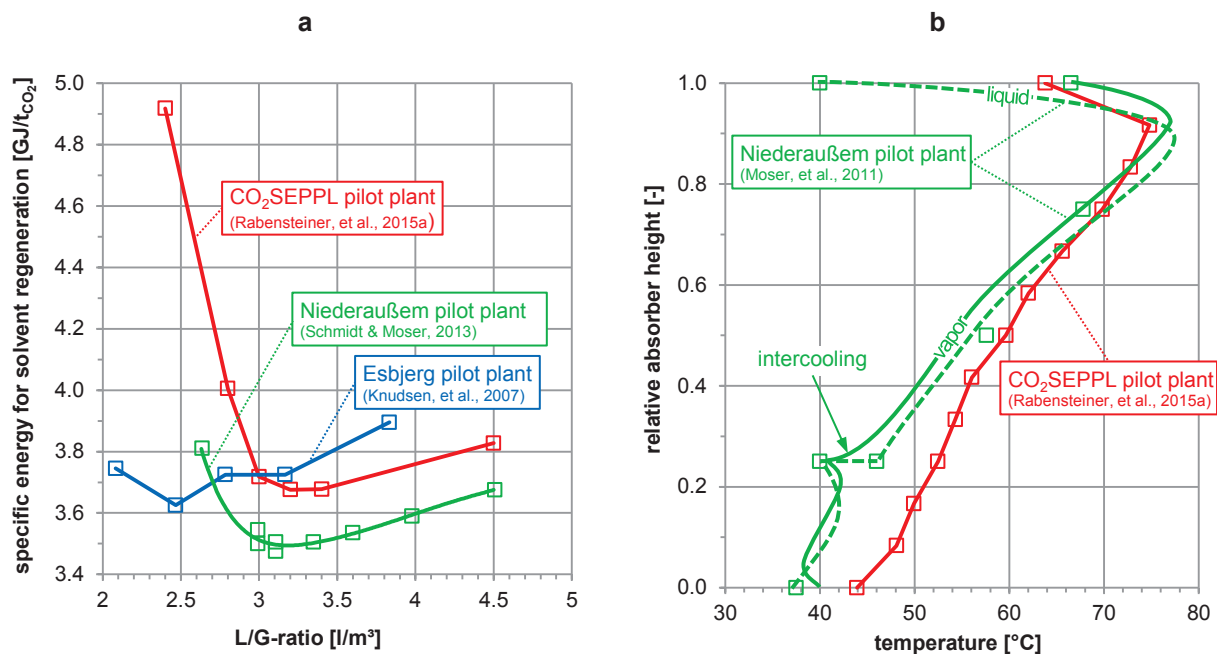
Fig. 6-2: **(a)** Specific energy for solvent regeneration as a function of the L/G-ratio for 30 wt% MEA. **(b)** Comparison of the absorber column temperature profile with and without absorber intercooling when using 30 wt% MEA.[1]

CO_2 capture with amine solvents results in the generation of a temperature maximum within the column due to heat released by absorption and reaction of CO_2 (Sachde & Rochelle, 2014). Bicarbonate (HCO_3^-) and carbamate ($R_1R_2NCOO^-$) are formed at the CO_2 absorption with primary and secondary amines (compare Section 4.1.1). Bicarbonate is unstable at higher temperatures (Schäffer, et al., 2010). The higher solvent temperature limits the maximum capacity of the solvent and reduces average driving forces through the column. The reduced solvent capacity results in the deterioration of the energy performance of the stripping system while the reduced driving forces can result in increased packing requirements in the absorber column (Sachde & Rochelle, 2014). Higher CO_2 loadings can be obtained by lowering the absorber temperature, provided that the slower kinetics (through temperature decrease) are sufficient to achieve near-equilibrium state. Absorber intercooling was found to improve absorption performance especially for high absorption capacity solvents (NETL, 2010).

The operation of the Niederaußem pilot plant is carried out with absorber intercooling (Schmidt & Moser, 2013). The solvent flowing downwards is cooled in a heat exchanger, whereby the temperature decreases, especially in the lower part of the column (Fig. 6-2b). This technology can save 0.1 GJ/t_{CO_2} (Schmidt & Moser, 2013). The measurement curves in Fig. 6-2a for the

---

[1] The lines from Moser, et al. (2011) in Fig. 6-2b are simulated temperature profiles. The set L/G-ratio at the CO_2SEPPL pilot plant is 3.2 l/m³. The set L/G-ratio at the Niederaußem pilot plant is unknown.

CO_2SEPPL and Niederaußem pilot plant are similar when this energy saving technique is taken into account.

The Esbjerg pilot plant is also equipped with an absorber intercooler. The measurements presented in Fig. 6-2a were carried out without absorber intercooling. The minimal specific energy for solvent regeneration is similar to those of the CO_2SEPPL pilot plant. The low optimal L/G-ratio can be attributed to inaccurate information about the flue gas or solvent flow rate in Knudsen, et al. (2007).

6.3 The impact of the solvent flow rate[1]

6.3.1 Basic considerations

The liquid to gas ratio (or solvent flow rate) has a strong influence on absorption/desorption processes. It is defined as the ratio of the liquid solvent volume flow rate and the gaseous flue gas volume flow rate when entering the bottom of the absorber column. The liquid and the gaseous flow rate for determining the L/G-ratio are measured at FIRC3.2 and FIRC1.2 (see flow scheme in Appendix A.1). In general, when assuming chemical equilibrium in the absorber column, the required lean solvent mass flow rate for a desired CO_2 separation efficiency can be determined by Eq. 6-1 (Oexmann, 2011). $\Delta\alpha$ is denoted as the CO_2 loading difference between the rich and lean solvent (Eq. 6-2).

$$\dot{m}_{lean} = \dot{m}_{CO_2} \cdot \frac{M_{lean}}{M_{CO_2}} \cdot \frac{\eta_{sep}}{\chi_{equ.\ amine}} \cdot \frac{1}{\Delta\alpha} \qquad \text{Eq. 6-1}$$

$$\Delta\alpha = \alpha_{rich} - \alpha_{lean} \qquad \text{Eq. 6-2}$$

$\dot{m}_{CO_2}$ is the mass flow rate of CO_2 in the flue gas at the absorber entry. M_{lean} and M_{CO_2} are the molar weight of the regenerated (lean) solvent and CO_2, respectively. $\chi_{equ.\ amine}$[2] indicates the mole fraction of active substance in the solvent. The lean solvent mass flow rate $\dot{m}_{lean}$ only depends on the CO_2 loading difference $\Delta\alpha$ for a fixed CO_2 separation efficiency η_{sep} and a constant mole fraction of active substance $\chi_{equ.\ amine}$. An increase in CO_2 loading difference leads to a decrease in the required lean solvent mass flow rate resulting in a reduction of auxiliary work. The required heat input for solvent regeneration q_{reb} (in GJ/t$_{CO_2}$) consists of

- Heat for reversing reaction (q_{abs,CO_2})
- Sensible heat for solvent heat up (q_{sens})
- Heat for the generation of stripping steam (q_{vap,H_2O})

and can be expressed as sum of the three terms (Oexmann & Kather, 2009b):

---

[1] Segments of this section have already been published in Rabensteiner, et al. (2014a; 2014b; 2014c; 2014d, 2015a; 2015c, 2015d).

[2] The CO_2 loading in the present work is indicated in mole per mole equivalent amine (mol$_{CO_2}$/mol$_{equ.\ amine}$) in order to make the CO_2 loadings comparable. The exception is the indication of CO_2 loading of the blend 28/17 wt% AMP/PIP. For this reason, the mole fraction of active substance in the solvent is indicated with mol$_{equ.\ amine}$/mol$_{solvent}$.

$$q_{reb} = q_{abs,CO_2} + q_{sens} + q_{vap,H_2O} \qquad \textbf{Eq. 6-3}$$

q_{abs,CO_2} is the heat required to strip the CO_2 from the solution, q_{sens} is the sensible heat to increase the temperature of the solution at the desorber inlet to the conditions in the reboiler (boiling point), and q_{vap,H_2O} is the heat of vaporization required to generate the water vapor (stripping steam) in the desorber (Oexmann, 2011). The specific energy for solvent regeneration q_{reb} can be estimated by Eq. 6-4 (Oexmann, 2011).

$$q_{reb} \approx \underbrace{\frac{\Delta h_{abs,CO_2}}{M_{CO_2}}}_{q_{abs,CO_2}} + \underbrace{\frac{c_p^l * \left(\vartheta_{reb}^l - \vartheta_{des,feed}^l\right)}{\Delta\alpha} \cdot \frac{M_{sol}}{M_{CO_2}\cdot\chi_{equ.\ amine}}}_{q_{sens}} + \underbrace{\Delta h_{vap_{H_2O}} \cdot \frac{1}{M_{CO_2}} \cdot \left(\frac{p_{H_2O}^g}{p_{CO_2}^g}\right)_{des,top}}_{q_{vap,H_2O}} \qquad \textbf{Eq. 6-4}$$

$\vartheta_{des,feed}^l$ is the temperature of the rich solvent at the desorber inlet, ϑ_{reb}^l is the boiling temperature of the rich solvent at desorber conditions, and $\left(p_{H_2O}^g/p_{CO_2}^g\cdot\right)_{des,top}$ is the partial pressure ratio of water and CO_2 at the desorber top.

The reboiler heat duty is entirely supplied by the stripping steam generated in the reboiler which consists mainly of H_2O and CO_2. Part of the steam condenses on its way up the column where the emerging latent heat supplies sensible heat as well as the heat of absorption/desorption. q_{vap,H_2O} solely denotes that part of the stripping steam which provides for the driving force, i.e. partial pressure difference, which transfers the physically dissolved molecular CO_2 from the liquid into the gas phase and remains uncondensed at the desorber top. The largest part of the remaining water vapor is condensed in the overhead condenser downstream of the desorber, so that q_{vap,H_2O} is ultimately dissipated to the cooling system (Oexmann, 2011).

The three terms of Eq. 6-3 and Eq. 6-4 are not mutually exclusive, but rather depend on each other as well as on the operational parameters of the pilot plant. A common misguide conclusion based on analysis of Eq. 6-3 is the statement that solvents with a low heat of absorption must also result in a low total reboiler heat duty (q_{reb}) (Oexmann & Kather, 2010). This is not the case, as this conclusion obscures the fact that q_{vap,H_2O} is in fact a function of q_{abs,CO_2}. High heat of absorption solvents profit from an increase in reboiler temperature in terms of a lower reboiler heat duty since the amount of stripping steam required is reduced (Oexmann, 2011).

q_{abs,CO_2} is independent of the solvent flow rate because this value corresponds to the CO_2 absorption heat. q_{sens} increases linearly with increasing solvent flow rate. The higher the CO_2 loading difference between the rich and the lean solvent, the lower the reboiler heat required for solvent heat up (q_{sens}) (see Eq. 6-4). A high CO_2 loading difference is coupled with low lean CO_2 loading due to the limited CO_2 loading capacity of each solvent. Low lean CO_2 loadings can be achieved by generating large amounts of stripping steam. The energy requirement increases enormously at very low solvent flow rates, depending on the CO_2 solubility of desorber conditions. The smaller the lean CO_2 loading, the more the CO_2 partial pressure in the desorber must be lowered by an increase of the water steam flow rate.

Those two opposite effects lead to the formation of a minimum specific energy for solvent regeneration. A qualitative trend according Posch (2012) is shown in Fig. 6-3.
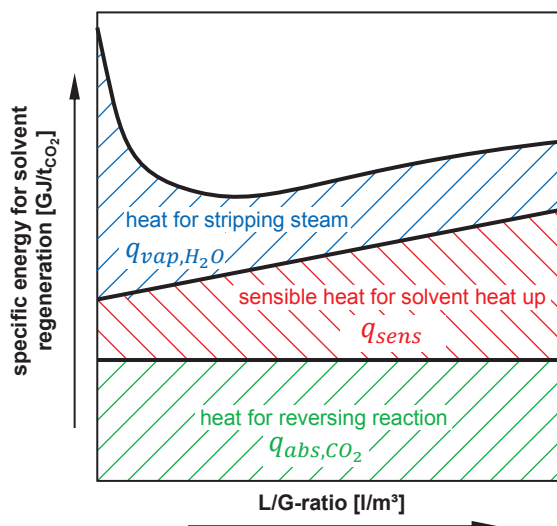
Fig. 6-3:   A qualitative view of correlation between specific energy for solvent regeneration and L/G-ratio (Posch, 2012).

The L/G-ratio threshold in Fig. 6-3 denotes the minimum amount of solvent flow rate required for desired CO_2 separation efficiency. The minimum solvent mass flow rate ($\dot{m}_{lean_{min}}$) results from the maximum achievable CO_2 loading difference, which depends on the solvent used. The minimum solvent mass flow rate at the L/G-ratio threshold for a desired CO_2 separation efficiency follows from Eq. 6-5 where $\Delta\alpha_{max}$ denotes the maximum CO_2 loading difference (Posch, 2012).

$$\dot{m}_{lean_{min}} = \dot{m}_{CO_2} \cdot \frac{M_{lean}}{M_{CO_2}} \cdot \frac{\eta_{sep}}{\chi_{equ.\,amine}} \cdot \frac{1}{\Delta\alpha_{max}} \qquad \text{**Eq. 6-5**}$$

6.3.2 Operating parameters

In the following sections, measurement results of the test campaign with 32 wt% EDA and 28/17 wt% AMP/PIP are partially compared with experimental data from the pilot plants in Esbjerg and Kaiserslautern. Technical data from these pilot plants are listed in Table 5-1. Known reference parameters are also reported in Table 6-4. Tests at the Kaiserslautern pilot plant were carried out with about 11 vol% (dry) and 5.8 vol% (dry) flue gas CO_2 content (Mangalapally & Hasse, 2011a). Since the CO_2 content of 11 vol% roughly corresponds to an operation with flue gases from a hard coal-fired boiler, this value is used as reference. Limited information is available about the investigations on the Esbjerg pilot plant; however, it can be assumed that the operating parameters are similar to those in Dürnrohr.

Pilot plant studies with aqueous piperazine were carried out at the J.J. Pickle and Tarong pilot plants. Technical data from these pilot plants are listed in Table 5-1. A series of experiments in which the L/G-ratio was changed was carried out at the Tarong pilot plant. Measuring points of the J.J. Pickle pilot plant based on secure and sufficient data are used for an energy comparison. Of the 14 measurement points of the J.J. Pickle pilot plant, three measurement points were taken where similar operating parameters were set as in Dürnrohr. These three measurement points were also recorded with variable L/G-ratio. Only a limited comparison of

measurement results generated at the J.J. Pickle pilot plant is possible due to the insufficient closing mass and energy balances of this pilot plant (Van Wagener, 2009).

All operating parameters of these test campaigns are listed in Table 6-4.

Table 6-4: Operating parameters of the series of measurements with varying L/G-ratio.

	Amine-based solvents										Amino acids			
	MEA	EDA			PIP			AMP/PIP			NaGly			KGly
	CO₂SEPPL pilot plant	CO₂SEPPL pilot plant	Kaiserslautern pilot plant	Esbjerg pilot plant	CO₂SEPPL pilot plant	J.J. Pickle pilot plant	Tarong pilot plant	CO₂SEPPL pilot plant	Kaiserslautern pilot plant	Esbjerg pilot plant	CO₂SEPPL pilot plant			CO₂SEPPL pilot plant
	(Rabensteiner, et al., 2015a)	(Rabensteiner, et al., 2014c)	(Mangalapally & Hasse, 2011a)	(Knudsen, et al., 2011)	(Rabensteiner, et al., 2015a)	(Plaza, 2011; Van Wagener, 2009)	(Cottrell, et al., 2013; Cousins, et al., 2012, 2011)		(Mangalapally & Hasse, 2011a)	(Knudsen, et al., 2011)	(Rabensteiner, et al., 2014b)			(Rabensteiner, et al., 2015c)
Concentration of active substance [wt%]	30	32	32	32	37.6	40.8[1]	40.8	28/17	28/17	28/17	15	25	40	40
└ [molal]	└ 7.0	└ 7.8	└ 7.8	└ 7.8	└ 7.0	└ 8.0[1]	└ 8.0	└ 4.4/2.4	└ 4.4/2.4	└ 4.4/2.4	└ 1.8	└ 3.4	└ 6.9	└ 5.9
L/G-ratio [l/m³]	var.	var.	var.	var.	var.	var.	var.	var.	var.	var.	var.	var.	var.	var.
Flue gas flow rate [m³/h]	90	90	-	-	100	~ 750[2]	~ 700[3]	100	-	-	50	50	50	50
└ F-factor [√Pa]	└ 1.50	└ 1.50	1.60	~ 2.00	└ 1.65	└ 1.50	└ 2.10	└ 1.65	1.60	~ 2.00	└ 0.84	└ 0.84	└ 0.84	└ 0.84
Desorber pressure [bar_abs]	2	2	~2[4]	-	2	2[4]	48 (±0.25)	2	~2[4]	-	2	2	2	2
Flue gas CO₂ content [vol% (dry)]	11.8 - 12.7	11.9 - 12.9	11.0	13.0	12.3 - 13.1	12.0[5]	9.8 – 13.0[6]	12.2 - 12.4	11.0	13.0	12.8 - 12.9	13.0 - 13.2	12.8 - 13.0	12.8 - 13.2
Regenerated solvent temp. [°C]	40	40	40	-	40	~ 40	33[7]	40	40	-	40	40	40	40
Flue gas temperature [°C]	40	40	47	-[8]	40	-[9]	45	40	47	-[8]	40	40	40	40
CO₂ separation efficiency [%]	90	90	90 (±1)	90	90 (±1)	-	82 (±5)	90 (±1)	90 (±1)	90	90 (±1)	90 (±1)	90 (±1)	90 (±1)

[1] Average value.
[2] Not specified. Calculated by L/G-ratio and solvent flow rate.
[3] No information available → Calculation by the captured CO_2 stream.
[4] Value in not specified. Pressure can be estimated by desorber temperature stated by Mangalapally & Hasse (2011a) for 32 wt% EDA and 28/17 wt% AMP/PIP and Van Wagener (2009) for 40.8 wt% PIP.
[5] No information exists whether the consideration of the water content.
[6] Measured in previous MEA-experiments (Cousins, et al., 2012).
[7] Indication of the temperature range in Cottrell, et al. (2013) (Fig. 4-3).
[8] The temperature of the flue gas will be higher than in Dürnrohr, since the flue gas is taken after the SO_2 scrubber and is fed directly (without pre-treatment) to the absorber (Knudsen, et al., 2007).
[9] The flue gas is artificially produced by the mixture of air and CO_2. The temperature of the inflowing flue gas is mainly dependent on the outside temperature because no flue gas heat exchanger exists and the pilot plant is outdoors. This results in very highly fluctuations of the flue gas temperature.

6.3.3 Specific energy for solvent regeneration

Fig. 6-4 shows a summary of measurement results from the investigated solvents. The characteristic course from Fig. 6-3 can be identified for each solvent. The aqueous solutions of amino acids investigated have a huge energy demand in comparison to the amine-based solvents. An extremely high solvent flow rate is required when using aqueous solutions of amino acids. Table 6-5 lists the specific energy for solvent regeneration (q_{reb}) and L/G-ratio in the optimum operating point for all investigated solvents. The specific energy for solvent regeneration is the lowest at the optimal operating point.
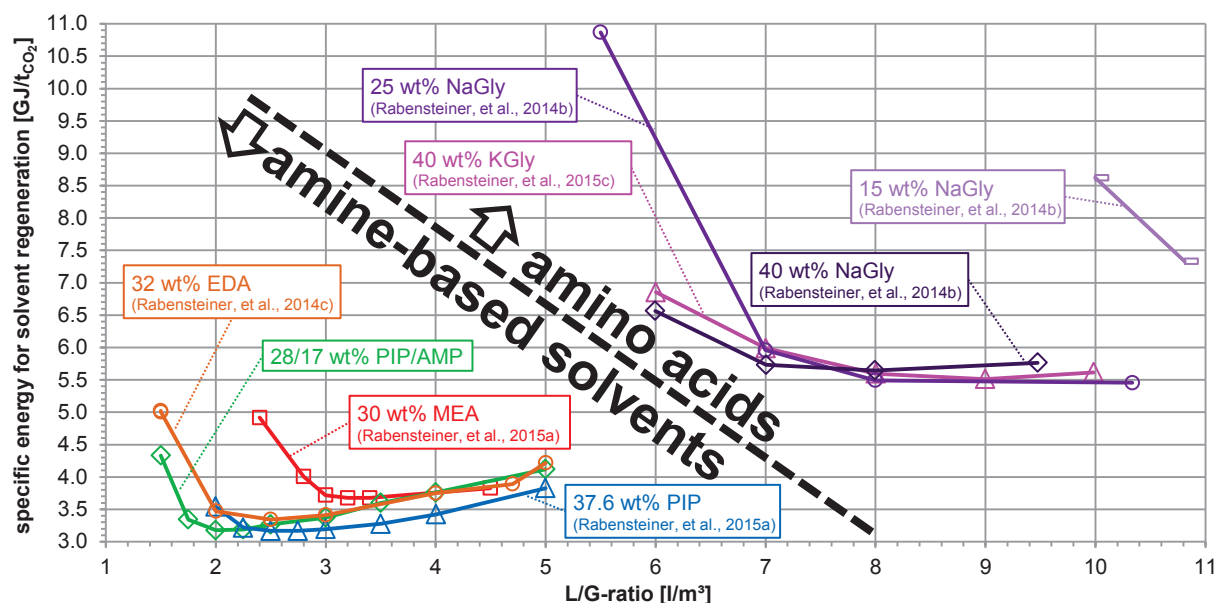
Fig. 6-4:   Specific energy for solvent regeneration as a function of the L/G-ratio for all investigated amine-based solvents and amino acids.

Table 6-5:   Specific energy for solvent regeneration and L/G-ratio at the optimum operating point for different solvents measured at the CO_2SEPPL pilot plant.

| | Amine-based solvents | | | | Amino acids | | | |
| | MEA | EDA | PIP | AMP/PIP | NaGly | | | KGly |
	(Rabensteiner, et al., 2015a)	(Rabensteiner, et al., 2014c)	(Rabensteiner, et al., 2015a)		(Rabensteiner, et al., 2014b)			(Rabensteiner, et al., 2015c)
Concentration of active substance [wt%]	30	32	37.6	28/17	15	25	40	40
└ [molal]	└ 7.0	└ 7.8	└ 7.0	└ 4.4/2.4	└ 1.8	└ 3.4	└ 6.9	└ 5.9
L/G-ratio [l/m³]	3.20	2.50	2.50	2.00	-[1]	8.00	7.00	9.00
Specific energy for solvent regeneration [GJ/t$_{CO_2}$]	3.68	3.34	3.17	3.18	-[1]	5.49[2]	5.73[3]	5.51

---

[1] The optimum operating point could not be achieved because of the high solvent flow rate.
[2] A lower q_{reb} of 5.46 GJ/t$_{CO_2}$ was measured at a L/G-ratio of 10.34 l/m³
[3] A lower q_{reb} of 5.65 GJ/t$_{CO_2}$ was measured at a L/G-ratio of 8.00 l/m³

6.3.3.1 Amine-based solvents

Fig. 6-5 shows the specific energy for solvent regeneration as a function of the L/G-ratio for the amine-based solvents investigated. The benchmark solvent 30 wt% MEA has a minimal specific energy for solvent regeneration of 3.68 GJ/t$_{CO_2}$ at an L/G-ratio of 3.2 l/m³ (Rabensteiner, et al., 2015a). As mentioned in Section 6.2, these values are consistent with literature. The minimal specific energy for solvent regeneration of approximately 3.2 GJ/t$_{CO_2}$ is measured at 37.6 wt% PIP and 28/17 wt% AMP/PIP. The required L/G-ratio to reach the optimal operating point is 2 l/m³ when using 28/17 wt% AMP/PIP. Thus 28/17 wt% AMP/PIP shows the most favorable energy characteristics. The measurement results of the individual solvents will be described in more detail below.
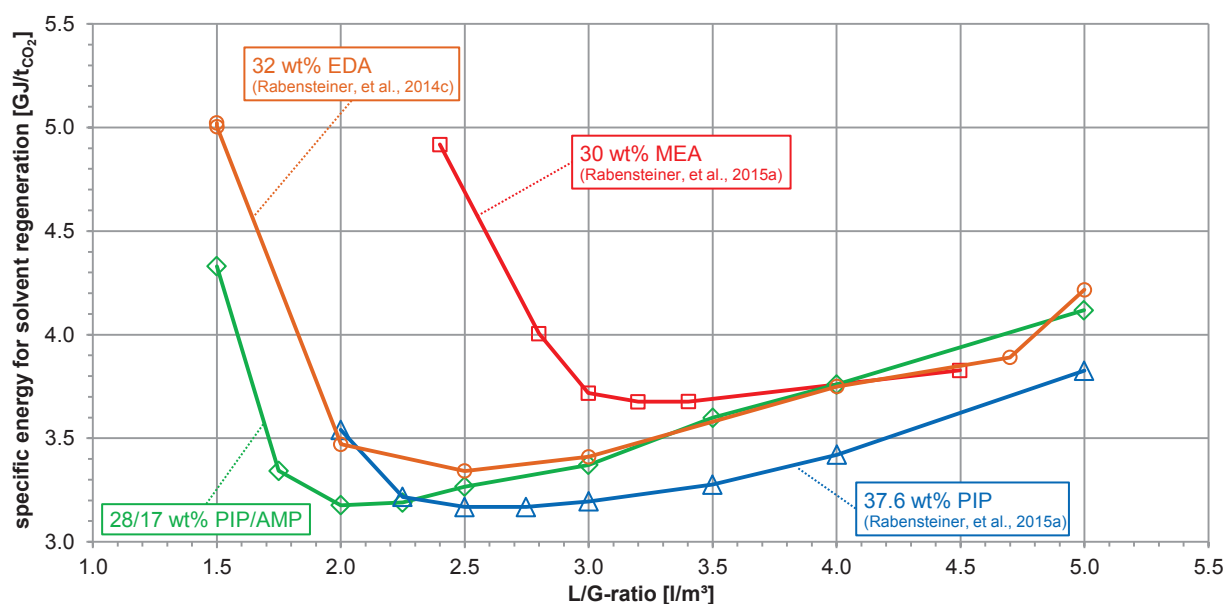
Fig. 6-5:   Specific energy for solvent regeneration as a function of the L/G-ratio for amine-based solvents.

Fig. 6-7 shows the measurement results generated at the CO$_2$SEPPL pilot plant for 32 wt% EDA (a) and 28/17 wt% AMP/PIP (b), in comparison to results from the Kaiserslautern pilot plant. The minimal specific energy for solvent regeneration when using 32 wt% EDA is 3.34 GJ/t$_{CO_2}$ (at an L/G-ratio of about 2.5 l/m³). The energy consumption can be reduced to 3.18 GJ/t$_{CO_2}$ when using 28/17 wt% AMP/PIP. Consequently, there is a 9 or 14 % reduction of the specific energy for solvent regeneration in comparison to the process with 30 wt% MEA. 28/17 wt% AMP/PIP is characterized by a low solvent flow rate of 2.0 l/m³ for reaching the optimal operating point. The heat dissipated by power plants is a crucial factor in the design of such plants. A reduction of the solvent flow rate leads to a lowering of the heat to be dissipated in the regenerated solvent cooler. It follows that smaller dimensions for the entire piping and aggregates lead to a further reduction in operating and capital costs.

The following section will explain the course of the measurement curve. q_{abs,CO_2} (heat for reversing reaction) in Eq. 6-3 and Eq. 6-4 is independent of the solvent flow rate because this value corresponds to the CO$_2$ absorption heat. The CO$_2$ loading difference between the rich and the lean solvent ($\Delta\alpha$) decreases linearly with increasing solvent flow rate, as can be seen in Fig.

6-11 for 32 wt% EDA and Fig. 6-13 for 28/17 wt% AMP/PIP. Some variables in Eq. 6-4 for the calculation of the q_{sens}-term are also dependent on solvent flow rate. The desorber sump temperature (ϑ_{reb}^l) drops with increasing solvent flow rate, as can be seen in Fig. 6-6 for 32 wt% EDA. ϑ_{reb}^l of 32 wt% EDA is 126.2 °C when a low L/G-ratio of 1.5 l/m³ is set. ϑ_{reb}^l drops to 121.4 °C when a high L/G-ratio of 5.0 l/m³ is set. The CO_2 enriched solvent temperature at the desorber inlet ($\vartheta_{des,feed}^l$) rises with increasing solvent flow rate. $\vartheta_{des,feed}^l$ of 32 wt% EDA for instance is 103.3 °C when a low L/G-ratio of 1.5 l/m³ is set (Fig. 6-6). $\vartheta_{des,feed}^l$ increases to 111.1 °C when a high L/G-ratio of 5.0 l/m³ is set. 32 wt% EDA must be warmed to 22.9 K when a low L/G-ratio of 1.5 l/m³ is set. This temperature difference ($\vartheta_{reb}^l - \vartheta_{des,feed}^l$) drops to 10.3 K when a high L/G-ratio of 5.0 l/m³ is set (Fig. 6-6). The temperature difference ($\vartheta_{reb}^l - \vartheta_{des,feed}^l$) shows a linear course by varying solvent flow rate. The specific heat capacity (c_p^l) is also depended on the solvent temperature. This dependence can be neglected because the average temperature of ϑ_{reb}^l and $\vartheta_{des,feed}^l$ remains almost constant by varying the solvent flow rate. The remaining variables in Eq. 6-4 (M_{sol}, M_{CO_2} and $\chi_{equ.\ amine}$) for the calculation of the q_{sens}-term are independent of the solvent flow rate. The sensible heat for solvent heat up (q_{sens}) must be proportional to the solvent flow rate because the terms $\vartheta_{reb}^l - \vartheta_{des,feed}^l$ and $\Delta\alpha$ are also linearly dependent on the solvent flow rate (Eq. 6-4).
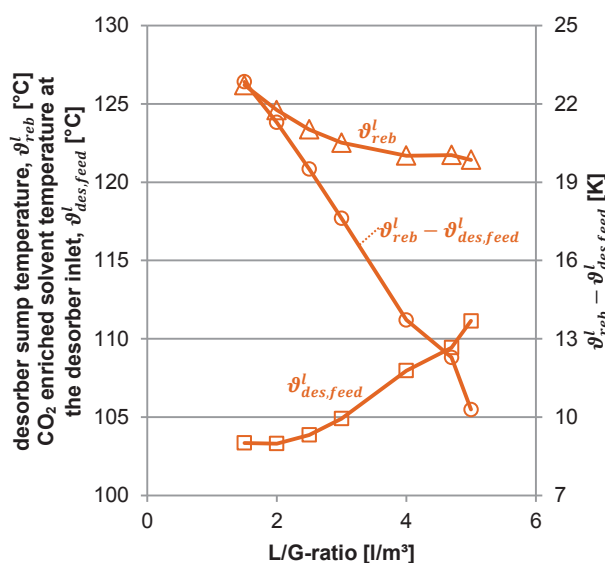
Fig. 6-6:   Decrease in temperature difference between desorber sump temperature and CO_2 enriched solvent temperature at the desorber inlet when using 32 wt% EDA.

A high CO_2 loading difference is coupled with low lean CO_2 loading due to the limited CO_2 loading capacity of each solvent. Low lean CO_2 loadings can be achieved by generating large amounts of stripping steam. The energy demand for stripping steam increases enormously at very low solvent flow rates, depending on the CO_2 solubility at desorber conditions. The smaller the lean CO_2 loading, the more the CO_2 partial pressure in the desorber must be lowered. The CO_2 partial pressure in the desorber drops by an increase of the water steam flow rate. Those two opposite effects lead to the formation of a minimum specific energy for solvent regeneration.

The water vapor stream at the top of the desorber column rises with increasing electrical heating rod power supply. The water vapor stream is linked with the temperature and pressure at the desorber top via the vapor pressure curve of water (Notz, 2009). Thus the amount of condensate generated in the overhead condenser rises with increasing power supply, resulting in an increase in sensible heat; however, this energy contribution can be normally neglected. The CO_2 partial pressure required to release the carbon dioxide in the desorber top is high when using 32 wt% EDA. This is made possible by the interaction of EDA´s high CO_2 loading of the regenerated solvent (Fig. 6-11) and the shape of the equilibrium curve at 120 °C (Fig. 6-12). In contrast to the MEA-process, only a moderate amount of steam has to be generated in order to reduce the CO_2 partial pressure to the required level. The required heat of evaporation (q_{vap,H_2O}) for the generation of stripping steam decreases. The minimal energy consisting of sensible heat (q_{sens}) and heat of evaporation shifts to smaller solvent flow rates. Fig. 6-12 shows the CO_2 loading with respect to the amount of amine ($mol_{CO_2}/mol_{equ.\ amine}$). Mangalapally & Hasse (2011a) represented the CO_2 loading as dependent on the amount of solvent ($mol_{CO_2}/kg_{solvent}$). The CO_2 loading difference as dependent on the amount of solvent (between the equilibrium curves) for 32 wt% EDA is larger than for 30 wt% MEA. The small solvent flow rate of 32 wt% EDA in comparison to the MEA-process is based on this fact.

The low energy consumption of 28/17 wt% AMP/PIP is also attributed to the high CO_2 partial pressure in the desorber (Fig. 6-14a). Less stripping steam has to be generated. The high CO_2 partial pressure during the regeneration of 28/17 wt% AMP/PIP also contributes to the very low solvent flow rate. Low-loaded AMP/PIP solvents have a particularly reduced CO_2 absorption enthalpy in comparison to MEA (Fig. 6-14b).

Investigations of 32 wt% EDA at the Kaiserslautern pilot plant show a minimal specific energy for solvent regeneration of 3.8 GJ/t_{CO_2} at an L/G-ratio of about 1.7 l/m³ (Mangalapally & Hasse, 2011a). Similar to the investigations on the CO_2SEPPL pilot plant, there is a reduction of the specific energy for solvent regeneration of 7 % compared to the process with 30 wt% MEA (Tönnis, et al., 2011). Kinetics have a high impact due to the low number of theoretical separation plates at the Kaiserslautern pilot plant (compare Table 5-2). The maximum CO_2 loading decreases (Fig. 6-11). The solvent has to be heavily regenerated which in turn leads to an increase of the specific energy for solvent regeneration. The distance between the equilibrium curves increases for decreasing CO_2 partial pressures (Fig. 6-12). The optimal operating point shifts to smaller solvent flow rates consequently. A high increase in specific energy for solvent regeneration is observed at a high solvent flow rate. This increase is more pronounced than in Dürnrohr. The kinetics have a broad influence on the maximal CO_2 loading at a high solvent flow rate (Fig. 6-11). Another reason for the different shape of the curves is the slightly lower CO_2 content of the flue gas; the consequences of this factor are discussed in Section 6.6.

No significantly higher energy demand was measured on the Kaiserslautern pilot plant for 28/17 wt% AMP/PIP in contrast to 32 wt% EDA. The fast kinetics of piperazine make it possible to achieve high CO_2 loadings despite the lower absorber column. The CO_2 loading of the regenerated solvent is higher, leading to low amounts of stripping steam in the desorber column.

The required energy for solvent regeneration with 32 wt% EDA on the pilot plant in Esbjerg amounts to 3.5 GJ/t$_{CO_2}$ without intercooling and vapor re-compression (Tönnis, et al., 2011). Tönnies, et al. (2011) indicated a 3 % improvement to 30 wt% MEA. The kinetics effect the MEA operation only slightly due to the longer absorber column. In this case, energy savings are small in comparison to the process with MEA because of the higher heat of CO_2 absorption of EDA (Fig. 6-12). An energy demand of 3.1 GJ/t$_{CO_2}$ was measured at the Esbjerg pilot plant (without absorber intercooling and vapor-recompression) for 28/17 wt% AMP/PIP (or 29/18 wt% AMP/PIP) according to Tönnis, et al., (2011). Similar measurement results were obtained at the CO_2SEPPL pilot plant for 32 wt% EDA and 28/17 wt% AMP/PIP.
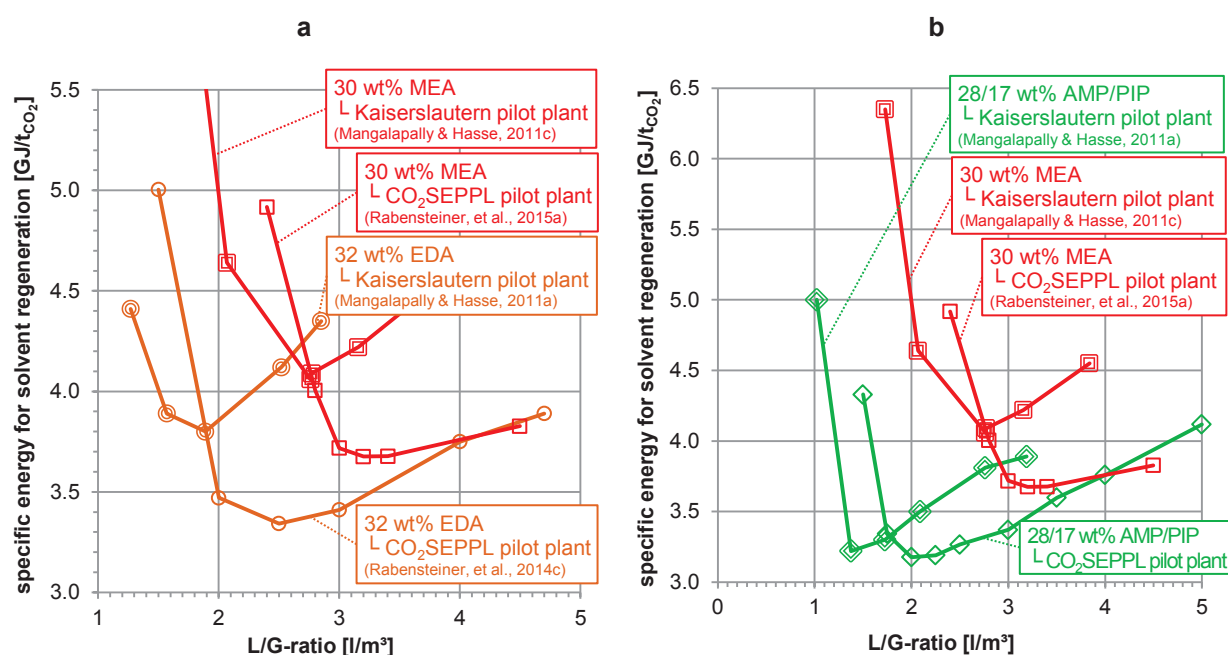
Fig. 6-7: Specific energy for solvent regeneration as a function of the L/G-ratio. Experimental data for 32 wt% EDA **(a)**, 28/17 wt AMP/PIP **(b)** and 30 wt% MEA generated at the CO_2SEPPL and Kaiserslautern pilot plant.

Fig. 6-8 shows the measurement results generated at the CO_2SEPPL pilot plant for 37.6 wt% PIP in comparison to results from the J.J. Pickle and Tarong pilot plant, in which aqueous piperazine was also tested. The energy demand can be reduced to 3.17 GJ/t$_{CO_2}$ at the CO_2SEPPL pilot plant in Dürnrohr, when using 37.6 wt% PIP, resulting in energy savings of 14 % in comparison to the process with 30 wt% MEA.
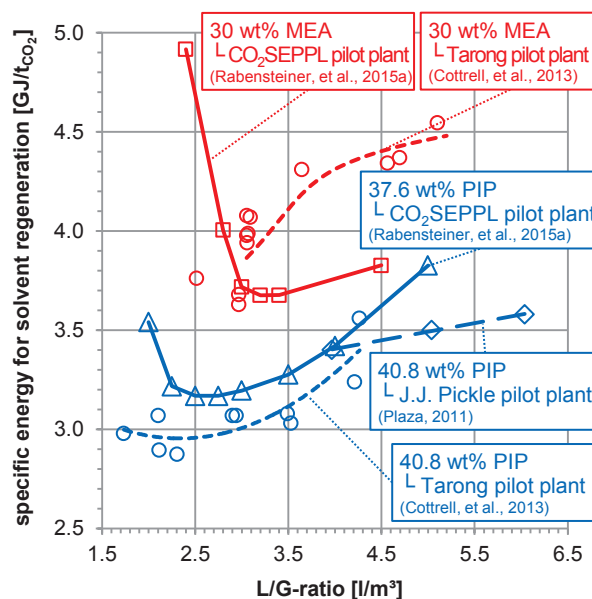
Fig. 6-8: Specific energy for solvent regeneration as a function of the L/G-ratio. Experimental data for concentrated piperazine and 30 wt% MEA generated at the CO_2SEPPL, J.J. Pickle and Tarong pilot plant. The lines for the J.J. Pickle and Tarong pilot plant are estimated curves.

The CO_2 absorption heat for 37.6 wt% PIP at the optimal operating point and mid-loading is 77 kJ/mol$_{CO_2}$ (Fig. 6-16). The CO_2 absorption heat increased to 88.5 kJ/mol$_{CO_2}$ when using 30 wt% MEA. That means that 13 % less heat is necessary to desorb the CO_2 from solution (q_{abs,CO_2}). The solvent must be regenerated to 0.12 mol$_{CO_2}$/mol$_{equ.\ amine}$ for both solvents (Fig. 6-15). The temperature in the desorber is approximately 120 °C. The CO_2 partial pressure in the desorber for the regeneration to 0.12 mol$_{CO_2}$/mol$_{equ.\ amine}$ (Fig. 6-16) is only slightly higher when using 37.6 wt% PIP. The heat of evaporation for producing stripping steam (q_{vap,H_2O}) is only slightly lower when using 37.6 wt% PIP.

The heat transfer coefficient in the main heat exchanger decreases because of the higher viscosity of piperazine solvents. This results in an increasing pinch temperature of the main heat exchanger. The pinch temperature is in the range of 4.9 to 5.5 K when using 30 wt% MEA. This temperature difference increases to 6.2 to 6.8 K when using 37.6 wt% PIP. A larger main heat exchanger was installed at the Tarong pilot plant in order to compensate for the lower heat transfer coefficient (Cottrell, et al., 2013).

The optimum operating point occurs at very low solvent flow rates when using 37.6 wt% PIP; it is between 2.5 and 2.75 l/m³ (Fig. 6-8). This means that up to 22 % less solvent has to be pumped in circuit in order to reach the optimal operating point in comparison to the process with 30 wt% MEA.

The lower solvent flow rate results in less solvent that must be heated in the desorber. The specific energy for solvent regeneration increases with increasing sensible heat (Oexmann, 2011). The specific heat capacity of the solvents is dependent on the CO_2 loading and temperature (Fig. 6-9). The specific heat capacities at the average CO_2 loading and desorber column temperature are equal for 30 wt% MEA and 37.6 wt% PIP (in Fig. 6-9 approximate with

40.8 wt% PIP). The heat transfer coefficient in the main heat exchanger is lower because of the reduced solvent flow rate, when using 37.6 wt% PIP. The high viscosity of piperazine reduces the heat transfer further. The temperature difference of the liquid phase in the desorber column (difference between the desorber sump temperature and incoming solvent temperature) is therefore higher when using 37.6 wt% PIP. Nevertheless, approximately 13 % of the sensible heat can be saved, compared to the process with 30 wt% MEA.
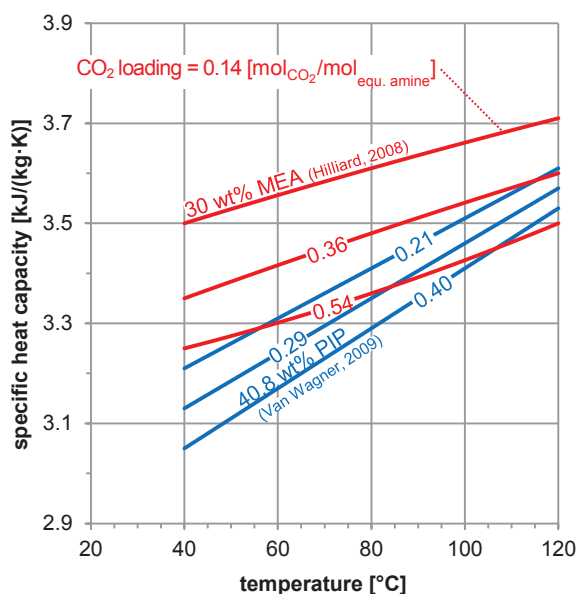
Fig. 6-9:   Comparison of the heat capacity from 8 m PIP (40.8 wt% PIP) and 30 wt% MEA.

There are high fluctuations in the measurement results of the J.J. Pickle and Tarong pilot plants. Fig. 6-8 shows the smooth lines of these measurement campaigns. Most measurement series at the J.J. Pickle pilot plant were carried out with high solvent flow rates. An increase in specific energy for solvent regeneration at a low solvent flow rate is not visible. The lower increase in energy demand with increasing solvent flow rate compared to the results generated at the CO_2SEPPL pilot plant is obvious. The J.J. Pickle pilot plant was expanded after completing measurements with basic configuration. An absorber intercooler and a two-stage flash were installed. After this conversion, 10 to 20 % lower energy consumption was measured than when using 30 wt% MEA with the same configuration (Dombrowski, 2010).

A the Tarong pilot plant, the minimum specific energy of 2.9 GJ/t_{CO_2} for solvent regeneration was measured. The energy demand of the 40.8 wt% PIP-process is nearly 15 % lower in comparison to the process with 30 wt% MEA (Cottrell, et al., 2013). This energy saving is similar to the measurements on the CO_2SEPPL pilot plant. Reasons for the lower energy demand compared to the CO_2SEPPL pilot plant are the significant higher desorber pressure, the slightly higher F-factor in the absorber column, and potentially also the slightly higher piperazine concentration. The effects of different F-factors and desorber pressures on the process are discussed in Sections 6.4 and 6.5, respectively. The absorber of the Tarong pilot plant is equipped with an intercooler as well. The location of the precise optimum solvent flow rate cannot be exactly located, but is apparently in the range of the optimal operating point of the CO_2SEPPL pilot plant. The CO_2 separation efficiency influences the location of the optimal

operating point. The test campaign at the Tarong pilot plant was not carried out with the standard CO_2 separation efficiency of 90 % but of 82 %. Less vapor steam needs to be generated in the desorber in this case. The gradient of the heat of evaporation below the optimal operating point is steeper than the gradient of sensible heat for L/G-ratios above the optimal operating point. Accordingly, the minimum energy (composed of sensible heat and heat of evaporation) shifts to smaller solvent flow rates (compare Section 6.9). The measured energy demand for 30 wt% MEA at the Tarong pilot plant is significantly higher than in Dürnrohr. This may be due to the low absorber column height. Since MEA has slower kinetics, only small CO_2 loadings are possible, resulting in lower lean loadings (Rabensteiner, et al., 2014c).

6.3.3.2 Amino acids

A series of measurements with varying L/G-ratios were carried out with 15, 25 and 40 wt% NaGly and 40 wt KGly. The specific energy for solvent regeneration cannot be reduced below 5.6 GJ/t$_{CO_2}$ with 25 wt% NaGly (Fig. 6-10). This represents an increase in specific energy for solvent regeneration by more than 50 % in comparison to the process with 30 wt% MEA. Another major disadvantage of aqueous NaGly solutions is the high required solvent flow rate. The optimal solvent flow rate when using 25 wt% NaGly is two to three times higher than for the process with 30 wt% MEA. This leads to an enormous increase in the required pump power and waste heat as well as an increase in the load of the reboiler to maintain the higher value of necessary sensible heat. The minimal regeneration energy of 40 wt% NaGly is similar. Decreasing NaGly concentrations (15 wt%) shift the optimum operating point to higher solvent flow rates.

This first series of measurements refutes claims of the low energy demand of aqueous NaGly (~ 3 GJ/t$_{CO_2}$) mentioned in literature (Lee, et al., 2007; Ogawa, 2013; Optimized Gas Treating, 2010; Weiland, et al., 2010a; 2010b) and summarized in Table 4-5. The optimal solvent flow rate is, in fact, much higher than described in these studies.
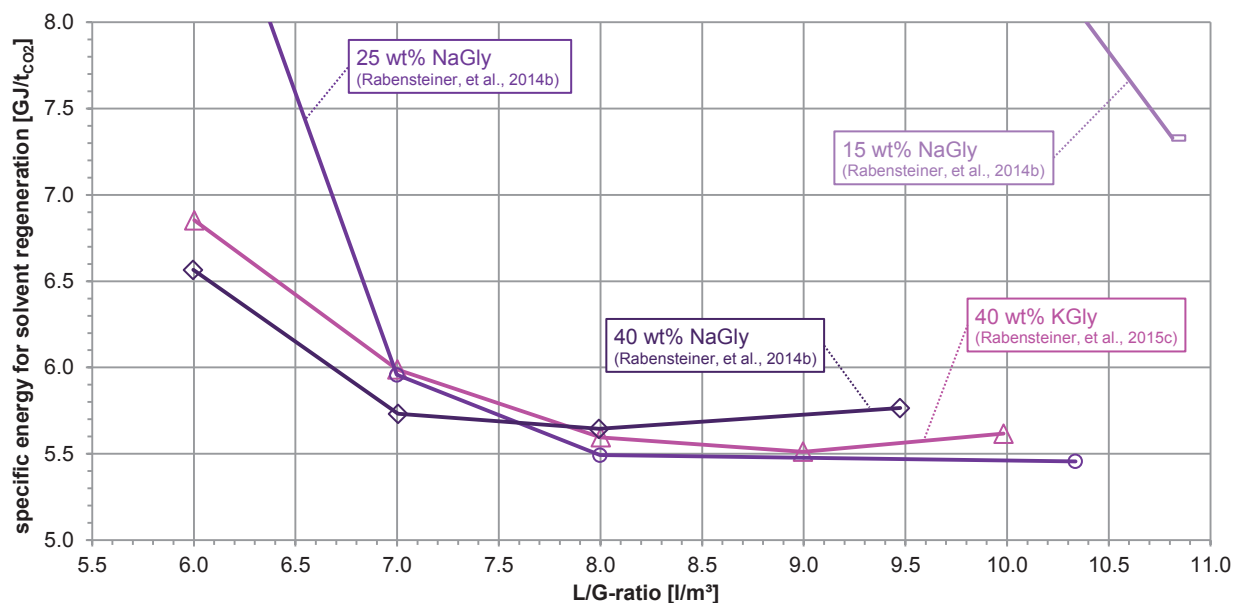
Fig. 6-10: Specific energy for solvent regeneration as a function of the L/G-ratio for all solvents based on amino acids.

A reduction in energy demand with aqueous KGly in comparison to aqueous NaGly is impossible, although mainly higher k_2-values were published (compare Fig. 4-13) and faster CO_2 absorption were proven (Rabensteiner, et al., 2014b) on laboratory-scale. The minimum specific energy for solvent regeneration for 40 wt% KGly was measured at an L/G-ratio of 9.0 l/m³, resulting in an unaltered high solvent flow rate in comparison to aqueous NaGly. The optimal solvent flow rate appears to be even higher than for 40 wt% NaGly because of the slightly lower active substance concentration in 40 wt% KGly. The low specific heat capacity of the amino acid solvents has no effects. It can be assumed that a decrease in the KGly concentration shifts the optimal operating point to even higher solvent flow rates, similar to the process with aqueous NaGly.

6.3.4 CO$_2$ loading

6.3.4.1 Amine-based solvents

Fig. 6-11 shows the CO_2 loading of 32 wt% EDA measured at the CO$_2$SEPPL pilot plant in comparison to the CO_2 loading measured at the Kaiserslautern pilot plant. The CO_2 loading difference between the rich and lean solvent drops with increasing L/G-ratio. The CO_2 equilibrium loading indicated in Fig. 6-11 refers to the absorber sump temperature (the lowest temperature in Fig. 6-19). The equilibrium CO_2 loading drops slightly with increasing solvent flow rate because of the higher absorber sump temperature at high solvent flow rates (Fig. 6-19). The enriched 32 wt% EDA solution is almost fully (equilibrium) loaded. No equilibrium loading can be achieved with 30 wt% MEA, in contrast to the CO$_2$SEPPL pilot plant. The rich loading decreases slightly by increasing L/G-ratio. The reason for this effect is the higher temperature in the absorber sump (Fig. 6-19). A high temperature reduces the equilibrium CO_2 loading of 32 wt% EDA. The maximal achievable CO_2 loading at the Kaiserslautern pilot plant is

reduced due to the low number of theoretical separation plates and the low flue gas CO_2 content. The slightly lower CO_2 concentration of the flue gas (in Kaiserslautern) leads to a reduction in CO_2 loading difference between rich and lean solvent.
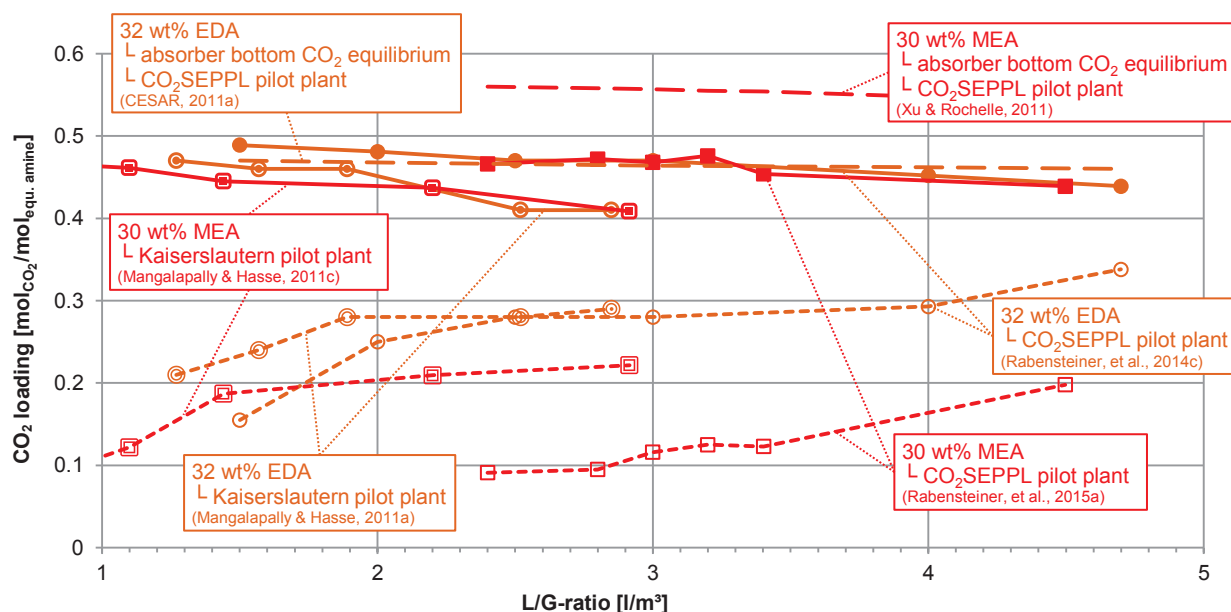
Fig. 6-11:   Dependence of the CO_2 loading on the L/G-ratio. Rich (filled symbols) and lean loading (unfilled symbols) for 32 wt% EDA and 30 wt% MEA, measured on the CO_2SEPPL and Kaiserslautern pilot plant.

Fig. 6-12 shows the CO_2 solubility data of 32 wt% EDA and the benchmark solvent 30 wt% MEA. 40 and 120 °C are approximately the temperatures present in the absorber and desorber. Data of different literature (CESAR, 2011a; Zhou, 2009) are consistent. The marked area indicates the flue gas CO_2 content of a hard coal-fired power plant. If one considers the absorber bottom temperature (lowest temperature in Fig. 6-19), it´s possible to see that equilibrium CO_2 loading is almost achieved at the CO_2SEPPL pilot plant when using 32 wt% EDA. Therefore, kinetics have only a slight influence on the process. The heat of CO_2 absorption drops with decreasing temperature and increasing CO_2 loading. Early research indicated mainly the CO_2 absorption heat of unloaded EDA solvents at low temperatures (Hikita, et al., 1977) and of loaded EDA solvents at very high temperatures, respectively (Weiland & Trass, 1971). 30 wt% MEA shows a progressive decline in the CO_2 absorption heat with increase in CO_2 loading (Xu & Rochelle, 2011), while 32 wt% EDA´s CO_2 absorption heat decreases linearly (Zhou, et al., 2010). The heat of CO_2 absorption of 32 wt% EDA is especially higher at low CO_2 loadings in comparison to CO_2 absorption heat of 30 wt% MEA (Fig. 6-12). The significant energy savings in comparison to the process with 30 wt% MEA cannot be attributed to the heat required to strip the CO_2 from the solution (q_{abs,CO_2}).

The process with 32 wt% EDA mainly benefits from the high CO_2 loading of the regenerated solvent. The required CO_2 partial pressure at the desorber top (approximation with the solubility curve for 120 °C and the lean CO_2 loading of 0.28 $mol_{CO_2}/mol_{equ.\ amine}$) is higher than 20 kPa for the optimal operating point (L/G-ratio = 2.5 l/m³). The CO_2 partial pressure at the desorber top is significantly lower when using 30 wt% MEA. The value is approximately 5 kPa for the optimal

operating point (L/G-ratio = 3.2 l/m³). The equilibrium data by Xu & Rochelle (2011) were used for the calculation of this value. Low amounts of stripping steam has to be generated when using 32 wt% EDA in comparison to the process with 30 wt% MEA. The heat of vaporization required to generate the water vapor (q_{vap,H_2O}) in the desorber drops significantly. The specific energy for solvent regeneration decreases according to Eq. 6-3 and Eq. 6-4.

Data about the specific heat capacity of EDA solvents are not available in literature. The temperature difference between desorber sump temperature and CO_2 enriched solvent temperature at the desorber inlet are similar for both solvents. It can be assumed that the sensible heat for solvent heat up (q_{sens}) is significantly lower than for the process with 30 wt% MEA because of the much lower solvent flow rate when using 32 wt% EDA. The optimal operating point of both solvents serves as reference once more. The significant energy savings in comparison to the process with 30 wt% MEA can be partially attributed to the lower sensible heat for solvent heat up (q_{sens}). The specific energy for solvent regeneration decreases according to Eq. 6-3 and Eq. 6-4.
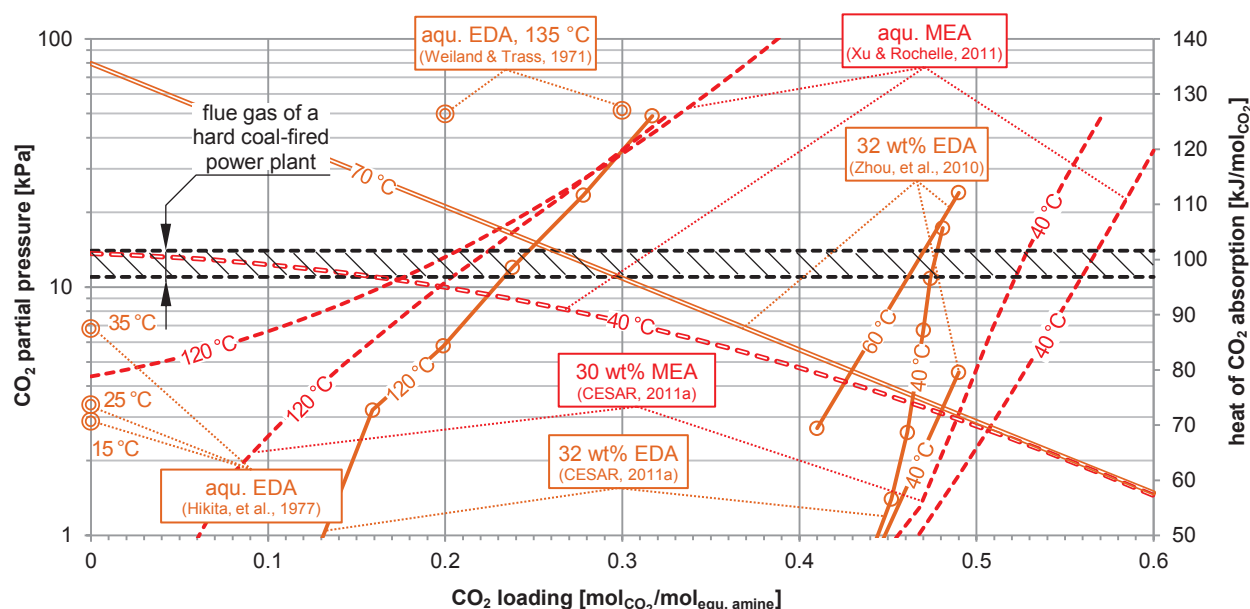
Fig. 6-12: CO_2 solubility (single line) and heat of CO_2 absorption at 40 °C (double line). Data regressed by Xu & Rochelle (2011) hold true for 17.6 to 44.3 wt% MEA.

Fig. 6-13 shows the CO_2 loading of the rich and lean solvents as a function of the L/G-ratio for 28/17 wt% AMP/PIP. The achievable rich loadings are similar to those of the Kaiserslautern pilot plant. The measured CO_2 loading of the regenerated solvent at the CO_2SEPPL pilot plant is higher because of the lower flue gas CO_2 content in the Kaiserslautern pilot plant. The achievable rich loading is significantly lower than the equilibrium CO_2 loading. The CO_2 equilibrium loading indicated in Fig. 6-13 refers to the absorber sump temperature (the lowest temperature in Fig. 6-21). The equilibrium CO_2 loading drops slightly with increasing solvent flow rate because of the higher absorber sump temperature at high solvent flow rates (Fig. 6-21). The achievable rich loading drops with increasing solvent flow rate, too. The reason is also the higher absorber sump temperature. The difference between achievable rich loading and equilibrium loading remains constant over the measuring range.
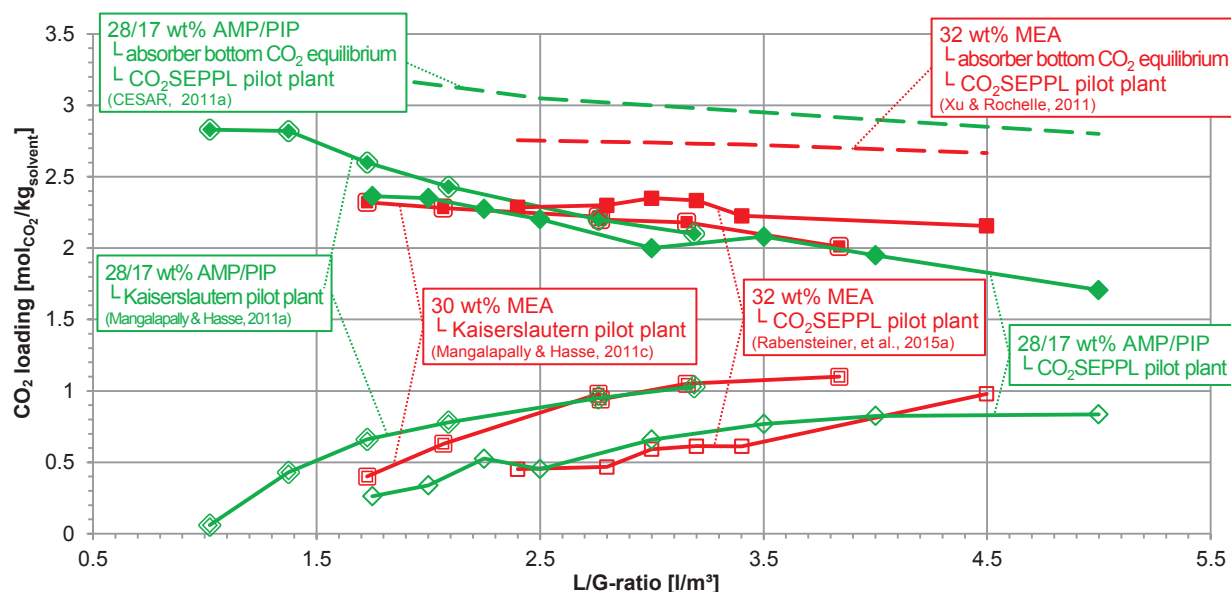
Fig. 6-13: Dependence of the CO_2 loading on the L/G-ratio. Rich (filled symbols) and lean loading (unfilled symbols) for 28/17 wt% AMP/PIP and 30 wt% MEA, measured on the CO_2SEPPL and Kaiserslautern pilot plant.

The equilibrium data for CO_2 solubility is plotted in Fig. 6-14a. CO_2 binding cannot be assigned to the individual amines by simple titration since 28/17 wt% AMP/PIP is a blend of two amines. The CO_2 loading is thus indicated in $mol_{CO_2}/kg_{solvent}$, unlike the remaining solvents tested, which consist of only one active component. The marked area indicates the flue gas CO_2 content of a hard coal-fired power plant. Looking at the absorber bottom temperature (lowest temperature in Fig. 6-21), one can see that equilibrium CO_2 loading is not achieved at the CO_2SEPPL pilot plant when using 28/17 wt% AMP/PIP.

The process with 28/17 wt% AMP/PIP benefits from the high CO_2 partial pressure at the desorber top. The required CO_2 partial pressure at the desorber top (approximation with the solubility curve for 120 °C and the lean CO_2 loading of 0.34 $mol_{CO_2}/kg_{solvent}$) is about 9 kPa for the optimal operating point (L/G-ratio = 2.0 l/m³). The CO_2 partial pressure at the desorber top is significantly lower when using 30 wt% MEA. The value is approximately 5 kPa for the optimal operating point (L/G-ratio = 3.2 l/m³). The equilibrium data by Xu & Rochelle (2011) were used for the calculation of this value. Low amounts of stripping steam have to be generated when using 28/17 wt% AMP/PIP in comparison to the process with 30 wt% MEA. The heat of vaporization required to generate the water vapor (q_{vap,H_2O}) in the desorber drops significantly. The specific energy for solvent regeneration decreases according to Eq. 6-3 and Eq. 6-4.

The heat of CO_2 absorption for a similar AMP/PIP solvent (24/12 wt% AMP/PIP) in comparison to 30 wt% MEA is shown in Fig. 6-14b. The CO_2 loading in this diagram is indicated in $mol_{CO_2}/mol_{equ.\ amine}$ as usual. 30 wt% MEA and 24/12 wt% AMP/PIP show a progressive decline in the CO_2 absorption heat with an increase in CO_2 loading (Xie, et al., 2013; Xu & Rochelle, 2011). At low CO_2 loadings, the AMP/PIP solvent has a significantly reduced heat of CO_2 absorption. The significant energy saving in comparison to the process with 30 wt% MEA can be partially attributed to the reduced amount of heat required to strip the CO_2 from the solution (q_{abs,CO_2}).

The optimal solvent flow rate is significantly lower when using 28/17 wt% AMP/PIP in comparison to the process with 30 wt% MEA. Data about the specific heat capacity of AMP/PIP solvents are not available in the literature. Nevertheless, only a small part of the energy saving can be attributed to the lower sensible heat for solvent heat up (q_{sens}). The reason is the significantly higher temperature difference between the desorber sump and desorber inlet temperature at the optimal operating point when using 28/17 wt% AMP/PIP. This temperature difference is increased by 31 % when using 28/17 wt% AMP/PIP in comparison to the optimal operation point of the MEA-process. The solvent flow rate is reduced by 37.5 % when using 28/17 wt% AMP/PIP in comparison to the optimal operation point of the MEA-process. q_{sens} therefore drops only slightly in comparison to the process with 30 wt% MEA.
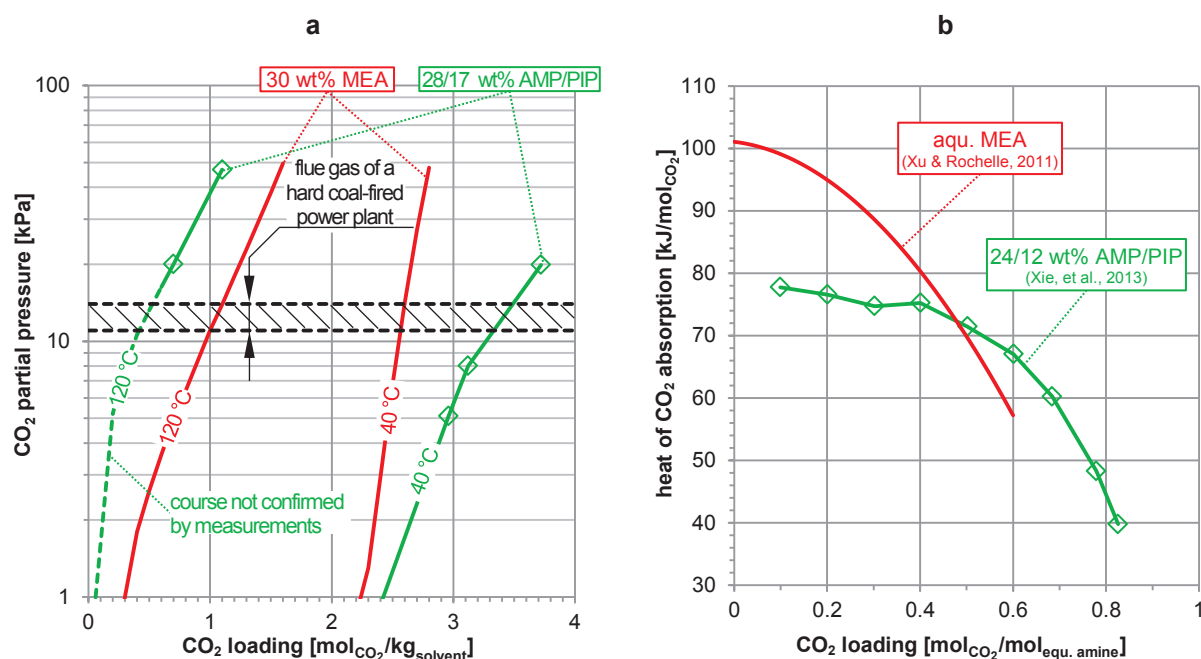
Fig. 6-14: **(a)** CO_2 solubility data for 28/17 wt% AMP/PIP and 30 wt% MEA (CESAR, 2011a). **(b)** Heat of CO_2 absorption for 24/12 wt° AMP/PIP (3/1.5 M AMP/PIP) and aqueous MEA (data regressed by Xu & Rochelle (2011) hold true for 17.6 to 44.3 wt% MEA) at 40 °C.

Fig. 6-15 shows the CO_2 loading of the rich and lean solvents as a function of the L/G-ratio for aqueous piperazine. The CO_2 loading difference between the rich and lean solvents is reduced if the L/G-ratio is increased. The CO_2 equilibrium loading indicated in Fig. 6-15 refers to the absorber sump temperature (the lowest temperature in Fig. 6-20). The equilibrium CO_2 loading drops slightly with increasing solvent flow rate because of the higher absorber sump temperature at high solvent flow rates (Fig. 6-20). 37.6 wt% PIP reaches no equilibrium loading in the absorber sump. The rich loading decreases slightly by increasing L/G-ratio. The reason for this is the higher temperature in the absorber column (Fig. 6-20). A high temperature reduces the equilibrium CO_2 loading of the aqueous piperazine solution (Fig. 6-16). The difference between achievable rich loading and equilibrium loading remains constant over the measurement range.

The comparison of the measured CO_2 loadings of the regenerated solvent shown in Fig. 4-3 demonstrates the risk of solidification over the entire range studied. The CO_2 loading of the regenerated solvent is at the edge of the solidification range under operating conditions when

small L/G-ratios are set. There is a particular risk of fast solidification in the regenerated solvent line between desorber and absorber, in case of a system failure. The entire line has to be trace heated during a brief system failure. A temperature above 35 to 40 °C (depending on the L/G-ratio) must be maintained at all times. The entire solvent inventory must circulate twice without regeneration to increase the CO_2 loading in order to ensure a safe plant shutdown at lower outdoor temperatures.

In addition to the three measurement points generated on the J.J. Pickle pilot plant, which were carried out under similar operating parameters as in the CO_2SEPPL pilot plant, CO_2 loadings of the remaining measurement points are plotted in Fig. 6-15. Higher CO_2 loadings and smaller CO_2 loading differences are recognized. The reason must be a lower CO_2 separation efficiency due to the same CO_2 flue gas concentration as in the CO_2SEPPL pilot plant. The absorption temperatures are significantly lower than in the CO_2SEPPL pilot plant because of the low inlet temperature of the artificially generated flue gas. This leads to higher CO_2 loadings of the enriched solvent. Solidification can easily be prevented thanks to the higher CO_2 loading of the regenerated solvent and the warmer climate in Austin. Higher CO_2 loadings by absorber intercooling cannot be reached at this pilot plant according to the measurement results of Chen, et al. (2010). The already low absorption temperature could be one reason for this.

The measured CO_2 loading at the Tarong pilot plant during operation is between 0.26 and 0.44 $mol_{CO_2}/mol_{equ.\ amine}$ (Fig. 4-3) (Cottrell, et al., 2013). Thus, also significantly higher CO_2 loadings were measured during operation of this system. The reason for this is the integrated absorber intercooler which increases the CO_2 equilibrium pressure, especially in the lower part of the column. A significant increase in CO_2 loading in the absorber column has already been proven by Sanpasertparnich, et al. (2011).
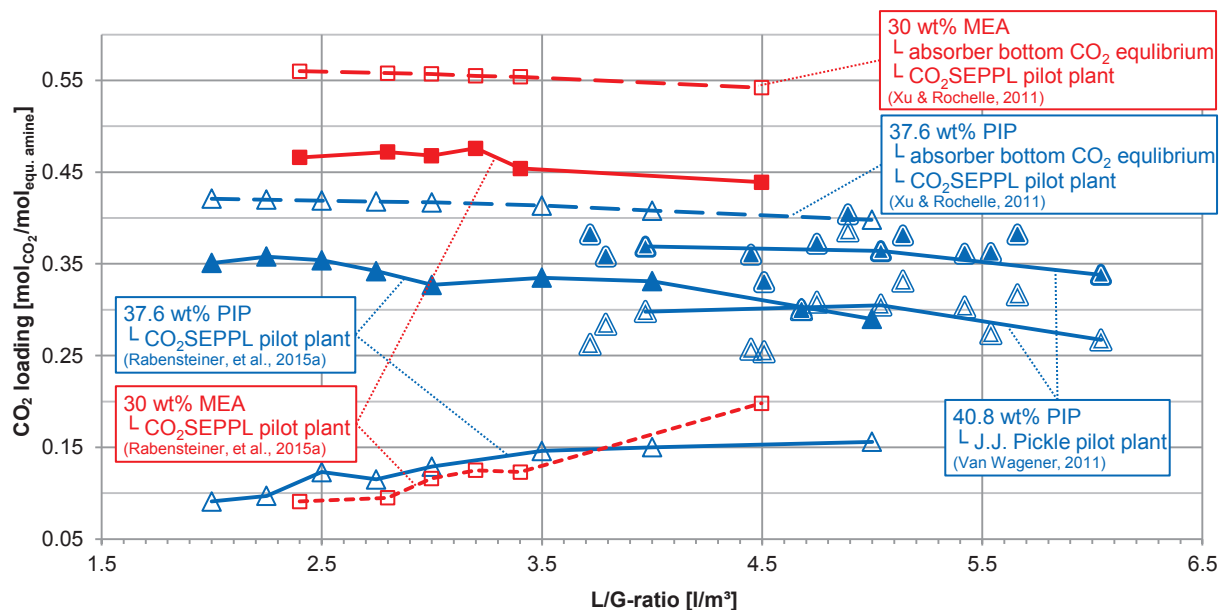
Fig. 6-15: Dependence of CO_2 loading on the L/G-ratio. Measured CO_2 loading of the rich (filled symbols) and lean solvent (unfilled symbols). Experimental data for concentrated piperazine generated at the CO_2SEPPL and J.J. Pickle pilot plant. Measurement results from Van Wagener (2009) connected with a line are the three measurement points in Fig. 6-8, where similar operating parameters as at the CO_2SEPPL pilot plant were set. The dashed lines indicate the equilibrium CO_2 loading at the prevailing temperature in the CO_2SEPPL pilot plant (according Fig. 6-16).

Fig. 6-16 shows the CO_2 solubility data of aqueous piperazine and monoethanolamine. The temperatures in the absorber and desorber are approximately 40 and 120 °C respectively. The marked area indicates the flue gas CO_2 content of a hard coal-fired power plant. Considering the absorber bottom temperature (lowest temperature in Fig. 6-20), it´s possible to recognize that equilibrium CO_2 loading cannot be achieved at the CO_2SEPPL pilot plant by using 37.6 wt% PIP. Aqueous MEA and PIP show a progressive decline in the CO_2 absorption heat with an increase in CO_2 loading. The CO_2 absorption heat of aqueous piperazine is significantly lower than of aqueous monoethanolamine. The significant energy saving in comparison to the process with 30 wt% MEA can mainly be attributed to the lower heat required to strip the CO_2 from the solution (q_{abs,CO_2}) when using 37.6 wt% PIP.

The process with 37.6 wt% PIP benefits from the high CO_2 partial pressure at the desorber top. The required CO_2 partial pressure at the desorber top (approximation with the solubility curve for 120 °C and the lean CO_2 loading of 0.12 $mol_{CO_2}/mol_{equ.\ amine}$) is about 7 kPa for the optimal operating point (L/G-ratio = 2.5 l/m³). The CO_2 partial pressure at the desorber top is slightly lower when using 30 wt% MEA. The value is approximately 5 kPa for the optimal operating point (L/G-ratio = 3.2 l/m³). The equilibrium data by Xu & Rochelle (2011) were used for the calculation of this value. Slightly lower amounts of stripping steam have to be generated when using 37.6 wt% PIP in comparison to the process with 30 wt% MEA. The heat of vaporization required to generate the water vapor (q_{vap,H_2O}) in the desorber drops. The specific energy for solvent regeneration decreases according to Eq. 6-3 and Eq. 6-4.

The lower solvent flow rate results in less solvent that must be heated in the desorber. The specific heat capacity of the solvents is dependent on the CO_2 loading and temperature (Fig. 6-9). The specific heat capacities at the average CO_2 loading and desorber column temperature are equal for 30 wt% MEA and 37.6 wt% PIP (in Fig. 6-9 approximate with 40.8 wt% PIP). The heat transfer coefficient in the main heat exchanger is lower because of the reduced solvent flow rate, when using 37.6 wt% PIP. The high viscosity of piperazine reduces the heat transfer further. The temperature difference of the liquid phase in the desorber column (difference of the desorber sump temperature and incoming solvent temperature) is therefore higher when using 37.6 wt% PIP. Nevertheless, approximately 13 % of the sensible heat (q_{sens}) can be saved, compared to the process with 30 wt% MEA.
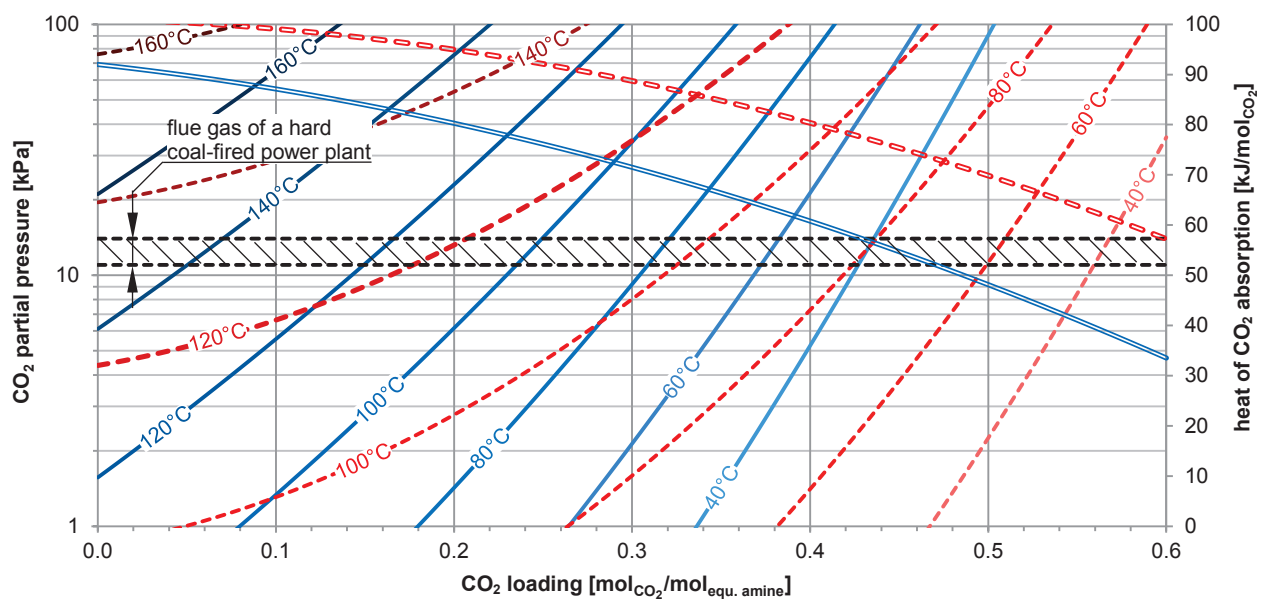
Fig. 6-16: CO_2 solubility (single line) and heat of CO_2 absorption at 40 °C (double line) regressed by Xu & Rochelle (2011) cover 7.2 to 50.4 wt% PIP (solid line) and 17.6 to 44.3 wt% MEA (dashed line).

Fig. 6-17 shows the CO_2 loading (a) and the flue gas CO_2 content (b) across the absorber height at different L/G-ratios when using 37.6 wt% PIP. The majority of CO_2 is absorbed in the upper part of the absorber column at low solvent flow rates. The region of the maximum CO_2 absorption moves downwards with increasing solvent flow rate. Fig. 6-17c shows the CO_2 loading of 28/17 wt% AMP/PIP across the absorber height at different L/G-ratios. No CO_2 absorption occurs at the upper half of the absorber column at L/G-ratios higher than 4 l/m³. In contrast, CO_2 is still absorbed over the entire absorber column at an L/G-ratio of 5 l/m³ when using 37.6 wt% PIP. Only a part of the column height is effectively used for CO_2 absorption at high solvent flow rates. The CO_2 absorption in the lowest quarter of the column is also very limited for all examined solvent flow rates.
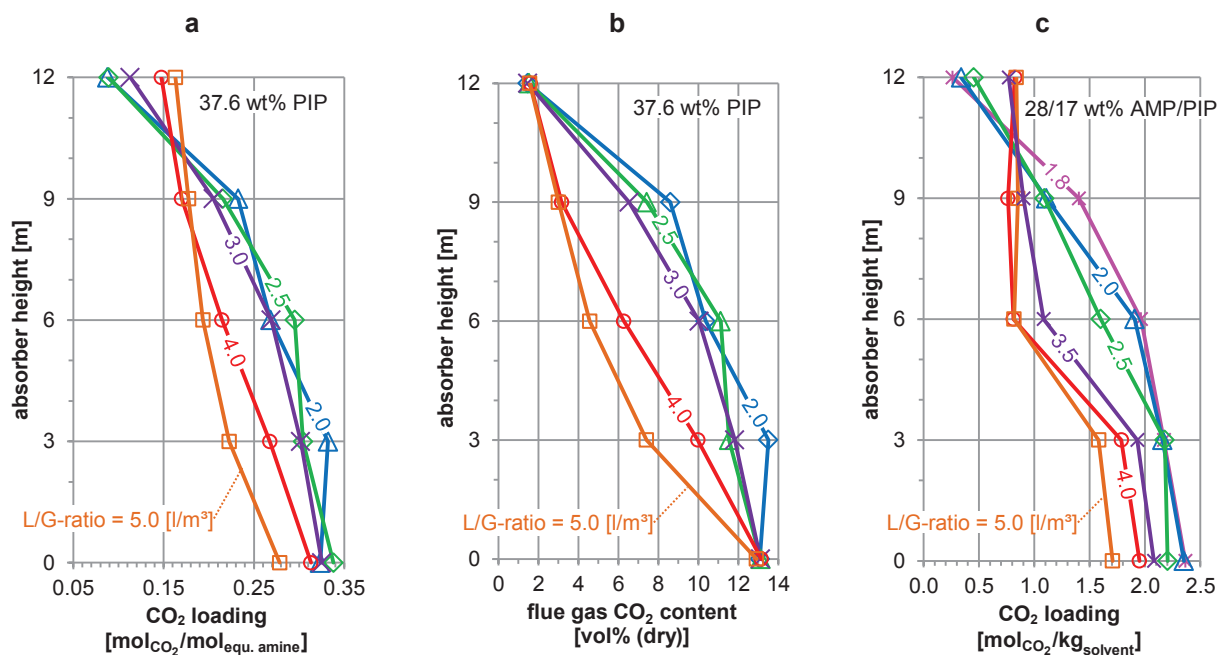
Fig. 6-17: Solvent CO_2 loading **(a)** and flue gas CO_2 content **(b)** across the absorber height when using 37.6 wt% PIP (Rabensteiner, et al., 2015a). CO_2 loading of 28/17 wt% AMP/PIP across the absorber height **(c)**.

6.3.4.2 Amino acids

CO_2 equilibrium loading cannot be reached in the absorber column for aqueous amino acids, when one compares the VLE-data of Fig. 4-12 with the CO_2 loadings of the rich solvent (Fig. 6-18). The equilibrium loading at the prevailing CO_2 partial pressure for 25 wt% NaGly is 0.58 $mol_{CO_2}/mol_{equ.\ amine}$ (approximation from the VLE-data of 30 wt% NaGly in Fig. 4-12). Due to the influence of the limited CO_2 absorption rate and contact time, only a CO_2 loading of 0.5 $mol_{CO_2}/mol_{equ.\ amine}$ can be achieved. Similar CO_2 loadings are possible when using 30 wt% MEA. The equilibrium CO_2 loading in this case is only 0.52 $mol_{CO_2}/mol_{equ.\ amine}$. The kinetics of NaGly strongly influence the measurement results. This explains the large deviation between the measured values and the simulation results. The kinetics of CO_2 absorption are neglected in the simulations.

The CO_2 loading of the regenerated solvent has to be lowered in the desorber due to the lower achievable CO_2 loading in the absorber column, which affects the entire process. To help explain the relationship between these factors, here is an example using the measurement results of the optimum operating point. A CO_2 loading of 0.47 $mol_{CO_2}/mol_{equ.\ amine}$ can be achieved in the absorber column when using 25 wt% NaGly and the L/G-ratio is set to 8 l/m³. This corresponds to a reduction of 0.09 $mol_{CO_2}/mol_{equ.\ amine}$ in comparison to the equilibrium loading. The measured CO_2 lean loading of this measurement point is 0.22 $mol_{CO_2}/mol_{equ.\ amine}$. This leads to a required equilibrium CO_2 partial pressure at the desorber top of about 2 to 3 kPa according to the VLE-data in Fig. 4-12 (assumption: desorber top temperature is 120 °C). The solvent would have to be regenerated only to about 0.31 $mol_{CO_2}/mol_{equ.\ amine}$ if equilibrium CO_2 loading can be achieved in the absorber. This corresponds to an equilibrium CO_2 partial pressure of about 8 kPa. For 30 wt% MEA and an L/G-ratio of 3.2 l/m³, the change of the CO_2

partial pressure because of kinetic effects is in the same order of magnitude. The partial pressures are significantly higher though when using MEA. More stripping steam has to be generated when using 25 wt% NaGly. A lowering of the rich loading leads to enormous increase in energy demand. This can also be seen in Fig. 6-41. Unfavorable conditions are created through the interaction of kinetics and VLE-properties of NaGly.

This interaction is another reason for the high solvent flow rate required. Fewer active components are available for the same amount of carbon dioxide when the NaGly concentration is decreased at a constant L/G-ratio. However, the CO_2 loading difference between rich and lean solvents has to be increased. The solvent has to be heavily regenerated, leading to an increase of the specific energy for solvent regeneration. The gradient of the heat of evaporation below the optimal operating point is steeper than the gradient of sensible heat for L/G-ratios above the optimal operating point (compare Fig. 6-10). The minimum of sensible heat and heat of evaporation shifts to higher solvent flow rates if the NaGly concentration is decreased.

The maximum CO_2 loading is reached at low solvent flow rates. There is only a small decrease in the rich CO_2 loading with an increasing L/G-ratio. The smaller decrease of the rich loading compared to 30 wt% MEA can be explained by the lower temperature differences in the absorber in the investigated range of operation (Fig. 6-22). The temperature in the absorber sump increases significantly when using 30 wt% MEA and changing the L/G-ratio from 2.0 to 4.5 l/m³. The higher temperature leads to a lower equilibrium CO_2 loading.
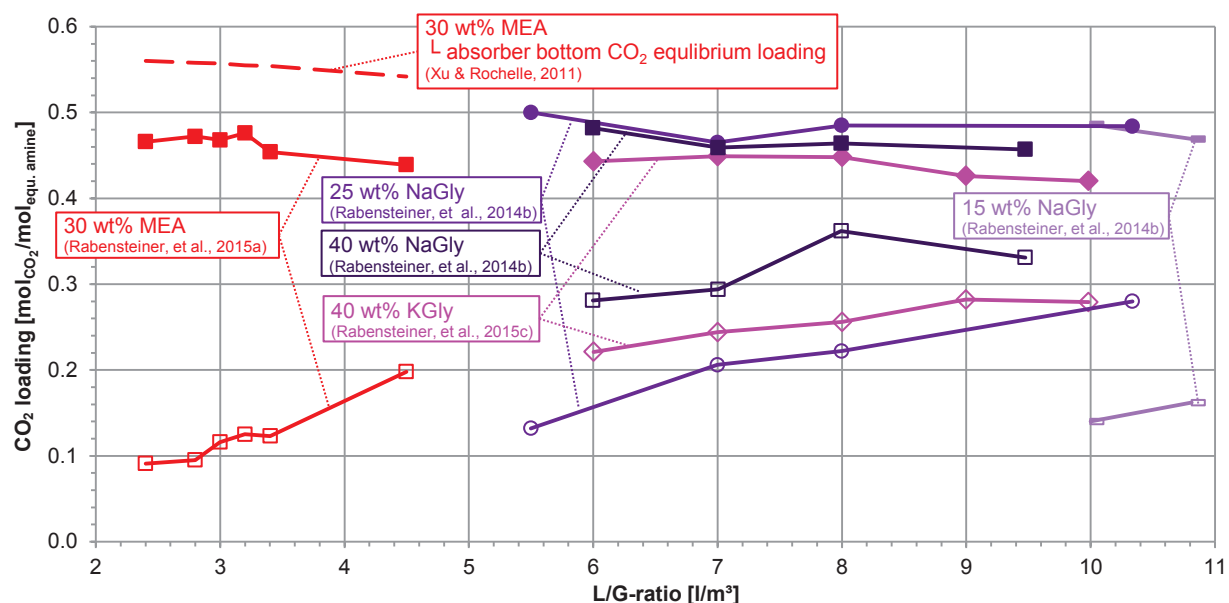
Fig. 6-18: Dependence of the CO_2 loading on the L/G-ratio. Measured CO_2 loading of the rich (filled symbols) and lean solvent (unfilled symbols) for aqueous NaGly and KGly and 30 wt% MEA.

Only VLE-data of aqueous KGly solutions up to KGly concentrations of 30 wt% are given in Portugal, et al. (2009) (Fig. 4-12). A trend can be observed with regard to the existing equilibrium CO_2 partial pressure in the absorber bottom when considering lower concentrated KGly solvents (1.13 and 10.78 wt% KGly). An equilibrium CO_2 loading of 0.6 $mol_{CO_2}/mol_{equ.\ amine}$ of 40 wt% KGly can be assumed for the existing CO_2 partial pressure of the untreated flue gas. The equilibrium CO_2 loading measured in the present work is slightly

lower in comparison to the values from Portugal, et al. (2009); therefore, it is possible to assume a slightly lower equilibrium CO_2 loading at the prevailing CO_2 partial pressure.

Equilibrium loading cannot be reached in the absorber column when using 40 wt% KGly either (Fig. 6-18). Because of the limited CO_2 absorption rate and contact time of the gaseous and liquid phase, only a CO_2 loading of 0.45 $mol_{CO_2}/mol_{equ. amine}$ can be achieved. The achievable CO_2 loading in the absorber column is even lower with aqueous NaGly, which has similar equilibrium CO_2 partial pressures. VLE data for aqueous KGly at higher temperatures are not available. It can be assumed that the same problem exists as for aqueous NaGly.

6.3.5 Absorption temperature

6.3.5.1 Amine-based solvents

The temperature of the treated flue gas is measured at a height of 12 m. The lowest temperature sensor is located in the sump of the absorber column and measures the temperature of the enriched solvent. The eleven intermediate temperature sensors measure a combination of the solvent and flue gas temperature which is denoted as absorption temperature in the following.

Fig. 6-19 shows the temperature profile of the absorber column for 32 wt% EDA. The highest absorption temperature is in the vicinity of the inlet of the regenerated solvent. The large temperature change at the top of the column suggests an intense reaction of carbon dioxide with the absorption solvent. The temperature in the lower part of the absorber column decreases due to the heat transfer from the liquid to the gaseous phase. Excessive solvent flow from the top to the bottom of the absorber column causes high downward transport of the absorption heat. The temperature across the entire lower absorber column increases at high solvent flow rates.

The temperature of the enriched solvent increases at high solvent flow rates. The temperature of the treated flue gas (top temperature measurement point) drops according to the law of energy conservation. This can be confirmed by the temperature profile.
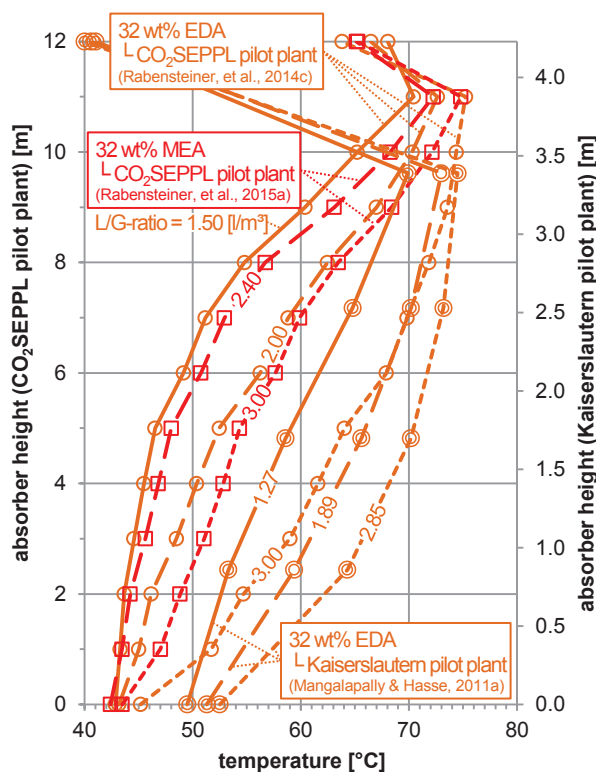
Fig. 6-19: Dependence of the absorber temperature profile on the L/G-ratio. Experimental data for 32 wt% EDA and 30 wt% MEA.

The CO_2 absorption heat for MEA and EDA increases at high temperatures (Fig. 6-12). Zhou, et al. (2010) investigate the absorption enthalpy of 42 wt% EDA. The concentration of MEA has little effect on the absorption enthalpy according to Carson, et al. (2000). If this behavior is assumed for EDA, then the curve of Zhou, et al. (2010) can be used for comparison, indicating a higher absorption enthalpy of EDA for low CO_2 loading numbers. The high absorption enthalpy of EDA in the upper part of the absorber column can contribute higher absorption temperatures.

For the purpose of comparing the measurement results of the Kaiserslautern pilot plant (which is only 4.25 m high) with the experimental data of the CO_2SEPPL pilot plant (Fig. 6-18), the temperature profiles have been adjusted in length. The temperature in the low part of the absorber rises particularly high due to the increased temperature of the entering flue gas (47 °C). The higher temperature is another reason for the low CO_2 loading of the rich solvent. The highest measuring point is located in the washing section and the corresponding temperature measured is in the range of 40 °C.

The temperature profile of 37.6 wt% PIP looks similar to that of 32 wt% EDA (Fig. 6-20). The temperature of the enriched solvent increases at high solvent flow rates whereas the temperature of the treated flue gas drops. This can be confirmed by the temperature profile. The same theoretical consideration is confirmed by the measured temperatures in the absorber column of the J.J. Pickle pilot plant. The prevailing absorption temperatures are generally lower than in the absorber of the CO_2SEPPL pilot plant because of the low inlet temperature of the flue gas (8 to 21 °C).

97
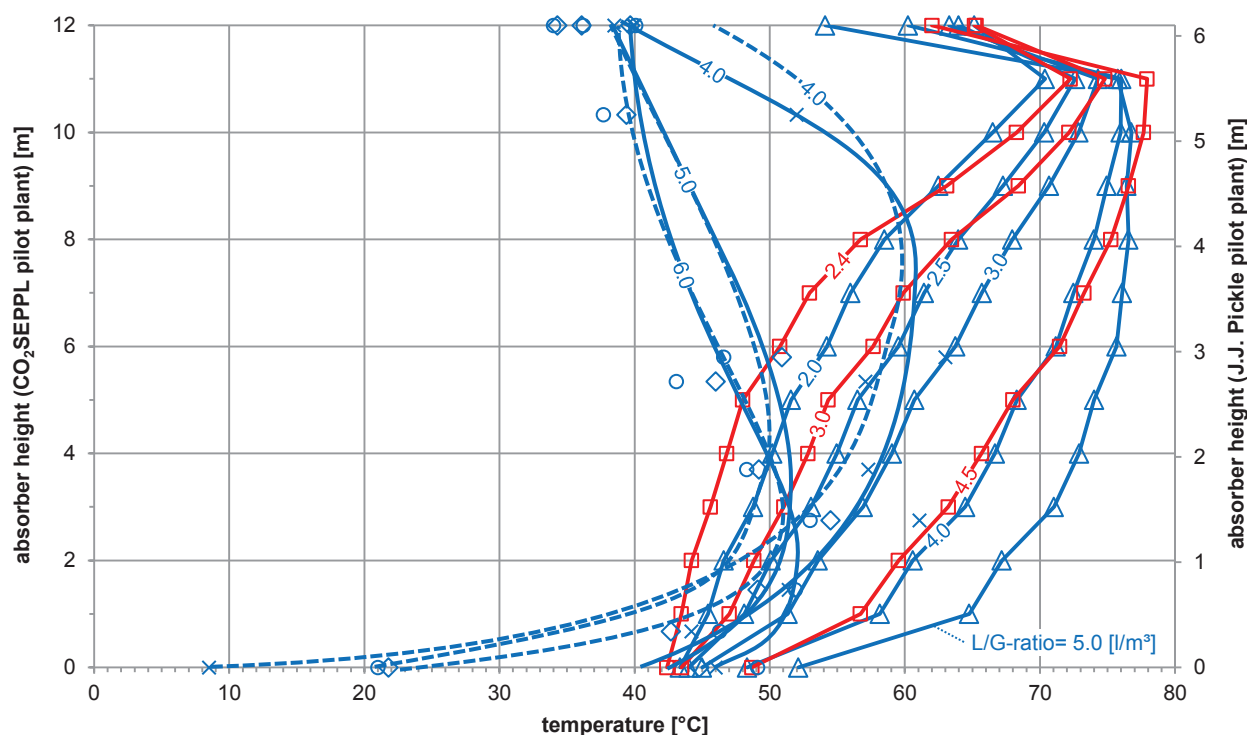
Fig. 6-20: Dependence of the absorber temperature profile on the L/G-ratio. Experimental data for 37.6 wt% PIP (Δ) and 30 wt% MEA (□) from the CO₂SEPPL pilot plant. The measured absorber temperature in the J.J. Pickle pilot plant for aqueous piperazine and L/G-ratios of 4.0 (X), 5.0 (◇) and 6.0 l/m³ (○) are also illustrated. The solvent temperature (solid line) and flue gas temperature (dashed line) was reconciled by Plaza (2011).

Fig. 6-21 shows the temperature profile of the absorber column for 28/17 wt% AMP/PIP. The temperature profiles have been adjusted in length in order to compare the measurement results of the Kaiserslautern pilot plant (which is only 4.25 m high) with the experimental data from the CO₂SEPPL pilot plant.
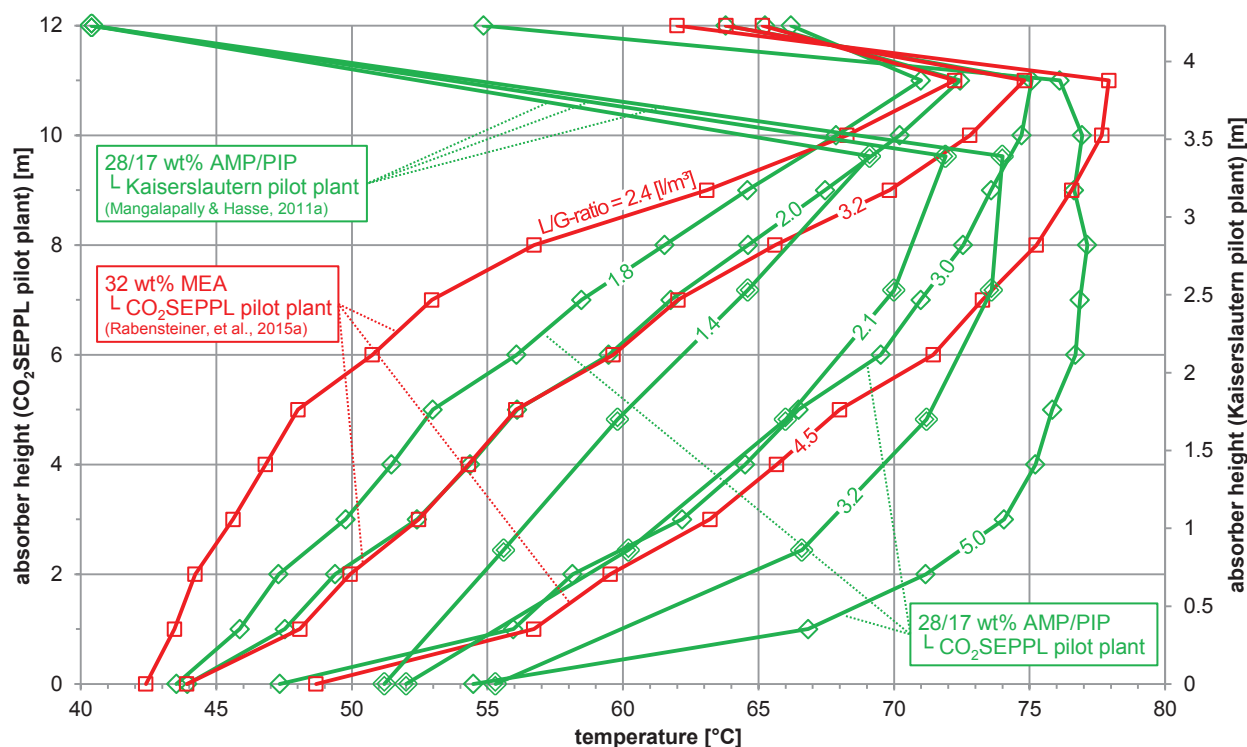
Fig. 6-21: Dependence of the absorber temperature profile on the L/G-ratio. Experimental data for 28/17 wt% AMP/PIP and 30 wt% MEA.

6.3.5.2 Amino acids

No large changes in the absorption temperature are visible for 25 wt% NaGly by varying solvent flow rate (Fig. 6-22b). The maximum absorption temperature is usually located directly below the inlet of the regenerated solvent. An exception is the increase of the L/G-ratio from 8.0 to 10.3 l/m³. There is a shift of the temperature curve over the entire absorber column. The maximum temperature is only 57 °C and occurs in the lower part of the column when the L/G-ratio is set to 10.3 l/m³. The reason for the sharp drop in absorption temperature is a balance in the enthalpy leaving with the liquid and the flue gas when the temperature bulge is located somewhere in the middle of the absorber column (Kvamsdal & Rochelle, 2008). This operation point is located between an L/G-ratio of 8.0 and 10.3 l/m³ when using 25 wt% NaGly (Fig. 6-22b) and between 7.0 and 8.0 l/m³ when using 40 wt% NaGly (Fig. 6-22c). A further increase of the solvent flow rate leads to reaching this critical value, which can be seen by a rapid change in the temperature of the temperature profile. The sharp temperature drop occurs exactly at the point where the treated flue gas temperature (highest temperature sensor) goes below 40 °C (Fig. 6-22b and Fig. 6-22c).

For 15 wt% NaGly, the temperature of the treated flue gas is below 40 °C when the smallest possible solvent flow rate (L/G-ratio = 10.0 l/m³) is set (Fig. 6-22a). The balance between the enthalpy of the liquid and the flue gas (Kvamsdal & Rochelle, 2008) consequently occurs at an L/G-ratio below 10.0 l/m³.
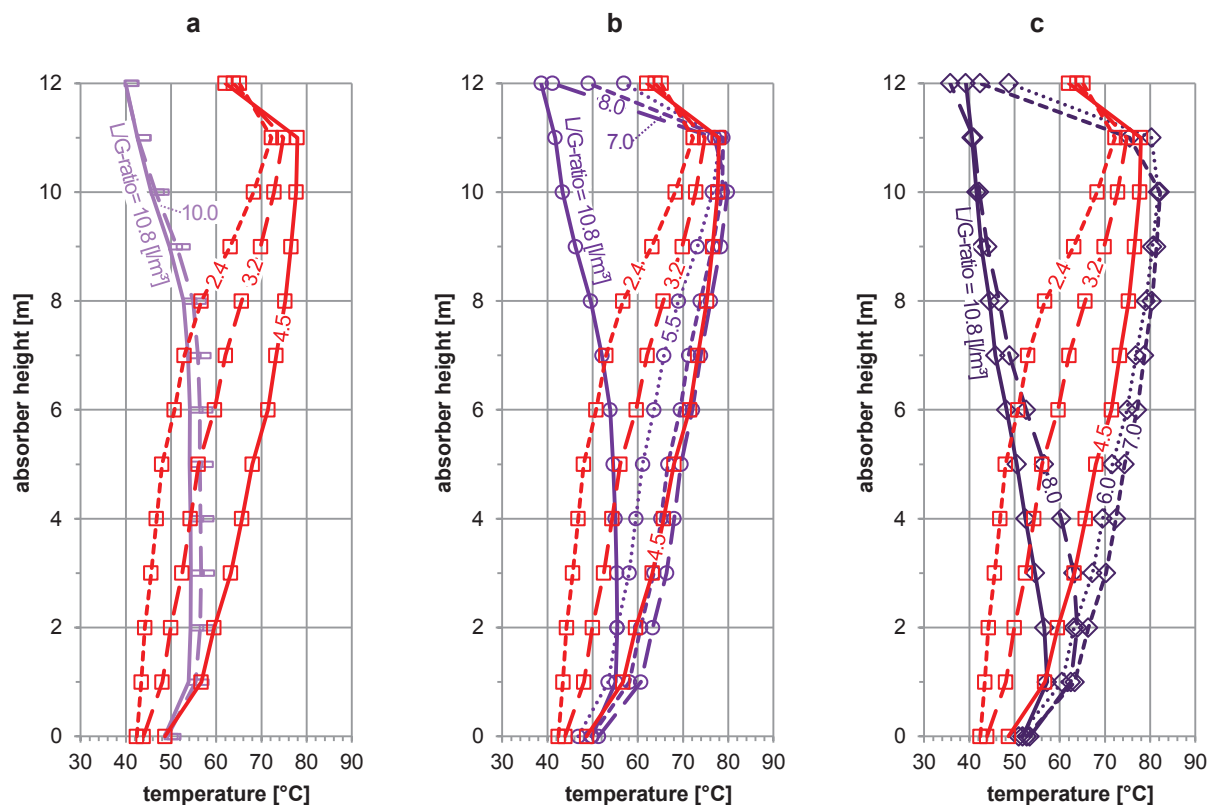
Fig. 6-22: Dependence of the absorber temperature profile on the L/G-ratio. Experimental data for 15 wt% NaGly **(a)**, 25 wt% NaGly **(b)** and 40 wt% NaGly **(c)** from Rabensteiner, et al. (2014b) and 30 wt% MEA (□) from Rabensteiner, et al. (2015a).

Fig. 6-23 shows the temperature profile of the absorber column for 40 wt% KGly and 40 wt% NaGly. The highest absorption temperature is close to the regenerated solvent inlet at lower solvent flow rates. The large temperature change at the top of the column suggests an intense reaction of carbon dioxide with the solvent. The temperature decreases due to heat transfer from the liquid to the gaseous phase in the lower part of the absorber column. The higher heat capacity of the solvent relative to the flue gas tends to push the heat of reaction to the bottom of the column at higher L/G-ratios (Kvamsdal & Rochelle, 2008). Consequently, the temperature across the lower absorber column increases, and the CO_2 enriched solvent temperature rises. The temperature of the treated flue gas drops according to the total energy balance. The temperature bulge magnitude will approach the solvent temperature limit at high solvent flow rate, while at low solvent flow rate, it will approach that of the gas limit (Kvamsdal & Rochelle, 2008).
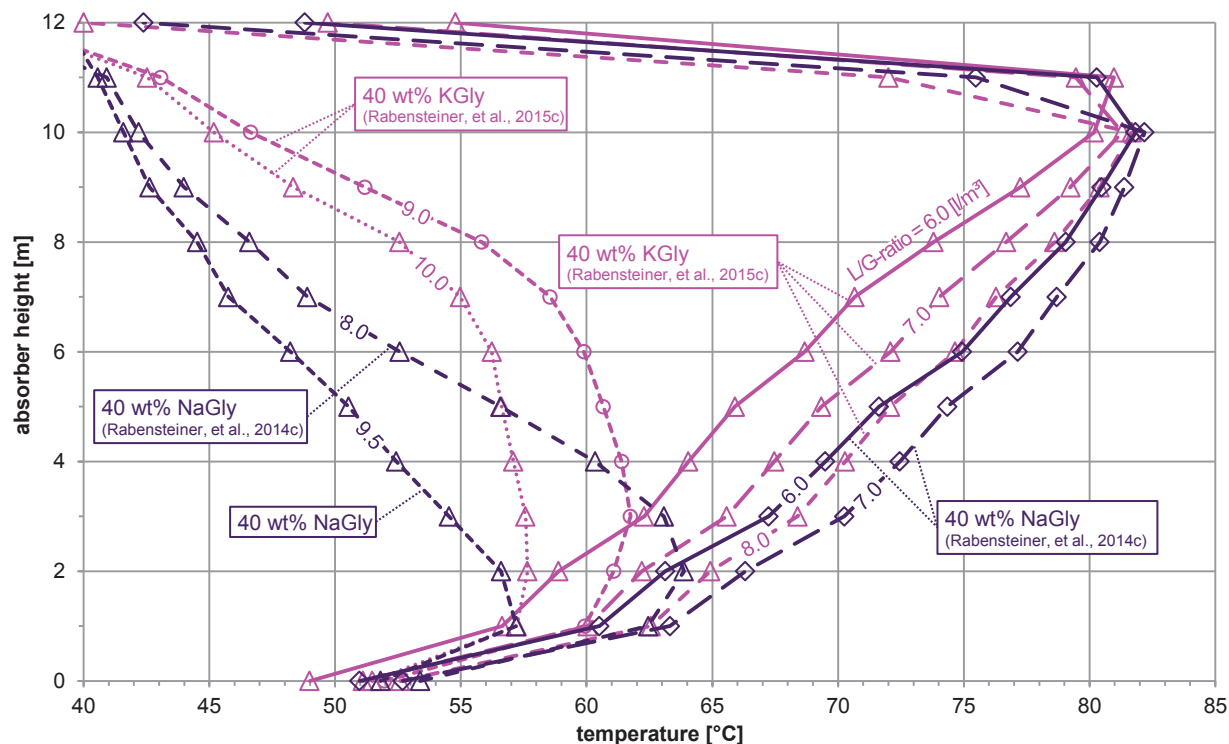
Fig. 6-23: Dependence of the absorber temperature profile on the L/G-ratio. Experimental data for 40 wt% KGly and 40 wt% NaGly.

There is a balance in the enthalpy leaving with the liquid and the flue gas when the temperature bulge is located somewhere in the middle of the absorber column (Kvamsdal & Rochelle, 2008). A further increase of the solvent flow rate leads to this critical value, which can be seen from a rapid change in the temperature of the liquid and flue gas leaving the absorber column. The rapid change in both the treated flue gas and CO_2 enriched solvent outlet temperature seems to appear where the maximal absorption temperature occurs at an absorber height of 10 m (Fig. 6-23). This is consistent with the numerical simulation of Kvamsdal & Rochelle (2008) for 30 wt% MEA. The rapid temperature change happens between an L/G-ratio of 8 and 9 l/m³ when using 40 wt% KGly. This temperature drop can already be observed at an L/G-ratio of between 7 and 8 l/m³ for 40 wt% NaGly. According to Kvamsdal & Rochelle (2008), a higher CO_2 absorption enthalpy of KGly could be the reason. It has been observed that the temperature drop occurs near the optimal operating point.

6.3.6 Pressure loss

The influence of the solvent flow rate on the pressure loss over the absorber column (PIRC 2.2 – PIR 2.3, compare Appendix A1) will be described on the basis of measurement results of 30 wt% MEA and 37.6 wt% PIP. The average pressure loss when using 37.6 wt% PIP is 3.5 mbar higher in comparison to the process with 30 wt% MEA (Fig. 6-24). The increased pressure loss has several possible reasons. The average absorption temperature (shown in Fig. 6-20) when using 37.6 wt% PIP is higher in comparison to the process with 30 wt% MEA. The operating flue gas flow rate in the column increases accordingly, resulting in a growing pressure drop. The dynamic viscosity of the solvent at average CO_2 loading and absorption temperature

is shown in Fig. 6-24. 37.6 wt% PIP has a higher viscosity during operation despite higher absorption temperatures.

The pressure drop dependency on liquid viscosity can be seen from the capacity factor according to traditional flooding and pressure drop charts (Strigle, 1993). The capacity factor is proportional to the square of the gas flow rate and to the liquid viscosity to the power 0.1 (assuming constant liquid density). The liquid hold-up is an important parameter in the pressure drop estimation in the correlations of Rocha, et al. (1993). The liquid hold-up and the pressure drop are expected to increase with increasing liquid viscosity.

The flooding velocity should decrease slightly with increased viscosity (to a power of about 0.05) according to traditional hydraulic diagrams. Experiments from Zakeri, et al. (2011) show a small flooding velocity increase with increased viscosity. This slight effect can be explained by an increased liquid density. The liquid density dependence is given by a power law exponent of -0.5 in a diagram given by Strigle (1993). A liquid density increase of 30 % will have a slightly greater influence on flooding velocity than a 600 % increase in liquid viscosity and is the reason for the observations by Zakeri, et al. (2011).
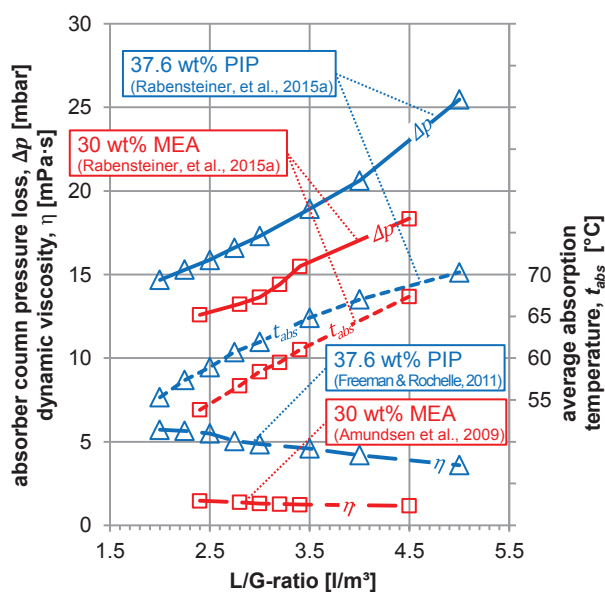
Fig. 6-24:   Absorber column pressure loss, viscosity of the solvent at the average absorption temperature and average absorption temperature as a function of the L/G-ratio for 37.6 wt% PIP and 30 wt% MEA.

The pressure distribution in the desorber column has a major impact on stable pilot plant operation. The power of the desorber heating rod influences the amount of steam generated. For example, when using 30 wt% MEA and changing the L/G-ratio from 2.8 to 2.4 l/m³, the pressure in the desorber sump rises strongly with increasing steam generation (Fig. 6-25). The pressure measured after the desorber washing section remains constant. The amount of steam is much higher for the amino acids used (represented by 40 wt% NaGly and 40 wt% KGly in Fig. 6-25), resulting in higher desorber sump pressures. The high solvent stream, which flows downstream in the desorber column, increases the desorber pressure further. The risk of solvent loss via the condensate return line rises with increasing desorber sump pressure,

resulting in unstable operation. A decrease in the flue gas flow rate counteracts this risk of instability during operation. The amount of steam generated and the downstream solvent flow rate as well as the amount of desorbed CO_2 decrease.

A formation of carbonate was observed in the desorber column during operation with 40 wt% KGly, leading to a further increase in desorber sump pressure. The solvent was in circulation for approximatively two weeks after the measurement procedure. Subsequent studies with the same solvent allowed only a stable operation with a flue gas flow rate less than 30 m³/h. There was further apparent deposition of carbonate in the desorber column during this period, resulting in a more sensitive operation.
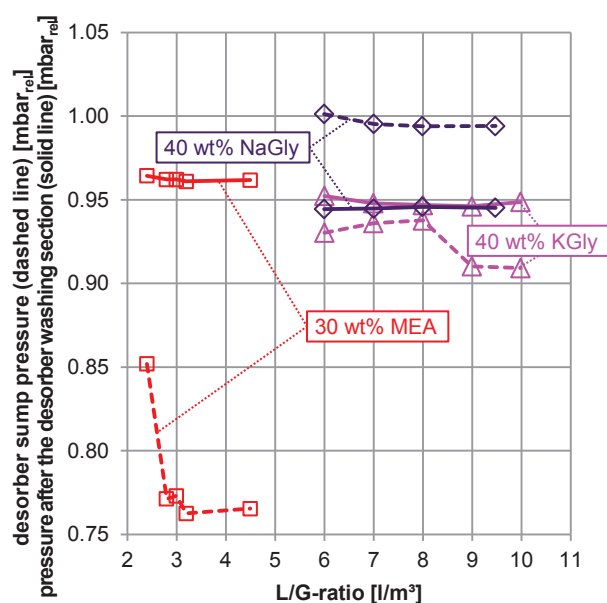
Fig. 6-25:   Pressure distribution in the desorber column (Rabensteiner, et al., 2015c).

6.3.7 Desorber sump temperature

The heat for solvent regeneration is taken from a water vapor stream out of the power plant process at full-scale plants. The desorber sump temperature determines the pressure of the steam which is removed from the power plant process. The desorber sump temperature drops with increasing solvent flow rate (Fig. 6-26). Whereas this temperature drop can be attributed to a low desorber sump pressure for amino acid-based solvents, no correlation of this kind can be found for amine-based solvents. The desorber sump pressure rises with increasing solvent flow rate when using amine-based solvents. The reason for the outlier in desorber sump pressure at a L/G-ratio of 3.4 l/m³ when using 30 wt% MEA is unknown.

The desorber sump temperature at the optimal operating point is similar when using amine-based solvents or 25 wt% NaGly. The desorber sump temperature is in the range of approximately 123 and 124 °C. The desorber sump temperature increases to above 126 °C when using high concentrated amino acid solvents (40 wt% NaGly and 40 wt% KGly).
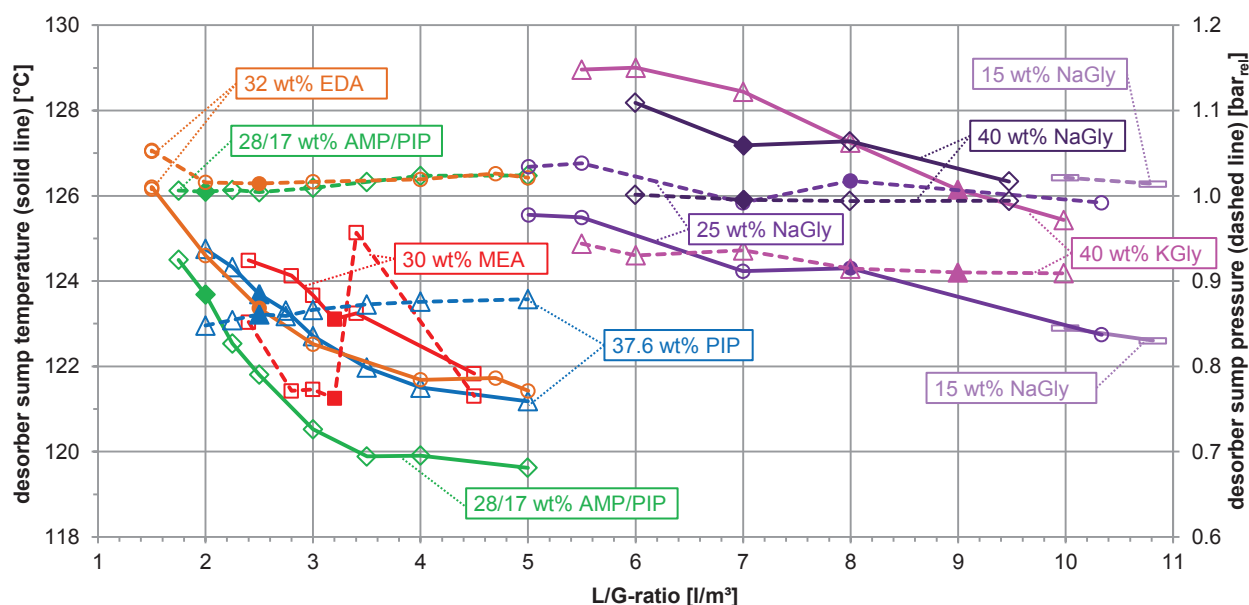
Fig. 6-26:   Desorber sump temperature (solid line) and desorber sump pressure (dashed line) as a function of the L/G-ratio. Filled symbols indicate optimal operating points.

6.4 Variation of the flue gas flow rate

The flue gas flow rate was varied in order to investigate mass transfer in the absorber column. The solvent flow rate is controlled so that the L/G-ratio remains constant. This measurement series allows us to study the kinetic effects. A decrease of the flue gas flow rate reduces the amount of CO_2 transferred between the phases. Less driving force is needed as a consequence. Mass transfer and kinetics limitations (if present) will therefore become less important (Mangalapally & Hasse, 2011a).

6.4.1 Basic considerations

The separation performance of an absorber column is dependent on the gas load of the column. The gas load is expressed by the F-factor (see Footnote 2 on page 54). Gas and liquid flow run with almost no mutual influence at low flue gas flow rates. This results in a low separation performance of the column. The interaction between liquid and gas in the absorber column is more intense at high flue gas flow rates. The separation efficiency increases until the flooding point of the column. The gas stream begins to entrain liquid at the flooding point, resulting in a loss of separation efficiency and drastic increase in energy demand (Sattler, 1988).

A flooding of the Raschig Super-Pak 250-Y structured packing used in the absorber column only occurs at F-factors above 3.5 √Pa (Raschig GmbH, 2015). Flooding is clearly indicated by a soaring *HETP*-value, resulting in a decreasing number of theoretical separation plates. Flooding can be dismissed since the flue gas blower only provides an F-factor of 2 √Pa (~ 120 m³/h) in the absorber column of the CO_2SEPPL pilot plant. Structured packings should be operated as close as possible to the flooding point in order to reach optimal separation efficiency. Normally a gas load of 40 to 80 % of the flooding load is sought (Mendes, 2011).

6.4.2 Measurement results[1]

Table 6-6 shows the most important operating parameters of this test campaign.

Table 6-6: Operating parameters of the test series with varying flue gas flow rate.

	MEA		EDA		PIP	AMP/PIP		NaGly
	CO_2 SEPPL pilot plant	Kaiserslautern pilot plant	CO_2 SEPPL pilot plant	Kaiserslautern pilot plant	CO_2 SEPPL pilot plant	CO_2 SEPPL pilot plant	Kaiserslautern pilot plant	CO_2 SEPPL pilot plant
	(Rabensteiner, et al., 2015a)	(Mangalapally & Hasse, 2011c)	(Rabensteiner, et al., 2014c)	(Mangalapally & Hasse, 2011a)	(Rabensteiner, et al., 2015a)		(Mangalapally & Hasse, 2011a)	(Rabensteiner, et al., 2014b)
Concentration of active substance [wt%]	30	30	32	32	37.6	28/17	28/17	25
└ [molal]	└ 7.0	└ 7.0	└ 7.8	└ 7.8	└ 7.0	└ 4.4/2.4	└ 4.4/2.4	└ 3.4
L/G-ratio [l/m³]	3.20	2.77	2.50	2.52	2.50	2.25	2.76	8.00
Flue gas flow rate [m³/h]	var.	var.	var.	var.	var.	var.	var.	var.
└ F-factor [√Pa]	var.	var.	var.	var.	var.	var.	var.	var.
Desorber pressure [bar$_{abs}$]	2	~ 2[2]	2	~ 2[2]	2	2	~ 2[2]	2
Flue gas CO_2 content [vol% (dry)]	11.6 - 12.7	11.0	11.9 - 12.0	11.0	12.7 - 13.0	12.1 - 13.0	11.0	12.8 - 13.2
Regenerated solvent temperature [°C]	40	40	40	40	40	40	40	40
Flue gas temperature [°C]	40	47	40	47	40	40	47	40
CO_2 separation efficiency[3] [%]	90	90	90	90	90	90	90	90

6.4.2.1 Amine-based solvents

For all amine-based solvents investigated, the specific energy for solvent regeneration drops with increasing flue gas flow rate (Fig. 6-27). The specific energy for solvent regeneration decreases to 3.00 GJ/t$_{CO_2}$ when using 37.6 wt% PIP and the highest possible F-factor of 2 √Pa is reached. This behavior indicates the fact that the reaction rate of piperazine is more than two times faster than that of MEA (Freeman, et al., 2010). At high flue gas flow rates, the energy demand can be reduced to 3.15 GJ/t$_{CO_2}$ when using 32 wt% EDA or 28/17 wt% AMP/PIP. The minimal specific energy for solvent regeneration is 3.50 GJ/t$_{CO_2}$ when using the benchmark solvent 30 wt% MEA. The minimal energy demand for the MEA-process was also measured at the highest possible flue gas flow rate. The curves in Fig. 6-27 show a regressive course. Only the process with 37.6 wt% PIP shows a nearly linear decrease in energy demand with rising flue gas flow rate.

In contrast, the energy demand measured at the Kaiserslautern pilot plant rises with increasing flue gas flow rate. The reason for this is the small number of theoretical separation plates in the absorber column (Table 5-2). The effects of physical and chemical properties of the absorption solvents can be better observed in the CO_2SEPPL pilot plant. The solvent must be heavily regenerated in the desorber due to the maximal loading decrease at high F-factors (Fig. 6-28). This results in an increase of the specific energy for solvent regeneration.

---

[1] Segments of this section have already been published in Rabensteiner, et al. (2014b; 2014c; 2014d; 2015b).

[2] Value in not specified. Pressure can be estimated by desorber temperature stated by Mangalapally & Hasse (2011a; 2011c).

[3] Deviation: ±1 %.

This could demonstrate that the kinetics of MEA, EDA and AMP/PIP are similar. A slightly steeper rise in the measurement curve of EDA as compared to MEA is a sign that the mass transfer kinetics of EDA are slightly slower than those of MEA (Mangalapally & Hasse, 2011a). This fact is also evident in other works (Kemper, et al., 2011; Zhou, 2009). The CO_2 absorption kinetics of AMP/PIP are slightly faster than those of MEA according to the measurement curves of Mangalapally & Hasse (2011a; 2011c) in Fig. 6-27.

The flue gas flow rate affects the desorber sump temperature. The pressure loss in the desorber column rises due to the larger amounts of steam at increasing flue gas flow rates. This results in a slight increase in desorber sump temperature. The fluctuation range of the desorber sump temperature is only 0.5 K (within the investigation area of Fig. 6-27) when using 37.6 wt% PIP, for instance. This effect can therefore be disregarded. The impact of the solvent flow rate on the desorber sump temperature is greater (compare Fig. 6-26).
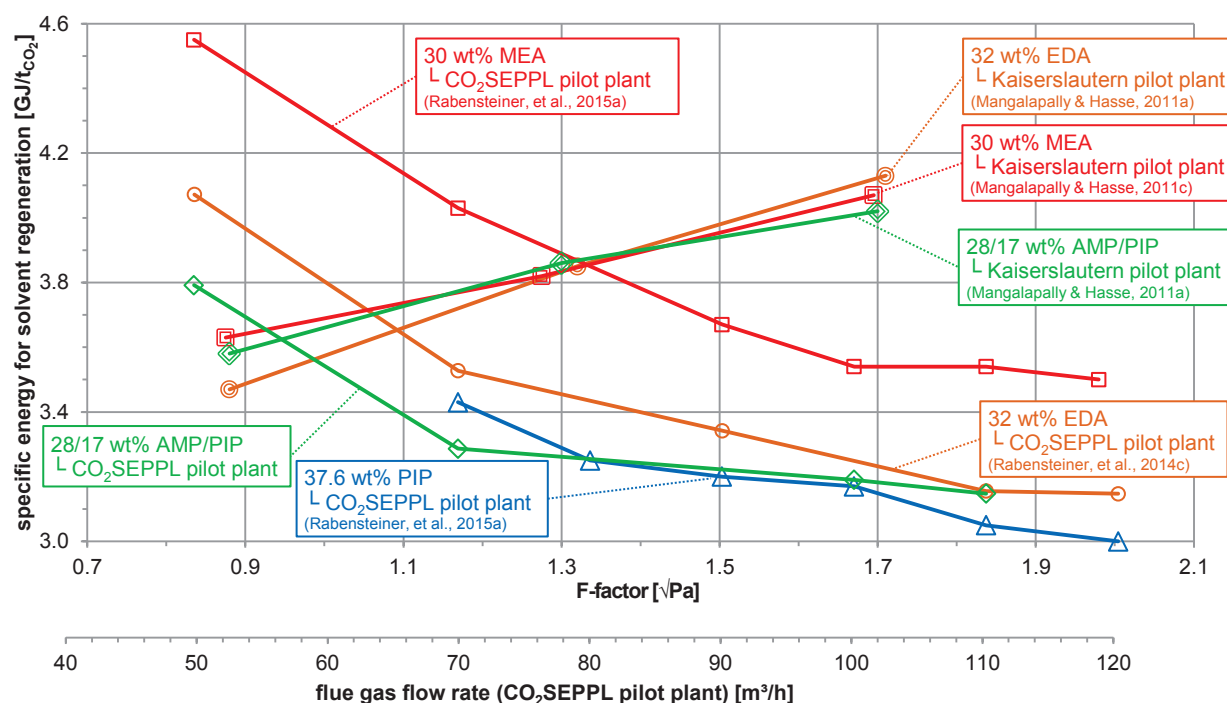
Fig. 6-27: Specific energy for solvent regeneration as a function of the flue gas flow rate.[1]

Fig. 6-28 shows a comparison of the rich and lean loadings for 30 wt% MEA, 32 wt% EDA and 28/17 wt% AMP/PIP as a function of the F-factor. The flue gas flow rate shows no remarkable impact on CO_2 loading despite the slightly higher absorption temperatures at high flue gas flow rates, as depicted in Fig. 6-29 for 30 wt% MEA. The remaining solvents investigated show the same behavior. This confirms the fact that the number of theoretical plates is sufficient for high F-factors.

---

[1] Both the pressure loss and the different absorber temperatures were taken into account when calculating the F-factor.

The influence of kinetics increases with increasing flue gas flow rate at the Kaiserslautern pilot plant. The CO_2 loading of the rich and lean solvents decreases because of the shorter contact time of the liquid and gaseous phase.
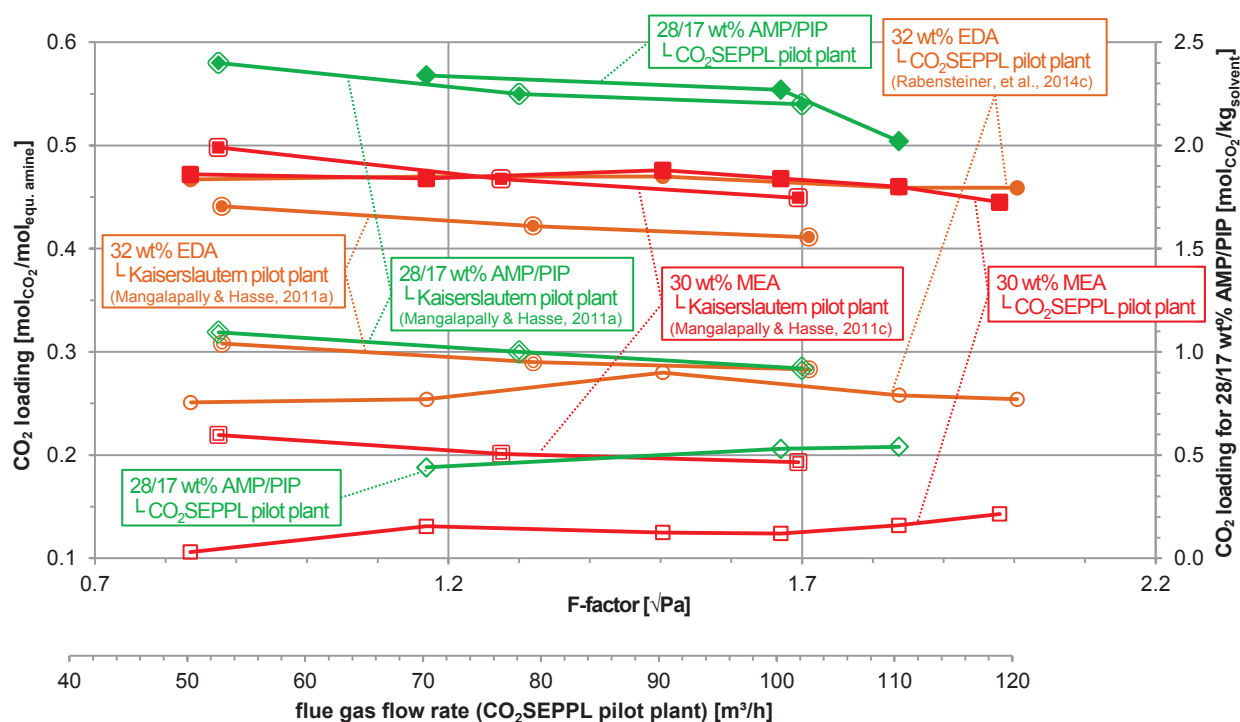
Fig. 6-28:   Dependence of the CO_2 loading of the rich (filled symbols) and lean (unfilled symbols) solvent on flue gas flow rate. Experimental data for 30 wt% MEA, 32 wt% EDA and 28/17 wt% AMP/PIP.

The maximal absorption temperature was always detected in the vicinity of the lean solvent inlet for the amine-based solvents investigated. A low flue gas flow rate shifts the temperatures in the absorber column to lower values. The released heat of CO_2 absorption rises with increasing the F-factor. This leads to an increase in the absorber temperature. Fig. 6-29 shows this behavior, based on 30 wt% MEA. The temperatures of the flue gas treated (highest temperature) and the absorber sump temperature (lowest temperature) increase to the same extent. The absorber sump temperature rises from 43.8 to 44.8 °C when the F-factor is increased from 1.17 to 1.98 √Pa. The treated flue gas temperature rises from 63.8 to 65.6 °C for the same case.

The temperature curve of 25 wt% NaGly in Fig. 6-29 will be explained in Section 6.4.2.2.
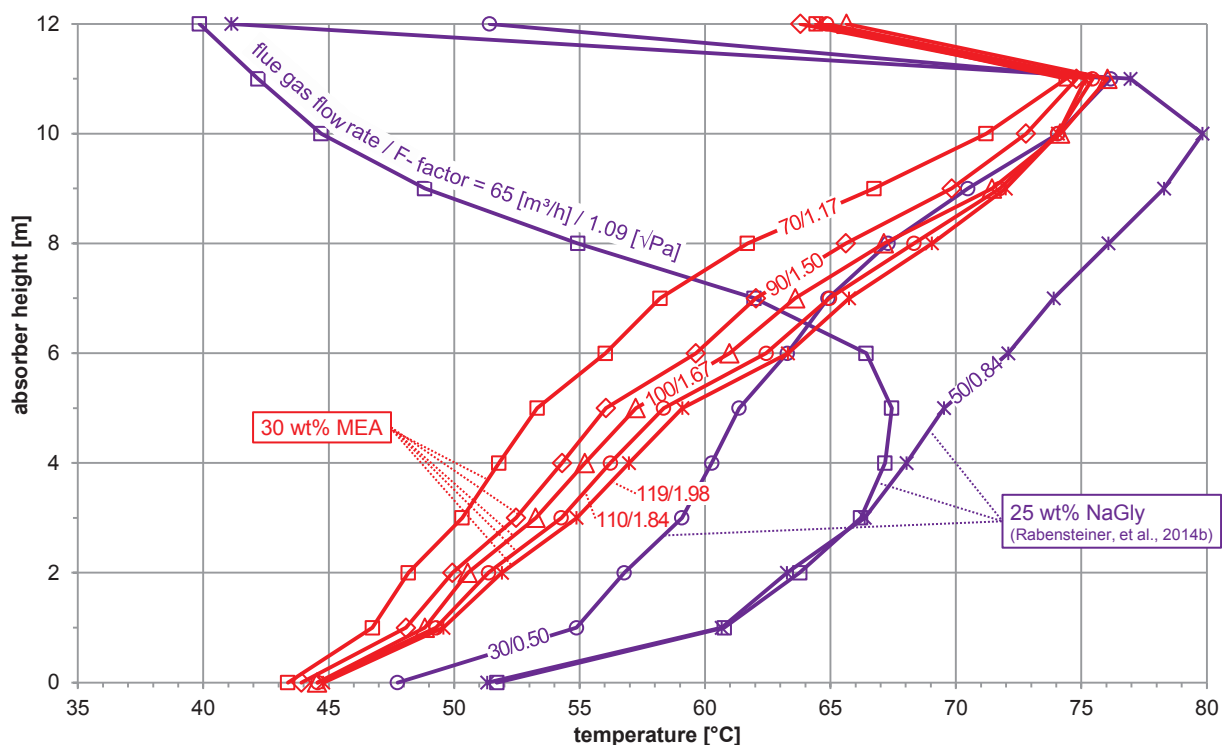
Fig. 6-29:   Absorber column temperature profile for different flue gas flow rates. Experimental data for 30 wt% MEA and 25 wt% NaGly.

Fig. 6-30 shows an increase in pressure loss in the entire absorber column (PIRC 2.2 – PIR 2.3, compare Appendix A1) by increasing flue gas flow rate, based on a comparison of 30 wt% MEA and 37.6 wt% PIP. The actual flue gas flow rate in the absorber column is also increased by the heat of absorption, resulting in a higher absorption temperature over the entire absorber column (compare Fig. 6-29 for 30 wt% MEA). The pressure loss is generally slightly higher for the process with 30 wt% MEA than it is with 37.6 wt% PIP. The absorber column pressure loss at an F-factor of 1.67 √Pa is 15.9 mbar when using 37.6 wt% PIP, for instance. In contrast, the pressure loss increases to 19.2 mbar at the same F-factor when using 30 wt% MEA. This is mainly due to the higher optimum solvent flow rate. The influence of the solvent flow rate (and the solvent viscosity) on the absorber column pressure loss can be seen in Fig. 6-24 for the same solvents. The increase in pressure loss is slightly flatter when using 37.6 wt% PIP. The reason is a smaller increase in the average absorption temperature caused by the lower CO_2 absorption enthalpy of piperazine. The average absorption temperatures of 30 wt% MEA and 37.6 wt% PIP are almost the same at a low flue gas flow rate. The difference between the average absorption temperatures increases to 2.5 K at high F-factors of around 2.00 √Pa. The lower absorption temperature results in a lower operating flue gas flow rate in the absorber column for the process with 37.6 wt% PIP.
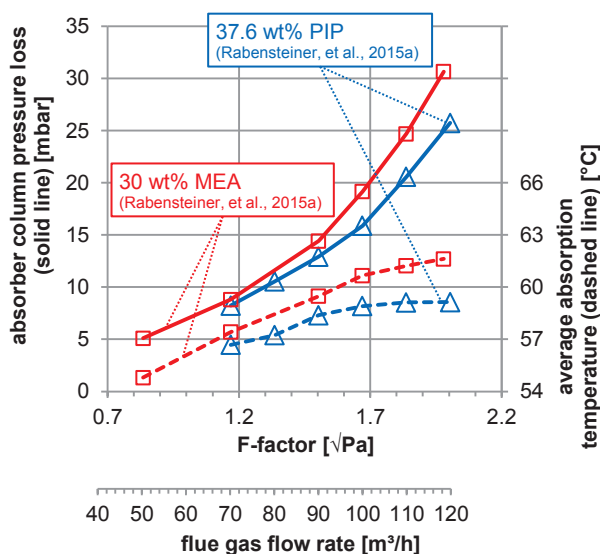
Fig. 6-30: Absorber column pressure loss and average absorption temperature as a function of flue gas flow rate. Experimental data for 30 wt% MEA and 37.6 wt% PIP.

6.4.2.2 Amino acids

This measurement series was carried out with 25 wt% NaGly for solvents based on amino acids. The flue gas flow rate varied between 30 and 65 m³/h, corresponding to an F-factor range of 0.50 to 1.09 √Pa (Fig. 6-31). A higher flue gas flow rate was not possible due to the limited solvent flow rate. The specific energy for solvent regeneration is extremely high (> 8 GJ/t_{CO_2}) at low flue gas flow rates. A reduction of the energy demand up to 5.08 GJ/t_{CO_2} is possible by increasing the flue gas flow rate.
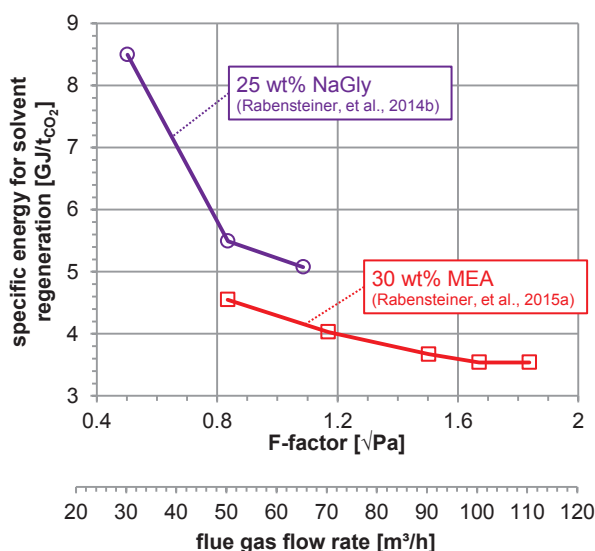
Fig. 6-31: Specific energy for solvent regeneration as a function of the flue gas flow rate. Experimental data for 30 wt% MEA and 25 wt% NaGly.

A variation of the flue gas flow rate in the investigation area has no significant effect on the CO_2 loading of amino acid solvents; this observation is similar to what was mentioned earlier for

amine-based solvents (Fig. 6-28). In addition to the absorption temperature of 30 wt% MEA, Fig. 6-29 shows the absorption temperature profile when using 25 wt% NaGly. 25 wt% NaGly shows a similar behavior as 30 wt% MEA at very low F-factors (0.5 and 0.84 √Pa). The absorption temperature increases in proportion to the F-factor within this operation range. This behavior applies to 30 wt% MEA, up to the maximum F-factor of 2 √Pa. For 25 wt% NaGly, a breakdown of the temperature profile occurs at an F-factor of 1.09 √Pa, where the highest temperature shifts to the lower part of the column. The highest temperature is at the top of the column at low F-factors, while at high F-factors, there is a flattening curve in this range.

6.5 Variation of the desorber pressure

6.5.1 Basic considerations

The partial pressures of both water vapor and carbon dioxide in Eq. 6-4 at the rich end of the desorber (desorber top) can be approximated by considering the equilibrium of the rich solution and its corresponding gas phase. The water vapor pressure and the equilibrium partial pressure of CO_2 are described by using fundamental thermodynamic interrelations in the simplified analysis (Oexmann & Kather, 2010).

Eq. 6-6 to Eq. 6-13 are taken from Gmehling & Kolb (1992). The enthalpy h and Gibbs free enthalpy g are defined by Eq. 6-6 and Eq. 6-7, respectively. u is the specific internal energy, P and $_T$ are the total pressure and temperature, respectively, v is the specific volume, and s is the specific entropy.

$$h \equiv u + P \cdot v \qquad \qquad \text{Eq. 6-6}$$

$$g \equiv u - T \cdot s + P \cdot v = h - T \cdot s \qquad \qquad \text{Eq. 6-7}$$

The partial derivative of the Gibbs free enthalpy is shown in Eq. 6-8.

$$\left(\frac{\partial g}{\partial T}\right)_{P,n_i} = -s \qquad \qquad \text{Eq. 6-8}$$

Eq. 6-9 follows by the combination of Eq. 6-7 and Eq. 6-8.

$$-h = \left(\frac{\partial g}{\partial T}\right)_{P,n_i} \cdot T - g \qquad \qquad \text{Eq. 6-9}$$

Differentiating g/T for T and substituting yields Eq. 6-10 and Eq. 6-11.

$$\left(\frac{\partial (g/T)}{\partial T}\right)_{P,n_i} = \frac{(\partial g/\partial T) \cdot T - (\partial T/\partial T) \cdot g}{T^2} \qquad \qquad \text{Eq. 6-10}$$

$$\left(\frac{\partial (g/T)}{\partial T}\right)_{P,n_i} = -\frac{h}{T^2} \qquad \qquad \text{Eq. 6-11}$$

The connection of the change of the Gibbs free enthalpy g_i and enthalpy h_i of component i in a mixture at a total constant pressure P is described by the Gibbs-Helmholtz equation in Eq. 6-12 or Eq. 6-13 (Gmehling & Kolb, 1992).

$$\left(\frac{\partial(g_i/T)}{\partial(1/T)}\right)_{P,n_i} = h_i$$

Eq. 6-12

$$\left(\frac{\partial(g_i/T)}{\partial T}\right)_{P,n_i} = -\frac{h_i}{T^2}$$

Eq. 6-13

The following calculation (Eq. 6-14 to Eq. 6-24) is taken from Oexmann & Kather (2010). The pressure dependency of the Gibbs free enthalpy for real gases is given by Eq. 6-14.

$$dg_i = d(\ln f_i) \cdot R \cdot T$$

Eq. 6-14

f_i is the vapor phase fugacity[1] of component i. Eq. 6-15 follows by substituting Eq. 6-14 into Eq. 6-12.

$$\left(\frac{\partial(\ln f_i)}{\partial(1/T)}\right)_{P,n_i} = -\frac{h_i}{R}$$

Eq. 6-15

Now consider the absorption of CO_2 from the gas into the liquid phase. The vapor phase fugacity coefficient φ_{CO_2} is 1 if ideal gas behavior is assumed for the vapor phase. Eq. 6-16 follows from Eq. 6-15 by assuming a constant total pressure P.

$$\frac{d\left(\ln p_{CO_2}^*\right)}{d(1/T)} = \frac{\Delta h_{abs,CO_2}}{R}$$

Eq. 6-16

Eq. 6-18 can be written by substituting Eq. 6-17 into Eq. 6-16.

$$dp_i = d(\ln p_i) \cdot p_i$$

Eq. 6-17

$$\frac{1}{p_{CO_2}^*} \cdot dp_{CO_2}^* = \frac{\Delta h_{abs,CO_2}}{R} \cdot \frac{1}{T^2} \cdot dT$$

Eq. 6-18

Similar consideration can be made for the water vapor pressure $p_{H_2O}^g$. The Clausius-Clapeyron equation for water is indicated in Eq. 6-19.

$$\frac{dp_{H_2O}^s}{dT} = \frac{\Delta h_{vap,H_2O}}{\Delta v \cdot T}$$

Eq. 6-19

Δv is the change in molar volume during the phase change. Assuming that the water vapor behaves as an ideal gas and that the molar volume of the vapor phase is much larger than of the fluid phase, Eq. 6-19 can be rewritten in a form that is easier to integrate (Eq. 6-20).

---

[1] The fugacity $f_i \equiv P \cdot \chi_i \cdot \varphi_i = p_i \cdot \varphi_i$ can be thought of as a "corrected partial pressure". The fugacity coefficient φ_i can be considered as "how closely the substance follows the behavior of an ideal gas" (Oexmann & Kather, 2010).

$$\frac{1}{p_{H_2O}^s} \cdot dp_{H_2O}^s = \frac{\Delta h_{vap,H_2O}}{R} \cdot \frac{1}{T^2} \cdot dT \qquad \text{Eq. 6-20}$$

Both Eq. 6-18 and Eq. 6-20 are differential equations and therefore describe the rate of change of the equilibrium partial pressures of CO_2 and water vapor pressure with the temperature. The integration of Eq. 6-18 and Eq. 6-20 yields Eq. 6-21 and Eq. 6-22 when assuming that the heat of evaporation of water and the heat of absorption of CO_2 are constant over the considered (small) range of temperatures.

$$p_{CO_2}^* = p_{CO_2,ref}^* \cdot e^{\left[\frac{|\Delta h_{abs,CO_2}|}{R} \cdot \left(\frac{1}{T} - \frac{1}{T_{ref}}\right)\right]} \qquad \text{Eq. 6-21}$$

$$p_{H_2O}^s = p_{H_2O,ref}^s \cdot e^{\left[\frac{|\Delta h_{vap,H_2O}|}{R} \cdot \left(\frac{1}{T} - \frac{1}{T_{ref}}\right)\right]} \qquad \text{Eq. 6-22}$$

Finally, the ratio of water vapor pressure and CO_2 equilibrium partial pressure can be expressed by combining Eq. 6-21 and Eq. 6-22 (Eq. 6-23).

$$\frac{p_{H_2O}^s}{p_{CO_2}^*} = \frac{p_{H_2O,ref}^s}{p_{CO_2,ref}^*} \cdot e^{\left[\frac{T - T_{ref}}{R \cdot T \cdot T_{ref}} \cdot \left(|\Delta h_{vap,H_2O}| - |\Delta h_{abs,CO_2}|\right)\right]} \qquad \text{Eq. 6-23}$$

Eq. 6-23 can be rewritten by Eq. 6-24 when assuming that the CO_2 stream is in chemical equilibrium with the loaded solvent and that the water vapor stream is saturated at the top of the desorber column (Oexmann & Kather, 2010).

$$\left(\frac{p_{H_2O}}{p_{CO_2}}\right)_{des,top} = \left(\frac{p_{H_2O}}{p_{CO_2}}\right)_{ref} \cdot e^{\frac{T_{des,feed}^l - T_{ref}}{R \cdot T_{des,feed}^l \cdot T_{ref}} \cdot \left(|\Delta h_{vap,H_2O}| - |\Delta h_{abs,CO_2}|\right)} \qquad \text{Eq. 6-24}$$

The partial pressure ratio between water steam and carbon dioxide at absorber temperature $(p_{H_2O}/p_{CO_2})_{ref}$ and the absorber temperature T_{ref} serve as reference in Eq. 6-24. The temperature $T_{des,feed}^l$ in the desorber is directly dependent on the desorber pressure and CO_2 loading of the solvent. The desorber sump temperature increases with increasing desorber pressure. In Eq. 6-24 it is apparent that solvents with a high CO_2 absorption enthalpy, such as MEA, benefit from high regeneration temperatures. This is the case when the CO_2 absorption enthalpy $\Delta h_{abs,CO_2}$ is higher than the evaporation enthalpy of water $\Delta h_{vap,H_2O}$ (~ 40 kJ/mol) (Oexmann, 2011). When working with solvents with a high CO_2 absorption enthalpy, high desorber sump temperatures yield a decreasing partial pressure ratio between water steam and carbon dioxide at the top of the desorber column. The energy for generating stripping steam decreases. This leads to a lower specific energy for solvent regeneration according Eq. 6-4.

6.5.2 Measurement results[1]

Table 6-7 shows the most important operating parameters of this test campaign. The desorber pressure indicated in this section was measured with PIRC 3.3, directly upstream of the pressure regulation valve (compare Appendix A.1).

Table 6-7:   Operating parameters of the test series with varying desorber pressures.

	MEA	EDA	PIP	AMP/PIP	NaGly
	(Fraubaum, 2013)	(Rabensteiner, et al., 2014c)	(Rabensteiner, et al., 2015a)		(Rabensteiner, et al., 2014b)
Concentration of active substance [wt%]	30	32	37.6	28/17	25
└ [molal]	7.0	7.8	7.0	4.4/2.4	3.4
L/G-ratio [l/m³]	2.80[2]	2.50	2.50	2.25	8.00
Flue gas flow rate [m³/h]	90	90	100	100	50
└ F-factor [√Pa]	1.50	1.50	1.65	1.65	0.84
Desorber pressure [bar$_{abs}$]	var.	var.	var.	var.	var.
Flue gas CO_2 content [vol% (dry)]	11.9 - 12.6	11.9 - 12.5	13.0 - 13.3	12.3 - 12.4	13.1 - 13.2
Regenerated solvent temperature [°C]	40	40	40	40	40
Flue gas temperature [°C]	40	40	40	40	40
CO_2 separation efficiency[3] [%]	90	90	90	90	90

6.5.2.1 Amine-based solvents

Fig. 6-32 shows the influence of the desorber pressure on the process. The pressure in the desorber unit varies between 1.6 and 2.6 bar$_{abs}$. It´s possible to see that the specific energy for solvent regeneration decreases with increasing desorber pressure. Solvents that show a high heat of absorption profit from a temperature swing between absorber and desorber column (compare Eq. 6-24). This applies for all of the solvents investigated, with the exception of 28/17 wt% AMP/PIP. The specific energy for solvent regeneration remains almost constant (~ 3.2 GJ/t$_{CO_2}$) for this solvent in the investigated range. An increase in the desorber operating pressure and reboiler temperature leads to less water vapor at the desorber head when using a solvent with a high heat of absorption. Less heat must be provided in the reboiler (Oexmann & Kather, 2010). 30 wt% MEA has proven to have the potential for especially high energy savings when it comes to desorber pressure increase. The efficiency even seems to be constant for desorber pressures higher than 2 bar$_{abs}$ for 32 wt% EDA. At high desorber pressures, the specific energy for solvent regeneration can be reduced to 3.0 GJ/t$_{CO_2}$ when using 37.6 wt% PIP.

The optimal operating point of the column depends on the evaporation temperature (Oexmann, 2011). As a result, not all tests from this measurement series were carried out with the optimal operating parameters. Slightly higher efficiencies can therefore be expected when there is a deviation from a desorber pressure of 2 bar$_{abs}$.

The temperature in the desorber is directly related to the desorber pressure and the CO_2 loading of the solvent. If the desorber pressure increases, the temperature in the desorber sump

---

[1] Segments of this section have already been published in Rabensteiner, et al. (2014b; 2014c; 2014d; 2015b).
[2] Fluctuation range: 2.8 to 2.9 l/m³ (Fraubaum, 2013).
[3] Deviation: ±1 %.

increases as well. The temperature increase in the desorber is limited with respect to the thermal degradation of the solvent.

Effects of thermal degradation will be discussed based on 32 wt% EDA. The desorber sump temperature is 123.4 °C in the reference case of 2 bar$_{abs}$ desorber pressure. Zhou, et al. (2010) investigated the thermal degradation of EDA solutions. The thermal degradation behavior of 32 wt% EDA is similar to 30 wt% MEA. The thermal degradation of 32 wt% EDA increases with increased CO_2 loading. No degradation of unloaded solvents occurs at temperatures below 135 °C. The desorber can be operated at 100 to 120 °C to avoid thermal degradation (Zhou, et al., 2010). The temperature in the desorber sump would lead to an amine loss of about 1 % per week for a 0.2 mol$_{CO_2}$/mol$_{equ. amine}$ loaded 32 wt% aqueous EDA solution. The amine loss rises to 3 % per week if the CO_2 loading is 0.4 mol$_{CO_2}$/mol$_{equ. amine}$. The thermal degradation rate decreases progressively with time according to Zhou (2009).

The specific volume of the CO_2 and water vapor mixture increases by lowering the desorber pressure. A disproportionately large increase of pressure loss occurs between the top of the desorber and the condensate separator (especially in the overhead condenser) due to the increase of the volume flow rate. The height of water column in the condensate return system is insufficient if the pressure loss continues to rise. Gas can escape through this line. This leads to high water loss and unstable operations.
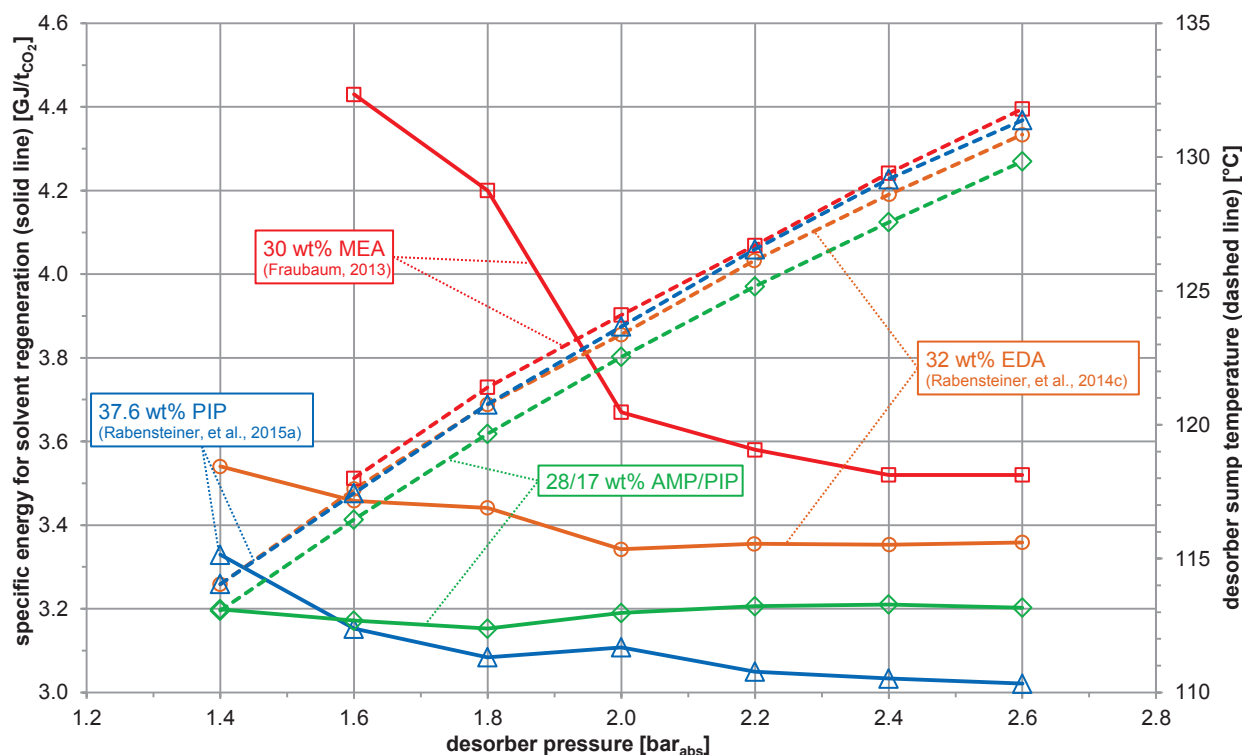
Fig. 6-32: Specific energy for solvent regeneration (solid line) and desorber sump temperature (dashed line) for different desorber pressures. Experimental data for 30 wt% MEA, 32 wt% EDA, 37.6 wt% PIP and 28/17 wt% AMP/PIP.

114

6.5.2.2 Amino acids

This test series was carried out with 25 wt% NaGly for aqueous solutions with amino acids. The CO_2 absorption enthalpy in aqueous NaGly is higher to the evaporation enthalpy of water $\Delta h_{vap,H_2O}$ (~ 40 kJ/mol) (Salazar, et al., 2010). At solvents with a high CO_2 absorption enthalpy, high desorber sump temperatures yield decreasing partial pressure ratio between water steam and carbon dioxide at the top of the desorber column. The energy for generating stripping steam decreases. This leads to a lower specific energy for solvent regeneration, according to Eq. 6-4. A lowering of the desorber pressure significantly increases the energy demand when using 25 wt% NaGly (Fig. 6-33). No considerable savings can be expected for pressures above the standard pressure of 2 bar$_{abs}$. The desorber temperature rises nearly linearly with increasing desorber pressure. The desorber pressure of the process with 25 NaGly is similar to the process with 30 wt% MEA.
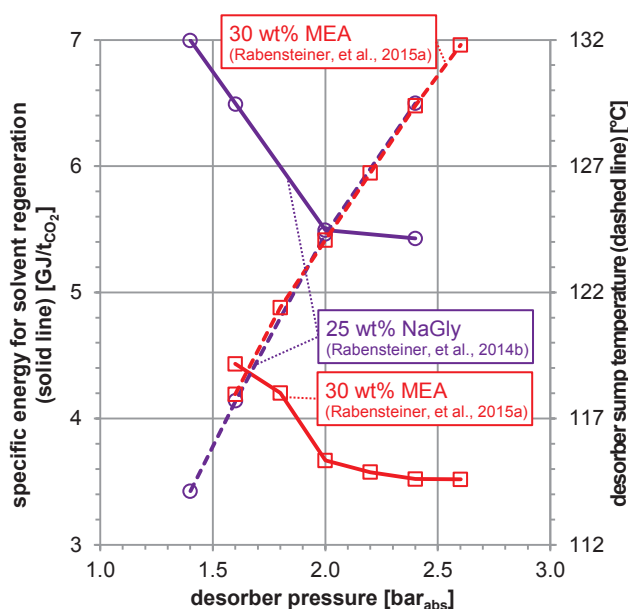
Fig. 6-33: Specific energy for solvent regeneration (solid line) and desorber sump temperature (dashed line) for different desorber pressures. Experimental data for 30 wt% MEA and 25 wt% NaGly.

The CO_2 loading of both the rich and lean solvents of all investigated amine and amino acid based solvents and the remaining absorption process does not depend on the desorber pressure. The temperature profile in the absorber column does not change.

6.6 Experiments with flue gas of a natural gas-fired boiler

A flue gas slipstream is branched off behind the induced draught fan of the power plant. The flue gas slipstream leads to the CO$_2$SEPPL pilot plant as explained in Section 5.2. The additional input of CO_2 or N_2 for varying flue gas CO_2 content was not planned. A change in fuel in power plant operation nevertheless produces a variation in CO_2 content. Test campaigns with flue gas of a natural gas-fired boiler are possible before and after the annual revision of the power plant. Using natural gas as the major fuel lowers the CO_2 content in the flue gas from the range of 11.3 to 13.3 vol% (dry) to 6.0 to 7.3 vol% (dry).

6.6.1 Basic considerations

Processes with a higher CO_2 concentration in the flue gas (higher CO_2 partial pressure) have a higher driving force for the reaction between CO_2 and the active absorption substance. The performance decreases for absorption processes with low CO_2 concentrations in the flue gas. The correlation between CO_2 partial pressure in the absorber column and the partial pressure ratio between water steam and carbon dioxide at the top of the desorber column can be seen from Eq. 6-24. The CO_2 partial pressure in the desorber increases with decreasing CO_2 partial pressure in the absorber.

An approach for the required energy demand when separating CO_2 from flue gases can be derived from the ideal gas law. The mixing of two or more ideal gas streams leads to an increase in entropy (Eq. 6-25) when assuming an adiabatic, ideal stirred tank (Fig. 6-34) (Posch, 2012).
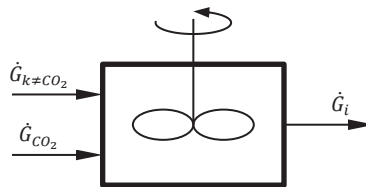
Fig. 6-34: Ideal stirred tank (Posch, 2012).

$$\Delta \dot{S}_{irr} = \dot{m}_{CO_2} \cdot R_{CO_2} \cdot \ln\frac{P}{p_{CO_2}} + \sum_{\substack{k=1 \\ k \neq CO_2}}^{N} \dot{m}_k \cdot R_k \cdot \ln\frac{P}{p_k} \qquad \text{Eq. 6-25}$$

The dissipated energy flow Ψ is calculated by Eq. 6-26 (Posch, 2012).

$$\Psi = T \cdot \Delta \dot{S}_{irr} \qquad \text{Eq. 6-26}$$

Ψ describes the minimum work required for a reversible, isothermal separation of the gaseous mixture into its components (Eq. 6-27) (Posch, 2012).

$$\dot{E} = \Psi \qquad \text{Eq. 6-27}$$

The minimum energy demand q_{reb} for a complete separation can be calculated with Eq. 6-28 by applying the ideal gas law for a gaseous mixture consisting out of N components (Posch, 2012).

$$q_{reb} = \frac{\dot{E}}{\dot{m}_{CO_2}} = \left(1 + \sum_{\substack{k=1 \\ k \neq CO_2}}^{N} \frac{\dot{m}_k}{\dot{m}_{CO_2}}\right) \cdot R \cdot T \cdot \sum_{i=1}^{N} \frac{1}{M_i} \cdot \ln\frac{1}{\chi_i} \qquad \text{Eq. 6-28}$$

For a binary mixture of N_2 and CO_2 at a temperature of 25 °C, Eq. 6-28 is quantified in Fig. 6-35 (Posch, 2012).

116
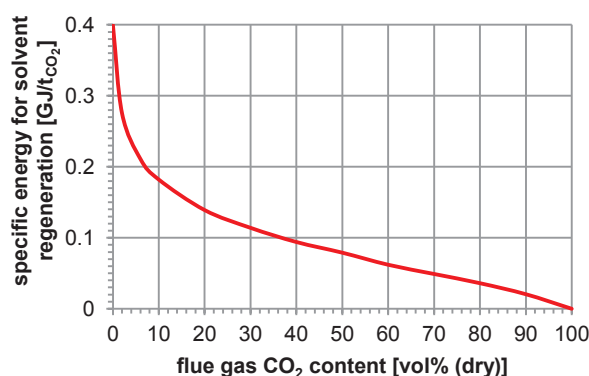
Fig. 6-35: Minimum specific energy consumption for CO_2 separation (Posch, 2012).

6.6.2 Measurement results[1]

Table 6-8 shows the most important operating parameters of this test campaign.

Table 6-8: Operating parameters of the test series with varying flue gas CO_2 content.

	MEA				EDA				PIP	
	CO_2 SEPPL pilot plant		Kaiserslautern pilot plant		CO_2 SEPPL pilot plant		Kaiserslautern pilot plant		CO_2 SEPPL pilot plant	
	(Rabensteiner, et al., 2015a)	(Posch, 2012)	(Mangalapally & Hasse, 2011c)		(Rabensteiner, et al., 2014c)		(Mangalapally & Hasse, 2011a)		(Rabensteiner, et al., 2015a)	(Rabensteiner, et al., 2015a; 2015b)
Concentration of active substance [wt%]	30	30	30	30	32	32	32	32	37.6	37.6
└ [molal]	└ 7.0	└ 7.0	└ 7.0	└ 7.0	└ 7.8	└ 7.8	└ 7.8	└ 7.8	└ 7.0	└ 7.0
L/G-ratio	var.	var.	var.	var.	var.	var.	var.	var.	var.	var.
Flue gas flow rate [m³/h]	90	70	-	-	90	110[2]	-	-	100	100
└ F-factor [√Pa]	└ 1.5	└ 1.2	1.6	1.6	└ 1.5	└ 1.8	1.6	1.6	└ 1.7	└ 1.7
Desorber pressure [bar_abs]	2	2	~ 2[3]	~ 2[3]	2	2	~ 2[3]	~ 2[3]	2	2
Flue gas CO_2 content [vol% (dry)]	11.8-12.7	~ 6.0	11.0	5.8	11.9-12.9	6.0-7.3	11.0	5.8	12.3-13.1	6.8
Regenerated solvent temperature [°C]	40	40	40	40	40	40	40	40	40	40
Flue gas temperature [°C]	40	40	47	47	40	40	47	47	40	40
CO_2 separation efficiency[4] [%]	90	90	90	90	90	90	90	90	90	90

Fig. 6-36 shows the specific energy needed for solvent regeneration as a function of the L/G-ratio for the differing flue gas CO_2 contents of 30 wt% MEA and 32 wt% EDA measured at the CO_2SEPPL and Kaiserslautern pilot plants. Fig. 6-37 represents the measurement results for 37.6 wt% PIP, once again in comparison to the benchmark solvent 30 wt% MEA. The attempts had to be carried out more quickly because of the short time slot of the investigations with a

---

[1] Segments of this section have already been published in Rabensteiner, et al. (2014c; 2015b).

[2] These investigations were accomplished as the first measurement series of the field campaign with 32 wt% EDA and still carried out with a flue gas rate of 110 m³/h. Increased pollution of the dust filter was observed after these experiments; hence, the flue gas flow rate had to be reduced to 90 m³/h.

[3] Value is not specified. Pressure can be estimated by desorber temperature stated by Mangalapally & Hasse (2011a; 2011c).

[4] Deviation: ±1 %.

natural gas-fired boiler. The distribution of the measuring points is therefore wider and they were connected partly (for 30 wt% MEA and 32 wt% EDA) with a smooth curve.

The mathematical formulation from Section 6.6.1 was experimentally confirmed at the CO_2SEPPL pilot plant by an increase in the minimum specific energy for solvent regeneration. The minimum energy demand increases from 3.68 to 4.27 GJ/t_{CO_2} (+16.0 %) when using 30 wt% MEA and low CO_2 concentrated flue gas (Fig. 6-36 and Fig. 6-37). Posch (2012) carried out experiments with flue gases from a natural gas-fired boiler at flue gas flow rates of only 70 m³/h. The reduction of the flue gas flow rate by 22 % leads to a further increase in specific energy for solvent regeneration according to Section 6.4.

For tests with flue gas out of a natural gas-fired boiler, the minimum energy demand increases from 3.17 to 3.55 GJ/t_{CO_2} (+12.0 %) when using 37.6 wt% PIP (Fig. 6-37). The lowest increase in energy demand from 3.34 to 3.60 GJ/t_{CO_2} is recognized by using 32 wt% EDA (Fig. 6-36). This represents an increase of only 7.8 % in energy demand. The higher flue gas flow rate during the experiments with low CO_2 concentrated flue gas is the reason for the small increase in energy demand. A 22 % higher flue gas flow rate (110 instead of 90 m³/h) was set during the 32 wt% EDA-experiments with low CO_2 concentrated flue gas, while both test series (high and low CO_2 concentrated flue gas) of 37.6 wt% PIP were carried out with the same flue gas flow rate. The impact of a higher flue gas flow rate is discussed in Section 6.4.
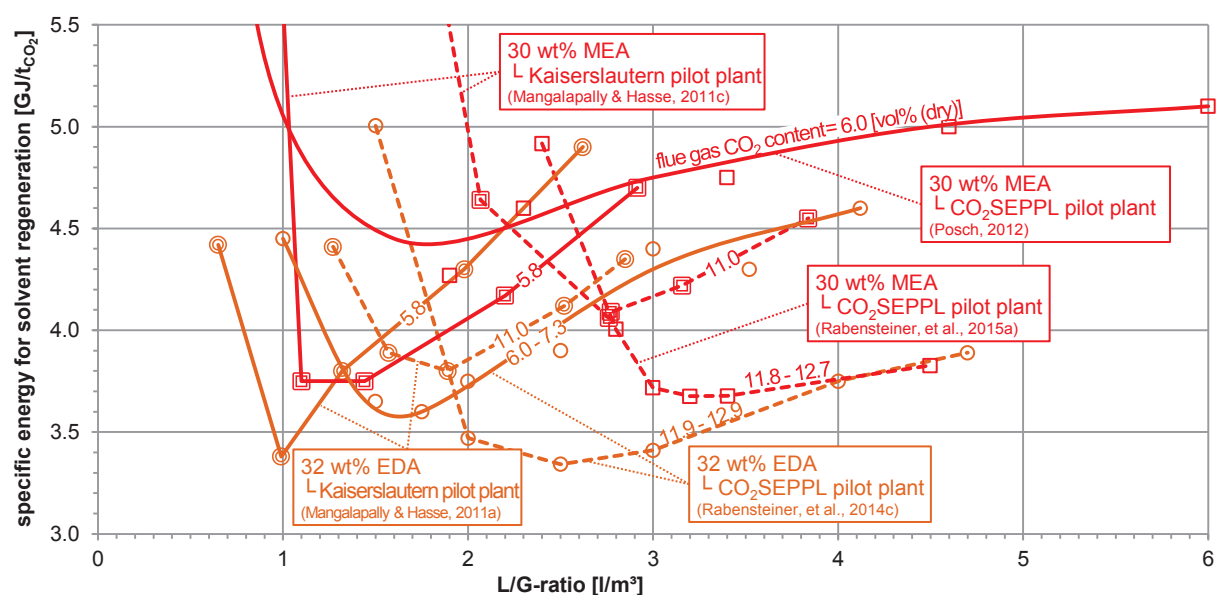
Fig. 6-36: Specific energy for solvent regeneration as a function of the L/G-ratio for flue gases with a high (dashed line) and low CO_2 content (solid line). Experimental data for 30 wt% MEA and 32 wt% EDA.
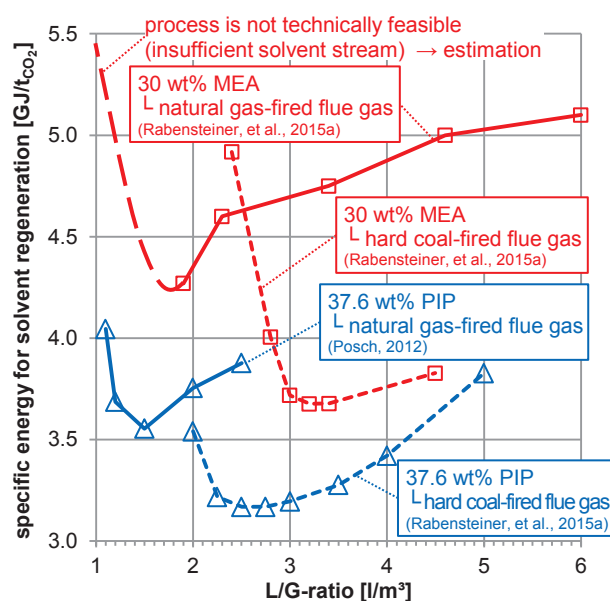
Fig. 6-37: Specific energy for solvent regeneration as a function of the L/G-ratio for flue gases of a hard coal- (dashed line) and natural gas-fired boiler (solid line). Experimental data for 30 wt% MEA and 37.6 wt% PIP.

The optimum L/G-ratio for the operation with flue gas of a natural gas-fired boiler decreases (compare Fig. 6-36 and Fig. 6-37) due to the higher CO_2 loading of the regenerated solvent (Fig. 6-38 and Fig. 6-39). Less vapor needs to be generated in the desorber. The gradient to the heat of evaporation below the optimal operating point is steeper than the gradient of sensible heat for L/G-ratios above the optimal operating point. Consequently, the minimum amount of sensible heat and heat of evaporation shifts to smaller solvent flow rates (Rabensteiner, et al., 2014b; 2014c).

Mangalapally & Hasse (2011a) performed experiments using two different flue gas CO_2 concentrations. The CO_2 concentration was set to 5.8 vol% (54 mbar CO_2 partial pressure) and 11.0 vol% (102 mbar). In contrast to the CO_2SEPPL pilot plant, the specific energy for solvent regeneration decreases if flue gases are used with a low CO_2 concentration (Fig. 6-36). The small number of theoretical separation plates has a strong influence on the measurements. Reasons behind the lower CO_2 loading of the rich solvent were explained in Section 6.3.3. The solvent must be heavily regenerated, leading to high specific energy for solvent regeneration. Less carbon dioxide has to be absorbed when using flue gases with a low CO_2 concentration. A smaller CO_2 loading difference is expected for equal solvent flow rates and CO_2 separation efficiencies, thus the CO_2 loading of the regenerated solvent increases and the heat of evaporation for stripping steam generation drops. As a result, the specific energy for solvent regeneration decreases.

Table 6-9 lists the L/G-ratio and specific energy required for solvent regeneration at the optimum operating points of different flue gas CO_2 contents.

Table 6-9: Specific energy for solvent regeneration and L/G-ratio at the optimum operating points of different flue gas CO_2 contents.

	MEA				EDA				PIP	
	CO$_2$ SEPPL pilot plant		Kaiserslautern pilot plant		CO$_2$ SEPPL pilot plant		Kaiserslautern pilot plant		CO$_2$ SEPPL pilot plant	
	(Rabensteiner, et al., 2015a)	(Posch, 2012)	(Mangalapally & Hasse, 2011c)		(Rabensteiner, et al., 2014c)		(Mangalapally & Hasse, 2011a)		(Rabensteiner, et al., 2015a)	(Rabensteiner, et al., 2015a; 2015b)
Concentration of active substance [wt%]	30	30	30	30	32	32	32	32	37.6	37.6
└ [molal]	7.0	7.0	7.0	7.0	7.8	7.8	7.8	7.8	7.0	7.0
Flue gas CO_2 content [vol% (dry)]	11.8-12.7	~ 6.0	11.0	5.8	11.9-12.9	6.0 - 7.3	11.0	5.8	12.3-13.1	6.8
L/G-ratio [l/m³]	3.20	1.90	2.76	1.10	2.50	1.75	1.89	0.99	2.50	1.50
Specific energy for solvent regeneration [GJ/t$_{CO_2}$]	3.68	4.27	4.06	3.75	3.34	3.60	3.80	3.38	3.17	3.55

The CO_2 loading of the rich and lean solvents for operation with the flue gases of a natural gas- and hard coal-fired boiler is shown in Fig. 6-38 (for 30 wt% MEA and 32 wt% EDA) and Fig. 6-39 (for 37.6 wt% PIP). The CO_2 loading of the rich 32 wt% EDA and 37.6 wt% PIP solvents clearly decreases for flue gases from a natural gas-fired boiler. There are two reasons for the decrease of the enriched CO_2 loading. Certainly, the equilibrium CO_2 loading decreases with decreasing CO_2 partial pressure (compare the VLE-data of aqueous MEA, EDA and PIP in Fig. 6-12 and Fig. 6-16). The difference between the equilibrium curves (for the partial pressure and absorber sump temperature respectively) for 30 wt% MEA and 37.6 wt% PIP can be seen in Fig. 6-38 and Fig. 6-39. Only one equilibrium curve for high CO_2 concentration is indicated for 32 wt% EDA in Fig. 6-38 because of insufficient VLE-data. The equilibrium CO_2 loading drops slightly with increasing solvent flow rate because of the higher absorber sump temperature at high solvent flow rates (compare Fig. 6-40). The second reason for the lower CO_2 loadings when operating with the flue gases of a natural gas-fired boiler is the lower absolute CO_2 flow rate, which reduces the CO_2 loading difference.
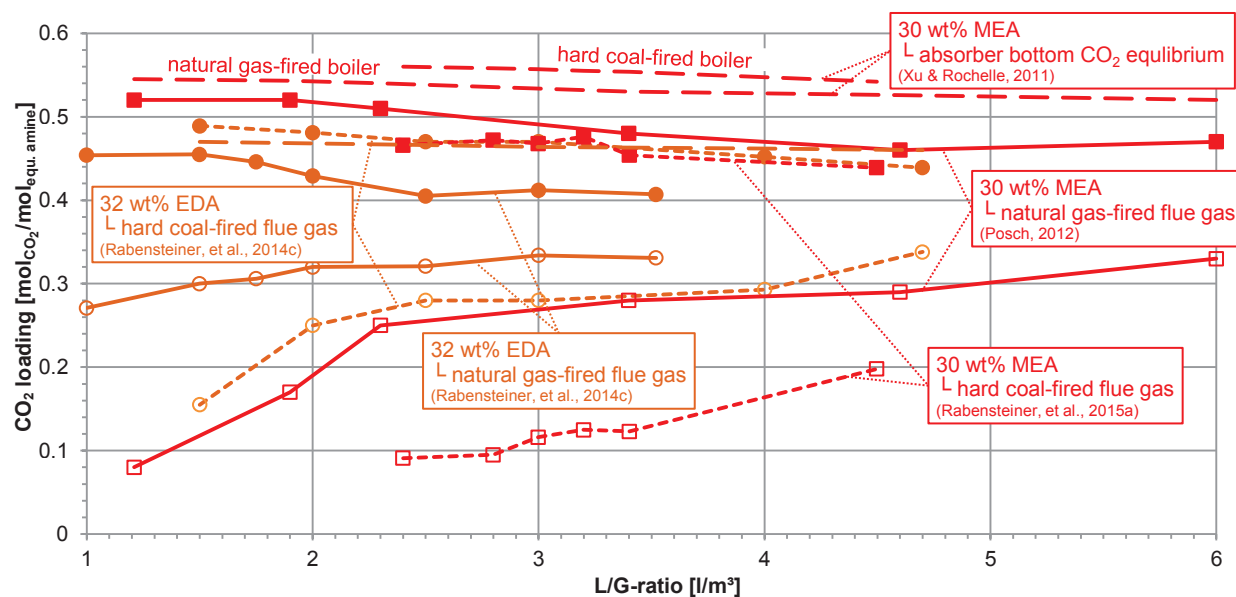
Fig. 6-38: CO$_2$ loading of the regenerated (unfilled symbols) and enriched (filled symbols) solvent for operation with flue gases of a hard coal- (dashed line) and natural gas-fired boiler (solid line). Experimental data for 30 wt% MEA and 32 wt% EDA.
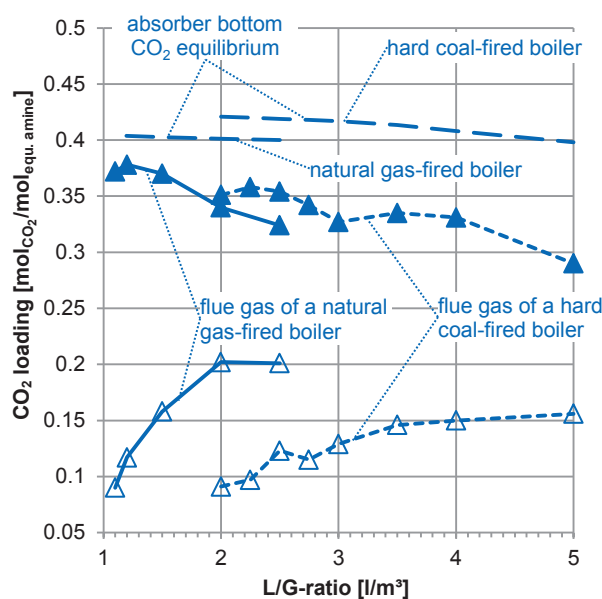
Fig. 6-39: CO$_2$ loading of the regenerated (unfilled symbols) and enriched (filled symbols) solvents for operation with the flue gases of a hard coal- (dashed line) and natural gas-fired boiler (solid line). Experimental data for 37.6 wt% PIP.

Fig. 6-40 shows the temperature profiles of the absorber column for operation with the flue gases of a natural gas- and coal-fired boiler for 32 wt% EDA (a) and 37.6 wt% PIP (b). The temperature curves are valid for L/G-ratios of 1.5, 2.5 and 4.0 l/m³ and 2.0 and 2.5 l/m³, respectively. The heat of absorption is higher for flue gases from a hard coal-fired boiler despite the smaller flue gas flow rate of the experiments with 32 wt% EDA. This is obvious from the higher temperatures at the inlet of the regenerated solvent. The different temperature profiles for the same solvent flow rates are attributed to different flue gas flow rates.

121
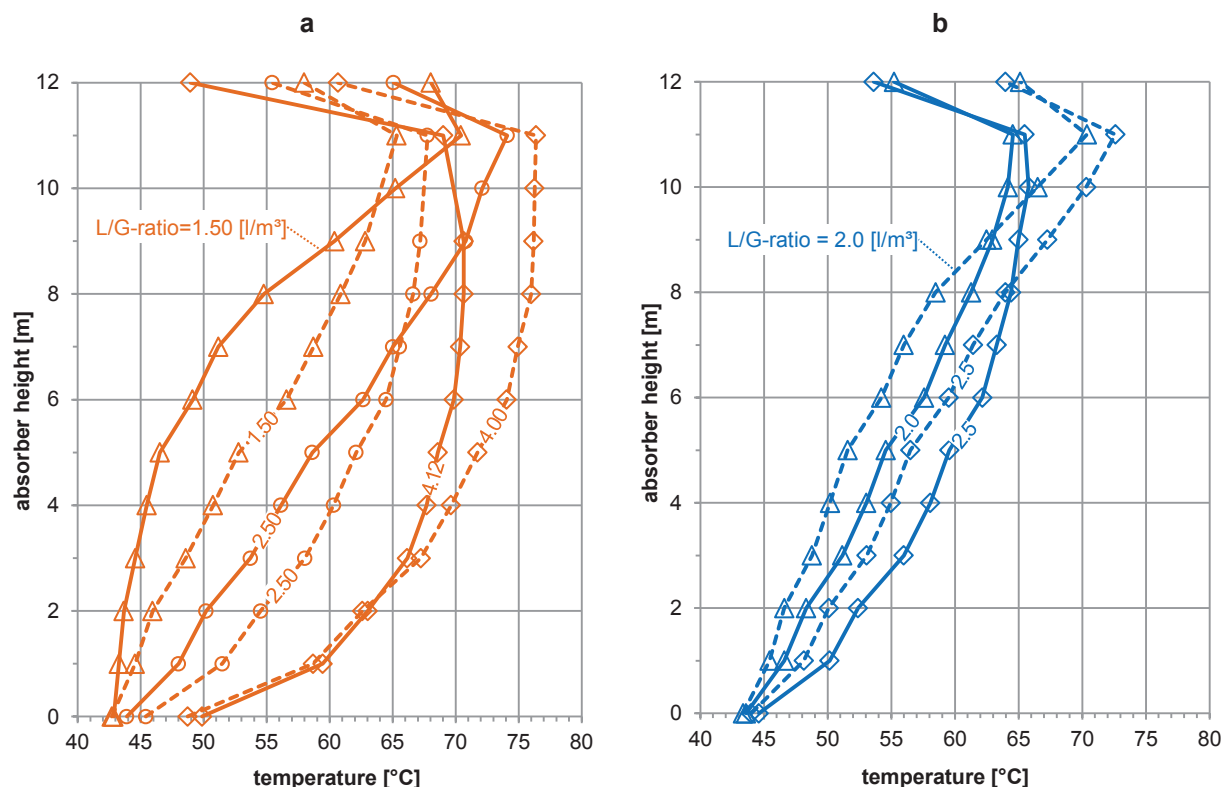
Fig. 6-40: Comparison of the absorber column temperature profile of 32 wt% EDA **(a)** and 37.6 wt% PIP **(b)** for operation with the flue gases of a coal-fired boiler (dashed line) and natural gas-fired boiler (solid line).

6.7 Variation in absorber heights

6.7.1 Basic considerations

The absorber column is considered as a plug flow reactor without diffusion for the following explanation. A reaction of pseudo-first order is assumed for instance. The balance of CO_2 along the axis z of the reactor yields Eq. 6-29 (Posch, 2012). u is the superficial velocity.

$$u \cdot \frac{\partial [CO_2]}{\partial z} = -k_{[CO_2]} \cdot [CO_2] \qquad \text{Eq. 6-29}$$

The concentration profile of CO_2 along the reactor axis is obtained by integration of Eq. 6-29 (Eq. 6-30). $z = 0$ at the regenerated solvent inlet (Posch, 2012).

$$[CO_2] = [CO_2]_{z=0} \cdot e^{\left(-k_{[CO_2]} \cdot \frac{z}{u}\right)} \qquad \text{Eq. 6-30}$$

A constant separation efficiency η_{sep} is assumed according to Eq. 6-31 (Posch, 2012). The rate of CO_2 absorption $k_{[CO_2]}$ decreases with increasing absorber column height h (Eq. 6-32).

$$\eta_{sep} = \left(1 - \frac{[CO_2]}{[CO_2]_{z=0}}\right) \cdot 100\% \qquad \text{Eq. 6-31}$$

122

$$k_{[CO_2]} = -\frac{u}{h} \cdot \ln\left(1 - \frac{\eta_{sep}}{100\%}\right)$$ **Eq. 6-32**

The CO_2 absorber column can be considered as a plug flow reactor. The reaction rate constant has to be increased for a constant CO_2 separation efficiency when the length of the plug flow reactor is reduced. An increase in the rate constant for CO_2 absorption can be achieved with higher amine concentrations in the solvent because the chemical reaction of CO_2 with amines is normally of second order (Aboundheir, et al., 2003). Consequently, the rate of CO_2 absorption additionally depends on the amine concentration and the temperature (Posch, 2012). A higher amine concentration is generally coupled with an increase in the viscosity and corrosivity of the solvent. The CO_2 absorption rate decreases along the absorber height as seen in Eq. 6-32. This means that the highest CO_2 absorption rate is at the regenerated solvent inlet. The CO_2 absorption rate decreases toward to the absorber bottom.

Lowering the absorber column height reduces the contact time of the liquid and gaseous phase. At a constant CO_2 separation efficiency and a constant solvent flow rate, the CO_2 loading difference between the rich and lean solvents has to stay the same. The rich loading is limited by the equilibrium CO_2 loading at the present absorption bottom temperature and the flue gas CO_2 content. The CO_2 absorption rate is no longer sufficient to reach a certain CO_2 loading in the absorber column through the reduction of the absorber column height and constant lean CO_2 loading. The CO_2 absorption rate is increased by lowering the regenerated solvent CO_2 loading. The CO_2 loading of the enriched solvent drops in the same way because of the constant CO_2 loading difference. The CO_2 absorption rate in the absorber column rises because of the average CO_2 loading across the absorber column. The CO_2 partial pressure has to be reduced at the top of the desorber in order to reduce the CO_2 loading of the regenerated solvent. The energy demand for stripping steam generation (q_{vap,H_2O}) thus rises according Eq. 6-4.

This interaction is a reason for the high solvent flow rate required when using amino acids. The solvent has to be heavily regenerated because of insufficient absorber column height of the CO_2SEPPL pilot plant. This leads to an increase of the specific energy for solvent regeneration. The gradient of the heat of evaporation below the optimal operating point is steeper than the gradient of sensible heat for L/G-ratios above the optimal operating point (compare Fig. 6-4).

6.7.2 Measurement results[1]

The effective absorber height of the CO_2SEPPL pilot plant can be varied between 3, 6, 9 and 12 m by manually opening and closing ball valves. Stationary operation conditions are hard to achieve with an absorber height of 3 m because the excess pressure in the desorber column leads to a minimum solvent mass flow rate (Posch, 2012). In other words, a disproportionately large increase of the pressure loss occurs between the top of the desorber and the condensate separator (especially in the overhead condenser) due to the increase of the volume flow rate. The height of the water column in the condensate return system is insufficient if the pressure

---

[1] Segments of this section have already been published in Rabensteiner, et al. (2014b; 2014c; 2014d; 2015b)

123

loss continues to rise. Thus, gas can escape through this line. This leads to high water loss and an unstable operation. Stable operation at 3 m absorber height is only possible with piperazine. But the energy demand escalates. This operating point was facilitated by the installation of structured packings in the water washing section of the desorber. In the previously conducted tests with 30 wt% MEA, 32 wt% EDA and 40 wt% NaGly, pall rings (15 x 0.3) were used. These internals have a higher pressure loss.

Table 6-10 shows the most important operating parameters of this test campaign.

Table 6-10: Operating parameters of the test series with varying absorber height.

	MEA	EDA	PIP	AMP/PIP	NaGly
	(Fraubaum, 2013)	(Rabensteiner, et al., 2014c)	(Rabensteiner, et al., 2015a)		(Rabensteiner, et al., 2014b)
Concentration of active substance [wt%]	30	32	37.6	28/17	40
└ [molal]	└ 7.0	└ 7.8	└ 7.0	└ 4.4/2.4	└ 5.9
L/G-ratio [l/m³]	2.80	2.50	2.50	2.25	8.00
Flue gas flow rate [m³/h]	90	90	100	100	50
└ F-factor [√Pa]	└ 1.50	└ 1.50	└ 1.65	└ 1.65	└ 0.84
Desorber pressure [bar$_{abs}$]	2	2	2	2	2
Flue gas CO_2 content [vol% (dry)]	12.4 - 12.5	11.9 - 12.2	13.1 - 13.3	12.7 - 13.1	12.9 - 13.0
Regenerated solvent temperature [°C]	40	40	40	40	40
Flue gas temperature [°C]	40	40	40	40	40
CO_2 separation efficiency[1] [%]	90	90	90	90	90

Fig. 6-41a shows the specific energy required for solvent regeneration at absorber heights of 6, 9 and 12 m. The specific energy for solvent regeneration increases with decreasing absorber height, as expected. The specific energy for solvent regeneration decreases continuously with increasing absorber height when using 30 wt% MEA. For 32 wt% EDA, 37.6 wt% PIP and 28/17 wt% AMP/PIP, only a slight increase in energy demand is recognized by a reduction of the absorber height from 12 to 9 m. A further decrease in absorber height to 6 m leads to a significant increase in energy demand for these solvents. A 6 m high column has approximately 17 theoretical separation plates. This roughly corresponds to the number of theoretical separation plates in the Kaiserslautern pilot plant. The measurement results for 32 wt% EDA and 28/17 wt% AMP/PIP are similar for this measurement point (compare Fig. 6-7). The lowest energy demand for each solvent is achieved at a maximum absorber height of 12 m. However, increased absorber height is linked to significant growth in investment costs.

The specific energy for solvent regeneration is increased by 18 % by lowering the absorber height from 12 to 6 m and using 30 wt% MEA. Only a 13 % increase in energy demand was measured when using 37.6 wt% PIP. The specific energy for solvent regeneration of the 37.6 wt% PIP-process with 6 m absorber height is still lower than in the standard case of the 30 wt% MEA-process.

The specific energy for solvent regeneration for 40 wt% NaGly, which is already high in the standard case of an absorber height of 12 m, rises sharply by lowering the absorber height. This is because of the enormous amount of stripping steam necessary to reduce CO_2 partial pressure at the top of the desorber column. The amount of stripping steam once again increases significantly by lowering the absorber column.

---

[1] Deviation: ±1 %.

Stationary operation conditions cannot be achieved by using 40 wt% NaGly and 6 m absorber height because of the high amounts of stripping steam. The pressure drop of the gas flow increases between the position in the desorber column where the condensate flows back and the condensate separator. The reflux gets stuck because of the high pressure at the condensate return. Consequently, the water column height in the siphon increases. There is a sudden reflux when a certain height of the water column is reached, which results in unstable operation.
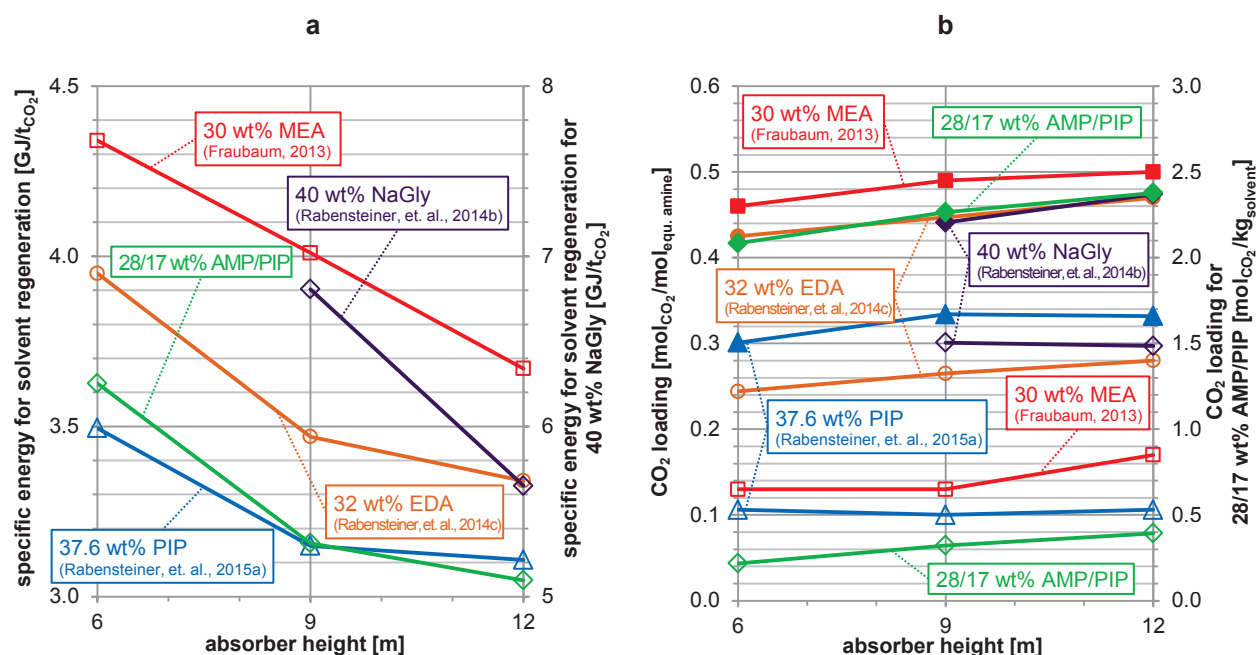
Fig. 6-41: Specific energy for solvent regeneration **(a)** and CO_2 loading **(b)** of the rich (filled symbols) and lean (unfilled symbols) solvents as a function of the absorber height. Experimental data for 30 wt% MEA, 32 wt% EDA, 37.6 wt% PIP, 28/17 wt% AMP/PIP and 40 wt% NaGly.

The CO_2 loading of the rich and lean solvents for different absorber heights is shown in Fig. 6-41b. An increase in the rich CO_2 loading can be observed by increasing the absorber height. This can be explained by the lower CO_2 loading of the regenerated solvent and the constant CO_2 loading difference. The low CO_2 loading of the regenerated solvent leads to an increased energy demand for solvent regeneration, which has been mentioned in previous sections.

Fig. 6-42 shows the CO_2 loading over the absorber column for different absorber heights when using 28/18 wt% AMP/PIP. The measurements are consistent with the calculations in Section 6.7.1. The reaction rate decreases along the absorber height as seen in Eq. 6-32. This means that the highest CO_2 absorption rate is located at the regenerated solvent inlet. The CO_2 absorption rate decreases towards the absorber bottom. The lower the absorber column height, the more uneven the CO_2 absorption is, across the absorber column. Minor amounts of carbon dioxide are absorbed in the lower part of the column when an absorber column height of 12 m is set. By contrast, the entire amount of carbon dioxide is absorbed in the upper part of the column when the height of 6 m is set.

125
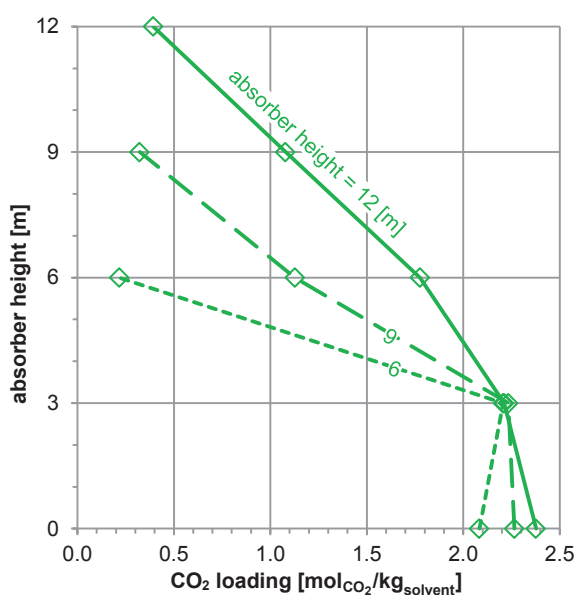
Fig. 6-42: CO_2 loading across the absorber column for different absorber heights. Experimental data for 28/17 wt% AMP/PIP.

The temperature distribution within the absorber column for different absorber heights is shown in Fig. 6-43. The temperature maximum for each solvent is in the vicinity of the lean solvent entry and is almost constant for each absorber height because of the consistent amount of absorption heat. The large temperature change at the top of the column suggests an intense reaction of carbon dioxide with the solvent. The absorption temperature decreases due to heat transfer from the liquid to the gaseous phase in the lower part of the absorber column.

A lowering of the effective absorber column height shifts the temperatures at the lower locations of the absorber column to higher values, resulting in higher CO_2 equilibrium loadings. The absorber sump temperature (lowest temperature measurement point) rises with decreasing effective absorber height. The temperature of the treated flue gas (top temperature measurement point) drops according to the law of energy conservation. The absorber sump temperature for 32 wt% EDA is 43.9 °C, for instance, when the total height of the column is used for CO_2 absorption. The treated flue gas temperature is 65.1 °C for the same setting. The treated flue gas temperature drops to 61.4 °C when the absorber column height is reduced to 6 m, while the absorber sump temperature rises to 47.0°C.

For the process with 40 wt% NaGly, the maximum temperature occurs at the bottom of the column due to the high L/G-ratio of the process. The higher heat capacity of the solvent relative to the flue gas tends to push the heat of reaction to the bottom (Kvamsdal & Rochelle, 2008). The temperature profiles of the process with 40 wt% NaGly therefore differ sharply from the remaining solvents. The treated flue gas temperature drops significantly downstream from the regenerated solvent inlet when absorber heights of 6 or 9 m are set. By contrast, the treated flue gas remains constant when using amine-based solvents.

The desorber sump temperature rises at low absorber column heights. The main reason is the higher amount of steam, resulting in an increased pressure loss in the desorber column. The increasing pressure in the desorber sump has little effect on the desorber sump temperature. A

halving of the absorber height from 12 to 6 m only leads to a desorber sump temperature increase of 1 K for 37.6 wt% PIP for instance.
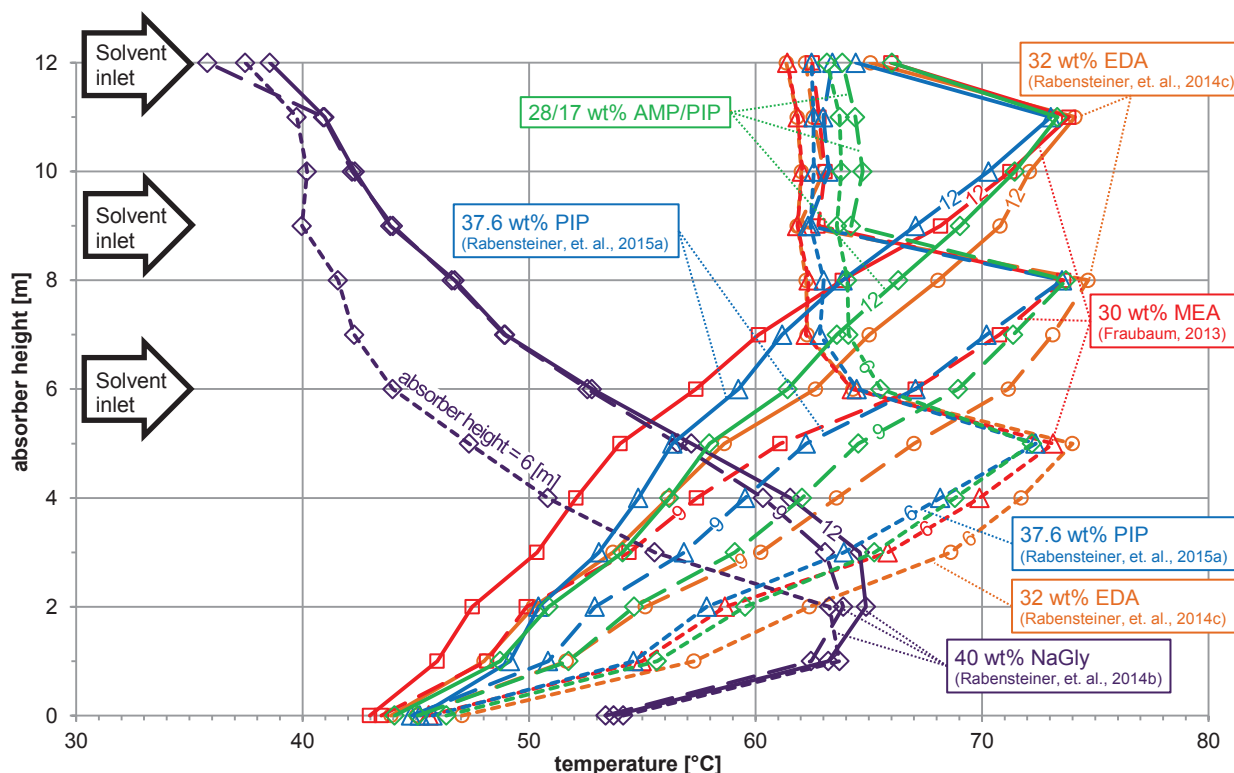
Fig. 6-43:   Absorber column temperature profile for different absorber heights. Experimental data for 30 wt% MEA, 32 wt% EDA, 37.6 wt% PIP, 28/17 wt% AMP/PIP and 40 wt% NaGly[1].

6.8 Variation of the absorption temperature

6.8.1 Basic considerations

Higher absorption temperatures lead to an increase in the rate constant for the reaction of CO_2 with the solvent. Increasing absorption temperatures result in decreasing CO_2 absorption capacities. A higher rate constant for absorption leads to a higher lean loading of the solvent for a constant CO_2 separation efficiency. This results in decreasing specific energy for solvent regeneration. Higher inlet temperatures shift the absorber temperature profile to higher values due to the increase in sensible heat within the absorber column. In general, higher solvent temperatures entail a reduction of CO_2 loading capacity (Cullinane, 2005).

A qualitative prediction cannot be given at this point due to the opposite nature of these two effects. It can be assumed that the kinetics don´t have a significant influence at the absorber bottom and that chemical equilibrium is achieved when the absorber height is set to 12 m. The lowering in CO_2 capacity at higher temperatures has a higher impact and leads to an increase in the specific energy required for solvent regeneration. In addition, the temperature has an

---

[1] The 40 wt% NaGly-experiments with an absorber height of 6 m are unstable.

influence on the viscosity of the solvent. This again affects the mass transfer. The effect of solvent viscosity on the mass transfer is described in Section 3.2.2.

6.8.2 Measurement results[1]

The absorption temperature can be varied by changing the regenerated solvent temperature or flue gas temperature. Table 6-11 shows the most important operating parameters of this test campaign.

Table 6-11: Operating parameters of the test series with varying absorption temperatures.

	MEA		EDA		PIP		NaGly
	(Fraubaum, 2013)		(Rabensteiner, et al., 2014c)		(Rabensteiner, et al., 2015a)		
Variation	Regenerated solvent temperature	Flue gas temperature	Regenerated solvent temperature	Flue gas temperature	Regenerated solvent temperature	Flue gas temperature	Regenerated solvent temperature
Concentration of active substance [wt%]	30	30	32	32	37.6	37.6	25
∟ [molal]	∟ 7.0	∟ 7.0	∟ 7.8	∟ 7.8	∟ 7.0	∟ 7.0	∟ 3.4
L/G-ratio	2.8	2.8	2.5	2.5	2.5	2.5	8.0
Flue gas flow rate [m³/h]	90	90	90	90	100	100	50
∟ F-factor [√Pa]	∟ 1.50	∟ 1.50	∟ 1.50	∟ 1.50	∟ 1.65	∟ 1.65	∟ 0.84
Desorber pressure [bar$_{abs}$]	2	2	2	2	2	2	2
Flue gas CO_2 content [vol% (dry)]	12.4	12.4	11.9 - 12.7	11.9 - 12.5	12.8 - 13.0	13.0 - 13.3	12.8 - 13.2
Regenerated solvent temperature [°C]	var.	40	var.	40	var.	40	var.
Flue gas temperature [°C]	40	var.	40	var.	40	var.	40
CO_2 separation efficiency[2] [%]	90	90	90	90	90	90	90

The assumption mentioned above can be seen in the flue gas temperature variation when using 32 wt% EDA (Fig. 6-44). The specific energy for solvent regeneration is 3.49 GJ/t$_{CO_2}$ when a high flue gas temperature of 51.7 °C is set. The energy demand decreases to 3.2 GJ/t$_{CO_2}$ when the flue gas temperature drops to 27.9 °C. A correlation with the solvent temperature is not clearly visible for 32 wt% EDA.

The temperature dependence of piperazine´s fast kinetics seems to affect the process only slightly, so that low temperature performance appears to be generally better. In particular, reducing the flue gas temperature shows a positive impact. 2.6 % of specific energy for solvent regeneration (2.97 instead of 3.08 GJ/t$_{CO_2}$) can be saved by reducing the flue gas temperature from 40.0 to 26.4 °C (minimum possible temperature).

No direct correlation between the absorption temperature and specific energy for solvent regeneration can be found for 30 wt% MEA and 25 wt% NaGly. The effects of temperature-dependent kinetics, mass transfer and CO_2 solubility seem to cancel each other out.

---

[1] Segments of this section have already been published in Rabensteiner, et al. (2014c; 2015b).
[2] Deviation: ±1 %.
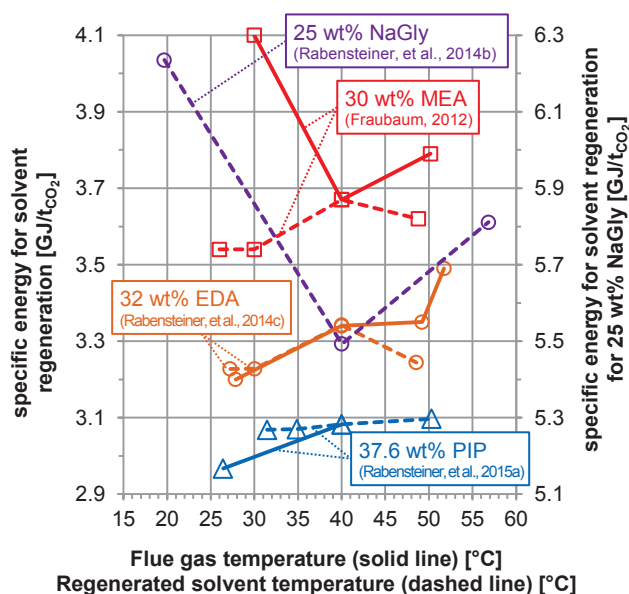
Fig. 6-44: Specific energy for solvent regeneration as a function of the flue gas temperature (solid line) and the regenerated solvent inlet temperature (dashed line). Experimental data for 30 wt% MEA, 32 wt% EDA, 37.6 wt% PIP and 25 wt% NaGly.

The absorption temperature has no visible effect on the CO_2 loadings. The effects of the absorption temperature on the desorber sump temperature are negligible. The small changes in desorber sump temperature can be affiliate to the different amounts of generated steam.

Fig. 6-45 shows the temperature profile of the absorber column at different flue gas temperatures. The temperature maximum for each solvent is in the vicinity of the lean solvent entry. The large temperature change at the top of the column suggests an intense reaction of carbon dioxide with the solvent. The absorption temperature decreases due to heat transfer from the liquid to the gaseous phase in the lower part of the absorber column. The flue gas temperature mainly affects the temperature profile in the lower part of the absorber column. The main reason for this is the lower water content of the cooler flue gas. More of the solvent´s water has to be vaporized for saturation during contact with the solvent. This results in the lower temperature of the enriched solvent.

For example, 73.9 °C is the maximal absorption temperature when a flue gas temperature of 27.9 °C is set when using 32 wt% EDA. When the flue gas temperature is set to 51.7 °C, the maximal absorption temperature rises to 76.3 °C. This results in an increase in the maximal absorption temperature of only 2.4 K. The temperature difference of the absorber sump increases by 21.3 K (54.9 instead of 33.6 °C) in contrast to the same flue gas temperature change.
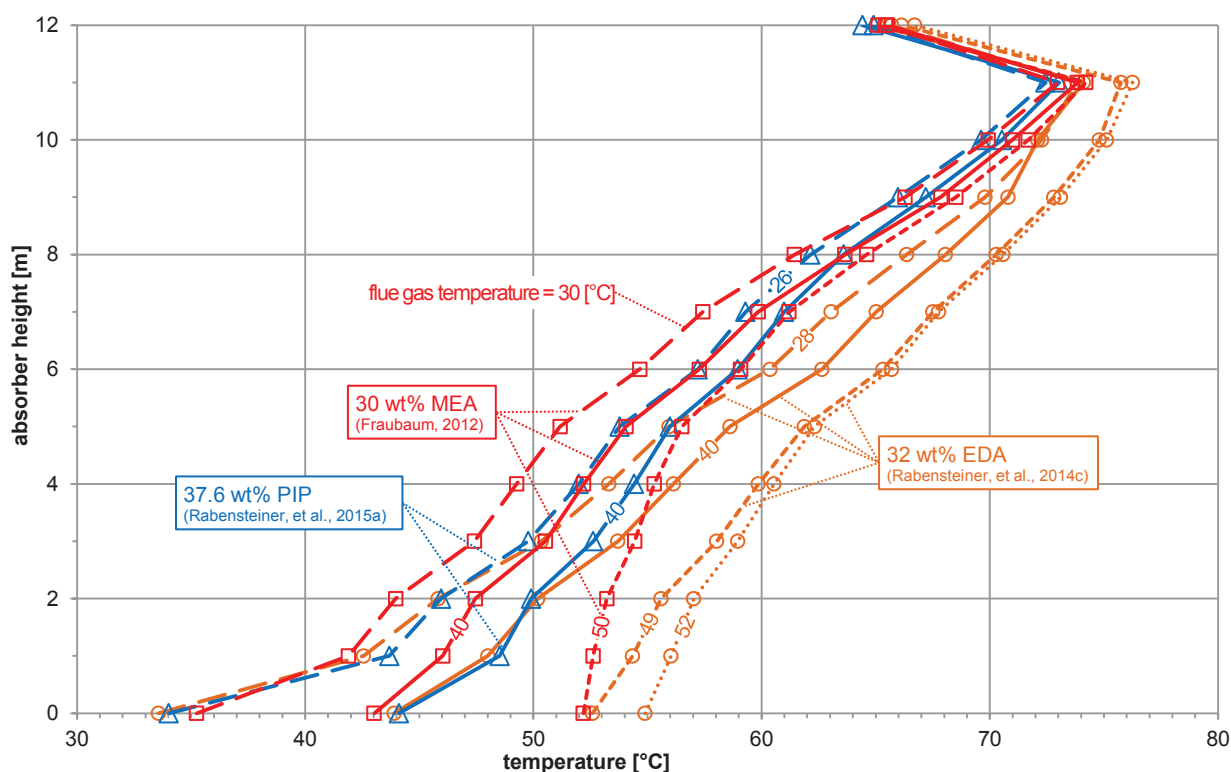
Fig. 6-45: Absorber column temperature profile for different flue gas temperatures. Experimental data for 30 wt% MEA, 32 wt% EDA and 37.6 wt% PIP.

The change of the regenerated solvent temperature affects only the exit temperature of the flue gas treated (highest temperature sensor in the absorber column) (Fig. 6-46). The absorption temperature of the remaining absorber height remains nearly constant when varying the regenerated solvent temperature. 59.9 °C is the treated flue gas temperature when a regenerated solvent temperature of 27.2 °C is set and using 32 wt% EDA for instance. The treated flue gas temperature rises to 68.7 °C when the flue gas temperature is increased to 48.6 °C.

The temperature maximum for each solvent, with the exception of 25 wt% NaGly, is in the vicinity of the lean solvent entry. The large temperature change at the top of the column suggests an intense reaction of carbon dioxide with the solvent. The absorption temperature decreases due to heat transfer from the liquid to the gaseous phase in the lower part of the absorber column.

The maximal absorption temperature of the 25 wt% NaGly-process is only directly at the regenerated solvent inlet when the highest regenerated solvent temperature of 56.8 °C is set. The average absorption temperature for the 25 wt% NaGly-process is higher than those of the other amine-based solvents because of the higher solvent flow rate and the higher specific heat capacity of the solvent in comparison to the flue gas. The maximal absorption temperature for the standard case (regenerated solvent temperature = 40 °C) is 79.8 °C when using 25 wt% NaGly. The maximal absorption temperature for the standard case is about 73 °C when one of the other solvents is used. There is already an enormous drop in the treated flue gas temperature when the regenerated solvent temperature is lowered to the standard temperature

of 40 °C when using 25 wt% NaGly. Lowering the regenerated solvent temperature to 20 °C results in a sharp decrease of the absorption temperature over the entire absorber column.
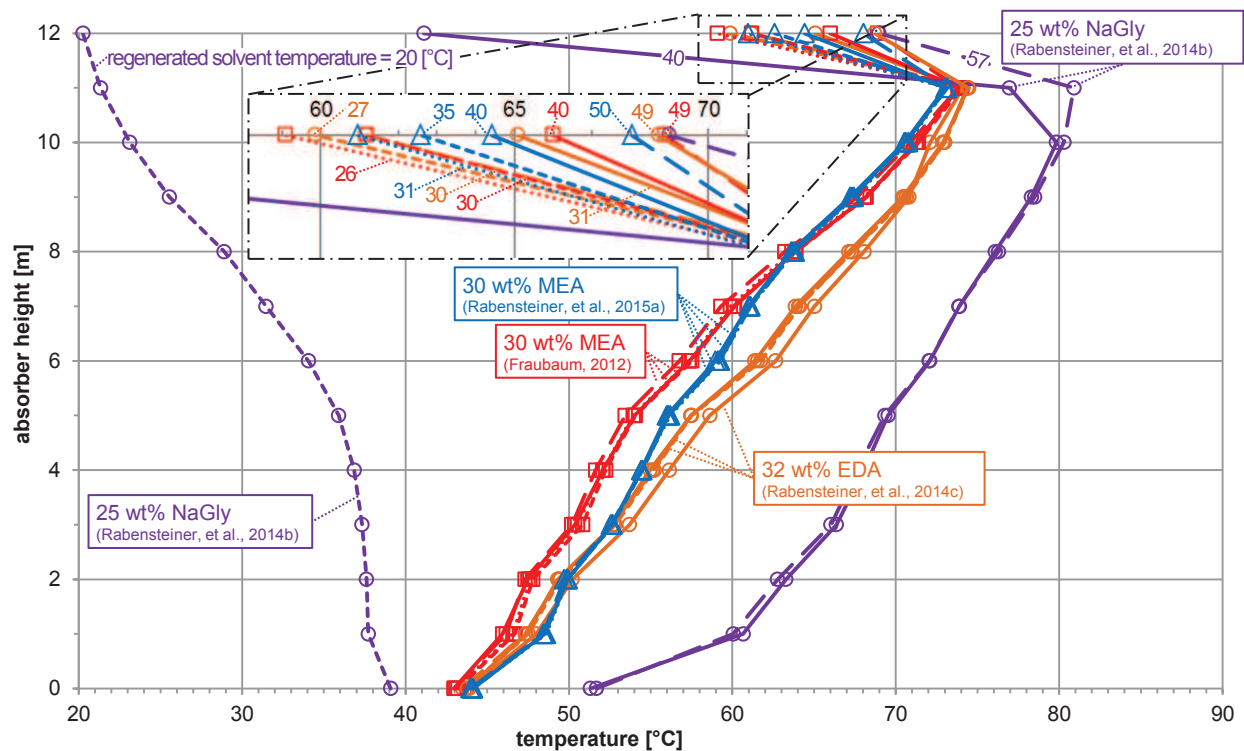
Fig. 6-46: Absorber column temperature profile for different regenerated solvent temperatures. Experimental data for 30 wt% MEA, 32 wt% EDA, 37.6 wt% PIP and 25 wt% NaGly.

6.9 Variation of the CO$_2$ separation efficiency

6.9.1 Basic considerations

Eq. 6-33 is obtained by transforming Eq. 6-1. The CO$_2$ loading difference $\Delta\alpha$ increases linearly with rising CO$_2$ separation efficiency when the lean solvent mass flow rate $\dot{m}_{lean}$ remains constant (Posch, 2012).

$$\Delta\alpha = \dot{m}_{CO_2} \cdot \frac{M_{lean}}{M_{CO_2}} \cdot \frac{\eta_{sep}}{\chi_{equ.\ amine}} \cdot \frac{1}{\dot{m}_{lean}}$$

Eq. 6-33

The CO$_2$ separation efficiency depends solely on the lean CO$_2$ loading (Eq. 6-34) when assuming that the absorber height is sufficient to achieve the equilibrium CO$_2$ loading in the absorber sump. Different absorption temperatures for the various operation points can also be dismissed. A higher CO$_2$ separation efficiency requires a lower residual CO$_2$ loading of the regenerated solvent. The CO$_2$ loading difference rises continuously (Posch, 2012).

$$\alpha_{lean} = \alpha_{rich} - \dot{m}_{CO_2} \cdot \frac{M_{lean}}{M_{CO_2}} \cdot \frac{\eta_{sep}}{\chi_{equ.\ amine}} \cdot \frac{1}{\dot{m}_{lean}}$$

Eq. 6-34

The CO_2 partial pressure in the desorber top has to be reduced in order to drop the CO_2 loading of the regenerated solvent. The heat of vaporization required to generate the water vapor (stripping steam) in the desorber (q_{vap,H_2O}) rises according to Eq. 6-4. The specific heat for solvent regeneration rises with increasing CO_2 separation efficiency.

6.9.2 Measurement results[1]

This measurement series was carried out with 30 wt% MEA (Fraubaum, 2013) and 32 wt% EDA (Rabensteiner, et al., 2014c). Table 6-12 shows the most important operating parameters of this test campaign.

Table 6-12:   Operating parameters of the test series with varying CO_2 separation efficiency.

	MEA		EDA	
	(Fraubaum, 2013)		(Rabensteiner, et al., 2014c)	
Concentration of active substance [wt%]	30	30	32	32
└ [molal]	└ 7.0	└ 7.0	└ 7.8	└ 7.8
L/G-ratio	var.	var.	var.	var.
Flue gas flow rate [m³/h]	90	90	90	90
└ F-factor [√Pa]	└ 1.50	└ 1.50	└ 1.50	└ 1.50
Desorber pressure [bar$_{abs}$]	2	2	2	2
Flue gas CO_2 content [vol% (dry)]	11.3 - 12.0	11.6 - 12.6	11.9 - 12.9	12.1 - 13.1
Regenerated solvent temperature [°C]	40	40	40	40
Flue gas temperature [°C]	40	40	40	40
CO_2 separation efficiency[2] [%]	90	80	90	80

The CO_2 loading difference increases linearly with respect to the CO_2 separation efficiency for a constant lean solvent flow rate. It is assumed that the rich CO_2 loading of the solvent is constant. The lean CO_2 loading decreases linearly with increasing CO_2 separation efficiency. The rich solvent does not achieve the equilibrium CO_2 loading for high CO_2 separation efficiencies since the partial pressure of CO_2 in the gas phase is the driving force for mass transfer. The CO_2 separation efficiencies close to the theoretical maximum enforce a disproportional increase in specific heat demand for the generation of stripping steam (Posch, 2012).

Fig. 6-47 shows the specific energy for solvent regeneration as a function of the L/G-ratio for the standard CO_2 separation efficiency of 90 % and 80 %. The curves exhibit the same shape and partially overlap at high L/G-ratios. There is only a higher difference at low solvent flow rates. The optimal operating point occurs at a smaller solvent flow rate because of the higher CO_2 loading of the regenerated solvent (Fig. 6-48). Less stripping steam needs to be generated in the desorber. The gradient of the heat of evaporation below the optimal operating point is steeper than the gradient of sensible heat for L/G-ratios above the optimal operating point. The minimum of sensible heat (q_{sens}) and heat of evaporation (q_{vap,H_2O}) shifts to smaller solvent flow rates. No significant differences were identified over the entire investigation range for 30 wt% MEA.

---

[1] Segments of this section have already been published in Rabensteiner, et al. (2014c).
[2] Deviation: ±1 %.
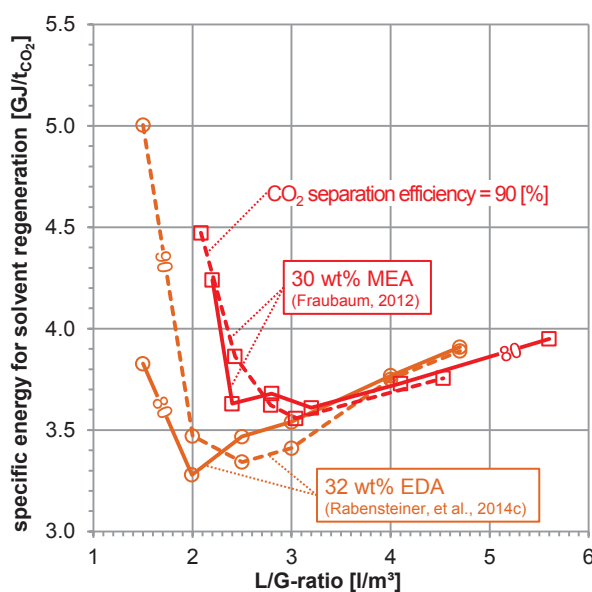
Fig. 6-47:   Specific energy for solvent regeneration in response to the CO_2 separation efficiency and the L/G-ratio. Experimental data for 30 wt% MEA and 32 wt% EDA for 90 (dashed line) and 80 % CO_2 separation efficiency (solid line).

Fig. 6-48 shows the CO_2 loading of the rich and lean solvent for different CO_2 separation efficiencies. The CO_2 loading difference between the rich and lean solvent drops with increasing L/G-ratio. The CO_2 equilibrium loading (not indicated in Fig. 6-48) refers to the absorber sump temperature (the lowest temperature in Fig. 6-49). The equilibrium CO_2 loading drops slightly with increasing solvent flow rate because of the higher absorber sump temperature at high solvent flow rates.

The CO_2 loading of the rich solvent is slightly higher at a CO_2 separation efficiency of 80 %. The reason is the lower sump temperature (compare Fig. 6-49) when setting a CO_2 separation efficiency of 80 %. The CO_2 loading of the regenerated solvent increases significantly at a CO_2 separation efficiency of 80 % because of the reduced amount of CO_2 absorbed.

Fig. 6-49 shows the temperature profile of the absorber column for different CO_2 separation efficiencies and L/G-ratios. The average absorption temperature for 90 % is higher than for 80 % CO_2 separation efficiency because of the reduced amount of CO_2 absorbed. Thus, less heat of absorption is released. Similar behavior is observed with 30 wt% MEA (Fraubaum, 2013).
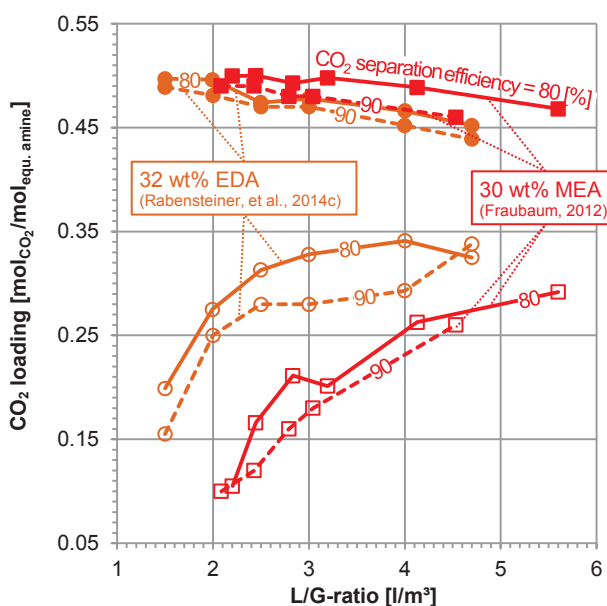
Fig. 6-48: Dependence of the CO_2 loading of the rich (filled symbols) and lean (unfilled symbols) 30 wt% MEA and 32 wt% EDA solution on L/G-ratio for 90 (dashed line) and 80 % CO_2 separation efficiency (solid line).
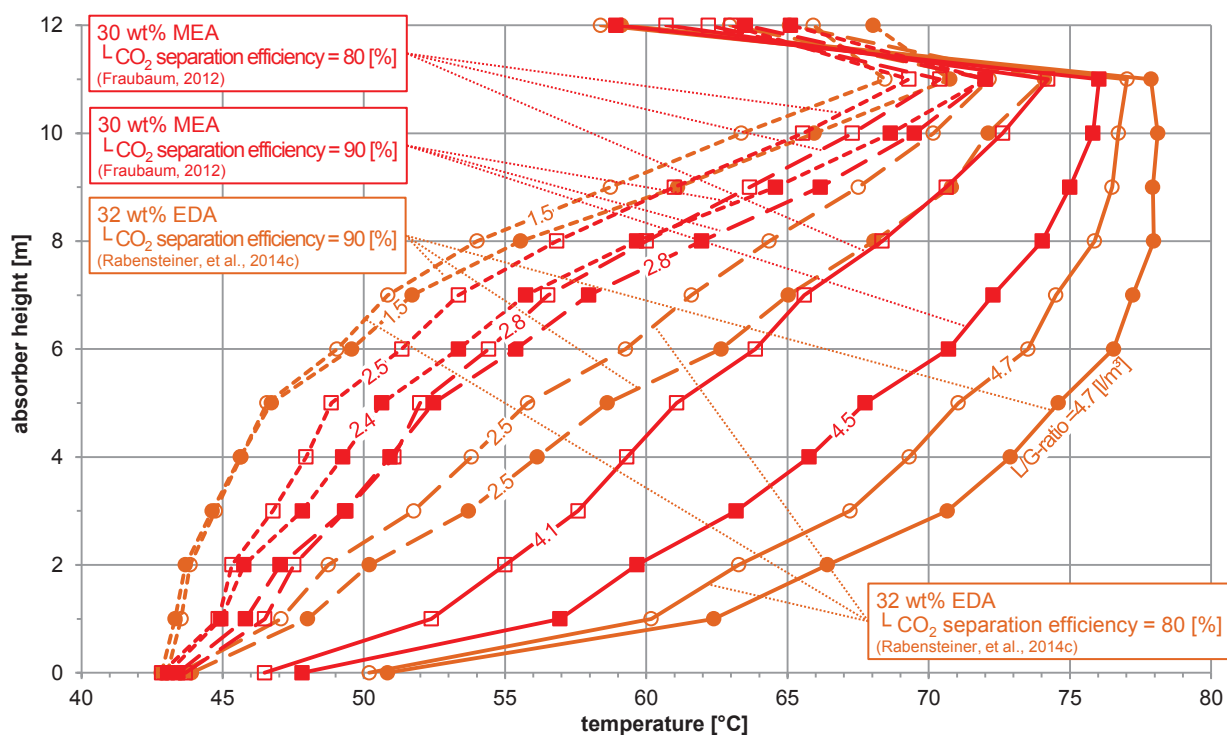
Fig. 6-49: Absorber column temperature profile for 90 (filled symbols) and 80 % CO_2 separation efficiency (unfilled symbols). Experimental data for 30 wt% MEA and 32 wt% EDA.

7 Pilot plant study with ionic liquids

Measurement series with the ionic liquid $[Ch_2][CO_3]$ will be described in the following section. The tests were carried out on the CO_2SEPPL and predecessor pilot plant, located on the Dürnrohr power plant.

Table 7-1 shows the most important operating parameters of this measurement campaign. The standard operating parameters of the measurement campaign on the predecessor pilot plant are listed on the left side of Table 7-1. Operating parameters of the remaining measurement points of the predecessor pilot plant can be taken from Wappel (2010).

Table 7-1: Operating parameters of the parameter study with aqueous $[Ch_2][CO_3]$.

Measurement series	Predecessor pilot plant Dürnrohr (Maierhofer, 2010; Wappel, 2010) Standard case (Section 7.1)	CO₂SEPPL pilot plant					
		Variation of the L/G-ratio (Section 7.2.1)	Variation of the flue gas flow rate (Section 7.2.2)	Effects of the absorption temperature (Section 7.2.3)			Decreased flue gas flow rate (Section 7.2.4)
				low	STD	high	
$[Ch_2][CO_3]$ concentration [wt%]	54	~ 77	~ 77	~ 77	~ 77	~ 77	~ 77
L/G-ratio [l/m³]	~ 14.0	2.0 – 5.0	4.0	4.6[1]	4.6[1]	4.6[1]	20.0
Flue gas flow rate [m³/h]	8.4	90	70 - 110	110	110	110	20
∟ F-factor [√Pa]	∟ 0.14	∟ 1.50	∟ 1.16-1.83	∟ 1.83	∟ 1.83	∟ 1.83	∟ 0.33
Desorber pressure [bar$_{abs}$]	1.24[2]	2.00	2.00	2.00	2.00	2.00	2.00
Flue gas CO_2 content [vol% (dry)]	12.4 - 12.8	12.4 - 12.8	12.4 - 12.8	12.4 - 12.8	12.4 - 12.8	12.4 - 12.8	12.4 - 12.8
Regenerated solvent temperature [°C]	40	40	40	~ 60	40	~ 25	50 - 62
Flue gas temperature [°C]	40	40	40	~ 50	40	~ 22	30 - 40
Desorber heating rod power [KW]	3.65	18	18	30	30	30	30
CO_2 separation efficiency [%]	26.2	17.4 - 25.2	21.8-28.4	16.0	25.6	33.2	max. 85.0
Specific energy for solvent regeneration [GJ/t$_{CO_2}$]	28.6	13.9 - 20.0	12.9-16.0	25.4	17.7	15.4	min. 24.0

7.1 Studies on the predecessor pilot plant

Tests on the predecessor pilot plant were carried out with 54 wt% $[Ch_2][CO_3]$. A description of this pilot plant can be found in Section 5.3.1. Stable pilot plant operation was the objective of this measurement campaign. Nine stable measuring points were recorded. Detailed evaluations of this measurement campaign can be found in Wappel (2010) and Maierhofer (2010).

Wappel (2010) defined a standard case (Table 7-1) for the ionic liquid. Prior to this, the pilot plant had been validated with 30 wt% MEA. The minimal specific energy for solvent regeneration is 4.4 GJ/t$_{CO_2}$ when using 30 wt% MEA. 90 % CO_2 separation efficiency was achieved with the benchmark solvent. Only small flue gas flow rates are processed because of the low absorber column height. The flue gas flow rate was further slightly reduced for the experiments with the ionic liquid. The solvent flow rate had been raised in order to provide sufficient solvent. The L/G-ratio was therefore significantly increased to 14 l/m³. Only a CO_2 separation efficiency of 26.2 % was achieved in the standard case. The specific energy for solvent regeneration is very high (28.6 GJ/t$_{CO_2}$) (Wappel, 2010).

---

[1] Maximal solvent flow rate.
[2] Regulated to 120 °C desorber sump temperature.

The CO_2 loading of 54 wt% $[Ch_2][CO_3]$ is in the range of 0.53 to 0.61 mol_{CO_2}/mol_{IL} during continuous operation. The maximum and minimum CO_2 loading of discontinuous operation should be determined. Only the absorber or desorber was operated over a longer period for this purpose. The CO_2 loading can be reduced to 0.53 mol_{CO_2}/mol_{IL} after a long regeneration period (~ 2 hours) without CO_2 absorption (in the absorber). This clearly indicates that the lean CO_2 loading cannot be lowered with pure regeneration compared to continuous operation. A further reduction of the lean CO_2 loading is difficult because of the low CO_2 partial pressure in the desorber top (compare Fig. 4-19). The CO_2 absorption rate decreases significantly because of the high CO_2 loading of the regenerated solvent (Aboundheir, et al., 2003). The measurement results of the screening experiments (Section 4.3.2) provide little information about the real CO_2 absorption rate in the pilot plant absorber column.

When a solvent temperature of 40 °C and a CO_2 partial pressure of 12 kPa are assumed, the equilibrium CO_2 loading in the absorber sump is 0.9 mol_{CO_2}/mol_{IL} (Fig. 4-19). No equilibrium CO_2 loading was achieved during continuous operation. The CO_2 loading can be significantly increased by pure absorption. Absorption without regeneration over a longer period (pure absorption) allowed CO_2 loadings of up to 0.85 mol_{CO_2}/mol_{IL}. Equilibrium CO_2 loading was therefore almost achieved in the absorber column. The separation performance of the process is generally better at high solvent flow rates because of the limited CO_2 loading difference between enriched and regenerated solvent.

Lowering the flue gas flow rate in order to minimize the effects of the slow kinetics increased residence time in the absorber column (not listed in Table 7-1). The CO_2 separation efficiency was increased to 49.7 % by reducing the flue gas flow rate to 5.8 m³/h. The L/G-ratio was increased to 31 l/m³. The main problem of CO_2 capture with the ionic liquid is the extremely slow CO_2 absorption rate caused by high CO_2 loadings.

7.2 Studies on the CO_2 SEPPL pilot plant

A $[Ch_2][CO_3]$ concentration of 77 wt% was set. The concentration was increased significantly compared to the experiments on the predecessor pilot plant in order to investigate the effects of the $[Ch_2][CO_3]$ concentration on the process. The advantage of this is the higher amount of active substance in the solvent circuit. The disadvantage is the strong increase in viscosity (compare Fig. 4-18). This results in a decrease in mass transfer.

7.2.1 Variation of the L/G-ratio

The effects of the solvent flow rate are observed in the first test series. The operating parameters are listed in Table 7-1. The CO_2 separation efficiency and the specific energy for solvent regeneration as a function of the L/G-ratio are shown in Fig. 7-1a. The CO_2 separation efficiency increases with increasing solvent flow rate. The standard CO_2 separation efficiency of 90 % is far from attained. Only a CO_2 separation efficiency between 17.4 and 25.2 % can be achieved, depending on the solvent flow rate. Nevertheless, there is a marked reduction in specific energy for solvent regeneration compared to the standard case of the predecessor pilot plant. The CO_2 separation efficiency of both measurement series (CO_2SEPPL and predecessor pilot plants) are similar. The better performance is mainly due to the longer absorber column.

The longer contact time of the two phases allows higher CO_2 loadings to be achieved. The optimal solvent flow rate decreases compared to the predecessor model experiments because of the increase in the active substance concentration and the higher CO_2 loadings. Higher solvent flow rates cannot be achieved due to the limited solvent pumping capacity.

3.5 GJ/t_{CO_2} is the minimal specific energy for solvent regeneration to reach 90 % CO_2 separation efficiency by using 30 wt% MEA (Rabensteiner, et al., 2015a). This means a huge increase in energy demand when using the ionic liquid. The optimal L/G-ratio is in the range of 3.2 l/m³ when using 30 wt% MEA. Consequently, more aqueous ionic liquid has to be pumped in a circuit to achieve the optimal operating point. More waste heat is produced because of the high solvent flow rate. The energy required for pumping is also increased. The inadequate performance of the ionic liquid is caused by the slow kinetics and the low mass transfer. The mass transfer is mainly hindered by the high viscosity of the ionic liquid (compare Fig. 4-18).
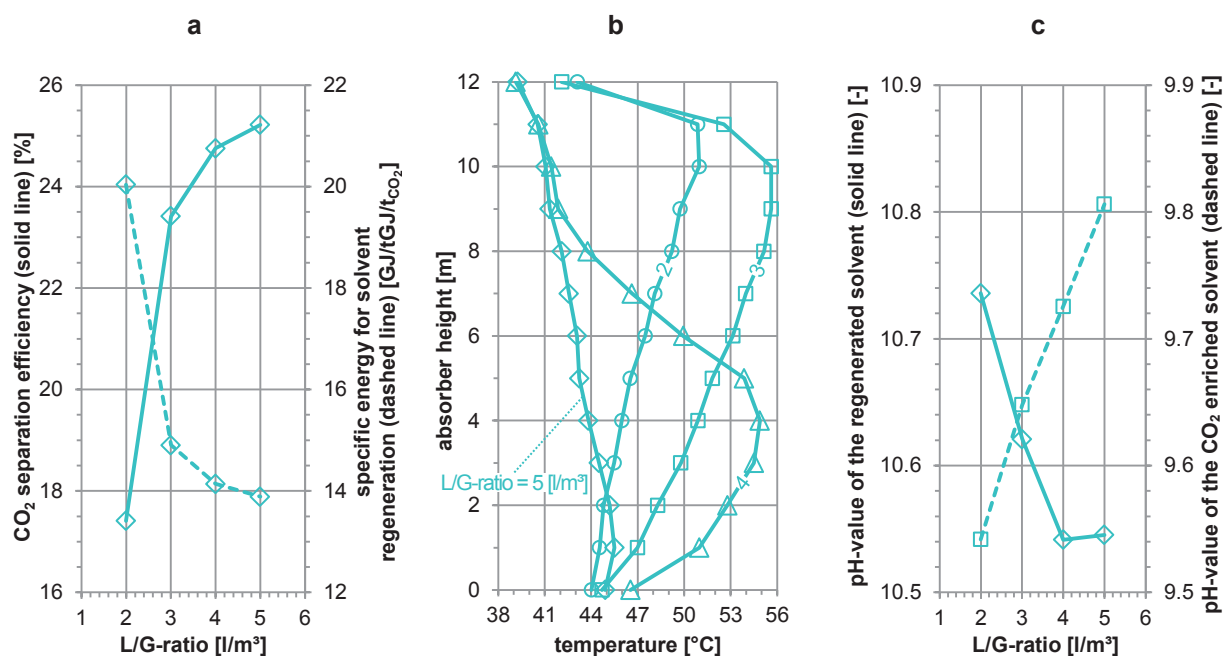
Fig. 7-1: **(a)** CO_2 separation efficiency (solid line) and specific energy for solvent regeneration (dashed line) as a function of the L/G-ratio. **(b)** Dependence of the absorber temperature profile on the L/G-ratio. **(c)** pH-value of the regenerated (solid line) and CO_2 enriched solvent (dashed line) as a function of the L/G-ratio. Experimental data for 77 wt% [Ch$_2$][CO$_3$].

Fig. 7-1b shows the temperature profile of the absorber column. The temperature of the flue gas treated is measured at a height of 12 m. The lowest temperature sensor is located in the sump of the absorber column and measures the temperature of the enriched solvent. The eleven intermediate temperature sensors measure a combination of the solvent and flue gas temperature, which is denoted as absorption temperature in the following. The maximum absorption temperature is in the upper part of the column at low solvent flow rates (L/G-ratio 2 to 3 l/m³). The absorption temperature over the entire column rises sharply when the L/G-ratio rises from 2 to 3 l/m³. The reason is the strong increase in CO_2 separation efficiency and the released absorption enthalpy associated with it. A further increase of the solvent flow rate shifts the absorption temperature maximum down. Excessive solvent stream from the top to the

bottom of the absorber column causes high downward transport of the absorption heat. The average absorption temperature on the absorber column decreases. The temperature of the enriched solvent increases at high solvent flow rates. The temperature of the treated flue gas drops according to the law of energy conservation. In general, the main absorption temperature of this series of experiments is very low in comparison to other solvents which were investigated on this pilot plant. The first reason for this is the small amount of CO_2 absorbed and the associated lower heat of absorption. Second is that the absorption enthalpy of the ionic liquid is significantly lower than those of the other solvents investigated (Section 4.3.5).

Fig. 7-1c shows the pH-value of the regenerated and enriched solvents as a function of the L/G-ratio. The pH-values for the enriched and regenerated solvents are linearly proportional to the CO_2 loading (Rabensteiner, et al., 2014b). The CO_2 loading of the enriched solvent decreases continuously with increasing solvent flow rate. In contrast, the CO_2 loading of the regenerated solvent increases. There seems to be a stagnation of the CO_2 loading of the regenerated solvent between 4 and 5 l/m³ - a sign that the optimum operating point has been reached.

7.2.2 Variation of the flue gas flow rate

The operating parameters of this measurement series are listed in Table 7-1. This measurement series allows the study of kinetic effects. A decrease in the flue gas flow rate reduces the amount of CO_2 transferred between the phases, which means that less driving force is needed. Mass transfer and kinetic limitations (if present) are thus less important (Mangalapally & Hasse, 2011a). Gas and liquid flow interact only moderately at low flue gas flow rates. This results in a reduction of the separation performance of the column. The turbulence in the absorber column is higher at higher flue gas flow rates. The separation efficiency increases until the flooding point of the column. A flooding of the used structured packings occurs only at F-factors above 3.5 √Pa (Schultes, 2008). There is no risk of flooding because the CO_2SEPPL pilot plant is only capable of F-factors up to 2 √Pa.

For 77 wt% [Ch$_2$][CO$_3$], the specific energy for solvent regeneration decreases to 12.9 GJ/t$_{CO_2}$, when the highest possible flue gas flow rate of 110 m³/h is set (Fig. 7-2a). The optimal L/G-ratio is 5 l/m³, according to the measurement results stated in Section 7.2.1. An L/G-ratio of 4 l/m³ has to be set because of the limiting solvent flow rate. The CO_2 separation efficiency decreases with increasing flue gas flow rate.
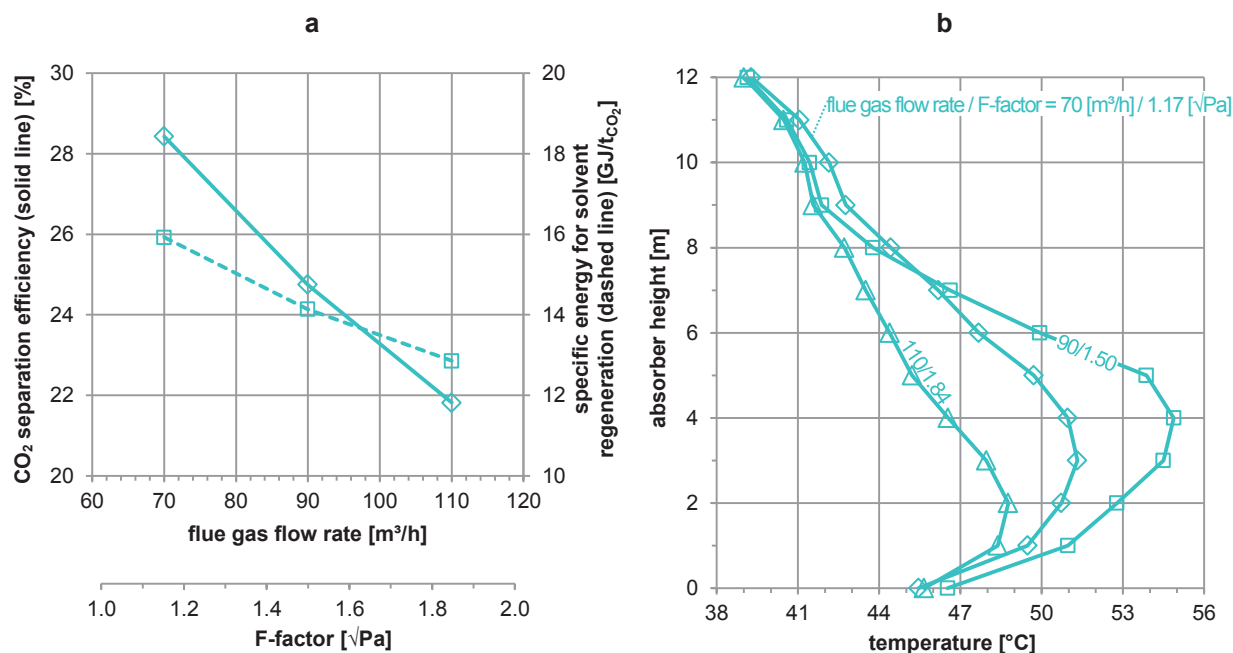
Fig. 7-2: **(a)** CO_2 separation efficiency (solid line) and specific energy for solvent regeneration (dashed line) as a function of the flue gas flow rate **(b)** Dependence of the absorber temperature profile on the flue gas flow rate. Experimental data for 77 wt% $[Ch_2][CO_3]$.

The mean absorption temperature decreases with increasing flue gas flow rate (Fig. 7-2b). Especially the temperature bulk in the lower part of the column rises. The temperature of the treated flue gas (highest temperature sensor) remains almost constant. The CO_2 enriched solvent temperature (lowest temperature sensor) increases slightly. The ratio of released heat of CO_2 absorption (amount of separated CO_2 molecules) to flue gas and solvent flow rate decreases with increasing flue gas flow rate, resulting in this temperature drop.

7.2.3 Effects of the absorption temperature

The operating parameters of this test series are listed in Table 7-1. The absorption temperature was changed by varying the flue gas temperature at the absorber entry and the regenerated solvent temperature. The maximal, minimal, and standard temperature of 40 °C of the flue gas and regenerated solvent were set. Higher absorption temperatures lead to an increase of the rate constant for the reaction of CO_2 with MEA (Posch, 2012) and other amines (Cullinane, 2005; Li, et al., 2007). This also applies for $[Ch_2][CO_3]$. A temperature increase reduces the viscosity of the solvent, too (compare Fig. 4-18). The CO_2 absorption process is also limited by the mass transfer. A low solvent viscosity caused by higher absorption temperatures leads to a higher mass transfer (compare Section 3.2.2). A low absorption temperature leads to higher CO_2 equilibrium loading level of the solvent. Low CO_2 loadings results in low CO_2 partial pressures in the desorber top. Large amounts of stripping steam must be generated to reduce the CO_2 partial pressure. This in turn leads to a high energy demand for generating stripping stream. A qualitative prediction cannot be made at this point due to the opposite nature of these two effects. Due to the slow kinetics and limited mass transfer of the ionic liquid, it is reasonable to assume that increased absorption temperatures lead to better performance.

139

As can be seen in Fig. 7-3, this basic idea was confirmed at the CO_2SEPPL pilot plant. A distinction is drawn between three different cases (high absorption temperature, standard case, and low absorption temperature in Table 7-1). As expected, the specific energy for solvent regeneration decreases with increasing absorption temperature. The same behavior was already observed at the predecessor pilot plant. The measured CO_2 loadings are higher than at the predecessor pilot plant. No conclusions can be drawn because of the different ionic liquid concentrations in both studies.
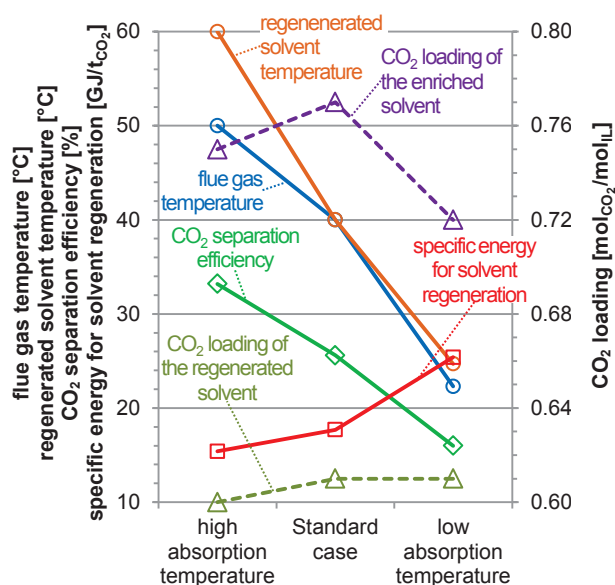
Fig. 7-3: Dependence of the CO_2 separation efficiency, specific energy for solvent regeneration and CO_2 loading of the enriched and regenerated solvent on the absorption temperature. Experimental data for 77 wt% $[Ch_2][CO_3]$.

7.2.4 Further investigations

The flue gas flow rate was drastically reduced in order to achieve the desired CO_2 separation efficiency of 90 %. The heating power was increased to 30 kW, which corresponds to the maximum power. An L/G-ratio of 20 l/m³ was set. Nevertheless, only a CO_2 separation efficiency of about 85 % (24 GJ/t_{CO_2}) was achieved. No improvement was achieved with a variation of the absorption temperature.

Experiments with a higher concentration ionic liquid were also carried out. The maximum and minimum CO_2 loading of an 85 wt% $[Ch_2][CO_3]$ solution were determined. Pure absorption without regeneration over an extended period (~ 2 hours) allows for CO_2 loadings of 0.82 mol_{CO_2}/mol_{IL}. The achievable CO_2 loading in continuous operation (normal operation with absorption and desorption) is significantly lower. A solvent regeneration down to 0.59 mol_{CO_2}/mol_{IL} is possible at the CO_2SEPPL pilot plant with pure desorption without absorption over an extended period (~ 2 hours). This clearly indicates that the lean CO_2 loading cannot be significantly lowered with pure regeneration compared to continuous operation. The same behavior had already been observed in the predecessor pilot plant.

A very high concentration ionic liquid (77 wt% $[Ch_2][CO_3]$) was used during the first measurement campaign on the CO_2SEPPL pilot plant (Sections 7.2.1, 7.2.2 and 7.2.3), which resulted in a very high solvent viscosity (Fig. 4-18). The concentration was significantly reduced to 50 to 60 wt% $[Ch_2][CO_3]$ in a other measurement campaign. This is roughly the concentration of the solution of measurement campaign carried out on the predecessor pilot plant. The specific energy for solvent regeneration increases enormously when using the lower concentration of solution.

The maximum and minimum CO_2 loading of a 57 wt% $[Ch_2][CO_3]$ solution was determined. A pure absorption without regeneration over an extended period (~ 2 hours) enables CO_2 loadings of 0.66 $mol_{CO_2}/mol_{equ.\ amine}$. A solvent regeneration down to 0.41 mol_{CO_2}/mol_{IL} is possible in the CO_2SEPPL pilot plant (without absorption over an extended period).

8   Emissions

Ammonia is the main oxidation product of the well-studied MEA-process (Schmidt & Moser, 2013). Thus NH_3 measurements of the flue gas treated were carried out in the course of the parametric study at the CO_2SEPPL pilot plant. Gas chromatography measurements were performed in order to determine other volatile components. No long-term studies have been conducted over the entire operating period of the CO_2SEPPL pilot plant. All solvents used were only in operation for a few hours at the time when the emission measurements were carried out. It is thus not surprising that the measured emissions are very low because the decomposition rate increases generally over time (Schmidt & Moser, 2013).

Emission measurements at the CO_2SEPPL pilot plant were carried out with 30 wt% MEA, 37.6 wt% PIP, 28/17 wt% AMP/PIP and 40 wt% KGly.

8.1 Preliminary studies

The degradation of MEA has been studied extensively and has recently been reviewed in detail by Reynolds, et al. (2015), Vega, et al. (2014), Rey, et al. (2013) and Gouedard, et al. (2012). The three pathways of MEA degradation are oxidative degradation, HSS formation and carbamate polymerization (Gouedard, et al., 2012; Vega, et al., 2014). Carbamate polymerization is also referred to as thermal degradation because it occurs primarily during thermal desorption of CO_2 and thermal amine regeneration (Rochelle, 2012). Emission measurements on a pilot plant-scale using MEA are reported in Schmidt & Moser (2013).

The only pilot plant study about piperazine degradation was carried out on the Tarong pilot plant (Cottrell, et al., 2013). A technical description of this pilot plant can be found in Section 5.3.3. Table 5-1 lists important technical data. The effect of flue gas components, including NO_x and SO_2, in addition to trace elements, on the performance of the piperazine-based process is almost unknown. This also entails the formation of degradation products from operation with piperazine in real flue gases, particularly as recently concerns have been raised regarding the formation of harmful products from PCC processes (Jackson & Attalla, 2011; Shao & Stangeland, 2009).

Results of emission measurements on a pilot plant-scale with aqueous KGly are not available in literature. The first studies about the degradation behavior of aqueous KGly were carried out by Sexton (2008a; 2008b). Experiments in a low gas flow apparatus with 18.45 wt% KGly (2 m KGly) were carried out in these studies. This solvent is resistant to oxidative degradation at 55 °C in the presence of Fe and Cu (determined by low gas flow apparatus experiments). Therefore, the alkanolamine structure may be more susceptible to oxidative degradation (Sexton, 2008b). The main oxidative degradation products are formate and acetate (Sexton, 2008b). Voice (2010) investigated oxidative degradation by quantification of the NH_3 production rate in a high gas flow apparatus. 30 wt% KGly (3.8 m KGly) shows a lower NH_3 production rate in comparison to 30 wt% MEA in this study.

Epp, et al. (2011) detected oxidation of KGly, albeit at a rate of about one-half to one-fourth that of MEA, by observing oxygen consumption, ammonia and formaldehyde production. Martin, et al. (2012) observed that KGly was extensively degraded at 140 °C in the presence of oxygen,

although losses may have been from amide polymerization at high temperature rather than oxidation.

Emission measurements on the Staudinger pilot plant with potassium salt of an undisclosed amino acid have been conducted by Siemens AG (Sandell, 2010). The loss of active substance due to degradation is not detectable. Even without an operation of the absorber water washing section, VOC (volatile organic compounds), formaldehyde, methylamine and nitrosamines were not detected in the CO_2 cleaned flue gas stream. Small amounts of HSS and nitrosamines can be removed with a reclaimer. The NH_3 concentration in the treated flue gas is smaller than 1 ppm (Sandell, 2010).

8.2 NH_3 emissions[1]

NH_3 concentration measurements of the treated flue gas at the CO_2SEPPL pilot plant were carried out using 30 wt% MEA, 37.6 wt% PIP, 28/17 wt% AMP/PIP and 40 wt% KGly. A stationary transmitter with a built-in electrochemical cell was used as the measurement device. Fig. 8-1 shows the measured NH_3 concentration of the treated flue gas at the outlet of the water washing section. All measurement results from this test series can be seen in Appendix B.

The solvent flow rate (L/G-ratio) was used as variable parameter. The most important operating parameters can be seen in Table 8-1. The water volume flow rate in the absorber washing section was kept constant at 470 l/h in this test series.

Table 8-1:   Operating parameters for emission measurements.

	MEA	PIP	AMP/PIP	KGly
Concentration of active substance [wt%]	30	37.6	28/17	40
└ [molal]	└ 7.0	└ 7.0	└ 4.4/2.4	└ 5.9
L/G-ratio [l/m³]	var.	var.	var.	var.
Flue gas flow rate [m³/h]	90	100	100	50
└ F-factor [√Pa]	└ 1.50	└ 1.65	└ 1.65	└ 0.84
Desorber pressure [bar$_{abs}$]	2	2	2	2
Flue gas CO_2 content [vol% (dry)]	12.6 – 12.8	12.9 – 13.2	11.9 – 12.4	12.8 – 13.2
Regenerated solvent temperature [°C]	40	40	40	40
Flue gas temperature [°C]	40	40	40	40
CO_2 separation efficiency[2] [%]	90	90	90	90

There are large differences in NH_3 emissions between the tested solvents (compare Fig. 8-1). Very low NH_3 emissions were measured for 37.6 wt% PIP and 28/17 wt% AMP/PIP (< 0.1 ppm). Absolute measurement values should not be used as comparison for these two solvents because of the large measuring range of the transmitter (0 – 500 ppm). Additionally, the NH_3 emissions of the process with 28/17 wt% AMP/PIP indicate no clear dependence on the solvent flow rate. The results of the measurement series with 28/17 wt% AMP/PIP are therefore not listed in Fig. 8-1. There is a significant increase in NH_3 emissions when using the benchmark solvent 30 wt% MEA (Fig. 8-1a). A NH_3 concentration up to 23 ppm was measured in the treated flue gas. The highest NH_3 concentration in the treated flue gas by far was measured during operation with 40 wt% KGly (Fig. 8-1c). The NH_3 concentration increased up to 249 ppm.

---

[1] Segments of this section have already been published in Rabensteiner, et al. (2015b; 2015c).
[2] Deviation: ±1 %.

The average absorption temperature increases with increasing solvent flow rate (compare Fig. 8-1a and Fig. 8-1b for 30 wt% MEA and 37.6 wt% PIP), resulting in increasing flue gas temperature at the entry of the water washing section. The average absorption temperature increases from 54.3 to 67.7 °C and from 54.4 to 70.7 C when using 30 wt% MEA and 37.6 wt% PIP, respectively. In contrast, the average absorption temperature rises only slightly when using 40 wt% KGly. There is a balance in the enthalpy leaving with the liquid and the flue gas when the temperature bulge is located somewhere in the middle of the absorber column (Kvamsdal & Rochelle, 2008). An increase of the solvent flow rate leads to reaching this critical value when using 40 wt% KGly. This can be seen from a rapid change in the average absorption temperature in Fig. 8-1c. The average absorption temperature decreases from 68.5 to 54.4 °C when the L/G-ratio rises from 8 to 9 l/m³.

The flue gas temperature at the outlet of the water washing section is approximately equal to the temperature of the flue gas at the inlet of the absorber (~ 40 °C) in order to keep the water balance of the entire system closed. Consequently, the temperature difference between the entering and exiting flue gas streams in the water washing section decreases with increasing solvent flow rate when using 30 wt% MEA and 37.6 wt% PIP, respectively. The temperature difference is very low and drops to 3.9 K when using 40 wt% KGly. The flue gas temperature at the water washing section entry drops even below 40 °C, the standard outlet temperature of the treated flue gas. The temperature difference in the absorber washing section is significantly higher and does not fall below 19.8 and 14.4 K when using 30 wt% MEA and 37.6 wt% PIP, respectively.

The flue gas stream down- and upstream to the water washing section is saturated. Lower amounts of condensate are produced in the water washing section at a low temperature difference in this section. Lower amounts of condensate apparently lead to an increase in NH_3 concentration in the treated flue gas when using 37.6 wt% PIP and 40 wt% KGly. For the process with 37.6 wt% PIP, the NH_3 concentration increases from 0.02 to 0.09 ppm when the L/G-ratio rises from 1.95 to 4.90 l/m³. The increase is almost linear. For the 40 wt% KGly-process, the NH_3 concentration increases from 95 to 234 ppm when the L/G-ratio rises from 6.0 to 10.0 l/m³. Two measurement points were recorded at an L/G-ratio of 8 l/m³ when 40 wt% KGly. One of these two measurement points indicates a strong increase in NH_3 concentration (249 ppm). The measurement curve of 30 wt% MEA shows no clear trend.

Another reason for the low NH_3 emissions during operation with aqueous piperazine could be the incomplete filling of the absorber water washing section during the operation. The absorber and desorber sump levels decreased slightly during this measuring campaign. The flue gas temperature at the outlet of the water washing section is approximately equal to the temperature of the flue gas at the inlet of the absorber (~ 40 °C) in order to keep the water balance of the entire system closed. Incomplete filling of the absorber water washing section must be therefore assumed. There is a continuous rise in the water level in reservoir of the water washing section during operation. The added water is not saturated with NH_3. Consequently, the emissions are very low until the filling is complete (Rabensteiner, et al., 2015b).
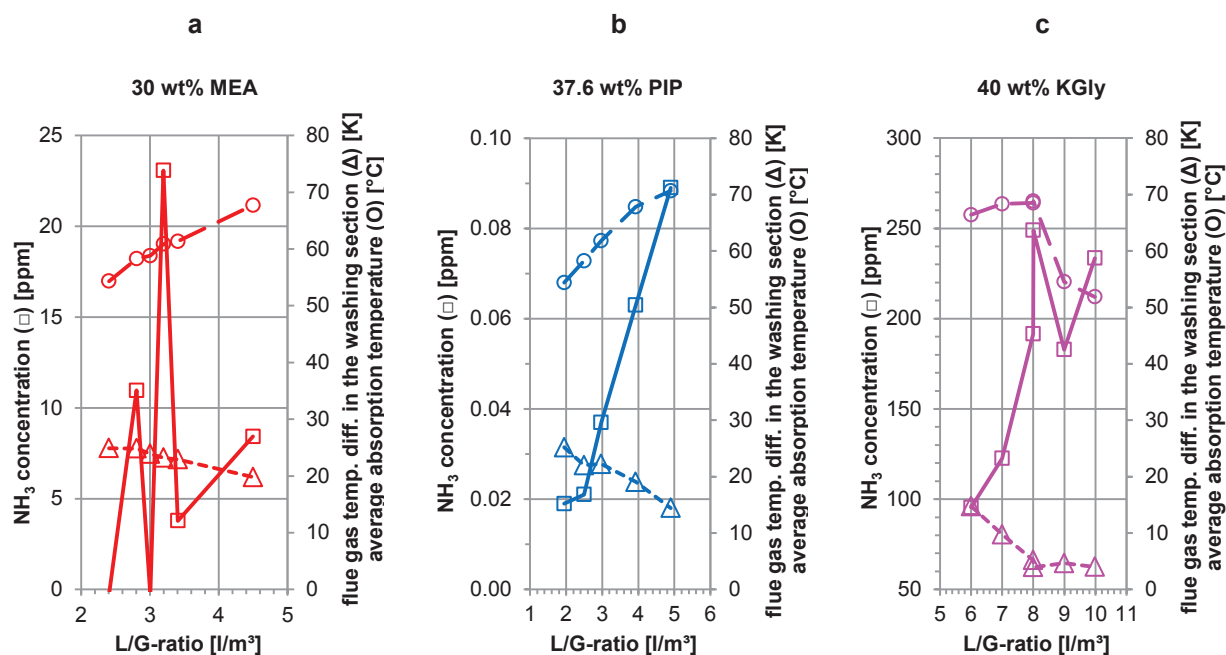
Fig. 8-1: Effect of the L/G-ratio on the NH_3 concentration of the treated flue gas. Experimental results for 30 wt% MEA **(a)**, 37.6 wt% PIP (Rabensteiner, et al., 2015b) **(b)** and 40 wt% KGly (Rabensteiner, et al., 2015c) **(c)**.

The NH_3 concentrations measured on the Tarong pilot plant with aqueous piperazine are significantly higher. An NH_3 concentration of 12 ppm was measured after 900 operating hours. The NH_3 concentration increases linearly with the runtime. NH_3 measurements were performed after only 700 hours of operation. Very small amounts of ammonia were emitted at the beginning of this measurement campaign, if a linear trend (continues even at low runtimes) is assumed. An increase in the desorber pressure leads to a steeper slop of the NH_3 concentration over time (Cottrell, et al., 2013).

8.3 Gas chromatographic measurements

Gas chromatography (GC) measurements on the CO_2SEPPL pilot plant were performed for 30 wt% MEA and 28/17 wt% AMP/PIP. Emissions were determined for the treated flue gas (which is emitted to the atmosphere) and the separated CO_2. An immediate gas analyses was not necessary because only stable components should be measured (compare Table 8-2). Gas bags (27 l) were used for gas sampling on site. Samples of the treated flue gas were taken downstream to the water washing section. The studies of Reynolds, et al. (2015) and Schmidt & Moser (2013) were used as reference when choosing test gases.

Table 8-2: Properties of test gases.[1]

		Concentration [ppm]	Boiling point [°C]	Vapor pressure (20 °C) [kPa]	Retention time [s]
Ammonia	NH_3	505 ± 10	-33.34	857.3	189.3
Formaldehyde	CH_2O	100 ± 10	-19	439.9	204.2
Acetaldehyde	C_2H_4O	44.6 ± 4.5	20.4	100.7	235.3
Propionaldehyde	C_3H_6O	9.68 ± 0.97	49	34.1	428.2
Acrolein	C_3H_4O	2.38 ± 0.24	52	29.5	443.3
Acetone	C_3H_6O	22.1 ± 1.1	56	24.6	486.3

A SHIMADZU GC-14B was used. The detail GC flow scheme can be found in Appendix A.2. The GC is equipped with a flame ionization detector (FID) and thermal conductivity detector (TCD). N_2 was used as a carrier gas for FID measurements. In contrast, He was used as carrier gas for the TCD measurements. A carrier gas flow rate of 50 ml/min was set. The furnace temperature was kept constant at 175 °C.

None of the components in the test gases were detected. A list of the detected peaks can be taken from Table 8-3.

Table 8-3: List of detected peaks.

Peak	Substance	t_{ret} [s]	Detector	30 wt% MEA flue gas	30 wt% MEA CO_2	28/17 wt% AMP/PIP flue gas	28/17 wt% AMP/PIP CO_2[2]
1	N_2		TCD	✓	✓	✓	✓
2	CO_2	64	TCD	✗	✓	✗	✓
3	unkn. C_xH_y	80	FID	✗	✗	✗	✓
4	unkn. non-C_xH_y	140	TCD	✓	✓	✗	✗
5	unkn. C_xH_y	165	FID, TCD	✓	✓	✓	✓
6	unkn. C_xH_y	180	FID	✓	✓	✓	✓
7	unkn. C_xH_y	203	FID	✓	✓	✓	✓
8	unkn. C_xH_y	418	FID	✓	✓	✗	✗

✓ Substance has been detected in at least one sample.
✗ Substance hasn´t been detected in any sample.

The results of the gas chromatographic analysis only partly allow for scientific discussion. In general, the concentrations of the components measured are below expectations. The NH_3 concentration measured by the stationary transmitter is significantly higher for 30 wt% MEA compared to 28/17 wt% AMP/PIP (compare Fig. 8-1a for 30 wt% MEA). NH_3 cannot be used as an indicator of other emissions in the treated flue gas. For example, the content of the unknown hydrocarbon which is indicated by peak 5 (Fig. 8-2a) is for 28/17 wt% AMP/PIP higher than for 30 wt% MEA. Peak 6 (Fig. 8-2b) is only slightly higher when using 30 wt% MEA. No conclusion can be drawn about the components in the separated CO_2 stream.

---

[1] N_2 is the remaining gas.
[2] Only one sample was taken from the CO_2 stream.
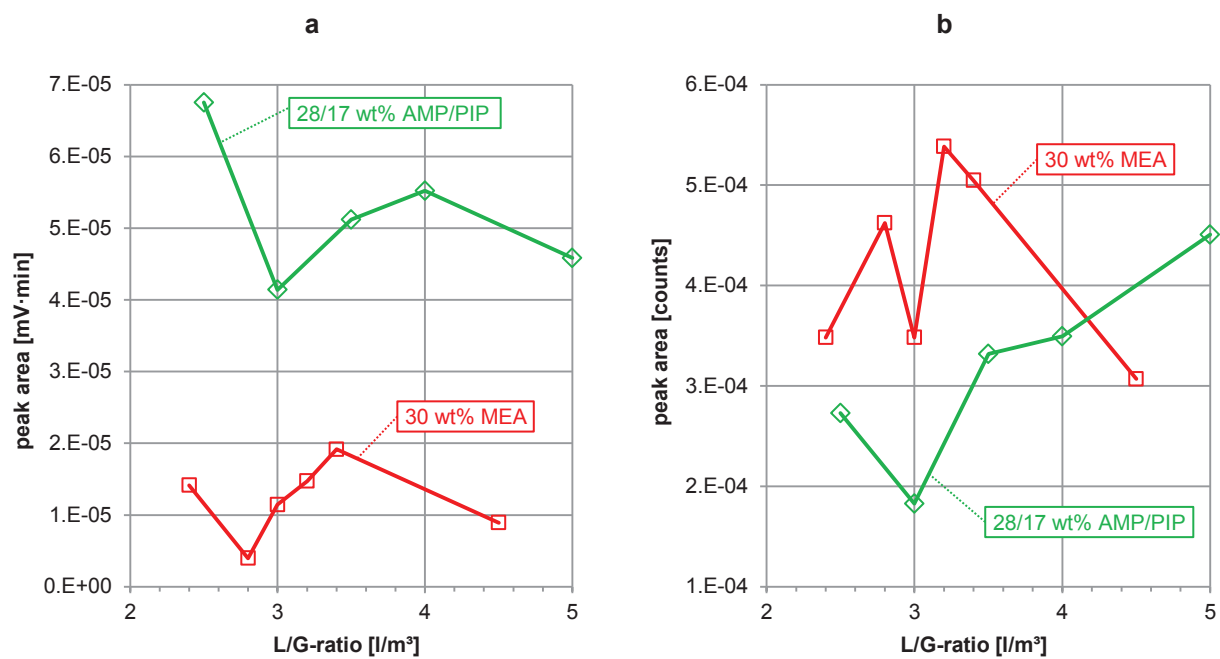
Fig. 8-2: Emission measurements of the treated flue gas. Peak area of peak 5 **(a)** and peak 6 **(b)** detected by FID as a function of the L/G-ratio.

9   Conclusions

This work presents a scientific investigation of the CO_2 post-combustion capture (PCC) process on pilot plant-scale. By producing realistic measurements, this work seeks to provide a major contribution to the design of full-scale plants. Realistic measurement conditions on the CO_2SEPPL pilot plant are ensured by the:

- Use of real flue gas out of the power plant process
- Nearly industrial heights of the absorber and desorber columns
- Closed CO_2 balance
- Closed energy balance.

Flue gas is taken directly from the hard coal-fired power plant in Dürnrohr, Austria. The influence of typical by-products of coal combustion on the PCC process can be observed. The presence of dust, soot, and other particles in the flue gas is reduced by an upstream dust filter. A pre-scrubber for SO_x reduction allows for a further application of the CO_2SEPPL pilot plant.

The influence of kinetics and mass transfer on the PCC process can be reduced by an absorber column of an almost industrial-scale. The height of the absorber column determines the contact time of the gaseous and liquid phase. The CO_2SEPPL absorber column is 12 m high. This is an above average absorber column height in comparison to other PCC pilot plants. High quality steels must be used for column construction in order to counteract the corrosive effect of several solvents. High absorber columns are therefore associated with enormous investment costs. Whether or not extremely high absorber columns (as the Staudinger and Niederaußem pilot plant) are economically viable to make operation of solvents with low kinetics feasible must be explored further.

Observation of the separated CO_2 stream is essential for the calculation of the specific energy for solvent regeneration. Balancing by CO_2 concentration and volume flow rate measurement of the incoming and exiting flue gas streams can be carried out during pilot plant operation. The balancing above the solvent stream occurs via CO_2 loading measurement of the CO_2 enriched and regenerated solvent in the laboratory. The calculations of the separated CO_2 amount via the solvent and flue gas stream provide same results.

The specific energy for solvent regeneration used in the present work refers to the separated amount of carbon dioxide and regeneration energy (GJ/t_{CO_2}). The regeneration energy is supplied by an electrical heating rod in the desorber sump. Heat losses are small and recognized by energy balancing thanks to completed thermal insulation of pilot plant components. Unlike pilot plants with high heat losses, as, for instance, the J.J. Pickle pilot plant, heat losses are not deducted when calculating the specific energy for solvent regeneration.

Studies with the benchmark solvent monoethanolamine (MEA) were performed in order to illustrate the realistic measurement conditions at the CO_2SEPPL pilot plant. Measurement results, generated at the pilot plants in Esbjerg (Denmark) and Niederaußem (Germany), two of the largest plants in the world, served as comparison. At the CO_2SEPPL pilot plant, there were only slight differences in the results, which were caused by different operating conditions and system configurations (e.g. absorber intercooler).

Due to the high costs of PCC, this technology and the entire CCS process is unprofitable and unfeasible without subsidies. The high investment costs for such plants are caused partially by the use of stainless and high-alloyed steel. Shorter absorber and desorber columns or non-corrosive solvents reduce investment costs considerably. However, the absorber height is limited by the reaction rate of the solvent. The solvent stream determines the size and design of the unit needed for the process, as well as its necessary cooling capacity, which is often a limiting factor in power plant construction. Additional costs are caused by the removal of any harmful components from the CO_2 cleaned flue gas, arising from volatility solvents and degradation products. Such high operating costs further hamper the widespread applicability of this technology. Operating costs are mainly dependent on the energy required for solvent regeneration. Fresh solvent must be continuous refilled due to the solvent loss caused by volatility and degradation. The running costs of solvent supply can be very high.

The use of different solvents affects all of the problems mentioned above. The most commonly used amine for CO_2 separation at present is 30 wt% MEA, which is used as benchmark solvent. Since MEA has already been used for flue gas cleaning for decades, and extensive and detailed studies of CO_2 separation with MEA exist, PCC capture with MEA can be considered a mature technology. Larger energy savings with this solvent can therefore be excluded from this analysis. The trend is towards the testing of new solvents that are attractive in terms of energy saving potential.

A minimum specific energy for solvent regeneration of 3.5 GJ/t$_{CO_2}$ has been determined for the benchmark solvent 30 wt MEA at the CO_2SEPPL pilot plant. For a better comparison of different measurement results, the solvent flow rate is always indicated as a function of the flue gas flow rate (L/G-ratio) in the present work. The minimal specific energy for solvent regeneration for 30 wt% MEA is measured at an L/G-ratio of 3.2 l/m³.

An intensive literature review was carried out in order to find attractive new solvents for PCC. Extensive laboratory tests were conducted to study CO_2 absorption capacity, kinetics and solvent regenerability. These studies were performed in order to determine in advance the behavior of the absorption solvent in pilot plant operation. Based on the preliminary laboratory studies, the aqueous amines ethylenediamine (EDA), piperazine (PIP), and 2-amino-2-methyl-1-propanol (AMP) were tested at the CO_2SEPPL pilot plant for their suitability as CO_2 absorption solvents.

The CO_2SEPPL pilot plant facilitates a detailed parameter study of various solvents due to the large number of variable operating parameters. Studies with flue gases of a natural gas-fired boiler and the related lower flue gas CO_2 content are possible in a short time range, before and after the annual power plant revision. A shorter absorber column can also be adjusted. The desorber pressure can be increased up to 3 bar$_{abs}$.

Piperazine-based solvents have large saving potential in terms of investment and operating costs due to their fast kinetics, low CO_2 absorption enthalpy, easily accomplished regeneration. Tests with piperazine-based solvents were carried out with 37.6 wt% PIP and 28/17 wt% AMP/PIP. The minimal specific energy demand for solvent regeneration of 37.6 wt% PIP is about 3.0 GJ/t$_{CO_2}$. The specific energy demand for solvent regeneration can be reduced by up to 15 % with piperazine in comparison to MEA. The solvent flow rate is by far the

149

most crucial operating parameter of the PCC process. The specific energy for solvent regeneration (consisting of heat for reversing reaction, sensible heat for solvent heat up, and energy for generating stripping steam) indicates a clearly recognizable minimum at a variety of L/G-ratios. 28/17 wt% AMP/PIP shows a favorable energy performance with a minimum specific energy for solvent regeneration of 3.1 GJ/t_{CO_2}.

The optimal L/G-ratio is 2.5 l/m³ when using 37.6 wt% PIP. The solvent flow rate is significantly lower than that of the process with 30 wt% MEA. Additionally, it can be further reduced by adding AMP to piperazine. This is achieved by the high CO_2 absorption capacity of AMP and results in significant savings in the design of plants. The lowest energy consumption was measured at an L/G-ratio of 2.0 l/m³ when using 28/17 wt% AMP/PIP. This means that almost 40 % less solvent has to be pumped in circulation. For studies with EDA, the concentration was set to 32 mass percent. A similar solvent flow rate as for 37.6 wt% PIP is required to reach the optimal operating point. The specific energy for solvent regeneration is slightly over 3.1 GJ/t_{CO_2} when using 32 wt% EDA.

All amine-based solvents show a decrease in regeneration energy with increasing flue gas flow rate. 37.6 wt% PIP in particular indicates a continuous decrease in energy demand up to the maximal flue gas flow rate of 120 m³/h because of its fast kinetics. For MEA, there is even a stagnation of energy for flue gas flow rates up to 100 m³/h in contrast. The importance of the industrial absorber column height was identifiable for the first time in this test series.

The fast kinetics of piperazine also have favorable effects on measurements by reducing absorber height. The achievable CO_2 loading in the absorber column decreases marginally. Only a small increase in specific energy for solvent regeneration (+13 %) is recognizable when the absorber height is reduced from 12 to 6 m. The specific energy for solvent regeneration is increased by 18 % when the absorber height is lowered from 12 to 6 m and when using 30 wt% MEA in contrast. Other amine-based solvents show only a small dependence on the desorber pressure compared to the benchmark solvent 30 wt% MEA. Substantial energy savings for higher desorber pressures (> 2 bar_{abs}) are only recognizable for 37.6 wt% PIP.

Experiments with the flue gas of a natural gas-fired boiler were conducted with 30 wt MEA, 32 wt% EDA, and 37.6 wt% PIP. There was an increase in energy demand due to the low driving force caused by the lower CO_2 partial pressure in the flue gas. There is a shift in the optimal operating point towards to smaller solvent flow rates because of a balance between energy demand for generating stripping steam and sensible heat for solvent heat up. All solvents exhibit an equal percentage increase in energy demand and reduction of solvent flow rate.

Piperazine-based solvents have a high resistance to thermal and oxidative degradation. This is demonstrated by the low concentration of volatile components (particularly NH_3) in the purified flue gas. With gas chromatography measurements it is apparent that elevated ammonia concentrations are not related to higher contents of other degradation products.

In order to prevent solidification, crystallization, and foaming during operation with piperazine-based solvents, additives have to be added and certain concentration ranges and operating areas must be avoided.

In addition to amine-based solvents, aqueous solutions of amino acids and ionic liquids were tested at the CO_2SEPPL pilot plant. The low or nonexistent vapor pressure of such solvents is their main advantage, and the expected emissions are small. However, the amino acids studied resulted partly in strongly increased concentrations of ammonia (the main degradation product) measured at the absorber outlet.

The laboratory studies of CO_2 absorption capacity, regenerability, and kinetics indicate that blends of primary (glycine) and secondary (proline and sarcosine) amino acids have no fundamentally favorable properties compared to simple solutions. Aqueous solutions of the amino acids sodium and potassium glycinate were tested at the CO_2SEPPL pilot plant. Amino acids and ionic liquids have a huge energy demand in comparison to the amine-based solvents tested. The increase in energy demand could be caused by the poor solvent regenerability and the related slow kinetics. The high viscosity of ionic liquids additionally complicates mass transfer in the columns. Based on the CO_2SEPPL pilot plant studies in Dürnrohr, this study concludes that amino acids and ionic liquids are not alternatives to amines

References

Aaron, D., Tsouris, C., 2005. Separation of CO_2 from flue gas: A review. Separation Science & Technology 40 (1-3), 321-348.

Aboundheir, A., Tontiwachwuthikul, P., Chakma, A., Idem, R., 2003. Kinetics of the reactive absorption of carbon dioxide in high CO_2-loaded, concentrated aqueous monoethanolamine solutions. Chemical Engineering Science, 58 (23-24), 5195-5210.

Abu-Zahra, M.R.M., Abbas, Z., Singh, P., Feron, P.H.M., 2013. Carbon dioxide post-combustion capture: Sovent technologies overview, status and future directions. In: Mendez-Vilas, A. (ed) *Materials and processes for energy: Communicating current research and technological developments*. Formatex Research Center, Badajoz, Spain, ISBN: 978-84-939843-7-3, 923–934.

Adeosum, A., Hadri, N.E.I., Goetheer, E.L.V., Abu-Zahra, M.R.M., 2013. Absorption of CO_2 by amine blends solutions: An experimental evaluation. Int. J. Eng. Sci. 3 (9), 12-23.

Aldous, R., Anderson, C., Anderson, R., Gerstenberger, M., Gurevich, B., Hooper, B., Jenkins, C., Kaldi, J., Kentish, S., Linton, V., Santos, S., Webley, P., 2013. CSLF Technology Assessment, CCS Technology Development: Gaps, Opportunities and Research Fronts. Cooperative Research Centre for Greenhouse Gas Technologies, Canberra, Australia, CO_2CRC Publication Number RPT13-4571.

Amundsen, T.G., Øi, L.E., Eimer, D.A., 2009. Density and viscosity of monoethanolamine + water + carbon dioxide from (25 to 80) °C. J. Chem. Eng. Data 54, 3096-3100.

Anderson, J.L., Dixon, J.K., Brennecke, J.F., 2007. Solubility of CO_2, CH_4, C_2H_6, C_2H_4, O_2, and N_2 in 1-hexyl-3-methylpyridinium bis(trifluoromethylsulfonyl)imide: Comparison to other ionic liquids. Acc. Chem. Res. 40, 1208-1216.

Aroua, M.K., Salleh, R.M., 2004. Solubility of CO_2 in aqueous piperazine and its modeling using the Kent-Eisenberg approach. Chem. Eng. & Technol. 27, 65-70.

Austgen, D.M., Rochelle, G.T., Chen, C.C., 1991. Model of vapor-liquid equilibria for aqueous acid gas-alkanolamine systems. 2. Representation of H_2S and CO_2 solubility in aqueous MDEA and carbon dioxide solubility in aqueous mixtures of MDEA with MEA or DEA. Ind. Eng. Chem. Res. 30, 543-555.

Bailey, D.W., Feron, P.H.M., 2005. Post-combustion decarbonisation processes. Oil & Gas Science and Technology, 60 (3), 461-474.

Baufumé, S., Hake, J.F., Linsen, J., Markewitz, P., 2011. Infrastrukturanalyse einer möglichen wasserstoffbasierten Stromerzeugung unter Berücksichtigung von Kohlendioxidabtrennung, -transport und –speicherung. In: 7. *International Energiewirtschaftstagung an der TU-Wien – Märkte um des Marktes Willen*, Technical University Vienna, Austria, February 16 - 18, 2011.

Behr, P., Maun, A., Deutgen, K., Tunnat, A., Oeljeklaus, G., Görner, K., 2011. Kinetic study on promoted potassium carbonate solutions for CO_2 capture from flue gas. Energy Procedia 4, 85-92.

Bishnoi, S., 2000. Carbon dioxide absorption and soution equlibrium in piperazine activated methyldiethanolamine. PhD thesis, The University of Texas at Austin, USA.

Bishnoi, S., Rochelle, G.T., 2000. Absorption of carbon dioxide into aqueous piperazine: Reaction kinetics, mass transfer and solubility. Chem. Eng. Sci. 55 (22), 5531-5543.

Blauwhoff, P.M.M., Versteeg, G.F., van Swaaij, W.P.M., 1984. A study on the reaction between CO_2 and alkanolamines in aqueous solutions. Chem. Eng. Sci. 38 (9), 1411-1429.

Bougie, F., Iliuta, M.C., 2012. Sterically hindered amine-based absorbents for the removal of CO_2 from gas streams. J. Chem. Eng. Data 57 (3), 635-669.

Brønsted, J.N., Guggenheim, E.A., 1927. Contribution to the theory of acid and basic catalysis. The mutarotation of glucose. J. Am. Chem. Soc., 49 (10), 2554-2584.

Brúder, P., Grimstvedt, A., Mejdell, T., Svendsen, H.F., 2011. CO_2 capture into aqueous solutions of piperazine activated 2-amino-2-methyl-1-propanol. Chem. Eng. Sci., 66 (23), 6193-6198.

Bundeskanzleramt, 2011., Verbot der geologischen Speicherung von Kohlenstoffdioxid sowie Änderung des Umweltverträglichkeitsprüfungsgesetzes 2000, des Bundes-Umwelthaftungs-gesetzes, der Gewerbeordnung 1994 sowie des Mineralrohstoffgesetzes. BGBl. Nr. 144/2011.

Bundesministerium für Umwelt, Naturschutz, Bau und Reaktorsicherheit, 2012. Gesetz zur Demonstration der dauerhaften Speicherung von Kohlendioxid (Kohlendioxid-Speicherungsgesetz - KSpG), BGBl. I S. 1726.

Caldas, J.N., Lacerda, A.I., 1988. Torres Recheadas. JR Editora Técnica Ltda, Rio de Janeiro, Brazil.

Caplow, M., 1968. Kinetics of carbamate formation and breakdown. J. Am. Chem. Soc. 90 (24), 6795-6803.

Carson, J.K., Marsh, K.N. & Mather, A.E., 2000. Enthalpy of solution of carbon dioxide in (water + monoethanolamine, or diethanolamine, or n-methyldiethanolamine) and (water + monoethanolamine + n-methyldiethanolamine) at T = 298.15 K. J. Chem. Theromdynamics 32 (9), 1285-1296.

CESAR, 2011a. EU-Project, CO_2 Enhanced Separation and Recovery (CESAR): Integrated research project partially funded by the European commission under the 7th frame work programm, Grant agreement number 213569, project duration from 01.02.2008 to 31.01.2011. http://www.co2cesar.eu.

CESAR, 2011b. Final publishable summary report. https://setis.ec.europa.eu/energy-research/sites/default/files/project/docs/CESARFinalReport31May2012.pdf

Chaffee, A.L., Knowles, G.P., Liang, Z., Zhang, J., Xiao, P., Webley, P.A., 2007. CO_2 capture by adsorption: Materials and process development. Int. J. Greenhouse Gas Control 1 (1), 11-18.

Chakraborty, A.K., Astarita, G., Bischoff, K.B., 1986. CO_2 absorption in aqueous solution of hindered amines. Chem. Eng. Sci. 41 (4), 997-1003.

Chakravarti, S., Gupta, A., Huneak, B., 2001. Advanced technology for the capture of carbon dioxide from flue gases. In: *First National Conference on Carbon Sequestration*, Washington, USA, May 15 - 17, 2001.

Chen, E., Rochelle, G.T., Perry, M., Briggs, S., Montgomery, R., Kennedy, B., Seibert, F., 2010. Absorber intercooling for 8 m pierazine and 9 m MEA with a simple stripper. In: Campaign Report for Ausgust 2010 - September 2010, The University of Texas at Austin, USA.

Chen, E., Rochelle, G.T., Seibert, F., 2006. Pilot plant for CO_2 capture with aqueous piperazine/potassium carbonate. In: *8th Internation Conference on Greenhouse Gas Control Technologies*, Trondheim, Norway, June 19 - 22, 2006.

Chen, H., Kovvali, A.S., Sirkar, K.K., 2000. Selective CO_2 separation from CO_2-N_2 mixtures by immobilized glycine-Na-glycerol membranes. Ind. Eng. Chem. Res. 39, 2447-2458.

Chen, L., Yong, S.Z., Ghoniem, A.F., 2012. Oxy-fuel combustion of pulverized coal: Characterization, fundamentals, stabilization and CFD modeling. Progress in Energy and Combustion Science 38 (2), 156-214.

Chen, X., 2011. Carbon dioxide theromdynamics, kinetics, and mass transfer in aqueous piperazine derivatives and other amines. PhD thesis, The University of Texas at Austin, USA.

Chen, X., Freeman, S.A., Rochelle, G.T., 2011. Foaming of aqueous piperazine and monoethanolamine for CO_2 capture. Int. J. Greenhouse Gas Control 5 (2), 381-386.

Chowdhury, F.A., Yamada, H., Higashii, T., Goto, K., Onoda, M., 2013. CO_2 capture by tertiary amine absorbents: A performance comparison study. Ind. Eng. Chem. Res., 52 (24), 8323-8331.

Ciftja, A.F., Hartono, A., da Silva, E.F., Svendsen, H.F., 2011. Study on carbamate stability in the AMP/CO_2/H_2O system from ^{13}C-NMR spectrosopy. Energy Procedia 4, 614-620.

CO_2CRC, 2015a. CO_2 capture/separation technologies. http://www.co2crc.com.au/aboutccs/cap_adsorption.html.

CO_2CRC, 2015b. Images & videos. http://www.co2crc.com.au/images/imagelibrary/gen_dia/spm1_media.jpg

Cottrell, A., 2012. Post combustion capture and the Tarong pilot plant. Presentation at the *APEC Clean Fossil Energy Technical and Policy Seminar*, Gold Coast, Australia, February 22 - 24, 2012.

Cottrell, A., Cousins, A., Huang, S., Dave, N., Do., T., Feron. P.H.M., McHugh, S., Sinclair, M., 2013. Concentrated piperazine based post-combustion-capture for Australian coal-fired power plants - Summary Report. Australian National Low Emissions Coal Research & Development, www.csiro.au.

Cousins, A., Cottrell, A., Huang, S., Feron, P.H.M., Lawson, A., 2012. Tarong CO_2 capture pilot plant. Energy Generation April - June 2012, 16-17.

Cousins, A., Wardhaugh, L.T., Feron, P.H.M., 2010. Preliminary analysis of process flow sheet modifications for energy efficient CO_2 capture from flue gases using chemical absorption. In: *Proceedings of Distillation & Absorption Conference*, Eindhoven, Netherlands, September 12 – 15, 2010, 187-192.

Cousins, A., Wardhaugh, L.T., Feron, P.H.M., 2011. Preliminary analysis of process flow sheet modification for energy efficient CO_2 capture from flue gases using chemical absorption. Chemical Engineering Research and Design 89 (8), 1237-1251.

Cuéllar-Franca, R.M., Azapagic, A., 2015. Carbon capture, storage and utilisation technologies: A critical analysis and comparison of their life cycle environmental impacts. Journal of CO_2 Utilization 9, 82-102.

Cullinane, J.T., 2005. Thermodynamics and kinetics of aqueous piperazine with potassium carbonate for carbon dioxide absorption. Topical Report from 01.01.2005 to 31.03.2005, The University of Texas at Austin, USA.

Cullinane, J.T., Rochelle, G.T., 2004. Carbon dioxide absorption with aqueous potassium carbonate promoted by piperazine. Chem. Eng. Sci. 59 (17), 3619-3630.

Cullinane, J.T., Rochelle, G.T., 2005. Thermodynamics of aqueous potassium carbonate, piperazine, and carbon dioxide. Fluid Phase Equilibria 227 (2), 197-213.

Cullinane, J.T., Rochelle, G.T., 2006. Kinetics of carbon dioxide absorption into aqueous potassium carbonate and piperazine. Ind. Eng. Chem. Res., 45, 2531-2545.

da Silva, E.F., Svendsen, H. F., 2007. Computational chemistry study of reactions, equilbrium and kinetics of chemical CO_2 absorption. Int. J. Greenhouse Gas Control 1 (2), 151-157.

Damiani, D., Litynski, J.T., McIlvried, H.G., Vikara, D.M., Srivastava, R.D., 2012. The US deparment of Energy´s R&D program to reduce greenhouse gas emissions through benefical uses of carbon dioxide. Greenhouse Gases: Sci. Technol. 2 (1), 9-19.

Danckwerts, P.V., 1951. Significance of liquid-film coefficients in gas absorption. Ind. Eng. Chem. 43 (6), 1460-1467.

Danckwerts, P.V., 1970. Gas-liquid reactions. McGraw-Hill Book Co, New York, USA.

Danckwerts, P.V., Sharma, M.M., 1966. The absorption of carbon dioxide into solutions of alkalis and amines (with some notws on hydrogen sulhide and carbonyl sulphide). Institution of Chemical Engineers, London, UK.

DECC, 2012. CCS roadmap storage strategy. Department of Energy & Climate Change, London, UK, www.decc.gov.uk.

Derks, P.W.J., Dijkstra, H.B.S., Hogendoorn, J.A., Versteeg, G.F., 2005. Solubility of carbon dioxide in aqueous piperazine solutions. AIChE J. 51 (8), 2311-2327.

Derks, P.W.J., Kleingeld, T., van Aken, C., Hogendoorn, J.A., Versteeg, G.F., 2006. Kinetics of absorption of carbon dioxide in aqueous piperazine solutions. Chem. Eng. Sci., 61 (20), 6837-6854.

Dombrowski, K., 2010. Evaluation of concentrated piperazine for CO_2 capture from coal-fired flue gases. Presentation at the *NETL CO_2 Capture Technology Meeting*, Pittsburg, USA, September 14 - 17, 2010.

Donaldsen, T.L., Nguyen, Y.N., 1980. Carbon dioxide reaction kinetics and transport in aqueous amine membranes. Ind. Eng. Chem. Fundamen. 19 (3), 260-266.

DOW Chemical Company, 2001. Ethyleneamines. DOW Chemical Company, Midland, USA, http://www.dow.com.

Dugas, R. E., 2007. Rate and equilibrium measurements of MEA/piperazine. Progess Report for October – December, 2006, The University of Texas at Austin, USA.

Dugas, R.E., 2006. Pilot plant study of carbon dioxide capture by aqueous monoethanolamine. Master thesis, The University of Texas at Austin, USA.

Dugas, R.E., 2009. Carbon dioxide absorption, desorption, and diffusion in aqueous piperazine and monoethanolamine. PhD thesis, The University of Texas at Austin, USA.

Dugas, R.E., Rochelle, G.T., 2009. Absorption and desorption rates of carbon dioxide with monoethanolamine and piperazine. Energy Procedia 1 (1), 1163-1169.

Eide-Haugmo, I., Brakstad, O.G., Hoff, K.A., Sørheim, K.R., da Silva, E.F., Svendsen, H.F., 2009. Environmental impact of amines. Energy Procedia 1 (1), 1297-1304.

Eide-Haugmo, I., Lepaumier, H., Einbu, A., Vernstad, K., da Silva, E.F., Svendsen, H.F, 2011. Chemical stability and biodegradability of new solvents for CO_2 capture. Energy Procedia 4, 1631-1636.

Epp, B., Fahlenkamp, H., Vogt, M., 2011. Degradation of solutions of monoethanolamine, diglycolamine and potassium glycinate in view of tail-end CO_2 absorption. Energy Procedia 4, 75-80.

Erga, O., Juliussen, O., Lidal, H., 1995. Carbon dioxide recovery by means of aqueous amines. Energy Conversion and Mangement, 36 (6-9), 387-392.

Ermatchkov, V., Kamps, Á.P.S., Speyer, D., Maurer, G., 2006. Solubility of carbon dioxide in aqueous solutions of piperazine in the low gas loading region. J. Chem. Eng. Data, 51 (5), 1788-1796.

European Parliament, 2008. Parliament and climate change: Carbon Capture and Storage. http://www.europarl.europa.eu/.

European Union, 2009. Directive 2009/31/EC of the European Parliament and of the Council of 23 April 2009 on the geological storage of carbon dioxide and amending Council Directive 85/337/EEC, European Parliament and Council Directives 2000/60/EC, 2001/80/EC, 2004/35/EC, 2006/12/EC, 2008/1/EC and Regulation (EC) No 1013/2006. Official Journal of the European Union, L 140, 114-135.

Fernandez, E.S., Goetheer, E.L.V., 2011. DECAB: Process development of a phase change absorption process. Energy Procedia 4, 868-875.

Feron, P. H.M., Adbroek, N.A., 2004. New solvents based on amino-acid salts for CO_2 capture form flue gases. In: *Proceedings of the 7th International Conference on Greenhouse Gas Control Technologies*, Vancouver, Canada, 5 - 9 May, 2004.

Figueroa, J.D., Fout, T., Plasynski, S., McIlvried, H., Srivastava, R.D., 2008. Advances in CO_2 capture technology - The U.S. Department of Energy´s Carbon Sequestration Program. Int. J. Greenhouse Gas Control 2, 9-20.

Fine, N.A., Nielsen, P.T., Rochelle, G.T., 2014. Decomposition of nitrosamines in CO_2 capture by aqueous piperazine or monoethanolamine. Environ. Sci. Technol. 48 (10), 5996-6002.

Fraubaum, M., 2013. Experimentelle Untersuchung der CO_2 Abscheidung aus Kohlekraftwerksrauchgases. Master thesis, Technical University Vienna, Austria.

Freeman, S.A., 2011. Thermal degradation and oxidation of aqueous piperazine for carbon dioxide capture. PhD thesis, The University of Texas at Austin, USA.

Freeman, S.A., Dugas, R.E., Van Wagener, D., Nguyen, T., Rochelle, G.T., 2009. Carbon dioxide capture with concentrated, aqueous piperazine. Energy Procedia 1 (1), 1489-1496.

Freeman, S.A., Dugas, R.E., Van Wagener, D., Nguyen, T., Rochelle, G.T., 2010. Carbon dioxide capture with concentrated, aqueous piperazine. Int. J. Greenhouse Gas Control 4 (2), 119-124.

Ghasem, N., Al-Marzougi, M., Rahim, N.A., 2013. Absorption of CO_2 from gas mixture employing gas-liquid membrane contactors via potassium glycinate solvent. Presentation at the *44th World Chemistry Congress*, Istanbul, Turkey, August 11 - 16, 2013.

Ghasem, N., Al-Marzougi, M., Rahim, N.A., 2014. Absorption of CO_2 from a natural gas via gas-liquid PVDF hollow fiber membrane contactors and potassium glycinate as solvent. Jurnal Teknologi, 69 (9), 121-126.

Gmehling, J., Kolb, B., 1992. Thermodynamik – Zweite überarbeitete Auflage, VCH Verlagsgesellschaft, Weiheim, Germany.

Gouedard, C., Picq, D., Launey, F., Carrette, P.L., 2012. Amine degradation in CO_2 capture. I. A review. Int. J. Greenhouse Gas Control 10, 244-270.

Harris, F., Kurnia, K.A., Mutalib, M.I.A., Thanapalan, M., 2009. Solubilities of carbon dioxide and densities of aqueous sodium glycinate solutions before and after CO_2 absorption. J. Chem. Eng. Data 54 (1), 144-147.

Hartono, A., Saeed, M., Ciftja, A.F., Svendsen, H.F., 2013. Binary and ternary VLE of the 2-amino-2-methyl-1-propanol (AMP)/piperazine (Pz)/water system. Chem. Eng. Sci. 91, 151-161.

Haszeldine, R.S., 2009. Carbon capture and storage: How green can black be?. Science 325, 1647-1652.

Haubrock, J., Hogendoorn, J.A., Versteeg, G.F., 2007. The applicability of activities in kinetic expressions: A more fundamental approach to represent the kinetics of the system CO_2-OH^--salt in terms of activities. Chem. Eng. Sci. 62 (21), 5753-5769.

Higbie, R., 1935. The rate of absorption of a pure gas into a still liquid during short periods of exposure. AIChE Transactions 31, 365-390.

Hikita, H., Asai, S., Ishikawa, H., Honda, M., 1977. The kinetics of reactions of carbon dioxide with monoisopropanolamine, diglycolamine and ethylenediamine by a rapid mixing method. Chem. Eng. J. 14 (1), 27-30.

Hikita, H., Asai, S., Katsu, Y., Ikuno, S., 1979. Absorption of carbon dioxide into aqueous monoethanolamine solutions. AIChE J. 25 (5), 793-800.

Hilliard, M.D., 2008. A predictive thermodynamic model for an aqueous blend of potassium carbonate, piperazine, and monoethanolamine for carbon dioxide capture from flue gas. PhD thesis, The University of Texas at Austin, USA.

Hobler, T., 1966. Mass transfer and absorbers. Pergamon Press, Oxford, UK.

Hook, R.J., 1997. An investigation of some sterically hindered amines as potential carbon dioxide scrubbing compounds. Ind. Eng. Chem. Res. 36 (5), 1779-1790.

Horn, M., Reichl, A., Schliepdiek, T., Schramm, H., 2014. Piloting of Siemens PostCap™ technology, 9,000 hours of operational experience including Mongstad technology qualification program. In: POWER-Gen Europe, Amsterdam, Netherlands, June 9 – 11, 2015.

House, K.Z., Harvey, C.F., Aziz, M.J., Schrag, D.P., 2009. The energy penalty of post-combustion CO_2 capture & storage and its implications for retrofitting the U.S. installed base. Energy Environ. Sci. 2, 193-205.

Huang, Q., Bhatnagar, S., Remias, J.E., Selegue, J.P., Liu, K., 2013. Thermal degradation of amino acid salts in CO_2 capture. Int. J. Greenhouse Gas Control 19, 243-250.

Idem, R., Supap, T, Shi, H, Gelowitz, D., Ball, M., Campbell, C., Tontiwachwuthikul, P., 2015. Practical experience in post-combustion CO_2 capture using reactive solvents in large pilot and demonstration plants. Int. J. Greenhouse Gas Control 40, 6-25.

IEA, 2002. Solutions for the 21st century - Zero emissions technologeis for fossil fiuels: Energy seurity, environmental protection and economic development. International Energy Agency (IEA), Paris, France, http://www.cslforum.org/publications/documents/TSRMay2002.pdf.

IEA, 2011. Clean energy Progress Report. International Energy Agency, Paris, France.

IEA, 2013. Technology Roadmap Carbon Capture and Storage, International Energy Agency, Paris, France.

IEA, UNIDO, 2011. Technolgy Roadmap: Carbon Capture and Storage in Industrial Applications. International Energy Agency (IEA), United Nations Industrial Development Organization (UNIDO), http://www.unido.org/fileadmin/user_media/News/2011/CCS_Industry _ Roadmap_WEB.pdf.

IPCC, 2005. Special Report on Carbon Dioxide Capture and Storage. Interfovernmental Panel on Climate Change, Cambridge University Press, Cambridge, UK and New York, USA.

IPCC, 2007. Zusammenfassung für politische Entscheidungsträger. In: Klimaänderung 2007: Wissenschaftliche Grundlagen - Beitrag der Arbeitsgruppe I zum Vierten Sachstandsbericht des Zwischenstaatlichen Ausschusses für Klimaänderung. Interfovernmental Panel on Climate Change, Cambridge University Press, Cambridge, UK and New York, USA.

IPCC, 2013. Climate Change 2013: The Physical Science Basis. Contribution of Working Group I to the Fifth Assesment Report. Intergovernmental Panel on Climate Change, Cambridge University Press, Cambridge, UK and New York, USA.

IPCC, 2014. Climate Change 2014: Synthesis Report. Contribution of Working Groups I, II and III to the Fifth Assessment Report. Intergovernmental Panel on Climate Change, Cambridge University Press, Cambridge, UK and New York, USA.

Jackson, P., Attalla, M., 2011. Environmental impacts of post-combustion capture - New insights. Energy Procedia 4, 2277-2284.

Jamal, A., Meisen, A., Lim, C.J., 2006. Kinetics of carbon dioxide absorption and desorption in aqueous alkanolamine solutions using a novel hemispherical contacotr - I. Experimental apparatus and mathamatical modeling. Chem. Eng. Sci. 61, 6571-6589.

Jansen, D., Gazzani, M., Manzolini, G., van Dijk, E., Carbo, M., 2015. Pre-combustion CO_2 capture. Int. J. Greenhouse Gas Control 40, 167-187.

Jensen, A., Christensen, R., 1955. Studies on carbamates - XI. The carbamate of ethylenediamine. Acta Chem. Scand. 9, 486-492.

Jensen, A., Jensen, J.B., Faurholt, C., 1952. Studies on carbamates - VI. The carbamate of glycine. Acta Chem. Scand. 6, 395-397.

Ji, L., Miksche, S.J., Rimpf, L.M., Farthing, G.A., 2009. CO_2 chemical solvent screening. Presentation at the *8th Annual Conference on Carbon Capture and Sequestration – DOE/NETL*, Pittsburgh, USA, May 4 – 7, 2009.

Kadiwala, S., Rayer, A.V., Henni, A., 2012. Kinetics of carbon dioxide (CO_2) with ethylenediamine, 3-amino-1-propanol in methanol and ethanol, and with 1-dimethylamino-1-propanol and 3-dimethylamino-1-propanol in water using stopped-flow technique. Chem. Eng. J. 179, 262-271.

Kamps, Á.P.S., Xia, J., Maurer, G., 2003. Solubility of CO_2 in (H_2O+piperazine) and in (H_2O+MDEA+piperazine). AICheE J. 49 (10), 2662-2670.

Kanniche, M., Gros-Bonnivard, R., Jaud, P., Valle-Marcos, J., Amann, J.M., Bouallou, C., 2010. Pre-combustion, post-combustion and oxy-combustion in thermal power plant for CO_2 capture. Applied Thermal Engineering 30 (1), 53-62.

Kemper, J., 2012. Kinetik und Stoffübertragung bei der reaktiven CO_2-Absorption/Desorption in speziellen Amin-Blends. PhD thesis, Ruhr University Bochum, Germany.

Kemper, J., Ewert, G., Grünewald, M., 2011. Absorption and regeneration performance of novel reactive amine solvents for post-combustion CO_2 capture. Energy Procedia 4, 232-239.

Khoo, H.H., Bu, J., Wong, R.L., Kuan, S.Y., Sharratt, P.N., 2011. Carbon capture and utilization: Preliminary life cycle CO_2, energy, and cost results of potential mineral carbonation. Energy Procedia 4, 2494-2501.

Kim, I., Svendsen, H.F., 2007. Heat of absorption of carbon dioxide (CO_2) in monoethanolamine (MEA) and 2-(aminoethyl)ethanolamine (AEEA) solutions. Ind. Eng. Chem. Res. 46 (17), 5803-5809.

Knudsen, J.N., Andersen, J., Jensen, J.N., Biede, O., 2011. Evaluation of process upgrades and novel solvents for the post combustion CO_2 capture process in pilot-scale. Energy Procedia 4, 1558-1565.

Knudsen, J.N., Jensen, J.N., 2009. Experience with the CASTOR/CESAR pilot plant. Presentation at the *Workshop on Operating Flexibility of Power Plants with CCS*, Imperial College, London, UK, November 12 – 12, 2009

Knudsen, J.N., Jensen, J.N., Vilhelmsen, P.J., Biede, O., 2007. First year operation experience with a 1 t/h CO_2 absorption pilot plant at Esbjerg coal-fired power plant. In: *Proceedings of European Congress of Chemical Engineering (ECCE-6)*, Copenhagen, Denmark, September 16 - 20, 2007.

Knudsen, J.N., Jensen, J.N., Vilhelmsen, P.J., Biede, O., 2009. Experience with CO_2 capture from coal flue gas in pilot-scale: Testing of different amine solvents. Energy Procedia 1 (1), 783-790.

Koch-Glitsch, 2015. Structured packing. Product data sheet, http://www.koch-glitsch.com /Document %20Library/KGSP.pdf.

Kohl, A., Nielsen, R., 1997. Gas Purification - 5th edition. Gulf Professional Publishing, Houston, USA, ISBN: 0-88415-220-0.

Kucka, L., 2003. Modellierung und Simulation der reaktiven Absorption von Sauergasen mit Alkanolaminelösungen (Berichte aus der Verfahrenstechnik). Shaker Verlag, Aachen, Germany, ISBN: 978-3832214388.

Kumar, P.S., Hogendoorn, J.A., Timmer, J.S., Feron, P.H.M., 2003a. Equilibrium solubility of CO_2 in aqueous potassium taurate solutions: Part 2. Experimental VLE data and model. Ind. Eng. Chem. Res. 42, 2841-2852.

Kumar, P.S., Hogendoorn, J.A., Versteeg, G.F., 2003b. Kinetics of the reaction of CO_2 with aqueous potassium salt of taurine and glycine. AIChE J. 49 (1), 203-213.

Kusakabe, K., Kuroda, T., Uchino, K., Hasegawa, Y., Morooka, S., 1999. Gas permeation properties of ion-exchanged faujasite-type zeolite membranes. AIChE J. 45 (6), 1220-1226.

Kutne, P., Kapadia, B.K., Meier, W., Aigner, M., 2011. Experimental analysis of the combustion behaviour of oxyfuel flames in a gas turbine model combustor. Proceedings of the Combustion Institute 33 (2), 3383-3390.

Kvamsdal, H.M., Rochelle, G.T., 2008. Effects of the temperature bulge in CO_2 absorption from flue gas by aqueous monoethanolamine. Ind. Eng. Chem. Res. 47 (3), 867-875.

Le Quéré, C., Peters, G.P., Andres, R.J., Andrew, R.M., Boden, T.A., Ciais, P., Friedlingstein, P., Houghton, R.A., Marland, G., Moriarty, R., Sitch, S., Tans, P., Arneth, A., Aravanitis, A., Bakker, D.C.E., Bopp, L., Candell, J.G., Chini, L.P., Doney, S.C., Harper, A., Harris, I., House, J.I., Jain, A.K., Jones, S.D., Kato, E., Keeling, R.F., Klein Goldewijk, K., Körtzinger, A., Koven, C., Lefévre, N., Omar, A., Ono, T., Park, G.H., Pfeil, B., Poulter, B., Raupach, M.R., Regnier, P., Rödenbeck, C., Saito, S., Schwinger, J., Segschneider, J., Stocker, B.D., Takahashi, T., Tilbrook, B., van Heuven, S., Viovy, N., Wanninkhof, R., Wiltshire, A., Zaehle, S., 2013. Global carbon budget 2013. Earth Syst. Sci. Data Discuss. 6, 689-760.

Lee, S., Choi, S.I., Maken, S., Song, H.J.; Shin, H.C.; Park, J.W. Jang, K.R., Kim, J.H., 2005. Physical properties of aqueous sodium glycinate solution as an absorbent for carbon dioxide removal. J. Chem. Eng. Data 50 (5), 1773-1776.

Lee, S., Song, H.J., Maken, S., Park, J.W., 2007. Kinetics of CO_2 absorption in aqueous sodium glycinate solutions. Ing. Eng. Chem. Res. 46, 1578-1583.

Lee, S., Song, H.J., Maken, S., Yoo, S.K., Park, J.W., Kim, S., Shim, J.G., Jang, K.R., 2008. Simulation of CO_2 removal with aqueous sodium glycinate solutions in a pilot plant. Korean J. Chem. Eng. 25 (1), 1-6.

Lerche, J., Dreuscher, H., 2011. Hocheffiziente Staubabscheidung - Voraussetzung für eine ungestörte CO_2-Wäsche. VGB PowerTech 4, 2011, 74-79.

Lévêque, M.A., 1928. Les lois de la transmission de chaleur par convection. Annales des Mines 12, 201-415.

Lewis, W.K., Whitman, W.G., 1924. Principles of gas absorption. Ind. Eng. Chem. Res. 16, 1215-1220.

Li, J., Henni, A., Tontiwachwuthikul, P., 2007. Reaction kinetics of CO_2 in aqueous ethylenediamine, ethyl ethanolamine, and diethyl monoethanolamine solutions in the temperature range of 298-313 K, Using the stopped-flow technique. Ind. Eng. Chem. Res. 46, 4426-4434.

Lu, H., Reddy, E.P., Smirniotis, P.G., 2006. Calcium oxide based sorbents for capture of carbon dioxide at high temperatures. Ind. Eng. Chem. Res. 45 (11), 3944-3949.

Lüdtke, K.H., 2004. Process Centrifugal Compressors. Springer-Verlag Berlin Heidelberg, Germany, ISBN: 978-3-662-09449-5.

Lukowicz, H., Chmielniak, T., Kochaniewicz, A., Mroncz, M., 2011. An analysis of the use of waste heat from exhaust gases of a brown-coal fired power plant for drying coal. Rynek Energii 1, 157-163.

Ma´mun, S., Nilsen, R., Svendsen, H.F., Juliussen, O., 2005. Solubility of carbon dioxide in 30 mas % monoethanolamine and 50 mass % methyldiethanolamine solutions. J. Chem. Eng. Data 50, 630-634.

Ma´mun, S., Svendsen, H.F., Hoff, K.A., Juliussen, O., 2007. Selection of new absorbents for carbon dioxide capture. Energy Conversion and Management 48 (1), 251-258.

Mahurin, S.M., Lee, J.S., Baker, G.A., Luo, H., Dai, S., 2010. Performance of nitrile-containing anions in task-specific ionic liquids for improved CO_2/N_2 separation. Journal of Membrane Science 353 (1-2), 177-183.

Maierhofer, M., 2010. Vergleich von MEA und einer ionischen Flüssigkeit als CO_2-Absorptionsmittel in einer Versuchsanlage. Master thesis, University of Leoben, Austria.

Majchrowicz, M.E., 2014. Amino acid salt solutions for carbon dioxide capture. PhD thesis, University of Twente, Netherlands.

Mangalapally, H.P., Hasse, H., 2011a. Pilot plant experiments for post combustion carbon dioxide capture by reactive absorption with novel solvents. Energy Procedia 4, 1-8.

Mangalapally, H.P., Hasse, H., 2011b. Pilot plant study of two new solvents for post combustion carbon dioxide capture by reactive absorption and comparison to monoethanolamine. Chem. End. Sci. Sci. 66 (22), 5512-5522.

Mangalapally, H.P., Hasse, H., 2011c. Pilot plant study of post combustion carbon dioxdie capture by reactive absorption: Medhodology, comparison of different structured packings, and comprehensive results for monoethanolamine. Chem. Eng. Res. Des. 89 (8), 1216-1228.

Markewitz, P., Kuckshinrichs, W., Leitner, W., Linsen, J., Zapp, P., Bongartz, R., Schreiber, A., Müller, T.E., 2012. Worldwide innovations in the development of carbon capture technolgies and the utilization of CO_2. Energy Environn Sci. 5, 7281-7305.

Martin, S., Lepaumier, H., Picq, D., Kittel, J., de Bruin, T., Faraj, A., Carrette, P.L., 2012. New amines for CO_2 capture. IV. Degradation, corrosion, and quantitative structure property relationship model. Ind. Eng. Chem. Res. 51 (18), 6283-6289.

Martínez-Berganza, I.G.S., 2012. Solidificación de Aminooácidos en la Captura de CO_2. Master thesis, Universidad Zaragoza, Spain.

Mayr, B., Prieler, R., Demuth, M., Potesser, M., Hochenauer, C., 2015. CFD and experimental analysis of a 115 kW natural gas fired lab-scale furnance under oxy-fuel and air-fuel conditions. Fuel 159, 864-875.

McDonell, V.G., 2006. Key combustion issues associated with syngas and high-hydrogen fuels. In: Smith, L., Karim, H., Etemad, S., Pfefferle, W.C. (ed) *The Gas Turbine Handbook*. U.S. Department of Energy-National Energy Technology Laboratory (NETL).

Meixner, K., Fuchs, I., Kinger, G., Gronald., G., Drosg, B., 2015. Biokunststoffproduktion mit Cyanbakterien. In: *8. Bundesalgenstammtisch - Die Rolle der Algenbiotechnologie in der Bioökonomie-Strategie*. München/Garching, Germany, September 7 – 8, 2015.

Melzer, L.S., 2012. Carbon dioxide enhanced oil recovery (CO_2 EOR): Factors involved in adding carbon capture, utilization and storage (CCUS) to enhanced oil recovery. Center for Climate and Energy Solutions, Midland, USA.

Mendes, M.F., 2011. HETP evaluation of structured and randomic packing distillation column. In: Markoš, J. (ed) Mass Transfer in Chemical Engineering Processes, InTech, Rijeka, Croatia, 41-68.

Merck Corporation, 2009. MSDS anhydrous piperazine. Merck Corporation, Whitehouse Station, USA.

Miessler, G.L., Fischer, P.J., Tarr, D.A., 1991. Inorganic Cemistry - 5th edition. Prentice Hall, Upper Saddle River, New Jersey, USA, ISBN: 978-0321811059.

Misiak, K., Sanchez Sanchez, C., van Os, P., Goetheer, E.L.V., 2013. Next generation post-combustion capture: Combined CO_2 and SO_2 removal. Energy Procedia 37, 1150-1159.

Moser, P., Schmidt, S., Sieder, G., Garcia, H., Stoffregen, T., 2011. Performance of MEA in a long-term test at the post-combustion capture pilot plant in Niederaussem. Int. J. Greenhouse Gas Control 5 (4), 620-627.

Muhammad, A., Abdul Mutalib, M.I., Murugesan, T., Shafeeq, A., 2009. Thermophysical properties of aqueous piperazine and aqueous (n-methyldiethanolamine plus piperazine) solutions at temperatures (298.15 to 338.15) K. J. Chem. Eng. Data 54 (8), 2317-2321.

Murdoch, K., Thibaud-Erkey, C., Sirkar, K.K., Obuskovic, G., 2001. Membrane based CO_2 removal from spacesuits. http://www.dsls.usra.edu/meetings/bio2001/pdf/138p.pdf.

Murdoch, K., Thibaud-Erkey, C., Sirkar, K.K., Obuskovic, G., Chen, H., 2002. Membrane-based CO_2 removal from breathing atmospheres. SAE Technical Paper 2000-01-2392, 2000, doi:10.4271/2000-01-2392.

Nagai, R., Taniguchi, N., 2014. Amino acids and proteins. In: Baynes, J.W., Dominiczak, M.H. (ed) *Medical Biochemistry – 4th edition*, Elsevier Ltd., ISBN: 978-1-4557-4580-7, 5-20.

NETL, 2010. Carbon dioxide capture by absorption with potassium carbonate. Poject Facts - Existing Plants, Emissions & Capture, National Energy Technology Laboratory (NETL), https://www.netl.doe.gov/File%20Library/research/coal/carbon%20capture/Proj280.pdf.

NETL, 2015. CO_2 utilization focus area, National Energy Technology Laboratory (NETL), http://www.netl.doe.gov/research/coal/carbon-storage/research-and-development/co2-utilization.

Nguyen, T., Hilliard, M.D., Rochelle, G.T., 2010. Amine volatility in CO_2 capture. Int. J. Greenhouse Gas Control 4 (5), 707-715.

Norton, T.T., Lin, Y.S., 2014. Ceramic-carbonate dual-phase membrane with improved chemical stability for carbon dioxide separation at high temperature. Solid State Ionics 263, 172-179.

Notz, R. J., 2009. CO_2-Abtrennung aus Kraftwerksabgasen mittels Reaktivabsorption. PhD thesis, University of Stuttgart, Germany.

Notz, R., Mangalapally, H.P., Hasse, H., 2011. Post combustion CO_2 capture by reactive absorption: Pilot plant description and results of systematic studies with MEA. Int. J. Greenhouse Gas Control 6, 84-112.

Oexmann, J., 2011. Post-combustion CO_2 capture: Energetic evaluation of chemical absorption processes in coal-fired steam power plants. PhD thesis, Technical University of Hamburg, Germany.

Oexmann, J., Hensel, C., Kather, A., 2008. Post-combustion CO_2 capture from coal-fired power plants: Preliminary evaluation of an integrated chemical absorption process with piperazine-promoted potassium carbonate. Int. J. Greenhouse Gas Control 2 (4), 539-552.

Oexmann, J., Kather, A., 2009a. Post-combustion CO_2 capture in coal-fired power plants: Comparison of integrated chemical absorption processes with piperazine promoted potassium carbonate and MEA. Energy Procedia 1 (1), 799-806.

Oexmann, J., Kather, A., 2009b. Post Combsution CO_2-Abtrennung in Kohlekraftwerken: Rauchgaswäschen mit chemischen Lösungsmitteln. VGB PowerTech 1-2, 2009, 92-103.

Oexmann, J., Kather, A., 2010. Minimising the regeneration heat duty of post-combustion CO_2 capture by wet chemical absorption: The misguided focus on low heat of absorption solvents. Int. J. Greenhouse Gas Control 4 (1), 36-43.

Ogawa, T., 2013. Carbon dioxide capture and utilization for gas engine. Energy and Power Engineering 5, 587-590.

Optimized Gas Treating, 2010. Capturing CO_2 with sodium glycinate. Optimzied Gas Treating, Inc. 4 (2). http://www.ogtrt.com/files/contactors/Contactor_Vol_4_No_2.pdf

Orr, J.F., 2009. CO_2 capture and storage: Are we ready?. Energy Environ.Sci. 2, 449-458.

Padurean, A., Cormos, C.C., Agachi, P.S., 2012. Pre-combustion carbon dioxide capture by gas-liquid absorption for integrated gasification combined cycle power plants. Int. J. Greenhouse Gas Control 7, 1-11.

Park, S.J., Jang, G.R., Park, I.H., 2006. Determination and calculation of physical properties for sodium glycinate as a CO_2 absorbent. Korean Chem. Eng. Res. 44 (3), 277-283.

Park, S.W., Son, Y.S., Park, D.W., Oh, K.J., 2008. Absorption of carbon dioxide into aqueous solution of sodium glycinate. Separation Science and Technology 43, 3003-3019.

Penny, D.E., Ritter, T.J., 1983. Kinetic study of the reaction between carbon dioxide and primary amines. J. Chem. Soc., Faraday Trans. 1 (79), 2103-2109.

Plaza, J.M., 2011. Modeling of carbon dioxide absorption using aqueous monoethanolamine, piperazine and promoted potassium carbonate. PhD thesis, The University of Texas at Austin, USA.

Plaza, J.M., Chen, E., Rochelle, G.T., 2009. Absorber intercooling in CO_2 absorption by piperazine-promoted potassium carbonate. AIChE J. 56 (4), 905-914.

Pohorecki, R., Moniuk, W., 1988. Kinetics of the reaction between carbon dioxide and hydroxyl ion in aqueous electrolyte solutions. Chem. Eng. Sci. 43 (7), 1677-1684.

Portugal, A.F., Derks, P.W.J., Versteeg, G.F., Magalhães, F.D., Mendes, A, 2007. Characterization of potassium glycinate for carbon dioxide absorption purposes. Chem. Eng. Sci. 62 (23), 6534-6547.

Portugal, A.F., Sousa, J.M., Magalhães, F.D., Mendes, A., 2009. Solubility of carbon dioxide in aqueous solutions of amino acid salts. Chem. Eng. Sci. 64 (9), 1993-2002.

Posch, S., 2012. Experimental and numerical investigations on post-combsution CO_2 capture from coal-fired power plants. PhD thesis, Technical University Vienna, Austria.

Posch, S., Haider, M., 2011. Stand der Technologieentwicklung und der weltweiten Demonstrationsvorhaben im Bereich CCS. In: *7. International Energiewirtschaftstagung an der TU-Wien – Märkte um des Marktes Willen*, Technical University Vienna, Austria, February 16 - 18, 2011.

Prieler, R., Demuth, M., Spoljaric, D., Hochenauer, C., 2014. Evaluation of a steady flamelet approach for use in oxy-fuel combustion. Fuel, 118, 55-68.

Rabensteiner, M., Kinger, G., Koller, M., Gronald, G., Hochenauer, C., 2014c. Pilot plant study of ethylenediamine as a solvent for post combustion carbon dioxide capture and comparison to monoethanolamine. Int. J. Greenhouse Gas Control 27, 1-14.

Rabensteiner, M., Kinger, G., Koller, M., Gronald, G., Hochenauer, C., 2015a. Investigation of carbon dioxide capture with aqueous piperazine on a post combustion pilot plant – Part I: Energetic review of the process. Int. J. Greenhouse Gas Control 39, 79-90.

Rabensteiner, M., Kinger, G., Koller, M., Gronald, G., Hochenauer, C., 2015b. Investigation of carbon dioxide capture with aqueous piperazine on a post combustion pilot plant – Part II: Parameter study and emission measurement. Int. J. Greenhouse Gas Control 37, 471-480.

Rabensteiner, M., Kinger, G., Koller, M., Gronald, G., Unterberger, S., Hochenauer, C., 2014b. Investigation of the suitability of aqueous sodium glycinate as a solvent for post combustion carbon dioxide capture on the basis of pilot plant studies and screening methods. Int. J. Greenhouse Gas Control 29, 1-15.

Rabensteiner, M., Kinger, G., Koller, M., Hochenauer, C., 2014a. Pilot plant studies of the CO_2 post-combustion process at the Dürnrohr power plant. VGB PowerTech 10, 2014, 61-66.

Rabensteiner, M., Kinger, G., Koller, M., Hochenauer, C., 2014d. Three years of working experience with different solvents at a realistic post combustion capture pilot plant. Energy Procedia 63, 1578-1584.

Rabensteiner, M., Kinger, G., Koller, M., Hochenauer, C., 2015c. PCC pilot plant studies with aqueous potassium glycinate. Int. J. Greenhouse Gas Control 42, 562-570.

Rabensteiner, M., Kinger, G., Koller, M., Hochenauer, C., 2015d. CO_2 post combustion pilot plant tests at the Dürnrohr power plant with amino acids. VGB PowerTech 11, 2015, 47-53.

Raschig GmbH, 2015. Raschig Super-Pak - Product Bulletin 501 - A new packing structure with innovative advantages. Product data sheet, http://s341789233.online.de/editor/assets /Info%20Raschig%20Super-Pak-501.pdf.

Ratz, A., 2010. Aufbau und Inbetreibnahme einer Versuchsanlage zur CO_2 Absorption, Master thesis, Leoben University of Mining, Austria.

Reddy, S., Johnson, D., Gilmartin, J., 2008. Fluor's econamine FG Plus[SM] technology for CO_2 capture at coal-fired power plants. In: *Power Plant Air Pollutant Control "Mega" Symposium*, Baltimore, USA, August 25 – 28, 2008.

Rey, A., Gouedard, C., Ledirac, N., Cohen, A., Dugay, J., Vial, J., Pichon, V., Bertomeu, L., Picq, D., Bontemps, D., Chopin, F., Carrette, P.L., 2013. Amine degradation in CO_2 capture. 2. New degradation products of MEA. Piperazine and alkylpyrazines: Analysis, mechanism of formation and toxicity. Int. J. Greenhouse Gas Control 19, 576-583.

Reynolds, A.J., Verheyen, T.V., Adeloju, S.B., Chaffee, A.L., Meuleman, E., 2015. Monoethanolamine degradation during pilot-scale post-combustion capture of CO_2 from a brown coal-fired power station. Energy Fuels 29 (11), 7441-7455.

Richards, G., Weiland, N., Strakey, P., 2006. Combusiton strategies for syngas and high-hydrogen fuel. In: Smith, L., Karim, H., Etemad, S., Pfefferle, W.C. (ed) *The Gas Turbine Handbook*. U.S. Department of Energy-National Energy Technology Laboratory (NETL).

Rocha, J.A., Bravo, J.L., Fair, J.R., 1993. Distillation columns containing structured packings: A comprehensive model for their performance. 1. Hydraulic models. Ind. Eng. Chem. 32, 641-651.

Rochelle, G.T., 2012. Thermal degradation of amines for CO_2 capture. Curr. Opin. Chem. Eng.1 (2), 183-190.

Rochelle, G.T., Bishnoi, S., Chi, S., Dang, H., Santos, J., 2001. Research needs for CO_2 capture from flue gas by aqueous absorption/stripping. Final report on DOE P.O. No. DE-AF26-99FT01029, January 17, 2001, Department of Chemical Engineering, University of Texas at Austin, USA.

Rochelle, G.T., Chen, E., Freeman, S., Van Wagener, D., Xu, Q., Voice, A.K., 2011. Aqueous piperazine as the new standard for CO_2 capture technology. Chem. Eng. J. 171 (3), 725-733.

Sachde, D., Rochelle, G.T., 2014. Absorber intercooling cofigurations using aqueous piperazine for capture from sources with 4 to 27% CO_2. Energy Procedia 63, 1637-1656.

Sada, E., Kumazawa, H., Butt, M.A., 1977. Absorption of carbon dioxide into aqueous solutions of ethylenediamine: Effect of interfacial turbulence. Chem. Eng. J. 13 (3), 213-217.

Saimpert, M., Puxty, G., Qureshi, S., Wardhaugh, L., Cousins, A., 2013. A new rate based absorber and desorber modelling tool. Chem. Eng. Sci. 96, 10-25.

Salazar, V., Sánchez-Vicente, Y., Pando, C., Renuncio, J.A.R., Cabañas, A., 2010. Enthalpies of absorption of carbon dioxide in aqueous sodium glycinate solutions at temperatures of (313.15 and 323.15) K. J. Chem. Eng. Data 55 (3), 1215-1218.

Sanchez Fernandez, E., Heffernan, K., van der Ham, L.V., Linders, M.J.G., Eggink, E., Schrama, F.N.H., Brilman, D.W.F., Goetheer, E.L.V., Vlugt, T.J.H., 2013. Conceptual design of a novel CO_2 capture process based on precipitating amino acid solvents. Ind. Eng. Chem. Res. 52 (34), 12223-12235.

Sandell, M.A., 2010. An overview of the current status of the Siemens POSTCAP process - Results from POSTCAP pilot plant operation. Presentation at the *Siemens Environmental Systems & Service*.

Sanpasertparnich, T., Idem, R., Tontiwachwuthikul, P., 2011. CO_2 absorption in an absorber column with a series of intercooler circuits. Energy Procedia 4, 1676-1682.

Sartori, G., Savage, D.W., 1983. Sterically hindered amines for CO_2 removal from gases. Ind. Eng. Chem. Fundamen. 22 (2), 239-249.

Sattler, K., 1988. Thermische Trennverfahren: Grundlagen, Auslegung, Apparate. VCH Verlagsgesellschaft, Weinheim, Germany, ISBN: 3-527-26727-1.

Schäffer, A., Brechtel, K., Scheffknecht, G., 2010. Untersuchung von wässrigen Mehrkomponentenaminsystemen - Waschlösungen zur Abtrennung von CO_2 aus Rauchgasen. VGB PowerTech 4, 2010, 66-71.

Scheffknecht, G., Al-Makhadmeh, L., Schnell, U., Maier, J., 2011. Oxy-fuel coal cobustion - A review of the current state-of-the-art. Int. J. Greenhouse Gas Control 5 (supplement), 16-35.

Scherer, V., Stolten, D., Franz, J., Riensche, E., 2012. CCS-Abscheidetechniken: Stand der Technik und Entwicklungen. Chemie Ingenieur Technik, Band 84 (7), 1026-1040.

Schmidt, S., 2014. Optimierung und experimentelle Untersuchung der CO_2-Abtrennung mit Monoethanolamin für braunkohlegefeuerte Kraftwerke. PhD thesis, Technische Universität München.

Schmidt, S., Moser, P., 2013. CO_2-Abtrennung mit Monoethanolamin für braunkohlegefeuerte Kraftwerke. VGB PowerTech 12, 2013, 35-41.

Schneider, R., Schramm, H., 2011. Environmental friendly and economic carbon capture from power plant flue gases: The SIEMENS PostCap technology. In. *1st Post Combustion Capture Conference*, Abu Dhabi, United Arab Emirates, May 17 – 19, 2011.

Schultes, M., 2008. Raschig Super-Pak - Eine neue Packungsstruktur mit innovativen Vorteilen im Vergleich. Chemie Ingenieur Technik 80 (7), 927-933.

Seiersten, M., 2001. Material selection for separation, transportation and disposal of CO_2. In: *Proceedings Corrosion 2001*, National Association of Corrosion Engineers, Houston, USA, Paper No. 01042, ISBN: 01042 2001 CP.

Sexton, A.J., 2008a. Amine oxidation in CO_2 capture processes. PhD thesis, The University of Texas at Austin, USA.

Sexton, A.J., 2008b. Oxidative degradation of amines. In: *CO_2 acpture by aqueous absorption - Summary of 2nd Quarterly Progress Reports 2008*, Department of Chemical Engineering, The University of Texas at Austin, USA, 81-106.

Shao, R., Stangeland, A., 2009. Amines used in CO_2 capture - Health and environmental impacts. Bellona Report, September 2009, Oslo, Norway, http://bellona.org/assets/sites/3/2015/06/fil_Bellona_report_September__2009_-_Amines_used_in_CO2_capture-11.pdf.

Sharma, M., 1965. Kinetics of reactions of carbonyl sulphide and carbon dioxide with amines and catalysis by Brönsted bases of the hydrolysis of COS. Taraday Soc. 61, 681-688.

Siemens AG, 2009. Capturing carbon for a better climate. Living Energy 1, November 2009.

Siemens AG, 2011. Lösungsmittel, Verfahren zur Bereitstellung einer Absorptionsflüssigkeit, Verwendung des Lösungsmittels und Verfahren zur Aktivierung eines Lösungsmittels. Patentnr. EP 2 481 469 A1.

Siemens AG, 2014. Siemens PostCap^{TM} technology CO_2 post combustion capture. – For combined sycle and steam power plant applications. Order No. E50001-D100-A192-X-7600, Siemens AG, Energy Sector, Erlangen, Germany

Singh, B., Stømman, A.H., Hertwich, E.G., 2011. Comparative life cycle environmental assessment of CCS technologies. Int. J. Greenhouse Gas Control, 5 (4), 911-921.

Smolak, A., 2011. GDK Mellach - Eine Antwort auf neue Herausforderungen. VERBUND Thermal Power GmbH & Co KG (VTP), http://www.aggm.at/files/get/204e9af3427224eb9f8c 96f 2f65f808b/infrastrukturausbau_ost_.

Song, H.J., Lee, S., Maken, S., Park, J.J., Park, J.W., 2006. Solubilities of carbon dioxide in aqueous solutions of sodium glycinate. Fluid Phase Equlibria 246 (1-2), 1-5.

Song, H.J., Lee, S., Park, K., Lee, J., Spah, D.C., Park., J.W., Filburn, T.P., 2008. Simplified estimation of regeneration energy of 30 wt % sodium glycinate solution for carbon dioxide absorption. Eng. Chem. Res. 47 (24), 9925-9930.

Stöger, P., 2011. Aufbau und Inbetriebnahme einer Versuchsanlage zur Abscheidung con CO_2 aus Kraftwerksracuhgasen. Master thesis, Technical University Vienna, Austria.

Strigle, R.F., 1993. Understand flow phenomena in packed column. Chem. Eng. 8, 79-83.

Styring, P., Jansen, D., de Coninck, H., Reith, H., Armstrong, K., 2011. Carbon Capture and Utilistation in the Green Economy – Using CO_2 to manufacture fuel, chemicals and materials. The Centre for Low Carbon Futures, CO2Chem Publishing, ISBN: 978-0-9572588-1-5.

Sulzer AG, 2015. Structured packings - Energy-efficient, innovative and profitable. Product data sheet, https://www.sulzer.com/de/-/media/Documents/ProductsAndServices/Separation_Tec hnology/Structured_Packings/Brochures/Structured_Packings.pdf.

Sun, W.C., Yong, C.B., Li, M.H., 2005. Kinetics of the absorption of carbon dioxide into mixed aqueous solutions of 2-amino-2-methyl-1-propanol and piperazine. Chem. Eng. Sci. 60 (2), 503-516.

Svensson, H., Hulteberg, V., Karlsson, H.T., 2013. Heat of absorption of CO_2 in aqueous solutions of N-methyldiethanolamine and piperazine. Int. J. Greenhouse Gas Control 17, 89-98.

Tan, Z., 2014. Air pollution and greenhouse gases - From basic concepts to engineering applications for air emission control. Springer Science+Business Media Singapore, ISBN: 978-981-287-212-8.

Thomas, C.T., 2005. Carbon dioxide capture for storage in deep geologic formations - Results from the CO_2 capture project. Volume 1: Capture and separation of carbon dioxide from combustion sources. Elservier Ltd., ISBN: 978-0-08-044570-0.

Tlili, N., Grévillot, G., Latifi, A., Valliéres, C., 2012. Electrical swing adsorption using new mixed matrix adsorbents for CO_2 capture and recovery: Experiments and modeling. Ind. Eng. Chem. Res. 51 (48), 15729-15737.

Tong, J., Zhang, L., Han, M., Huang, K., 2015. Electrochemical separation of CO_2 from a simulated flue gas with high-temperature ceramic-carbonate membrane: New observations. Journal of Membrane Science 477, 1-6.

Tönnis, I., Mangalapally, H.P., Hasse, H., 2011. Pilot plant studies of new solvents for post combustion CO_2 capture. Presentation at the *International Conference on Energy Process Engineering*, Frankfurt, Germany, June 20 – 22, 2011.

Trass, O., Weiland, R.H., 1971. Absorption of carbon dioxide in ethylenediamine solutions - II. Pilot plant study of absorption and regeneration. Can. J. Chem. Eng. 49, 773-781.

Union Carbide Chemical Co., 1957. Gas Treating Chemicals, Vol. 1.

Vaidya, P.D., Konduru, P., Vaidyanathan, M., Kenig, E.Y., 2010. Kinetics of carbon dioxide removal by aqueous alkaline amino acid salts. Ind. Eng. Chem. Res. 49 (21), 11067-11072.

van Holst, J., Versteeg, G.F., Brilman, D.W.F., Hogendoorn, J.A., 2009. Kinetic study of CO_2 with various amino acid salts in aqueous solution. Chem. Eng. Sci. 64 (1), 59-68.

Van Wagener, D.H., 2009. Modeling stripper performance for CO_2 removal with amine solvents. In: *CO_2 acpture by aqueous absorption - Summary of 1st Quarterly Progress Reports 2009*, Department of Chemical Engineering, The University of Texas at Austin, USA, 35-49.

VDI, 2006. VDI-Wärmeatlas – Zehnte, berarbeitete und erweiterte Auflage. Verein Deutscher Ingenieure (VDI), VDI-Gesellschaft Verfahrenstechnik und Chemieingenieurwesen (GVC), Springer-Verlag Berlin Heidelberg, Germany, ISBN: 978-3-540-25504-8.

Vega, F., Sanna, A., Navarrete, B., Maroto-Valer, M.M., Cortés, V., 2014. Degradation of amine-based solvents in CO_2 capture process by chemical absorption. Greenhouse Gases: Sci. Technol. 4(6), 707-733.

Versteeg, G.F., Oyevaar, M.H., 1989. The reaction between CO_2 and diethanolamine at 298 K. Chem. Eng. Sci. 44 (5), 1264-1268.

Versteeg, G.F., van Dijck, L.A.J., van Swaaij, W.P.M., 1996. On the kinetics between CO_2 and alkanolamins both in aqueous and non-aqueous solutions. Chemical Engineering Communications 144 (1), 113-158.

Voice, A.K., 2009. Degradation of amine solvents for carbon capture CO_2. In: *CO_2 acpture by aqueous absorption - Summary of 2nd Quarterly Progress Reports 2009*, Department of Chemical Engineering, The University of Texas at Austin, USA, 203-215.

Voice, A.K., 2010. Degradation of MEA and other amines. In: *CO_2 acpture by aqueous absorption - Summary of 4th Quarterly Progress Reports 2009*, Department of Chemical Engineering, The University of Texas at Austin, USA, 154-165.

Wall, T. Liu, Y.; Spero, C., Elliott, L., Khare, S., Rathnam, R., Zeenathal, F., Moghtaderi, B., Buhre, B., Sheng, C., Gupta, R., Yamada, T., Makino, K., Yu, J., 2009. An overview on oxyfuel coal combustion - State of the art research and technology development. Chem. Eng. Res. Des. 87 (8), 1003-1016.

Wang, M., Lawal., A., Stephenson, P., Sidders, J., Ramshaw, C., 2011. Post-combustion CO_2 capture with chemical absorption: A state-of-the-art review. Chem. Eng. Res. Des. 89 (9), 1609-1624.

Wappel, D., 2010. CO_2-Abtrennung mit ionischen Flüssigkeiten. PhD thesis, University of Leoben, Austria.

Wappel, D., Gronald, G., Kalb, R., Draxler, J., 2010. Ionic liquids for post-combustion CO_2 absorption. Int. J. Greenhous Gas Control 4 (3), 486-494.

Wasserscheid, P., Welton, T., 2008. Ionic liquids in synthsis – 2nd editon. Wiley-VCH Verlag GmbH & Ci. KGaA, Weinheim, Germany. ISBN: 9783527312399.

Weiland, R.H., Hatcher, N.A., Nava, J. L., 2010b. Benchmarking solvents for carbon capture. In: *Distillation & Absorption*, Eindhoven University of Technology, Netherlands, September 12 – 15, 2010.

Weiland, R.H., Hatcher, N.A., Nava, J.L., 2010a. Post-combsution CO_2 capture with amino-acid salts. In: *GPA Europe Meeting*, Lisbon, Portugal, September 22 – 24, 2010.

Weiland, R.H., Trass, O., 1971. Absorption of carbon dioxide in ethylenediamine solutions - I. Absorption kinetics and eqilibrium. Can. J. Chem. Eng. 49 (6), 767-772.

Westerterp, K.R., van Swaaij, W.P.M., Beenakers, A.A.C.M., 1984. Chemical Reactor Design and Operation – 2nd edition. Wiley, New York, USA, ISBN: 978-0-471-91730-4.

Witkowski, A., Maijkut, M., 2012. The impact of CO_2 compression systems on the compressor power required for a pulverized coal-fired power plant in post-combustion carbon dioxide sequestration. The Archive of Mechanical Engineering 59 (3), 343-360.

Xie, Q., Aroonwilas, A., Veawab, A., 2013. Measurment of heat of CO_2 absortion into 2-amino-2-methyl-1-propanol (AMP)/piperazine (PZ) blends using differential reaction calorimeter. Energy Procedia 37, 826-833.

Xu, Q., Rochelle, G.T., 2011. Total pressure and CO_2 solubility at high temperature in aqueous amines. Energy Procedia 4, 117-124.

Xu, S., Wang, Y.W., Otto, F.D., Mather, A.E., 1996. Kinetics of the reaction of carbon dioxide with 2-amino-2-methyl-1-propanol solutions. Chem. Eng. Sci. 51 (6), 841-850.

Yan, S., He, Q., Zhao, S., Zhai, H., Cao, M., Ai, P., 2015. CO_2 removal from biogas by using green amino acid salts: Performance evaluation. Fuel Process. Technol. 129, 203-212.

Yoon, S.J., Lee, H., 2003. Substituent effect in amine-CO_2 interaction investigated by NMR and IR spectroscopies. Chem. Lett. 32, 344-345.

Zaimes, G.G., Khanna, V., 2013. Microalgal biomass production pathways: Evaluation of life cycle environmental impacts. Biotechnolgy for Biofuels 6 (88).

Zakeri, A., Einbu, A., Wiig, P.O., Øi, L.E., Svendsen, H.F., 2011. Experimental investigation of pressure drop, liquid hold-up and mass transfer parameters in a 0.5 m diameter absorber column. Energy Procedia 4, 606-613.

Zhou, S., 2009. Ethylenediamine as a solvent for CO_2 capture. In: *CO_2 acpture by aqueous absorption - Summary of 2nd Quarterly Progress Reports 2009*, Department of Chemical Engineering, The University of Texas at Austin, USA, 97-123.

Zhou, S., Chen, X., Nguyen, T., Voice, A.K., Rochelle, G.T., 2010. Aqueous ethylenediamine for CO_2 capture. ChemSusChem 3, 913-918.

Appendix

A Technical flow sheets

A.1 - CO$_2$SEPPL

Last updated on 26.01.2016

CO₂ to atmosphere or CO₂ compression unit

FIR 3.1

sampling

PIRC 3.3

TIRC 3.3

phase separator EF3.1

V-W3.3

CO₂ cooler WT3.1

CO₂ to the atmosphere

sampling

demister

500 mm siphon

desorption unit Des3.1

LIR 3.1
PIR 3.1
TIR 3.1
LA 3.1

desorber sump Des3.2

HZ3.1

25 kW

PIR 3.2
TIR 3.2
TIR 2.16

desorber water washing section 1 x 2 m Raschig Super-Pak 200-X
desorber column 2 x 4 m Raschig Super-Pak 250-Y

lean solvent pump PU3.1

TIR 2.15
TIR 3.5
TIR 2.14

TIR 3.4

main heat exchanger WT2.2

QIR-pH 2.2

sampling

V-W3.6

Lean solvent cooler WT3.2

FIRC 3.2

FIR 2.2

TIRC 3.6

QIR-pH 3.1
TIR 2.1

sampling

rich solvent pump PU2.2

absorber sump Abs2.2

HZ2.1

1 kW

PIRC 2.2
LA 2.1
PIRC 2.1

QIR-CO2 1.2

absorber water washing section 1 x 2 m Raschig Super-Pak 200-X

absorption unit Abs2.1

absorber column 4 x 3 m Raschig Super-Pak 250-Y

FIR 2.1

sampling

PIR 2.4
PIR 2.3
TIR 2.12.1

demister

venting/ discharge

TIR 2.11
TIR 2.12
TIR 2.9
TIR 2.10
TIR 2.7
TIR 2.8
TIR 2.5
TIR 2.6
TIR 2.3
TIR 2.4
TIR 2.2

CO₂ cleaned flue gas to the atmosphere

QIR-NH3 2.3
QIR-CO2 2.1
TIRC 2.13

deionate refill

sampling

washing water buffer BB2.1

HZ2.2

0.2 kW

washing water pump PU2.1

washing water cooler WT2.1

V-W2.13

TIRC 1.1

FIC 2.3

pre-scrubber column 1 x 2 m Raschig Super-Pak 200-X

pre-scrubber VW1.1

FIC 1.2

NaOH refill

LA 1.1

TIRC 1.2

FIRC 1.1

pre-scrubber sump VW1.2

HZ1.1

1.5 kW

pre-scrubber pump PU1.1

QIR-pH 1.1

phase separator EF1.1

1500 mm siphon

flue gas cooler WT1.1

V-W1.1

frequency converter FU1.1

flue gas blower G1.1

dust filter F1.1

compressed air

power plant flue gas

A.2 - Gas chromatograph

B. Measurement results

B.1 - 30 wt% MEA

	Variation of the L/G-ratio (Section 6.2, 6.3, 6.6)						Variation of the L/G-ratio (emission measurements) (Section 8)					
	25.03.14	25.03.14	24.03.14	25.03.14	25.03.14	24.03.14	04.11.15	04.11.15	04.11.15	03.11.15	04.11.15	04.11.15
	15:21	10:30	18:57	13:18	18:06	21:09	12:29	10:20	14:38	23:04	17:42	19:46
	00:30	00:25	00:30	00:30	00:30	00:30	00:30	00:30	00:30	00:30	00:30	00:30
	15:50	10:54	19:26	13:47	18:35	21:38	12:58	10:49	15:07	23:33	18:11	20:15
$conc_{lean}$ [wt%]	30.26	29.96	31.07	29.96	30.47	30.16	-	-	-	-	-	-
$conc_{rich}$ [wt%]	29.96	29.76	30.67	29.96	29.96	29.96	-	-	-	-	-	-
QIR-pH 1.1 [-]	8.61	9.46	6.90	8.65	8.52	7.34	-	-	-	-	-	-
QIR-pH 2.1 [-]	8.60	8.61	8.65	8.64	8.63	8.71	8.39	8.40	8.42	8.38	8.46	8.56
QIR-pH 3.1 [-]	10.40	10.27	10.21	10.11	10.14	9.94	10.52	10.39	10.29	10.19	10.20	10.09
α_{rich} [$mol_{CO_2}/mol_{equ.\ amine}$]	0.47	0.47	0.47	0.48	0.45	0.44	-	-	-	-	-	-
α_{lean} [$mol_{CO_2}/mol_{equ.\ amine}$]	0.09	0.10	0.12	0.13	0.12	0.20	-	-	-	-	-	-
QIR 1.2 [$vol\%_{CO_2}$ (dry)]	11.81	12.64	12.68	11.79	12.65	12.62	12.61	12.66	12.65	12.79	12.64	12.63
QIR 2.1 [$vol\%_{CO_2}$ (dry)]	1.44	1.51	1.66	1.35	1.34	1.27	1.60	1.07	1.44	1.71	1.61	1.40
FIRC 1.1 [m³/h]	90.00	90.00	90.06	90.00	89.94	90.02	89.98	89.99	89.99	90.01	89.97	90.03
FIR 2.1 [m³/h]	85.24	82.89	72.33	84.03	83.24	81.94	83.26	82.85	83.26	83.85	83.60	84.23
FIR 3.1 [m³/h]	5.07	5.43	5.44	5.13	5.56	5.51	4.62	5.38	5.35	5.37	5.32	5.37
FIR 2.2 [l/h]	179.74	211.39	230.32	241.24	257.75	347.07	185.66	215.43	230.09	258.23	263.59	346.09
FIRC 3.2 [l/h]	187.23	218.33	233.75	249.23	264.78	350.12	186.89	217.74	233.50	249.49	265.05	350.08
PIRC 2.1 [mbar]	52.22	52.50	51.09	53.80	54.76	56.89	51.62	52.42	52.83	53.66	53.75	56.61
PIRC 2.2 [mbar]	22.79	23.07	21.66	24.38	25.33	27.46	22.19	22.99	23.40	24.22	24.32	27.18
PIR 2.3 [mbar]	10.19	9.83	8.01	9.96	9.84	9.12	9.99	9.86	9.94	9.98	9.92	9.79
PIR 2.4 [mbar]	6.70	6.40	5.50	6.59	6.47	6.34	6.51	6.50	6.55	6.63	6.60	6.56
PIR 3.1 [bar_{rel}]	0.85	0.77	0.77	0.76	0.96	0.77	1.02	1.01	1.01	1.01	1.01	1.01
PIR 3.2 [bar_{rel}]	0.96	0.96	0.96	0.96	0.96	0.96	0.97	0.97	0.97	0.97	0.97	0.97
PIRC 3.3 [bar_{rel}]	1.00	1.00	1.00	1.00	1.00	1.00	1.00	1.00	1.00	1.00	1.00	1.00
LIR 3.1 [cm]	57.12	58.37	53.45	57.87	54.47	54.87	53.13	52.81	51.97	52.97	51.02	49.49
TIRC 1.1 [°C]	41.67	41.38	41.36	42.04	41.82	41.66	42.02	42.00	41.99	41.99	42.00	41.97
TIRC 1.2 [°C]	40.04	40.30	40.01	40.01	40.08	40.23	40.18	40.22	40.28	40.07	40.34	40.25
TIR 2.1 [°C]	42.40	43.07	43.47	43.91	44.50	48.68	42.63	43.37	43.78	44.37	44.79	47.95
TIR 2.2 [°C]	43.46	45.49	47.01	48.08	49.59	56.72	43.82	46.06	46.93	48.89	49.35	56.30
TIR 2.3 [°C]	44.22	46.91	48.84	49.94	51.44	59.53	44.60	47.63	48.71	51.03	51.77	59.84
TIR 2.4 [°C]	45.61	48.83	51.05	52.47	54.14	63.21	46.07	49.94	51.16	53.91	54.64	63.69
TIR 2.5 [°C]	46.82	50.36	52.83	54.30	55.98	65.67	47.24	51.51	52.76	55.79	56.48	66.28
TIR 2.6 [°C]	48.01	51.85	54.33	56.05	57.82	68.00	48.57	53.42	54.67	57.81	58.55	68.81
TIR 2.7 [°C]	50.76	54.95	57.65	59.64	61.51	71.45	51.24	57.17	58.26	61.49	62.20	72.36
TIR 2.8 [°C]	52.95	57.08	59.89	62.03	63.93	73.26	53.41	59.71	60.49	63.79	64.51	74.04
TIR 2.9 [°C]	56.72	60.99	63.46	65.61	67.53	75.25	57.28	64.13	64.46	67.46	68.07	75.90
TIR 2.10 [°C]	63.10	66.58	68.40	69.83	71.58	76.55	62.99	69.23	69.09	71.14	71.72	76.99
TIR 2.11 [°C]	68.26	70.96	72.15	72.80	74.47	77.66	68.51	73.04	72.79	74.11	74.42	78.02
TIR 2.12 [°C]	72.24	74.30	74.80	74.81	76.13	77.93	72.92	75.42	75.25	76.04	76.17	78.33
TIR 2.12.1 [°C]	65.15	65.65	65.29	63.80	64.71	62.00	66.90	66.85	66.06	65.28	64.97	61.82
TIR 2.13 [°C]	43.52	41.58	18.68	42.03	42.00	39.99	42.00	42.02	42.14	42.08	42.04	42.01
TIR 2.14 [°C]	41.75	42.66	43.00	43.28	43.94	47.43	42.10	43.07	43.54	44.26	44.79	48.21
TIR 2.15 [°C]	108.67	108.88	108.54	108.85	108.93	110.30	108.72	108.99	108.87	109.00	109.04	110.30
TIR 2.16 [°C]	105.90	105.91	105.53	105.98	106.28	107.30	105.64	105.97	105.83	105.98	106.07	107.30
TIR 3.1 [°C]	124.49	124.13	123.67	123.11	123.25	121.83	125.10	124.52	123.93	123.41	123.10	121.86
TIR 3.2 [°C]	108.41	103.13	97.83	98.32	98.83	99.03	106.82	100.73	98.25	98.04	98.35	99.36
TIR 3.3 [°C]	4.48	5.44	6.93	4.98	6.09	5.56	10.20	10.10	9.38	10.49	9.27	9.09
TIR 3.4 [°C]	124.17	123.77	123.33	122.80	123.02	121.53	124.42	123.87	123.40	122.78	122.67	121.51
TIR 3.5 [°C]	47.20	47.92	47.94	48.51	49.14	52.60	47.52	48.42	48.87	49.57	50.10	53.48
TIR 3.6 [°C]	40.03	39.98	40.01	40.04	40.00	40.00	40.05	39.98	40.01	40.02	40.01	39.98
ϑ_{out} [°C]	10.88	10.05	5.74	9.15	8.44	5.55	6.32	4.71	6.79	3.25	5.39	4.53
h_{abs} [m]	12.00	12.00	12.00	12.00	12.00	12.00	12.00	12.00	12.00	12.00	12.00	12.00
NH_3 conc. [ppm]	-	-	-	-	-	-	-0.27	10.96	-0.29	23.07	3.78	8.42
P_{des} [kW]	21.30	18.60	17.10	16.05	17.40	18.15	21.30	18.30	17.10	17.10	17.10	18.00
Δp_{abs} [mbar]	12.60	13.24	13.65	14.41	15.50	18.35	12.20	13.14	13.46	14.24	14.40	17.39
Δp_{des} [mbar]	-112.41	-190.88	-189.01	-198.41	-7.54	-196.38	48.86	41.76	41.24	40.47	41.32	43.11
L/G-ratio [l/m³]	**2.40**	**2.80**	**3.00**	**3.20**	**3.40**	**4.50**	**2.40**	**2.81**	**3.00**	**3.20**	**3.40**	**4.50**
η_{sep} [%]	89.06	89.39	88.35	89.78	90.61	91.10	88.71	92.51	89.89	88.09	88.65	90.10
q_{reb} [GJ/t_{CO_2}]	4.92	4.01	3.72	3.68	3.68	3.83	4.57	3.75	3.61	3.64	3.66	3.78

	Variation of the flue gas flow rate (Section 6.4)					
	26.03.14	25.03.14	25.03.14	26.03.14	26.03.14	26.03.14
	07:48	21:30	13:18	09:37	11:29	14:20
	00:30	00:30	00:30	00:20	00:30	00:30
	08:17	21:59	13:47	09:56	11:58	14:49
$conc_{lean}$ [wt%]	30.42	30.37	29.96	30.67	30.57	30.57
$conc_{rich}$ [wt%]	30.06	30.06	29.96	30.47	30.57	30.47
QIR-pH 1.1 [-]	8.27	8.46	8.65	8.19	8.15	8.02
QIR-pH 2.1 [-]	8.57	8.60	8.64	8.61	8.63	8.64
QIR-pH 3.1 [-]	10.29	10.19	10.11	10.21	10.16	10.16
α_{rich} [$mol_{CO_2}/mol_{equ.\ amine}$]	0.47	0.47	0.48	0.47	0.46	0.45
α_{lean} [$mol_{CO_2}/mol_{equ.\ amine}$]	0.11	0.13	0.13	0.12	0.13	0.14
QIR 1.2 [$vol\%_{CO_2}$ (dry)]	12.69	12.51	11.79	12.70	11.97	11.63
QIR 2.1 [$vol\%_{CO_2}$ (dry)]	1.20	1.62	1.35	1.32	1.25	1.20
FIRC 1.1 [m³/h]	**49.95**	**70.04**	**90.00**	**100.11**	**109.99**	**118.53**
FIR 2.1 [m³/h]	52.76	66.40	84.03	93.23	104.46	112.54
FIR 3.1 [m³/h]	3.37	4.27	5.13	6.14	6.46	6.71
FIR 2.2 [l/h]	134.09	188.11	241.24	271.47	299.01	323.18
FIRC 3.2 [l/h]	138.94	194.14	249.23	276.91	304.36	326.69
PIRC 2.1 [mbar]	37.88	44.14	53.80	60.87	69.10	78.82
PIRC 2.2 [mbar]	8.45	14.72	24.38	31.44	39.67	49.39
PIR 2.3 [mbar]	3.35	5.90	9.96	12.28	14.98	18.73
PIR 2.4 [mbar]	2.35	4.11	6.59	7.94	9.68	11.34
PIR 3.1 [bar_{rel}]	0.99	0.99	0.76	1.01	1.01	1.02
PIR 3.2 [bar_{rel}]	0.95	0.95	0.96	0.97	0.97	0.97
PIRC 3.3 [bar_{rel}]	1.00	1.00	1.00	1.00	1.00	1.00
LIR 3.1 [cm]	58.69	57.44	57.87	52.42	51.29	49.93
TIRC 1.1 [°C]	42.23	42.00	42.04	41.88	41.64	41.69
TIRC 1.2 [°C]	39.76	40.09	40.01	40.18	40.10	40.08
TIR 2.1 [°C]	42.26	43.37	43.91	44.54	44.56	44.78
TIR 2.2 [°C]	44.74	46.75	48.08	48.83	49.28	49.57
TIR 2.3 [°C]	45.74	48.17	49.94	50.55	51.37	51.91
TIR 2.4 [°C]	47.35	50.32	52.47	53.25	54.27	54.88
TIR 2.5 [°C]	48.63	51.79	54.30	55.22	56.23	56.97
TIR 2.6 [°C]	49.78	53.31	56.05	57.24	58.35	59.10
TIR 2.7 [°C]	51.94	56.03	59.64	60.98	62.44	63.31
TIR 2.8 [°C]	54.03	58.21	62.03	63.60	64.96	65.75
TIR 2.9 [°C]	57.39	61.69	65.61	67.14	68.33	69.05
TIR 2.10 [°C]	63.26	66.73	69.83	71.45	71.75	71.99
TIR 2.11 [°C]	69.40	71.21	72.80	74.16	74.05	74.07
TIR 2.12 [°C]	74.12	74.40	74.81	76.05	75.45	75.17
TIR 2.12.1 [°C]	63.71	64.43	63.80	65.64	64.85	64.58
TIR 2.13 [°C]	42.16	41.91	42.03	41.96	41.96	41.75
TIR 2.14 [°C]	41.67	42.83	43.28	43.65	43.85	44.03
TIR 2.15 [°C]	107.49	108.04	108.85	109.31	109.61	109.95
TIR 2.16 [°C]	104.73	105.37	105.98	106.56	106.79	107.05
TIR 3.1 [°C]	123.82	123.31	123.11	123.65	123.50	123.44
TIR 3.2 [°C]	98.48	97.54	98.32	99.18	99.23	99.22
TIR 3.3 [°C]	4.14	2.58	4.98	5.90	7.76	8.68
TIR 3.4 [°C]	123.53	123.01	122.80	123.44	123.31	123.25
TIR 3.5 [°C]	46.77	47.83	48.51	49.05	49.39	49.68
TIR 3.6 [°C]	40.02	40.06	40.04	39.98	39.98	40.01
ϑ_{out} [°C]	5.06	4.65	9.15	9.35	12.85	12.91
h_{abs} [m]	12.00	12.00	12.00	12.00	12.00	12.00
NH_3 conc. [ppm]	-	-	-	-	-	-
P_{des} [kW]	11.70	13.80	16.05	18.90	19.80	20.79
Δp_{abs} [mbar]	5.10	8.82	14.41	19.15	24.69	30.65
Δp_{des} [mbar]	42.75	32.41	-198.41	44.45	42.06	45.35
L/G-ratio [l/m³]	3.20	3.20	3.20	3.20	3.20	3.19
η_{sep} [%]	90.32	87.95	89.78	90.82	90.67	90.81
q_{reb} [GJ/t_{CO_2}]	4.55	4.03	3.68	3.54	3.54	3.50

173

B.2 - 32 wt% EDA

	Variation of the L/G-ratio (Section 6.3, 6.6, 6.9)								Variation of the flue gas flow rate (Section 6.4)				
	24.07.13	24.07.13	23.07.13	22.07.13	24.07.13	22.07.13	30.07.13	25.07.13	21.08.13	21.08.13	22.07.13	21.08.13	21.08.13
	12:56	17:08	11:16	18:24	22:09	22:13	16:13	10:05	11:36	16:18	18:24	20:37	19:05
	00:30	00:30	00:30	00:30	00:30	00:30	00:30	00:30	00:30	00:30	00:30	00:30	00:30
	13:25	17:37	11:45	18:53	22:38	22:42	16:42	10:34	12:05	16:47	18:53	21:06	19:34
$conc_{lean}$ [wt%]	32.12	31.80	32.33	32.17	31.90	31.69	31.42	31.37	31.58	30.57	32.17	30.62	31.05
$conc_{rich}$ [wt%]	30.30	31.16	30.78	30.84	31.42	30.84	30.89	31.21	30.20	29.31	30.84	29.56	30.20
QIR-pH 1.1 [-]	7.08	6.75	7.69	8.05	7.87	7.99	8.18	7.71	8.07	7.85	8.05	7.30	7.57
QIR-pH 2.1 [-]	7.93	7.92	8.02	8.10	8.24	8.44	8.46	8.59	7.93	7.99	8.10	8.12	8.15
QIR-pH 3.1 [-]	10.32	10.31	10.01	9.80	9.70	9.61	9.44	9.52	9.71	9.65	9.80	9.66	9.66
α_{rich} [$mol_{CO_2}/mol_{equ.\ amine}$]	0.49	0.49	0.48	0.47	0.47	0.45	0.44	0.43	0.47	0.47	0.47	0.46	0.46
α_{lean} [$mol_{CO_2}/mol_{equ.\ amine}$]	0.16	0.16	0.25	0.28	0.28	0.29	0.34	0.32	0.25	0.25	0.28	0.26	0.25
QIR 1.2 [$vol\%_{CO_2}$ (dry)]	11.98	12.14	12.00	11.87	12.05	11.99	12.87	12.06	12.39	12.31	11.87	12.40	12.34
QIR 2.1 [$vol\%_{CO_2}$ (dry)]	1.25	1.46	1.32	1.33	1.33	1.33	1.43	1.33	1.16	1.27	1.33	1.40	1.35
FIRC 1.1 [m³/h]	90.03	89.97	89.98	90.01	89.98	89.99	90.02	90.00	**50.03**	**70.01**	**90.01**	**110.00**	**120.01**
FIR 2.1 [m³/h]	83.48	83.44	84.37	83.59	84.08	84.14	83.52	83.06	49.61	66.11	83.59	103.04	111.84
FIR 3.1 [m³/h]	5.38	5.37	5.39	5.35	5.23	5.39	5.84	5.38	3.31	4.29	5.35	6.52	7.10
FIR 2.2 [l/h]	108.55	106.00	157.47	199.61	238.44	333.53	373.69	394.87	102.81	153.64	199.61	251.15	277.71
FIRC 3.2 [l/h]	117.38	117.32	156.19	195.00	233.76	311.34	365.72	388.88	108.64	151.93	195.00	238.12	259.61
PIRC 2.1 [mbar]	64.82	64.82	65.96	66.39	68.15	70.22	72.40	82.66	51.35	57.80	66.39	78.97	86.52
PIRC 2.2 [mbar]	21.65	21.65	22.80	23.23	24.99	27.05	29.24	31.63	8.19	14.64	23.23	35.80	43.35
PIR 2.3 [mbar]	9.95	10.01	10.11	9.48	9.92	9.45	9.28	9.29	3.28	6.07	9.48	14.72	17.60
PIR 2.4 [mbar]	6.53	6.57	6.65	6.59	6.62	6.70	6.59	6.60	2.33	4.23	6.59	9.63	11.45
PIR 3.1 [bar_{rel}]	1.05	1.05	1.02	1.01	1.02	1.02	1.03	1.02	1.00	1.01	1.01	1.03	1.04
PIR 3.2 [bar_{rel}]	1.03	1.03	1.00	1.00	1.01	1.01	1.01	1.00	0.99	1.00	1.00	1.02	1.03
PIRC 3.3 [bar_{rel}]	1.00	1.00	1.00	1.00	1.00	1.00	1.00	1.00	1.00	1.00	1.00	1.00	1.00
LIR 3.1 [cm]	52.36	52.50	51.41	51.03	50.71	48.97	47.69	43.70	47.79	48.40	51.03	45.84	44.80
TIRC 1.1 [°C]	40.84	40.72	40.82	40.60	40.92	40.74	40.84	40.59	40.61	40.78	40.60	41.18	41.20
TIRC 1.2 [°C]	40.22	40.18	40.12	40.05	39.98	40.02	39.96	39.80	40.05	40.04	40.05	40.08	39.98
TIR 2.1 [°C]	42.83	42.86	43.18	43.90	45.18	48.74	50.83	52.22	42.93	43.35	43.90	44.23	44.47
TIR 2.2 [°C]	43.31	43.28	45.01	48.01	51.71	58.69	62.39	64.94	45.02	46.51	48.01	48.64	49.18
TIR 2.3 [°C]	43.68	43.67	46.15	50.19	54.69	62.62	66.42	68.31	46.27	48.18	50.19	51.18	52.00
TIR 2.4 [°C]	44.63	44.57	48.49	53.71	58.99	67.25	70.66	72.25	48.47	51.08	53.71	54.82	55.63
TIR 2.5 [°C]	45.62	45.48	50.38	56.14	61.59	69.64	72.89	74.04	50.37	53.31	56.14	57.39	58.20
TIR 2.6 [°C]	46.72	46.52	52.46	58.62	64.04	71.74	74.59	75.38	52.17	55.41	58.62	59.88	60.63
TIR 2.7 [°C]	49.56	49.13	56.24	62.65	67.91	74.06	76.54	76.89	55.58	59.21	62.65	63.91	64.86
TIR 2.8 [°C]	51.71	51.17	58.83	65.03	69.83	74.94	77.23	77.23	57.97	61.75	65.03	66.18	66.84
TIR 2.9 [°C]	55.55	54.78	62.48	68.06	71.85	76.01	77.97	77.87	61.86	65.34	68.06	69.02	69.72
TIR 2.10 [°C]	61.11	60.39	67.00	70.80	73.56	76.20	77.94	77.62	66.60	69.14	70.80	71.63	72.03
TIR 2.11 [°C]	65.95	65.23	70.29	72.11	74.38	76.28	78.11	77.83	70.57	72.08	72.11	73.50	73.71
TIR 2.12 [°C]	70.75	70.43	72.64	74.11	75.24	76.39	77.87	77.12	73.37	73.91	74.11	74.65	74.73
TIR 2.12.1 [°C]	68.03	68.05	66.49	65.07	63.82	60.66	59.12	56.12	63.74	65.22	65.07	65.76	66.01
TIR 2.13 [°C]	41.02	41.18	41.90	40.43	41.68	40.83	41.01	38.67	35.35	41.05	40.43	40.46	40.49
TIR 2.14 [°C]	42.74	42.68	43.20	44.27	45.77	49.26	51.15	52.18	42.80	43.41	44.27	44.38	44.47
TIR 2.15 [°C]	106.24	106.17	106.19	106.74	107.75	111.16	113.21	114.53	104.42	105.67	106.74	107.56	108.12
TIR 2.16 [°C]	103.33	103.35	103.31	103.86	104.90	107.97	109.44	111.14	101.48	102.92	103.86	104.86	105.30
TIR 3.1 [°C]	126.16	126.20	124.60	123.37	122.52	121.69	121.73	121.43	123.97	123.62	123.37	123.96	124.20
TIR 3.2 [°C]	109.09	109.24	96.87	95.70	97.24	100.08	101.17	102.93	91.91	94.68	95.70	96.87	96.65
TIR 3.3 [°C]	24.34	24.56	23.54	23.62	23.58	22.84	25.07	23.64	22.53	5.34	23.62	22.67	22.69
TIR 3.4 [°C]	125.88	125.85	124.31	123.13	122.36	121.47	121.55	121.28	123.34	123.24	123.13	123.66	123.96
TIR 3.5 [°C]	47.94	47.95	48.32	49.59	51.32	54.95	57.02	58.22	47.18	48.40	49.59	50.07	50.26
TIR 3.6 [°C]	40.08	40.04	40.00	40.01	39.98	40.07	40.02	39.91	40.02	40.05	40.01	39.98	40.06
ϑ_{out} [°C]	34.63	29.74	31.34	29.93	25.77	24.35	31.68	27.16	24.86	26.10	29.93	20.82	23.25
h_{abs} [m]	12.00	12.00	12.00	12.00	12.00	12.00	12.00	12.00	12.00	12.00	12.00	12.00	12.00
NH_3 conc. [ppm]	-	-	-	-	-	-	-	-	-	-	-	-	-
P_{des} [kW]	22.50	22.35	14.94	14.79	15.36	16.83	18.84	18.45	10.38	12.63	14.79	18.30	20.15
Δp_{abs} [mbar]	11.70	11.64	12.69	13.74	15.07	17.61	19.96	22.34	4.91	8.57	13.74	21.08	25.75
Δp_{des} [mbar]	23.95	22.96	11.04	12.00	11.19	13.15	15.68	16.68	8.46	10.15	12.00	11.83	13.58
L/G-ratio [l/m³]	**1.50**	**1.50**	**2.00**	**2.50**	**3.00**	**4.00**	**4.70**	**5.00**	2.50	2.50	2.50	2.50	2.50
η_{sep} [%]	90.64	89.19	90.12	89.93	90.14	89.99	90.09	90.14	90.50	90.51	89.93	89.90	90.37
q_{reb} [GJ/t_{CO_2}]	5.02	5.00	3.47	3.34	3.41	3.75	3.89	4.22	4.07	3.53	3.34	3.16	3.15

	Variation of the desorber pressure (Section 6.5)							Variation in absorber heights (Section 6.7)			Variation of the flue gas temperature (Section 6.8)			
	01.08.13	01.08.13	01.08.13	22.07.13	01.08.13	01.08.13	01.08.13	20.08.13	20.08.13	22.07.13	22.08.13	22.07.13	22.08.13	23.08.13
	13:48	11:35	08:02	18:24	17:15	20:30	22:16	14:37	17:50	18:24	16:37	18:24	23:06	11:43
	00:30	00:30	00:30	00:30	00:30	00:30	00:30	00:30	00:30	00:30	00:30	00:30	00:30	00:30
	14:17	12:04	08:31	18:53	17:44	20:59	22:45	15:06	18:19	18:53	17:06	18:53	23:35	12:12
$conc_{lean}$ [wt%]	31.69	31.53	31.00	32.17	31.64	31.10	31.05	33.19	34.16	32.17	30.94	32.17	30.94	30.84
$conc_{rich}$ [wt%]	31.16	30.62	31.05	30.84	30.23	30.30	29.98	32.44	32.65	30.84	30.25	30.84	30.30	29.19
QIR-pH 1.1 [-]	4.74	6.62	7.39	8.05	8.18	8.08	8.01	7.62	7.06	8.05	5.55	8.05	2.53	8.23
QIR-pH 2.1 [-]	8.09	8.09	8.09	8.10	8.08	8.10	8.10	8.28	8.63	8.10	8.17	8.10	8.05	8.02
QIR-pH 3.1 [-]	9.65	9.66	9.67	9.80	9.65	9.66	9.66	9.68	9.80	9.80	9.74	9.80	9.65	9.59
α_{rich} [$mol_{CO_2}/mol_{equ. amine}$]	0.49	0.48	0.48	0.47	0.48	0.48	0.47	0.45	0.43	0.47	0.48	0.47	0.46	0.46
α_{lean} [$mol_{CO_2}/mol_{equ. amine}$]	0.27	0.27	0.29	0.28	0.27	0.27	0.27	0.27	0.24	0.28	0.26	0.28	0.27	0.26
QIR 1.2 [$vol\%_{CO_2}$ (dry)]	12.24	12.37	12.46	11.87	12.25	12.13	12.25	12.19	11.98	11.87	12.47	11.87	12.37	12.49
QIR 2.1 [$vol\%_{CO_2}$ (dry)]	1.36	1.36	1.52	1.33	1.36	1.34	1.39	1.38	1.33	1.33	1.37	1.33	1.32	1.32
FIRC 1.1 [m³/h]	90.02	90.00	89.99	90.01	89.95	90.00	90.02	89.97	89.99	90.01	90.02	90.01	89.99	90.01
FIR 2.1 [m³/h]	83.54	83.58	83.43	83.59	83.50	83.62	83.65	83.25	81.11	83.59	81.65	83.59	83.59	84.29
FIR 3.1 [m³/h]	5.43	5.45	5.45	5.35	5.42	5.30	5.35	5.27	5.19	5.35	5.92	5.35	4.93	4.90
FIR 2.2 [l/h]	196.30	198.59	199.03	199.61	199.34	206.07	199.08	198.32	204.43	199.61	198.99	199.61	198.81	200.10
FIRC 3.2 [l/h]	194.95	195.01	194.99	195.00	194.93	195.05	194.96	194.76	194.88	195.00	195.01	195.00	194.97	195.03
PIRC 2.1 [mbar]	66.31	66.39	66.82	66.39	66.76	66.89	66.83	65.75	64.56	66.39	68.53	66.39	64.56	64.10
PIRC 2.2 [mbar]	23.14	23.23	23.66	23.23	23.59	23.72	23.67	22.58	21.40	23.23	25.37	23.23	21.39	20.93
PIR 2.3 [mbar]	9.48	9.54	9.97	9.48	9.87	9.91	9.93	9.88	9.49	9.48	10.03	9.48	8.96	8.95
PIR 2.4 [mbar]	6.56	6.59	6.60	6.59	6.52	6.59	6.59	6.65	6.39	6.59	6.55	6.59	6.27	6.19
PIR 3.1 [bar_{rel}]	0.44	0.63	0.82	1.01	1.21	1.41	1.61	1.01	1.02	1.01	1.02	1.01	1.01	1.01
PIR 3.2 [bar_{rel}]	0.42	0.61	0.81	1.00	1.20	1.40	1.60	1.00	1.00	1.00	1.01	1.00	1.00	1.00
PIRC 3.3 [bar_{rel}]	**0.40**	**0.60**	**0.80**	**1.00**	**1.20**	**1.40**	**1.60**	1.00	1.00	1.00	1.00	1.00	1.00	1.00
LIR 3.1 [cm]	48.85	49.16	49.18	51.03	49.38	49.50	49.43	42.45	45.48	51.03	44.59	51.03	45.10	47.66
TIRC 1.1 [°C]	41.10	41.03	40.91	40.60	40.87	40.79	40.86	41.29	41.36	40.60	27.89	40.60	51.64	67.95
TIRC 1.2 [°C]	40.12	40.07	39.82	40.05	40.14	39.92	39.89	40.07	39.97	40.05	**27.85**	40.05	**49.24**	**51.74**
TIR 2.1 [°C]	43.93	43.83	43.55	43.90	43.92	43.73	43.62	45.04	47.04	43.90	33.57	43.90	52.59	54.90
TIR 2.2 [°C]	47.97	47.97	47.43	48.01	47.93	47.84	47.76	51.65	57.29	48.01	42.56	48.01	54.35	56.03
TIR 2.3 [°C]	50.10	49.96	49.54	50.19	50.02	50.01	49.78	55.14	62.38	50.19	45.83	50.19	55.59	57.02
TIR 2.4 [°C]	53.46	53.34	52.79	53.71	53.45	53.47	53.25	60.23	68.62	53.71	50.35	53.71	58.03	58.96
TIR 2.5 [°C]	55.85	55.75	55.17	56.14	55.92	55.91	55.63	63.59	71.73	56.14	53.30	56.14	59.86	60.54
TIR 2.6 [°C]	58.26	58.20	57.51	58.62	58.29	58.24	58.06	67.00	74.00	58.62	55.95	58.62	61.88	62.32
TIR 2.7 [°C]	62.37	62.30	61.47	62.65	62.15	62.25	62.01	71.16	64.31	62.65	60.37	62.65	65.32	65.70
TIR 2.8 [°C]	64.85	64.80	63.90	65.03	64.69	64.83	64.45	73.13	62.29	65.03	63.05	65.03	67.51	67.75
TIR 2.9 [°C]	67.77	67.90	67.05	68.06	67.88	67.85	67.60	74.69	62.24	68.06	66.35	68.06	70.28	70.58
TIR 2.10 [°C]	70.86	70.94	70.26	70.80	70.83	70.85	70.65	61.93	61.85	70.80	69.80	70.80	72.81	73.10
TIR 2.11 [°C]	72.80	72.97	72.61	72.11	72.82	72.80	72.74	63.00	62.02	72.11	72.28	72.11	74.80	75.13
TIR 2.12 [°C]	74.40	74.56	74.16	74.11	74.36	74.27	74.26	62.54	61.84	74.11	73.85	74.11	75.74	76.26
TIR 2.12.1 [°C]	65.41	65.62	65.27	65.07	65.62	65.36	65.28	62.22	61.36	65.07	65.70	65.07	66.14	66.71
TIR 2.13 [°C]	41.13	41.32	41.01	40.43	40.95	41.08	41.23	41.01	36.96	40.43	24.71	40.43	50.67	53.66
TIR 2.14 [°C]	44.31	44.18	43.82	44.27	44.30	44.07	43.99	45.41	47.47	44.27	35.28	44.27	52.41	54.53
TIR 2.15 [°C]	99.67	102.09	104.32	106.74	108.56	110.35	112.05	108.94	114.11	106.74	105.74	106.74	107.82	108.04
TIR 2.16 [°C]	96.47	99.20	101.43	103.86	106.02	107.97	109.64	105.91	110.65	103.86	103.12	103.86	105.04	105.27
TIR 3.1 [°C]	114.04	117.60	120.75	123.37	126.13	128.61	130.84	124.54	125.44	123.37	124.20	123.37	123.43	123.23
TIR 3.2 [°C]	90.49	91.85	93.80	95.70	98.34	99.22	100.83	96.46	102.51	95.70	95.26	95.70	96.85	97.51
TIR 3.3 [°C]	24.08	23.71	23.54	23.62	24.27	24.14	23.94	23.43	23.82	23.62	22.23	23.62	21.99	22.06
TIR 3.4 [°C]	113.85	117.36	120.48	123.13	125.88	128.34	130.53	123.89	124.94	123.13	123.92	123.13	123.13	123.01
TIR 3.5 [°C]	49.09	49.20	48.96	49.59	49.88	49.84	49.87	51.00	53.38	49.59	41.47	49.59	57.03	58.99
TIR 3.6 [°C]	39.98	40.04	40.00	40.01	40.02	39.96	40.02	40.04	39.98	40.01	39.98	40.01	39.95	39.94
ϑ_{out} [°C]	29.03	29.88	20.47	29.93	32.57	27.20	24.39	21.69	19.33	29.93	25.67	29.93	16.63	23.91
h_{abs} [m]	12.00	12.00	12.00	12.00	12.00	12.00	12.00	**9.00**	**6.00**	**12.00**	12.00	12.00	12.00	12.00
NH_3 conc. [ppm]	-	-	-	-	-	-	-	-	-	-	-	-	-	-
P_{des} [kW]	15.54	15.36	15.26	14.79	14.73	14.63	14.76	15.84	17.76	14.79	16.20	14.79	14.40	14.55
Δp_{abs} [mbar]	13.66	13.69	13.69	13.74	13.72	13.81	13.74	12.70	11.91	13.74	15.34	13.74	12.43	11.98
Δp_{des} [mbar]	15.64	15.02	11.86	12.00	12.29	14.16	14.12	8.63	13.55	12.00	10.19	12.00	10.58	10.60
L/G-ratio [l/m³]	2.50	2.50	2.50	2.50	2.50	2.50	2.50	2.50	2.50	2.50	2.50	2.50	2.50	2.50
η_{sep} [%]	90.04	90.18	89.13	89.93	90.02	90.10	89.87	89.87	90.00	89.93	90.13	89.93	90.52	90.56
q_{reb} [GJ/t_{CO_2}]	3.54	3.46	3.44	3.34	3.36	3.35	3.36	3.47	3.95	3.34	3.20	3.34	3.35	3.45

175

	Variation of the regenerated solvent temperature (Section 6.8)				Variation of the L/G-ratio (η_{sep} = 80 %) (Section 6.9)							
	22.08.13	22.08.13	22.07.13	22.08.13	31.07.13	30.07.13	25.07.13	25.07.13	25.07.13	31.07.13	26.07.13	25.07.13
	09:37	08:03	18:24	12:27	16:24	21:26	23:23	18:20	15:01	20:52	11:02	13:36
	00:30	00:30	00:30	00:30	00:30	00:30	00:30	00:30	00:30	00:30	00:30	00:30
	10:06	08:32	18:53	12:56	16:53	21:55	23:52	18:49	15:30	21:21	11:31	14:05
$conc_{lean}$ [wt%]	31.12	31.64	32.17	30.25	33.37	31.05	31.12	31.09	31.41	31.85	30.62	31.21
$conc_{rich}$ [wt%]	29.34	29.77	30.84	29.72	32.15	30.41	30.73	31.53	30.52	30.52	30.30	31.69
QIR-pH 1.1 [-]	2.16	2.23	8.05	7.54	7.29	7.97	3.02	6.12	7.18	6.06	8.32	7.36
QIR-pH 2.1 [-]	8.05	8.05	8.10	8.04	7.95	7.96	8.10	8.19	8.28	8.31	8.40	8.35
QIR-pH 3.1 [-]	10.04	9.95	9.80	9.48	10.00	9.81	9.69	9.56	9.48	9.31	9.36	9.43
α_{rich} [$mol_{CO_2}/mol_{equ.\,amine}$]	0.47	0.46	0.47	0.46	0.50	0.50	0.47	0.48	0.46	0.47	0.45	0.46
α_{lean} [$mol_{CO_2}/mol_{equ.\,amine}$]	0.25	0.25	0.28	0.26	0.20	0.28	0.31	0.33	0.34	0.34	0.33	0.34
QIR 1.2 [$vol\%_{CO_2}$ (dry)]	12.66	12.58	11.87	12.54	12.11	13.05	12.22	12.15	13.48	12.30	12.28	13.54
QIR 2.1 [$vol\%_{CO_2}$ (dry)]	1.41	1.39	1.33	1.44	2.65	2.89	2.74	2.71	3.04	2.68	2.67	2.98
FIRC 1.1 [m³/h]	89.99	89.99	90.01	89.99	89.96	89.93	90.01	90.01	89.97	89.98	90.01	90.03
FIR 2.1 [m³/h]	83.73	83.92	83.59	83.82	84.79	82.75	84.66	84.76	84.38	82.37	84.69	85.28
FIR 3.1 [m³/h]	5.47	5.38	5.35	5.40	4.72	5.12	4.83	4.80	5.34	4.83	4.87	5.38
FIR 2.2 [l/h]	199.02	198.97	199.61	197.43	106.72	158.72	199.24	240.29	336.93	335.76	377.54	374.56
FIRC 3.2 [l/h]	194.94	195.03	195.00	194.96	117.43	156.22	194.97	233.80	311.38	311.30	365.71	365.60
PIRC 2.1 [mbar]	66.04	66.18	66.39	67.08	64.99	65.49	66.28	67.37	69.75	69.65	71.67	72.14
PIRC 2.2 [mbar]	22.87	23.02	23.23	23.91	21.82	22.33	23.12	24.20	26.58	26.49	28.51	28.98
PIR 2.3 [mbar]	9.42	9.46	9.48	10.26	10.24	9.91	9.76	9.73	9.50	9.41	9.56	9.60
PIR 2.4 [mbar]	6.62	6.67	6.59	6.63	6.81	6.58	6.83	6.82	6.67	6.62	6.81	6.83
PIR 3.1 [bar_{rel}]	1.01	1.02	1.01	1.02	1.01	1.01	1.01	1.01	1.02	1.01	1.01	1.02
PIR 3.2 [bar_{rel}]	1.00	1.01	1.00	1.01	1.00	1.00	1.00	1.00	1.00	1.00	1.00	1.00
PIRC 3.3 [bar_{rel}]	1.00	1.00	1.00	1.00	1.00	1.00	1.00	1.00	1.00	1.00	1.00	1.00
LIR 3.1 [cm]	47.76	48.06	51.03	47.94	45.20	51.40	50.27	49.65	48.58	47.07	46.88	48.12
TIRC 1.1 [°C]	41.22	41.40	40.60	41.08	40.95	40.90	40.79	40.85	40.84	40.95	40.95	40.90
TIRC 1.2 [°C]	40.08	39.83	40.05	40.05	40.11	39.93	39.77	39.94	40.10	39.90	39.99	40.14
TIR 2.1 [°C]	43.70	43.48	43.90	-	43.04	42.71	43.50	44.77	47.57	47.75	49.84	50.19
TIR 2.2 [°C]	47.51	47.33	48.01	47.38	43.53	44.07	47.06	50.18	55.92	56.51	60.11	60.17
TIR 2.3 [°C]	49.47	49.37	50.19	49.32	43.85	44.94	48.74	52.84	59.28	59.78	63.52	63.27
TIR 2.4 [°C]	52.84	52.72	53.71	52.73	44.74	46.86	51.76	56.43	63.31	63.83	67.38	67.21
TIR 2.5 [°C]	55.22	55.12	56.14	54.96	45.65	48.30	53.80	58.60	65.56	66.03	69.41	69.31
TIR 2.6 [°C]	57.50	57.46	58.62	57.48	46.57	49.78	55.80	60.77	67.60	67.98	70.96	71.05
TIR 2.7 [°C]	61.75	61.55	62.65	61.38	49.05	53.05	59.27	64.09	70.51	70.63	73.26	73.52
TIR 2.8 [°C]	64.11	64.06	65.03	63.87	50.84	55.12	61.60	65.99	71.89	71.85	74.15	74.50
TIR 2.9 [°C]	67.33	67.31	68.06	67.13	54.01	58.59	64.35	68.29	73.61	73.25	75.23	75.88
TIR 2.10 [°C]	70.66	70.51	70.80	70.43	58.73	63.12	67.51	70.45	74.80	74.33	75.64	76.50
TIR 2.11 [°C]	72.97	73.00	72.11	72.89	63.37	67.18	70.17	72.11	75.68	75.02	75.97	76.72
TIR 2.12 [°C]	74.46	74.36	74.11	74.42	68.45	71.02	72.15	73.38	76.20	75.41	75.70	77.02
TIR 2.12.1 [°C]	59.86	61.17	65.07	68.72	65.92	65.44	62.96	61.81	60.86	58.91	56.12	58.38
TIR 2.13 [°C]	41.99	41.97	40.43	41.82	40.99	38.98	41.13	40.97	41.79	36.40	40.96	43.00
TIR 2.14 [°C]	43.76	43.63	44.27	43.83	42.83	42.53	43.78	45.26	48.33	48.39	50.44	50.37
TIR 2.15 [°C]	106.43	106.47	106.74	106.47	105.45	105.33	105.76	106.34	108.13	108.58	110.92	110.52
TIR 2.16 [°C]	103.77	103.72	103.86	103.71	102.57	102.64	103.06	103.66	105.34	105.62	107.24	106.79
TIR 3.1 [°C]	123.67	123.67	123.37	123.66	125.64	124.31	122.49	121.27	120.48	120.12	119.49	119.93
TIR 3.2 [°C]	95.84	95.94	95.70	95.78	100.50	95.01	95.37	95.58	97.22	97.37	98.96	98.57
TIR 3.3 [°C]	21.70	21.76	23.62	22.08	24.68	24.18	23.60	23.98	24.06	23.79	23.91	23.87
TIR 3.4 [°C]	123.40	123.36	123.13	123.38	125.22	123.94	122.23	121.06	120.36	119.93	119.36	119.81
TIR 3.5 [°C]	49.08	48.92	49.59	49.23	47.90	47.62	48.96	50.69	53.99	53.93	56.08	56.08
TIR 3.6 [°C]	**27.23**	**30.06**	**40.01**	**48.56**	40.02	40.01	40.04	40.03	40.04	39.91	39.98	39.97
ϑ_{out} [°C]	19.15	16.40	29.93	25.88	31.00	21.69	24.08	28.56	31.57	25.00	30.28	30.67
h_{abs} [m]	12.00	12.00	12.00	12.00	12.00	12.00	12.00	12.00	12.00	12.00	12.00	12.00
NH_3 conc. [ppm]	-	-	-	-	-	-	-	-	-	-	-	-
P_{des} [kW]	15.39	15.33	14.79	15.18	14.76	14.22	13.47	13.68	15.51	14.88	15.45	16.38
Δp_{abs} [mbar]	13.46	13.56	13.74	13.65	11.58	12.42	13.36	14.48	17.09	17.08	18.95	19.37
Δp_{des} [mbar]	9.94	9.13	12.00	10.54	13.58	10.00	9.50	11.73	13.37	12.89	13.90	14.01
L/G-ratio [l/m³]	2.50	2.50	2.50	2.50	**1.50**	**1.99**	**2.50**	**3.00**	**4.00**	**4.00**	**4.70**	**4.70**
η_{sep} [%]	90.06	90.16	89.93	89.70	80.07	80.05	79.69	79.74	79.81	80.26	80.34	80.27
q_{reb} [GJ/t_{CO_2}]	3.23	3.23	3.34	3.24	3.83	3.28	3.47	3.54	3.61	3.77	3.91	3.76

	Variation of the L/G-ratio (operation with flue gas of a natural gas-fired boiler) (Section 6.6)							
	30.04.13	30.04.13	30.04.13	30.04.13	30.04.13	30.04.13	30.04.13	30.04.13
	-	-	-	-	-	-	-	-
	-	-	-	-	-	-	-	-
	-	-	-	-	-	-	-	-
$conc_{lean}$ [wt%]	32.58	32.58	32.73	32.87	33.51	32.73	32.55	-
$conc_{rich}$ [wt%]	32.04	32.22	32.44	32.76	33.19	32.05	31.51	-
QIR-pH 1.1 [-]	-	-	-	-	-	-	-	-
QIR-pH 2.1 [-]	-	-	-	-	-	-	-	-
QIR-pH 3.1 [-]		-	-	-	-	-	-	-
α_{rich} [mol_{CO_2}/$mol_{equ.\ amine}$]	0.45	0.46	0.45	0.43	0.41	0.41	0.41	-
α_{lean} [mol_{CO_2}/$mol_{equ.\ amine}$]	0.27	0.30	0.31	0.32	0.32	0.33	0.33	-
QIR 1.2 [$vol\%_{CO_2}$ (dry)]	-	-	-	-	-	-	-	-
QIR 2.1 [$vol\%_{CO_2}$ (dry)]	-	-	-	-	-	-	-	-
FIRC 1.1 [m³/h]	-	-	-	-	-	-	-	-
FIR 2.1 [m³/h]	-	-	-	-	-	-	-	-
FIR 3.1 [m³/h]	-	-	-	-	-	-	-	-
FIR 2.2 [l/h]	-	-	-	-	-	-	-	-
FIRC 3.2 [l/h]	-	-	-	-	-	-	-	-
PIRC 2.1 [mbar]	-	-	-	-	-	-	-	-
PIRC 2.2 [mbar]	-	-	-	-	-	-	-	-
PIR 2.3 [mbar]	-	-	-	-	-	-	-	-
PIR 2.4 [mbar]	-	-	-	-	-	-	-	-
PIR 3.1 [bar_{rel}]	-	-	-	-	-	-	-	-
PIR 3.2 [bar_{rel}]	-	-	-	-	-	-	-	-
PIRC 3.3 [bar_{rel}]	-	-	-	-	-	-	-	-
LIR 3.1 [cm]	-	-	-	-	-	-	-	-
TIRC 1.1 [°C]	-	-	-	-	-	-	-	-
TIRC 1.2 [°C]	-	-	-	-	-	-	-	-
TIR 2.1 [°C]	-	-	-	-	-	-	-	-
TIR 2.2 [°C]	-	-	-	-	-	-	-	-
TIR 2.3 [°C]	-	-	-	-	-	-	-	-
TIR 2.4 [°C]	-	-	-	-	-	-	-	-
TIR 2.5 [°C]	-	-	-	-	-	-	-	-
TIR 2.6 [°C]	-	-	-	-	-	-	-	-
TIR 2.7 [°C]	-	-	-	-	-	-	-	-
TIR 2.8 [°C]	-	-	-	-	-	-	-	-
TIR 2.9 [°C]	-	-	-	-	-	-	-	-
TIR 2.10 [°C]	-	-	-	-	-	-	-	-
TIR 2.11 [°C]	-	-	-	-	-	-	-	-
TIR 2.12 [°C]	-	-	-	-	-	-	-	-
TIR 2.12.1 [°C]	-	-	-	-	-	-	-	-
TIR 2.13 [°C]	-	-	-	-	-	-	-	-
TIR 2.14 [°C]	-	-	-	-	-	-	-	-
TIR 2.15 [°C]	-	-	-	-	-	-	-	-
TIR 2.16 [°C]	-	-	-	-	-	-	-	-
TIR 3.1 [°C]	-	-	-	-	-	-	-	-
TIR 3.2 [°C]	-	-	-	-	-	-	-	-
TIR 3.3 [°C]	-	-	-	-	-	-	-	-
TIR 3.4 [°C]	-	-	-	-	-	-	-	-
TIR 3.5 [°C]	-	-	-	-	-	-	-	-
TIR 3.6 [°C]	-	-	-	-	-	-	-	-
ϑ_{out} [°C]	-	-	-	-	-	-	-	-
h_{abs} [m]	12.00	12.00	12.00	12.00	12.00	12.00	12.00	12.00
NH_3 conc. [ppm]	-	-	-	-	-	-	-	-
P_{des} [kW]	-	-	-	-	-	-	-	-
Δp_{abs} [mbar]	-	-	-	-	-	-	-	-
Δp_{des} [mbar]	-	-	-	-	-	-	-	-
L/G-ratio [l/m³]	**1.00**	**1.50**	**1.75**	**2.00**	**2.50**	**3.00**	**3.52**	**4.12**
η_{sep} [%]	-	-	-	-	-	-	-	-
q_{reb} [GJ/t_{CO_2}]	4.45	3.65	3.60	3.75	3.90	4.40	4.30	4.60

B.3 - 37.6 wt% PIP

	Variation of the L/G-ratio (Section 6.3, 6.6)								Variation of the flue gas flow rate (Section 6.4)					
	22.07.14	22.07.14	22.07.14	22.07.14	22.07.14	22.07.14	22.07.14	23.07.14	23.07.14	23.07.14	22.07.14	22.07.14	23.07.14	23.07.14
	14:49	16:08	12:09	18:43	20:14	21:12	22:11	09:47	11:48	13:53	11:05	12:09	15:53	18:35
	00:30	00:30	00:30	00:30	00:30	00:30	00:30	00:30	00:30	00:30	00:30	00:30	00:30	00:30
	15:18	16:37	12:38	19:12	20:43	21:41	22:40	10:16	12:17	14:22	11:34	12:38	16:22	19:04
$conc_{lean}$ [wt%]	37.76	37.62	37.49	36.82	36.96	37.76	37.49	36.96	36.89	36.56	37.49	37.49	36.82	37.09
$conc_{rich}$ [wt%]	37.09	36.62	36.69	36.56	36.49	36.82	36.82	36.16	36.29	36.02	37.71	36.69	36.56	37.22
QIR-pH 1.1 [-]	7.90	7.52	8.35	5.02	8.71	8.62	8.54	8.28	7.95	6.33	8.48	8.35	8.55	7.91
QIR-pH 2.1 [-]	8.42	8.46	8.50	8.52	8.57	8.63	8.68	8.84	8.46	8.45	8.49	8.50	8.51	8.54
QIR-pH 3.1 [-]	10.61	10.59	10.46	10.39	10.32	10.24	10.19	10.07	10.40	10.38	10.47	10.46	10.39	10.43
α_{rich} [$mol_{CO_2}/mol_{equ.\ amine}$]	0.35	0.36	0.35	0.34	0.33	0.34	0.33	0.29	0.36	0.36	0.33	0.35	0.35	0.35
α_{lean} [$mol_{CO_2}/mol_{equ.\ amine}$]	0.09	0.10	0.12	0.12	0.13	0.15	0.15	0.16	0.12	0.11	0.12	0.12	0.11	0.11
QIR 1.2 [$vol\%_{CO_2}$ (dry)]	12.74	12.90	12.77	12.90	12.95	13.00	13.07	12.32	12.95	12.87	12.73	12.77	12.89	12.86
QIR 2.1 [$vol\%_{CO_2}$ (dry)]	1.59	1.29	1.52	1.33	1.52	1.58	1.69	1.35	1.45	1.62	1.53	1.52	1.36	1.54
FIRC 1.1 [m³/h]	99.99	100.02	100.00	100.05	99.99	99.98	99.95	100.03	70.02	79.97	90.01	100.00	109.99	120.00
FIR 2.1 [m³/h]	92.42	91.64	92.91	91.45	92.14	92.37	92.90	85.88	65.82	74.62	83.18	92.91	103.08	111.99
FIR 3.1 [m³/h]	6.34	6.52	6.34	6.55	6.46	6.39	6.44	6.17	4.68	5.16	5.62	6.34	7.19	7.22
FIR 2.2 [l/h]	175.60	197.37	219.15	241.76	263.71	307.63	351.92	444.07	154.17	175.12	196.92	219.15	242.29	264.27
FIRC 3.2 [l/h]	173.42	195.03	216.47	238.04	259.62	302.57	345.73	432.00	151.93	173.50	194.95	216.47	238.10	259.60
PIRC 2.1 [mbar]	41.48	41.93	42.70	43.19	44.01	45.62	47.33	50.73	28.93	32.86	37.58	42.70	49.96	59.37
PIRC 2.2 [mbar]	26.76	27.22	27.98	28.48	29.30	30.91	32.62	35.97	14.21	18.15	22.87	27.98	35.25	44.65
PIR 2.3 [mbar]	12.07	11.93	12.11	11.89	12.00	11.98	12.00	10.51	5.99	7.61	9.96	12.11	14.68	18.91
PIR 2.4 [mbar]	7.82	7.72	7.86	7.74	7.83	7.86	7.93	7.00	4.11	5.22	6.44	7.86	9.42	11.31
PIR 3.1 [bar_{rel}]	0.85	0.85	0.86	0.86	0.87	0.87	0.88	0.88	0.84	0.83	0.86	0.86	0.85	0.88
PIR 3.2 [bar_{rel}]	0.97	0.97	0.97	0.97	0.97	0.97	0.97	0.97	0.96	0.96	0.96	0.97	0.98	0.98
PIRC 3.3 [bar_{rel}]	1.00	1.00	1.00	1.00	1.00	1.00	1.00	1.00	1.00	1.00	1.00	1.00	1.00	1.00
LIR 3.1 [cm]	33.49	33.07	33.13	32.99	32.98	32.21	31.30	29.57	37.32	36.23	34.32	33.13	32.50	30.94
TIRC 1.1 [°C]	40.87	40.67	41.26	41.12	41.00	40.91	40.91	40.95	41.14	40.74	40.86	41.26	40.57	40.93
TIRC 1.2 [°C]	39.98	40.07	39.88	40.16	39.98	40.02	40.00	40.03	40.21	40.17	39.67	39.88	39.82	39.74
TIR 2.1 [°C]	43.36	43.74	44.00	44.60	45.00	46.41	48.33	52.12	43.71	43.77	43.67	44.00	44.01	44.12
TIR 2.2 [°C]	45.44	46.74	48.13	49.92	51.33	54.79	58.14	64.77	46.90	47.38	47.75	48.13	48.65	48.61
TIR 2.3 [°C]	46.60	48.35	50.09	51.99	53.57	57.38	60.59	67.18	48.19	48.67	49.51	50.09	50.21	50.32
TIR 2.4 [°C]	48.78	50.91	53.07	55.20	56.91	61.06	64.47	71.03	50.59	51.25	52.53	53.07	53.00	53.30
TIR 2.5 [°C]	50.20	52.66	54.96	57.19	59.05	63.25	66.67	72.90	52.08	52.76	54.30	54.96	54.84	55.00
TIR 2.6 [°C]	51.57	54.11	56.50	58.75	60.71	64.98	68.29	74.01	53.52	54.25	55.91	56.50	56.41	56.46
TIR 2.7 [°C]	54.23	57.05	59.52	61.95	63.74	68.03	71.18	75.67	56.15	57.01	58.82	59.52	59.59	59.65
TIR 2.8 [°C]	55.98	59.02	61.43	63.92	65.70	69.74	72.48	76.08	57.88	58.77	60.70	61.43	61.55	61.60
TIR 2.9 [°C]	58.49	61.58	63.96	66.40	67.96	71.66	73.99	76.56	60.35	61.24	63.20	63.96	64.15	64.21
TIR 2.10 [°C]	62.48	65.44	67.26	69.42	70.67	73.34	74.94	76.41	63.98	64.77	66.60	67.26	67.63	67.67
TIR 2.11 [°C]	66.50	69.13	70.31	72.18	72.86	74.87	75.97	76.77	67.86	68.46	69.89	70.31	70.85	70.65
TIR 2.12 [°C]	70.37	72.22	72.61	73.96	74.30	75.45	76.02	75.77	71.55	71.63	72.37	72.61	73.09	72.92
TIR 2.12.1 [°C]	65.14	65.05	63.97	64.10	63.29	61.85	60.24	54.11	64.08	64.06	63.75	63.97	64.64	64.32
TIR 2.13 [°C]	41.49	40.95	42.05	40.42	41.00	41.12	41.60	26.93	41.94	42.54	41.90	42.05	42.08	41.50
TIR 2.14 [°C]	43.25	43.60	43.88	44.69	45.16	46.74	48.30	51.86	43.57	43.80	43.63	43.88	44.06	44.03
TIR 2.15 [°C]	107.47	107.79	108.24	108.63	108.95	110.39	111.71	114.11	106.60	106.95	107.87	108.24	108.09	108.24
TIR 2.16 [°C]	103.71	104.05	104.36	104.79	105.13	106.22	107.31	111.14	103.12	103.36	103.92	104.36	104.50	104.64
TIR 3.1 [°C]	124.75	124.33	123.70	123.30	122.71	121.97	121.50	121.18	123.52	123.40	123.63	123.70	123.85	123.81
TIR 3.2 [°C]	102.12	98.33	96.57	97.30	97.04	98.19	99.07	102.31	94.83	95.63	95.84	96.57	96.70	96.55
TIR 3.3 [°C]	-	-	-	-	-	-	-	-	-	-	-	-	-	-
TIR 3.4 [°C]	124.34	124.08	123.37	123.12	122.49	121.81	121.28	120.91	123.21	123.16	123.17	123.37	123.64	123.70
TIR 3.5 [°C]	49.99	50.39	50.64	51.50	52.00	53.54	55.07	58.05	49.94	50.14	50.26	50.64	50.97	51.15
TIR 3.6 [°C]	39.97	40.01	40.05	40.03	39.99	40.02	40.01	39.85	40.01	40.10	39.97	40.05	40.00	40.00
ϑ_{out} [°C]	26.07	21.26	23.40	23.62	22.05	22.06	21.98	25.25	28.30	30.46	22.00	23.40	33.57	22.05
h_{abs} [m]	12.00	12.00	12.00	12.00	12.00	12.00	12.00	12.00	12.00	12.00	12.00	12.00	12.00	12.00
NH_3 conc. [ppm]	-	-	-	-	-	-	-	-	-	-	-	-	-	-
P_{des} [kW]	18.45	17.40	16.68	17.10	17.10	17.55	18.30	19.80	12.60	13.50	15.00	16.68	18.30	19.65
Δp_{abs} [mbar]	14.69	15.30	15.87	16.60	17.30	18.93	20.62	25.47	8.23	10.54	12.91	15.87	20.57	25.74
Δp_{des} [mbar]	-123.66	-116.49	-109.11	-113.88	-104.06	-98.44	-96.02	-90.11	-121.51	-129.53	-107.84	-109.11	-125.67	-97.26
L/G-ratio [l/m³]	**2.00**	**2.25**	**2.50**	**2.75**	**3.00**	**3.50**	**4.00**	**5.00**	2.50	2.50	2.50	2.50	2.50	2.50
η_{sep} [%]	88.97	91.19	89.47	90.92	89.66	89.29	88.56	90.19	89.76	88.72	89.39	89.47	90.66	89.54
q_{reb} [GJ/t_{CO_2}]	3.54	3.22	3.17	3.17	3.20	3.28	3.42	3.83	3.43	3.25	3.20	3.17	3.05	3.00

	Variation of the desorber pressure (Section 6.5)							Variation in absorber heights (Section 6.7)			Variation of the flue gas temperature (Section 6.8)	
	24.07.14	24.07.14	24.07.14	24.07.14	24.07.14	24.07.14	24.07.14	24.07.14	24.07.14	24.07.14	25.07.14	23.07.14
	14:33	11:50	10:27	09:28	16:17	17:38	19:01	09:28	20:10	21:48	12:06	19:37
	00:30	00:30	00:30	00:30	00:30	00:30	00:30	00:30	00:20	00:20	00:20	00:30
	15:02	12:19	10:56	09:57	16:46	18:07	19:30	09:57	20:29	22:07	12:25	20:06
$conc_{lean}$ [wt%]	37.76	37.76	36.82	36.56	38.15	38.55	37.89	36.56	37.09	38.42	38.82	37.56
$conc_{rich}$ [wt%]	37.62	37.22	36.42	36.42	36.96	37.09	36.82	36.42	38.29	38.55	37.49	36.42
QIR-pH 1.1 [-]	8.92	9.04	9.50	5.45	8.84	8.79	8.73	5.45	8.67	8.56	7.99	7.44
QIR-pH 2.1 [-]	8.48	8.55	8.62	8.64	8.48	8.49	8.49	8.64	8.58	8.74	8.66	8.52
QIR-pH 3.1 [-]	10.39	10.37	10.40	10.35	10.40	10.41	10.43	10.35	10.45	10.54	10.45	10.46
α_{rich} [$mol_{CO_2}/mol_{equ. amine}$]	0.35	0.34	0.35	0.35	0.36	0.35	0.33	0.35	0.33	0.30	0.34	0.35
α_{lean} [$mol_{CO_2}/mol_{equ. amine}$]	0.12	0.11	0.11	0.11	0.10	0.10	0.11	0.11	0.10	0.11	0.09	0.11
QIR 1.2 [$vol\%_{CO_2}$ (dry)]	13.28	13.04	13.06	13.08	13.27	13.09	13.14	13.08	13.21	13.31	13.29	12.96
QIR 2.1 [$vol\%_{CO_2}$ (dry)]	1.65	1.74	1.54	1.55	1.54	1.27	1.49	1.55	1.41	1.60	1.48	1.33
FIRC 1.1 [m³/h]	100.02	99.99	99.98	100.00	100.01	100.00	99.97	100.00	100.01	99.98	99.98	100.03
FIR 2.1 [m³/h]	92.16	92.22	96.43	91.65	92.18	92.61	92.18	91.65	92.17	92.16	92.25	92.11
FIR 3.1 [m³/h]	6.65	6.43	6.48	6.42	6.70	6.70	6.58	6.42	6.69	6.67	7.14	6.55
FIR 2.2 [l/h]	219.10	218.63	217.18	219.60	220.06	220.12	220.18	219.60	219.73	221.06	219.12	219.36
FIRC 3.2 [l/h]	216.50	216.46	216.50	216.54	216.56	216.51	216.62	216.54	216.48	216.51	216.40	216.54
PIRC 2.1 [mbar]	43.43	43.38	44.03	42.98	43.61	43.82	43.70	42.98	42.58	41.13	46.94	43.38
PIRC 2.2 [mbar]	28.72	28.66	29.32	28.27	28.90	29.11	28.99	28.27	27.87	26.42	32.24	28.67
PIR 2.3 [mbar]	12.01	12.04	12.77	11.91	12.04	12.09	12.02	11.91	12.03	11.96	12.55	11.97
PIR 2.4 [mbar]	7.73	7.79	8.28	7.71	7.76	7.82	7.78	7.71	7.79	7.77	7.98	7.73
PIR 3.1 [bar_{rel}]	0.30	0.49	0.69	0.88	1.05	1.24	1.43	0.88	0.86	0.87	0.87	0.87
PIR 3.2 [bar_{rel}]	0.39	0.58	0.77	0.97	1.17	1.37	1.56	0.97	0.97	0.97	0.98	0.97
PIRC 3.3 [bar_{rel}]	**0.40**	**0.60**	**0.80**	**1.00**	**1.20**	**1.40**	**1.60**	1.00	1.00	1.00	1.00	1.00
LIR 3.1 [cm]	30.61	30.67	32.21	32.06	30.72	30.44	30.33	32.06	32.79	35.41	28.47	32.11
TIRC 1.1 [°C]	41.10	41.07	40.96	41.02	40.84	40.68	40.70	41.02	41.03	41.02	24.33	40.97
TIRC 1.2 [°C]	40.34	39.99	40.27	41.28	39.95	39.90	40.01	41.28	39.96	39.79	**26.42**	**40.03**
TIR 2.1 [°C]	44.37	44.13	44.27	45.18	44.11	44.07	44.15	45.18	44.80	45.74	34.02	44.11
TIR 2.2 [°C]	48.51	48.48	48.47	49.16	48.40	48.52	48.51	49.16	50.85	54.61	43.69	48.53
TIR 2.3 [°C]	49.92	49.76	49.77	50.43	49.76	49.81	49.77	50.43	52.91	57.85	45.96	49.91
TIR 2.4 [°C]	52.74	52.59	52.53	53.09	52.53	52.71	52.56	53.09	56.85	63.90	49.77	52.62
TIR 2.5 [°C]	54.45	54.34	54.28	54.83	54.28	54.44	54.38	54.83	59.54	68.17	52.00	54.42
TIR 2.6 [°C]	55.95	55.98	55.79	56.33	55.89	56.15	55.88	56.33	62.23	72.37	53.78	55.99
TIR 2.7 [°C]	58.85	58.88	58.87	59.25	58.82	59.07	58.90	59.25	67.07	64.48	57.21	58.96
TIR 2.8 [°C]	60.82	60.82	60.75	61.18	60.77	61.21	60.90	61.18	70.21	62.84	59.30	61.00
TIR 2.9 [°C]	63.41	63.41	63.46	63.85	63.38	63.91	63.59	63.85	73.55	63.02	62.15	63.59
TIR 2.10 [°C]	66.83	66.69	66.82	67.07	66.87	67.51	67.05	67.07	62.33	62.43	65.98	67.20
TIR 2.11 [°C]	70.25	69.97	70.17	70.29	70.43	70.90	70.54	70.29	63.24	62.57	69.62	70.54
TIR 2.12 [°C]	73.00	72.60	72.84	73.04	73.08	73.45	73.10	73.04	62.99	62.56	72.45	73.04
TIR 2.12.1 [°C]	64.72	64.21	64.39	64.44	64.90	64.89	64.72	64.44	63.39	62.48	64.91	64.42
TIR 2.13 [°C]	41.60	41.09	47.04	41.64	41.58	41.98	41.38	41.64	41.51	41.43	26.68	41.09
TIR 2.14 [°C]	44.32	44.15	44.30	45.42	44.07	44.10	44.16	45.42	44.91	46.01	34.19	43.99
TIR 2.15 [°C]	100.61	103.07	105.64	107.86	109.54	111.53	113.13	107.86	108.82	111.14	106.64	107.66
TIR 2.16 [°C]	96.36	99.14	101.93	104.41	106.26	108.49	110.30	104.41	105.33	107.45	103.30	104.13
TIR 3.1 [°C]	114.05	117.45	120.76	123.67	126.55	129.18	131.38	123.67	124.23	124.83	124.29	123.73
TIR 3.2 [°C]	91.79	91.92	94.53	96.36	98.14	100.55	102.10	96.36	98.03	101.50	95.33	96.19
TIR 3.3 [°C]	-	-	-	-	-	-	-	-	-	-	-	-
TIR 3.4 [°C]	113.81	117.24	120.51	123.44	126.35	129.00	131.19	123.44	123.96	124.55	124.10	123.51
TIR 3.5 [°C]	50.27	50.38	51.03	51.82	50.96	51.24	51.39	51.82	51.86	53.37	42.35	50.73
TIR 3.6 [°C]	40.05	40.01	39.97	40.00	40.02	40.02	39.99	40.00	39.91	39.97	39.95	40.01
ϑ_{out} [°C]	27.71	25.79	22.95	21.85	32.28	28.07	26.83	21.85	26.03	22.03	28.75	22.17
h_{abs} [m]	12.00	12.00	12.00	12.00	12.00	12.00	12.00	**12.00**	**9.00**	**6.00**	12.00	12.00
NH_3 conc. [ppm]	-	-	-	-	-	-	-	-	-	-	-	-
P_{des} [kW]	18.15	16.74	16.65	16.65	16.80	16.80	16.50	16.65	17.40	19.20	18.00	16.80
Δp_{abs} [mbar]	16.71	16.62	16.54	16.37	16.86	17.02	16.96	16.37	15.83	14.45	19.68	16.69
Δp_{des} [mbar]	-91.00	-89.26	-87.70	-89.25	-120.86	-130.89	-130.46	-89.25	-118.89	-102.02	-107.90	-96.69
L/G-ratio [l/m³]	2.50	2.50	2.50	2.50	2.50	2.50	2.50	2.50	2.50	2.50	2.50	2.50
η_{sep} [%]	89.02	88.22	89.65	89.55	89.79	91.45	89.98	89.55	90.57	89.43	90.20	90.95
q_{reb} [GJ/t_{CO_2}]	3.33	3.15	3.08	3.11	3.05	3.03	3.02	3.11	3.15	3.50	2.97	3.08

	Variation of the regenerated solvent temperature (Section 6.8)				Variation of the L/G-ratio (operation with flue gas of a natural gas-fired boiler) (Section 6.6)				
	23.07.14	23.07.14	23.07.14	23.07.14	01.05.14	01.05.14	01.05.14	01.05.14	30.04.14
	21:19	20:37	19:37	22:20	05:09	03:49	01:56	23:49	22:22
	00:15	00:15	00:30	00:15	00:10	00:20	00:20	00:20	00:20
	21:33	20:51	20:06	22:34	05:18	04:08	02:15	00:08	22:41
$conc_{lean}$ [wt%]	37.49	37.36	37.56	37.22	37.36	37.09	37.76	37.76	37.36
$conc_{rich}$ [wt%]	36.56	36.76	36.42	36.89	37.49	36.96	37.09	37.36	36.16
QIR-pH 1.1 [-]	5.23	5.43	7.44	5.12	8.81	8.82	8.82	8.83	8.84
QIR-pH 2.1 [-]	8.53	8.52	8.52	8.52	8.59	8.60	8.65	8.75	8.84
QIR-pH 3.1 [-]	10.67	10.58	10.46	10.21	10.63	10.53	10.35	10.11	10.04
α_{rich} [$mol_{CO_2}/mol_{equ.\,amine}$]	0.35	0.36	0.35	0.36	0.37	0.38	0.37	0.34	0.32
α_{lean} [$mol_{CO_2}/mol_{equ.\,amine}$]	0.11	0.12	0.11	0.11	0.09	0.12	0.16	0.20	0.20
QIR 1.2 [$vol\%_{CO_2}$ (dry)]	12.91	12.98	12.96	12.78	6.78	6.81	6.83	6.81	6.85
QIR 2.1 [$vol\%_{CO_2}$ (dry)]	1.21	1.29	1.33	1.20	0.86	0.83	0.62	0.59	0.85
FIRC 1.1 [m³/h]	100.00	100.02	100.03	99.96	99.96	100.03	100.00	100.00	99.98
FIR 2.1 [m³/h]	92.36	92.30	92.11	92.48	97.78	97.68	97.62	97.93	98.11
FIR 3.1 [m³/h]	6.54	6.56	6.55	6.53	3.28	3.24	3.37	3.44	3.35
FIR 2.2 [l/h]	219.30	219.29	219.36	219.09	94.47	102.77	128.16	171.23	213.76
FIRC 3.2 [l/h]	216.45	216.45	216.54	216.54	95.85	104.50	130.34	173.38	216.54
PIRC 2.1 [mbar]	43.20	43.31	43.38	43.77	41.02	41.31	41.82	42.93	43.90
PIRC 2.2 [mbar]	28.48	28.59	28.67	29.06	25.59	25.87	26.38	27.48	28.44
PIR 2.3 [mbar]	11.91	11.95	11.97	12.35	13.08	13.14	13.13	13.19	13.18
PIR 2.4 [mbar]	7.82	7.80	7.73	7.84	8.71	8.76	8.76	8.79	8.81
PIR 3.1 [bar_{rel}]	0.87	0.87	0.87	0.88	0.87	0.86	0.87	0.87	0.87
PIR 3.2 [bar_{rel}]	0.97	0.97	0.97	0.97	0.95	0.95	0.95	0.95	0.95
PIRC 3.3 [bar_{rel}]	1.00	1.00	1.00	1.00	1.00	1.00	1.00	1.00	1.00
LIR 3.1 [cm]	31.71	31.92	32.11	32.01	35.51	35.58	35.28	35.12	34.41
TIRC 1.1 [°C]	41.02	41.39	40.97	40.90	41.67	41.33	41.69	41.67	41.58
TIRC 1.2 [°C]	39.99	40.09	40.03	39.94	40.04	40.11	39.97	39.92	40.05
TIR 2.1 [°C]	44.08	44.14	44.11	43.97	42.96	43.02	43.07	43.60	44.60
TIR 2.2 [°C]	48.61	48.45	48.53	48.42	43.11	43.34	44.06	46.60	50.15
TIR 2.3 [°C]	49.93	49.89	49.91	49.71	43.27	43.51	44.73	48.32	52.39
TIR 2.4 [°C]	52.65	52.68	52.62	52.57	43.66	44.12	46.17	51.16	55.98
TIR 2.5 [°C]	54.45	54.50	54.42	54.46	44.04	44.69	47.32	53.04	58.07
TIR 2.6 [°C]	56.20	56.09	55.99	56.10	44.42	45.18	48.28	54.56	59.56
TIR 2.7 [°C]	59.26	59.12	58.96	59.20	45.82	46.79	50.67	57.59	62.16
TIR 2.8 [°C]	61.10	61.03	61.00	61.12	46.82	48.05	52.27	59.23	63.28
TIR 2.9 [°C]	63.83	63.65	63.59	63.76	48.64	49.89	54.55	61.27	64.42
TIR 2.10 [°C]	67.45	67.27	67.20	67.35	51.54	53.04	57.75	62.94	64.99
TIR 2.11 [°C]	70.76	70.54	70.54	70.61	55.31	56.64	60.61	64.16	65.79
TIR 2.12 [°C]	73.12	73.14	73.04	73.15	59.35	60.08	62.69	64.55	65.48
TIR 2.12.1 [°C]	60.96	62.59	64.42	68.02	56.39	56.33	56.29	55.22	53.63
TIR 2.13 [°C]	41.46	41.51	41.09	41.36	41.03	41.00	40.83	41.01	40.94
TIR 2.14 [°C]	44.12	44.17	43.99	43.95	42.26	42.33	42.57	43.40	44.72
TIR 2.15 [°C]	107.76	107.74	107.66	107.68	106.80	106.95	107.56	109.08	111.06
TIR 2.16 [°C]	104.31	104.21	104.13	104.15	102.82	102.90	103.42	104.72	106.30
TIR 3.1 [°C]	123.84	123.72	123.73	123.79	124.67	124.32	123.40	121.88	120.64
TIR 3.2 [°C]	96.25	96.31	96.19	96.24	99.69	95.12	94.36	95.66	97.40
TIR 3.3 [°C]	-0.33	0.44	1.35	-0.55	-4.65	-4.04	-0.25	1.45	4.53
TIR 3.4 [°C]	123.53	123.52	123.51	123.47	123.91	123.65	122.70	121.30	120.10
TIR 3.5 [°C]	50.89	50.90	50.73	50.72	48.42	48.53	48.71	49.60	50.94
TIR 3.6 [°C]	**31.46**	**34.90**	**40.01**	**50.33**	40.14	39.98	39.98	40.02	39.96
ϑ_{out} [°C]	20.30	21.46	22.17	19.28	13.11	12.72	13.15	15.45	16.43
h_{abs} [m]	12.00	12.00	12.00	12.00	12.00	12.00	12.00	12.00	12.00
NH_3 conc. [ppm]	-	-	-	-	-	-	-	-	-
P_{des} [kW]	16.80	16.80	16.80	16.80	11.10	10.20	10.20	10.80	10.80
Δp_{abs} [mbar]	16.58	16.64	16.69	16.72	12.50	12.73	13.25	14.29	15.26
Δp_{des} [mbar]	-98.30	-100.05	-96.69	-93.56	-83.03	-88.55	-87.36	-82.08	-84.87
L/G-ratio [l/m³]	2.50	2.50	2.50	2.50	**1.10**	**1.20**	**1.50**	**2.00**	**2.50**
η_{sep} [%]	91.70	91.24	90.95	91.71	88.10	88.50	91.45	91.79	88.33
q_{reb} [GJ/t_{CO_2}]	3.07	3.07	3.08	3.10	4.05	3.69	3.55	3.75	3.88

	Variation of the L/G-ratio (NH₃ measurement) (Section 8)				
	30.09.14	30.09.14	30.09.14	30.09.14	30.09.14
	20:41	13:13	14:57	16:29	18:34
	00:30	00:30	00:30	00:30	00:30
	21:10	13:42	15:26	16:58	19:03
$conc_{lean}$ [wt%]	36.82	37.36	37.02	36.56	37.22
$conc_{rich}$ [wt%]	36.11	36.69	36.87	36.62	37.09
QIR-pH 1.1 [-]	-	-	-	-	-
QIR-pH 2.1 [-]	-	-	-	-	-
QIR-pH 3.1 [-]	-	-	-	-	-
α_{rich} [$mol_{CO_2}/mol_{equ.\ amine}$]	0.32	0.34	0.33	0.31	0.28
α_{lean} [$mol_{CO_2}/mol_{equ.\ amine}$]	0.09	0.09	0.11	0.15	0.16
QIR 1.2 [$vol\%_{CO_2}$ (dry)]	12.92	13.08	13.11	13.12	13.15
QIR 2.1 [$vol\%_{CO_2}$ (dry)]	-	-	-	-	-
FIRC 1.1 [m³/h]	-	-	-	-	-
FIR 2.1 [m³/h]	-	-	-	-	-
FIR 3.1 [m³/h]	-	-	-	-	-
FIR 2.2 [l/h]	-	-	-	-	-
FIRC 3.2 [l/h]	-	-	-	-	-
PIRC 2.1 [mbar]	-	-	-	-	-
PIRC 2.2 [mbar]	-	-	-	-	-
PIR 2.3 [mbar]	-	-	-	-	-
PIR 2.4 [mbar]	-	-	-	-	-
PIR 3.1 [bar_{rel}]	-	-	-	-	-
PIR 3.2 [bar_{rel}]	-	-	-	-	-
PIRC 3.3 [bar_{rel}]	-	-	-	-	-
LIR 3.1 [cm]	-	-	-	-	-
TIRC 1.1 [°C]	-	-	-	-	-
TIRC 1.2 [°C]	-	-	-	-	-
TIR 2.1 [°C]	-	-	-	-	-
TIR 2.2 [°C]	-	-	-	-	-
TIR 2.3 [°C]	-	-	-	-	-
TIR 2.4 [°C]	-	-	-	-	-
TIR 2.5 [°C]	-	-	-	-	-
TIR 2.6 [°C]	-	-	-	-	-
TIR 2.7 [°C]	-	-	-	-	-
TIR 2.8 [°C]	-	-	-	-	-
TIR 2.9 [°C]	-	-	-	-	-
TIR 2.10 [°C]	-	-	-	-	-
TIR 2.11 [°C]	-	-	-	-	-
TIR 2.12 [°C]	-	-	-	-	-
TIR 2.12.1 [°C]	-	-	-	-	-
TIR 2.13 [°C]	-	-	-	-	-
TIR 2.14 [°C]	-	-	-	-	-
TIR 2.15 [°C]	-	-	-	-	-
TIR 2.16 [°C]	-	-	-	-	-
TIR 3.1 [°C]	-	-	-	-	-
TIR 3.2 [°C]	-	-	-	-	-
TIR 3.3 [°C]	-	-	-	-	-
TIR 3.4 [°C]	-	-	-	-	-
TIR 3.5 [°C]	-	-	-	-	-
TIR 3.6 [°C]	-	-	-	-	-
ϑ_{out} [°C]	-	-	-	-	-
h_{abs} [m]	12.00	12.00	12.00	12.00	12.00
NH₃ conc. [ppm]	0.02	0.02	0.04	0.06	0.09
P_{des} [kW]	-	-	-	-	-
Δp_{abs} [mbar]	-	-	-	-	-
Δp_{des} [mbar]	-	-	-	-	-
L/G-ratio [l/m³]	**2.00**	**2.50**	**3.00**	**4.00**	**5.00**
η_{sep} [%]	89.69	90.12	89.72	90.17	89.64
q_{reb} [GJ/t_{CO_2}]	-	-	-	-	-

181

B.4 - 28/17 wt% AMP/PIP

	Variation of the L/G-ratio (Section 6.3, 8)								Variation of the flue gas flow rate (Section 6.4)			
	23.09.15	23.09.15	23.09.15	22.09.15	22.09.15	22.09.15	22.09.15	22.09.15	01.10.15	01.10.15	23.09.15	24.09.15
	16:21	13:21	11:22	15:14	13:30	17:17	19:44	21:32	20:54	23:55	11:22	17:02
	00:30	00:30	00:30	00:30	00:30	00:15	00:30	00:15	00:30	00:30	00:30	00:10
	16:50	13:50	11:51	15:43	13:59	17:31	20:13	21:46	21:23	00:24	11:51	17:11
$conc_{lean}$ [wt%]	-	-	-	-	-	-	-	-	-	-	-	-
$conc_{rich}$ [wt%]	-	-	-	-	-	-	-	-	-	-	-	-
QIR-pH 1.1 [-]	14.87	14.88	14.88	14.88	14.88	14.88	14.88	14.88	14.88	14.88	14.88	14.88
QIR-pH 2.1 [-]	8.67	8.71	8.77	8.59	8.61	8.79	8.89	8.97	8.65	8.65	8.77	8.75
QIR-pH 3.1 [-]	11.07	10.79	10.69	10.59	10.50	10.48	10.50	10.48	10.75	10.65	10.69	10.64
α_{rich} [mol_{CO_2}/$kg_{solvent}$]	2.36	2.35	2.27	2.20	2.00	2.08	1.95	1.71	-	2.34	2.27	2.02
α_{lean} [mol_{CO_2}/$kg_{solvent}$]	0.26	0.34	0.53	0.45	0.66	0.77	0.82	0.84	-	0.44	0.53	0.54
QIR 1.2 [$vol\%_{CO_2}$ (dry)]	12.42	12.43	12.43	12.35	12.40	12.20	12.30	11.90	12.90	12.99	12.43	12.10
QIR 2.1 [$vol\%_{CO_2}$ (dry)]	1.44	1.28	1.44	1.41	1.43	1.42	1.36	1.27	1.82	1.57	1.44	1.24
FIRC 1.1 [m³/h]	100.02	100.01	100.02	100.02	100.02	99.97	99.97	99.99	**50.04**	**69.96**	**100.02**	**110.00**
FIR 2.1 [m³/h]	93.13	92.99	93.38	93.56	93.28	94.41	94.04	94.92	52.50	66.22	93.38	103.44
FIR 3.1 [m³/h]	6.20	6.25	6.19	6.40	6.34	6.33	6.33	6.21	3.27	4.39	6.19	6.78
FIR 2.2 [l/h]	149.58	169.79	189.74	213.37	255.56	298.94	340.85	428.40	94.96	132.54	189.74	209.16
FIRC 3.2 [l/h]	151.90	173.55	194.96	216.52	259.64	302.65	345.83	431.68	98.15	136.79	194.96	214.35
PIRC 2.1 [mbar]	34.02	34.98	35.80	37.23	39.79	42.25	45.02	52.02	14.36	21.25	35.80	44.01
PIRC 2.2 [mbar]	28.62	29.59	30.41	31.84	34.40	36.85	39.63	46.63	8.97	15.85	30.41	38.61
PIR 2.3 [mbar]	12.24	12.11	12.03	12.20	12.08	12.08	11.84	11.91	3.40	6.03	12.03	14.79
PIR 2.4 [mbar]	7.91	7.83	7.81	7.97	7.96	8.05	7.88	8.11	2.38	4.24	7.81	9.54
PIR 3.1 [bar_{rel}]	1.01	1.00	1.01	1.00	1.01	1.02	1.02	1.02	1.01	1.03	1.01	1.02
PIR 3.2 [bar_{rel}]	0.97	0.97	0.97	0.97	0.97	0.97	0.97	0.97	0.96	0.96	0.97	0.98
PIRC 3.3 [bar_{rel}]	1.00	1.00	1.00	1.00	1.00	1.00	1.00	1.00	1.00	1.00	1.00	1.00
LIR 3.1 [cm]	44.20	43.90	43.57	46.89	46.37	44.08	41.44	35.09	46.97	45.21	43.57	40.91
TIRC 1.1 [°C]	41.22	41.30	41.36	41.33	41.62	41.55	41.47	41.66	41.51	41.42	41.36	41.29
TIRC 1.2 [°C]	40.01	40.05	40.19	40.04	40.27	39.85	39.92	40.08	39.83	39.89	40.19	40.01
TIR 2.1 [°C]	43.53	43.94	44.48	45.00	47.34	49.33	51.52	54.48	43.06	43.36	44.48	44.75
TIR 2.2 [°C]	45.86	47.53	49.22	51.06	55.96	59.68	62.68	66.83	45.72	47.07	49.22	50.11
TIR 2.3 [°C]	47.30	49.38	51.40	53.28	58.14	62.84	66.60	71.17	47.73	49.39	51.40	52.06
TIR 2.4 [°C]	49.77	52.41	54.89	56.89	62.18	66.64	70.33	74.06	50.15	52.40	54.89	55.61
TIR 2.5 [°C]	51.47	54.36	57.09	59.14	64.51	68.85	72.10	75.22	51.49	54.21	57.09	57.78
TIR 2.6 [°C]	52.98	56.10	58.79	61.12	66.48	70.41	73.40	75.84	53.10	55.91	58.79	59.82
TIR 2.7 [°C]	56.07	59.48	62.24	64.60	69.51	72.75	75.05	76.69	56.05	59.05	62.24	63.01
TIR 2.8 [°C]	58.47	61.77	64.36	66.58	70.99	73.91	75.59	76.86	58.10	61.32	64.36	65.34
TIR 2.9 [°C]	88.84	-	20.23	68.72	72.55	74.70	50.85	77.13	60.88	64.14	20.23	-
TIR 2.10 [°C]	64.59	67.46	69.26	70.85	73.58	74.95	75.97	76.64	64.33	67.06	69.26	69.85
TIR 2.11 [°C]	67.87	70.21	71.56	72.68	74.71	75.62	76.43	76.94	67.48	69.70	71.56	71.98
TIR 2.12 [°C]	70.99	72.44	73.17	73.80	75.08	75.58	76.08	76.11	70.77	72.24	73.17	73.26
TIR 2.12.1 [°C]	66.20	65.25	64.70	64.09	63.79	61.17	59.54	54.86	63.44	65.45	64.70	64.97
TIR 2.13 [°C]	41.89	41.99	42.28	42.48	41.97	42.48	41.96	42.16	41.99	41.97	42.28	41.44
TIR 2.14 [°C]	43.43	44.02	44.75	45.17	47.15	48.65	50.55	53.62	43.04	43.48	44.75	44.84
TIR 2.15 [°C]	104.19	104.63	105.08	105.44	107.12	109.27	111.79	112.42	101.80	103.13	105.08	105.62
TIR 2.16 [°C]	101.06	101.48	101.97	102.19	103.84	105.60	107.69	111.47	98.75	100.17	101.97	102.53
TIR 3.1 [°C]	124.50	123.69	122.54	121.81	120.53	119.89	119.91	119.62	122.36	122.53	122.54	122.82
TIR 3.2 [°C]	97.07	93.09	93.54	95.00	96.30	97.63	99.27	102.44	88.27	92.08	93.54	94.21
TIR 3.3 [°C]	21.01	19.21	21.38	21.62	12.79	20.84	21.29	21.70	15.70	16.27	21.38	12.35
TIR 3.4 [°C]	124.08	123.25	122.13	121.39	120.21	119.74	119.63	119.43	121.84	122.10	122.13	122.39
TIR 3.5 [°C]	49.28	49.92	50.74	51.10	53.00	54.67	56.63	59.67	47.96	48.79	50.74	50.75
TIR 3.6 [°C]	40.01	40.07	40.01	40.03	40.00	40.04	39.99	40.03	40.04	39.99	40.01	39.85
ϑ_{out} [°C]	11.48	12.72	15.48	24.03	23.95	21.95	19.35	17.67	13.89	9.48	15.48	14.82
h_{abs} [m]	12.00	12.00	12.00	12.00	12.00	12.00	12.00	12.00	12.00	12.00	12.00	12.00
NH_3 conc. [ppm]	-0.29	-0.29	-0.25	-0.24	-0.21	-0.25	-0.25	-0.26	-0.29	-0.26	-0.25	-0.29
P_{des} [kW]	17.10	16.50	16.35	16.80	17.40	18.36	19.50	20.85	9.60	12.30	16.35	17.97
Δp_{abs} [mbar]	16.39	17.48	18.39	19.63	22.33	24.77	27.78	34.73	5.57	9.82	18.39	23.82
Δp_{des} [mbar]	35.36	32.39	35.02	31.23	39.79	44.14	52.96	56.56	54.32	66.74	35.02	45.43
L/G-ratio [l/m³]	**1.75**	**2.00**	**2.25**	**2.50**	**3.00**	**3.50**	**4.00**	**5.00**	2.25	2.25	2.25	2.25
η_{sep} [%]	89.73	90.89	89.76	89.91	89.81	89.70	90.24	90.52	85.57	88.98	89.76	90.90
q_{reb} [GJ/t_{CO_2}]	3.34	3.18	3.19	3.27	3.37	3.60	3.76	4.12	3.79	3.29	3.19	3.15

	Variation of the desorber pressure (Section 6.5)							Variation in absorber heights (Section 6.7)		
	24.09.15	24.09.15	24.09.15	23.09.15	23.09.15	23.09.15	23.09.15	01.10.15	01.10.15	01.10.15
	15:03	13:43	12:21	11:22	20:37	21:52	22:58	09:57	12:23	14:53
	00:30	00:30	00:30	00:30	00:30	00:30	00:10	00:15	00:25	00:20
	15:32	14:12	12:50	11:51	21:06	22:21	23:07	10:11	12:47	15:12
$conc_{lean}$ [wt%]	-	-	-	-	-	-	-	-	-	-
$conc_{rich}$ [wt%]	-	-	-	-	-	-	-	-	-	-
QIR-pH 1.1 [-]	14.88	14.88	14.82	14.88	14.82	14.76	14.74	14.78	14.88	14.88
QIR-pH 2.1 [-]	8.74	8.73	8.73	8.77	8.76	8.74	8.74	8.76	8.84	9.04
QIR-pH 3.1 [-]	10.65	10.65	10.65	10.69	10.73	10.67	10.66	10.70	10.80	11.02
α_{rich} [$mol_{CO_2}/kg_{solvent}$]	2.27	2.29	2.30	2.27	2.30	2.29	2.27	2.38	2.27	2.08
α_{lean} [$mol_{CO_2}/kg_{solvent}$]	0.58	0.59	0.52	0.53	0.54	0.53	0.56	0.39	0.32	0.22
QIR 1.2 [$vol\%_{CO_2}$ (dry)]	12.40	12.35	12.36	12.43	12.28	12.28	12.33	13.06	12.97	12.68
QIR 2.1 [$vol\%_{CO_2}$ (dry)]	1.41	1.48	1.41	1.44	1.36	1.38	1.39	1.60	1.34	1.43
FIRC 1.1 [m³/h]	99.99	99.98	100.03	100.02	100.02	99.99	99.95	99.97	100.00	100.03
FIR 2.1 [m³/h]	93.43	93.60	93.40	93.38	92.63	92.60	92.64	93.28	92.78	92.98
FIR 3.1 [m³/h]	6.22	6.16	6.17	6.19	6.11	6.15	6.18	6.30	6.34	6.14
FIR 2.2 [l/h]	186.71	188.29	190.06	189.74	194.69	194.45	194.30	187.88	188.41	188.55
FIRC 3.2 [l/h]	194.97	194.99	194.97	194.96	194.97	194.95	194.97	195.11	194.93	194.94
PIRC 2.1 [mbar]	36.33	36.50	36.52	35.80	36.12	36.49	36.68	38.27	36.20	33.49
PIRC 2.2 [mbar]	30.94	31.10	31.12	30.41	30.72	31.09	31.29	32.89	30.81	28.10
PIR 2.3 [mbar]	12.31	12.35	12.31	12.03	12.17	12.19	12.20	12.54	13.42	12.51
PIR 2.4 [mbar]	7.98	8.01	7.98	7.81	7.89	7.90	7.90	8.13	7.92	7.93
PIR 3.1 [bar_{rel}]	0.45	0.63	0.83	1.01	1.21	1.40	1.60	1.04	1.04	1.03
PIR 3.2 [bar_{rel}]	0.39	0.58	0.78	0.97	1.17	1.37	1.56	0.98	0.97	0.97
PIRC 3.3 [bar_{rel}]	**0.40**	**0.60**	**0.80**	**1.00**	**1.20**	**1.40**	**1.60**	1.00	1.00	1.00
LIR 3.1 [cm]	41.93	41.96	41.91	43.57	42.03	42.06	42.48	43.93	46.66	48.91
TIRC 1.1 [°C]	41.28	41.26	41.56	41.36	41.26	41.24	41.37	41.53	41.36	41.03
TIRC 1.2 [°C]	40.06	40.03	40.18	40.19	39.95	40.00	40.03	39.99	40.14	39.89
TIR 2.1 [°C]	44.48	44.45	44.52	44.48	44.42	44.41	44.41	44.07	45.09	46.35
TIR 2.2 [°C]	49.37	49.34	49.60	49.22	49.59	49.43	49.20	48.72	51.74	55.65
TIR 2.3 [°C]	51.47	51.52	51.58	51.40	51.72	51.60	51.44	50.87	54.64	59.54
TIR 2.4 [°C]	54.99	54.93	55.02	54.89	55.14	55.06	54.89	54.13	59.09	65.25
TIR 2.5 [°C]	57.15	57.06	57.19	57.09	57.38	57.27	57.16	56.20	62.05	68.81
TIR 2.6 [°C]	58.98	58.85	58.95	58.79	59.16	59.13	59.11	57.97	64.54	72.22
TIR 2.7 [°C]	62.40	62.22	62.31	62.24	62.60	62.49	62.38	61.43	68.96	65.52
TIR 2.8 [°C]	64.56	64.41	64.51	64.36	64.74	64.58	64.49	63.59	71.39	64.11
TIR 2.9 [°C]	-	-	-	20.23	-	-	-	66.31	73.72	64.05
TIR 2.10 [°C]	69.33	69.14	69.32	69.26	69.46	69.36	69.38	69.04	64.22	63.60
TIR 2.11 [°C]	71.55	71.38	71.52	71.56	71.62	71.61	71.58	71.46	64.73	63.79
TIR 2.12 [°C]	73.17	73.07	73.10	73.17	73.15	73.16	73.09	73.33	64.41	63.72
TIR 2.12.1 [°C]	65.56	65.32	65.43	64.70	65.43	65.00	65.20	66.03	63.84	63.16
TIR 2.13 [°C]	42.00	42.03	41.95	42.28	41.05	40.96	40.98	42.10	41.97	41.99
TIR 2.14 [°C]	44.72	44.69	44.73	44.75	44.66	44.62	44.68	44.16	45.35	46.64
TIR 2.15 [°C]	98.80	100.97	103.07	105.08	106.89	108.45	110.00	104.85	106.91	110.40
TIR 2.16 [°C]	94.88	97.42	99.82	101.97	103.94	105.73	107.42	101.82	103.89	107.30
TIR 3.1 [°C]	113.05	116.46	119.66	122.54	125.17	127.57	129.84	123.09	123.90	124.82
TIR 3.2 [°C]	87.23	89.44	91.72	93.54	95.61	96.88	98.26	94.50	95.79	101.38
TIR 3.3 [°C]	20.09	19.84	19.73	21.38	20.05	19.97	20.07	14.17	15.17	14.21
TIR 3.4 [°C]	112.73	116.08	119.31	122.13	124.75	127.25	129.48	122.65	123.58	124.40
TIR 3.5 [°C]	49.86	50.00	50.25	50.74	50.55	50.71	50.86	49.92	51.29	52.96
TIR 3.6 [°C]	39.98	40.05	40.05	40.01	40.02	40.09	40.03	40.00	39.93	39.97
ϑ_{out} [°C]	14.88	15.33	15.24	15.48	11.65	11.22	11.23	12.03	16.23	17.28
h_{abs} [m]	12.00	12.00	12.00	12.00	12.00	12.00	12.00	**12.00**	**9.00**	**6.00**
NH_3 conc. [ppm]	-0.30	-0.28	-0.26	-0.25	-0.30	-0.32	-0.36	-0.17	-0.22	-0.24
P_{des} [kW]	16.65	16.35	16.35	16.35	16.35	16.35	16.35	16.80	17.55	19.50
Δp_{abs} [mbar]	18.63	18.75	18.81	18.39	18.55	18.91	19.08	20.35	17.39	15.59
Δp_{des} [mbar]	60.20	54.61	53.50	35.02	42.62	38.01	36.12	66.19	62.42	58.98
L/G-ratio [l/m³]	2.25	2.25	2.25	2.25	2.25	2.25	2.25	2.25	2.25	2.25
η_{sep} [%]	89.93	89.35	89.88	89.76	90.15	90.04	89.98	89.18	90.88	89.99
q_{reb} [GJ/t_{CO_2}]	3.20	3.17	3.15	3.19	3.21	3.21	3.20	3.05	3.16	3.63

B.5 - 15 wt% NaGly

	Variation of the L/G-ratio (Section 6.3)	
	03.12.13	03.12.13
	16:10	13:45
	00:30	00:30
	16:39	14:14
$conc_{lean}$ [wt%]	18:14	16:19
$conc_{rich}$ [wt%]	15.35	15.59
QIR-pH 1.1 [-]	8.19	8.21
QIR-pH 2.1 [-]	8.50	8.51
QIR-pH 3.1 [-]	10.32	10.24
α_{rich} [$mol_{CO_2}/mol_{equ.\ amine}$]	0.49	0.47
α_{lean} [$mol_{CO_2}/mol_{equ.\ amine}$]	0.14	0.16
QIR 1.2 [$vol\%_{CO_2}$ (dry)]	12.80	12.88
QIR 2.1 [$vol\%_{CO_2}$ (dry)]	1.21	1.29
FIRC 1.1 [m³/h]	49.99	49.95
FIR 2.1 [m³/h]	51.32	51.49
FIR 3.1 [m³/h]	3.32	3.37
FIR 2.2 [l/h]	426.51	463.13
FIRC 3.2 [l/h]	431.99	466.38
PIRC 2.1 [mbar]	30.06	38.66
PIRC 2.2 [mbar]	8.47	8.45
PIR 2.3 [mbar]	3.26	3.29
PIR 2.4 [mbar]	2.35	2.38
PIR 3.1 [bar_{rel}]	1.02	1.01
PIR 3.2 [bar_{rel}]	0.95	0.95
PIRC 3.3 [bar_{rel}]	1.00	1.00
LIR 3.1 [cm]	33.88	36.76
TIRC 1.1 [°C]	42.14	42.14
TIRC 1.2 [°C]	39.85	39.93
TIR 2.1 [°C]	49.23	48.62
TIR 2.2 [°C]	55.48	53.87
TIR 2.3 [°C]	56.43	54.32
TIR 2.4 [°C]	56.66	54.42
TIR 2.5 [°C]	56.54	54.28
TIR 2.6 [°C]	56.38	54.10
TIR 2.7 [°C]	56.33	54.15
TIR 2.8 [°C]	55.92	53.72
TIR 2.9 [°C]	54.85	52.79
TIR 2.10 [°C]	51.28	49.61
TIR 2.11 [°C]	46.62	45.61
TIR 2.12 [°C]	42.68	42.55
TIR 2.12.1 [°C]	39.78	39.97
TIR 2.13 [°C]	38.91	39.27
TIR 2.14 [°C]	49.88	49.27
TIR 2.15 [°C]	115.90	115.66
TIR 2.16 [°C]	112.99	113.07
TIR 3.1 [°C]	122.90	122.60
TIR 3.2 [°C]	113.12	110.68
TIR 3.3 [°C]	11.75	11.42
TIR 3.4 [°C]	122.76	122.51
TIR 3.5 [°C]	55.10	54.59
TIR 3.6 [°C]	40.00	40.01
ϑ_{out} [°C]	4.83	6.22
h_{abs} [m]	12.00	12.00
NH_3 conc. [ppm]	-	-
P_{des} [kW]	21.60	18.30
Δp_{abs} [mbar]	5.22	5.16
Δp_{des} [mbar]	74.14	67.25
L/G-ratio [l/m³]	**10.00**	**10.81**
η_{sep} [%]	90.33	89.68
q_{reb} [GJ/t_{CO_2}]	8.62	7.33

B.6 - 25 wt% NaGly

	Variation of the L/G-ratio (Section 6.3)					Variation of the flue gas flow rate (Section 6.4)			Variation of the desorber pressure (Section 6.5)			
	28.11.13	28.11.13	27.11.13	27.11.13	27.11.13	29.11.13	27.11.13	29.11.13	28.11.13	28.11.13	27.11.13	28.11.13
	13:00	14:01	15:54	18:48	21:11	11:12	18:48	13:04	20:25	18:02	18:48	16:25
	00:30	00:30	00:30	00:30	00:30	00:17	00:30	00:30	00:30	00:30	00:30	00:30
	13:29	14:30	16:23	19:17	21:40	11:28	19:17	13:33	20:54	18:31	19:17	16:54
$conc_{lean}$ [wt%]	26.06	26.18	25.81	25.69	25.69	-	25.69	24.82	25.81	25.44	25.69	25.69
$conc_{rich}$ [wt%]	26.06	25.44	25.57	25.51	25.32		-	25.51	25.07	25.57	25.32	25.51	25.44
QIR-pH 1.1 [-]	8.20	8.17	8.55	8.50	8.48	6.53	8.50	8.49	7.94	8.04	8.50	8.09
QIR-pH 2.1 [-]	8.54	8.55	8.62	8.61	8.63	8.53	8.61	8.57	8.60	8.57	8.61	8.57
QIR-pH 3.1 [-]	10.51	10.49	10.13	10.06	9.84	10.25	10.06	10.07	10.11	10.11	10.06	10.12
α_{rich} [$mol_{CO_2}/mol_{equ.\ amine}$]	0.50	0.50	0.47	0.49	0.48	-	0.49	0.47	0.47	0.48	0.49	0.49
α_{lean} [$mol_{CO_2}/mol_{equ.\ amine}$]	0.16	0.13	0.21	0.22	0.28	-	0.22	0.24	0.23	0.23	0.22	0.22
QIR 1.2 [$vol\%_{CO_2}$ (dry)]	13.09	13.13	12.99	13.20	12.95	13.02	13.20	12.79	13.11	13.09	13.20	13.13
QIR 2.1 [$vol\%_{CO_2}$ (dry)]	1.99	1.32	1.35	1.30	1.17	2.47	1.30	1.29	1.27	1.37	1.30	1.29
FIRC 1.1 [m³/h]	49.95	50.00	50.02	50.04	50.06	**30.05**	50.04	**65.02**	50.03	50.03	50.04	50.00
FIR 2.1 [m³/h]	41.83	50.60	53.61	50.88	49.97	18.22	50.88	62.17	43.07	49.01	50.88	49.00
FIR 3.1 [m³/h]	3.14	3.30	4.28	5.00	3.32	2.16	5.00	3.95	3.32	3.27	5.00	3.29
FIR 2.2 [l/h]	222.16	241.35	303.56	348.71	451.22	209.64	348.71	452.70	351.29	348.73	348.71	351.01
FIRC 3.2 [l/h]	216.53	238.08	302.66	345.81	446.88	207.90	345.81	449.10	345.69	345.88	345.81	345.73
PIRC 2.1 [mbar]	41.43	42.12	45.30	45.33	40.91	38.51	45.33	46.00	32.95	42.86	45.33	42.81
PIRC 2.2 [mbar]	8.47	9.15	9.99	10.02	7.95	5.54	10.02	13.04	9.41	9.90	10.02	9.85
PIR 2.3 [mbar]	2.90	3.30	3.57	3.24	3.12	2.06	3.24	4.97	2.67	3.22	3.24	3.20
PIR 2.4 [mbar]	2.22	2.40	2.54	2.36	2.30	1.38	2.36	3.60	2.06	2.32	2.36	2.31
PIR 3.1 [bar_{rel}]	1.03	1.04	0.99	1.02	0.99	1.00	1.02	1.01	0.43	0.62	1.02	1.39
PIR 3.2 [bar_{rel}]	0.95	0.95	0.94	0.96	0.94	0.93	0.96	0.94	0.35	0.54	0.96	1.33
PIRC 3.3 [bar_{rel}]	1.00	1.00	1.00	1.00	1.00	1.00	1.00	1.00	**0.40**	**0.60**	**1.00**	**1.40**
LIR 3.1 [cm]	40.22	41.62	42.29	41.35	37.02	40.19	41.35	34.25	37.30	39.58	41.35	40.69
TIRC 1.1 [°C]	42.81	42.84	42.49	41.74	42.67	41.08	41.74	42.01	42.33	42.45	41.74	42.97
TIRC 1.2 [°C]	40.20	40.00	39.94	39.82	40.09	39.79	39.82	40.61	40.22	40.22	39.82	40.09
TIR 2.1 [°C]	46.04	46.85	49.69	51.32	49.87	47.74	51.32	51.70	51.34	51.22	51.32	51.30
TIR 2.2 [°C]	51.80	53.44	58.14	60.67	55.12	54.87	60.67	60.77	60.54	60.27	60.67	60.38
TIR 2.3 [°C]	53.73	55.44	60.63	63.27	55.43	56.78	63.27	63.78	63.39	63.08	63.27	63.27
TIR 2.4 [°C]	56.09	58.07	63.53	66.37	55.34	59.08	66.37	66.20	66.61	66.29	66.37	66.46
TIR 2.5 [°C]	57.39	59.55	65.12	68.04	55.01	60.27	68.04	67.18	68.21	67.84	68.04	68.11
TIR 2.6 [°C]	58.83	61.04	66.65	69.53	54.56	61.36	69.53	67.44	69.82	69.43	69.53	69.61
TIR 2.7 [°C]	61.05	63.58	69.39	72.09	53.87	63.28	72.09	66.42	72.44	72.12	72.09	72.29
TIR 2.8 [°C]	62.86	65.74	71.23	73.90	52.07	64.90	73.90	61.96	74.07	73.68	73.90	73.97
TIR 2.9 [°C]	65.86	68.99	73.82	76.09	49.55	67.30	76.09	54.93	76.43	75.98	76.09	76.22
TIR 2.10 [°C]	70.05	73.20	76.56	78.30	46.20	70.48	78.30	48.83	78.46	78.19	78.30	78.34
TIR 2.11 [°C]	74.03	76.51	78.67	79.84	43.32	74.07	79.84	44.69	80.13	79.78	79.84	79.97
TIR 2.12 [°C]	76.71	78.25	78.84	76.96	41.70	76.17	76.96	42.18	76.57	76.52	76.96	76.95
TIR 2.12.1 [°C]	57.05	56.90	49.06	41.13	38.63	51.42	41.13	39.85	41.01	41.19	41.13	41.40
TIR 2.13 [°C]	20.46	41.98	46.06	39.88	36.50	47.52	39.88	42.01	11.28	37.59	39.88	38.24
TIR 2.14 [°C]	45.60	46.44	49.82	51.86	50.23	47.46	51.86	53.07	52.18	51.98	51.86	51.81
TIR 2.15 [°C]	114.18	114.82	116.10	116.71	115.47	114.01	116.71	116.68	107.65	110.98	116.71	120.79
TIR 2.16 [°C]	111.02	111.61	112.11	112.94	112.63	110.93	112.94	113.78	104.96	107.62	112.94	117.26
TIR 3.1 [°C]	125.55	125.49	124.23	124.30	122.74	124.23	124.30	123.76	114.12	117.71	124.30	129.49
TIR 3.2 [°C]	114.32	113.97	107.47	106.58	104.08	109.93	106.58	105.82	101.64	103.31	106.58	107.91
TIR 3.3 [°C]	11.73	11.49	11.24	54.27	10.15	10.39	54.27	10.41	10.47	10.61	54.27	10.34
TIR 3.4 [°C]	125.30	125.31	124.03	124.19	122.65	123.96	124.19	123.59	114.00	117.54	124.19	129.36
TIR 3.5 [°C]	50.33	51.54	54.89	56.73	55.47	52.54	56.73	58.16	56.31	56.50	56.73	57.16
TIR 3.6 [°C]	39.94	40.00	39.98	40.02	40.00	40.09	40.02	40.02	40.04	40.00	40.02	39.99
ϑ_{out} [°C]	1.24	0.98	2.27	1.27	0.20	3.70	1.27	4.93	1.26	1.40	1.27	1.69
h_{abs} [m]	12.00	12.00	12.00	12.00	12.00	12.00	12.00	12.00	12.00	12.00	12.00	12.00
NH_3 conc. [ppm]	-	-	-	-	-	-	-	-	-	-	-	-
P_{des} [kW]	30.00	29.40	15.90	15.00	14.70	13.50	15.00	17.40	18.90	17.40	15.00	14.70
Δp_{abs} [mbar]	5.57	5.86	6.43	6.78	4.83	3.48	6.78	8.08	6.74	6.68	6.78	6.65
Δp_{des} [mbar]	81.95	85.50	56.95	57.07	53.09	64.37	57.07	64.62	86.02	76.16	57.07	57.71
L/G-ratio [l/m³]	**5.01**	**5.50**	**7.00**	**8.00**	**10.34**	8.00	8.00	8.00	8.00	8.00	8.00	8.00
η_{sep} [%]	85.80	90.06	89.50	90.08	90.85	89.22	90.08	90.56	90.25	89.67	90.08	90.31
q_{reb} [GJ/t_{CO_2}]	11.72	10.87	5.96	5.49	5.46	8.50	5.49	5.07	7.00	6.49	5.49	5.43

	Variation of the regenerated solvent temperature (Section 6.8)		
	29.11.13	27.11.13	02.12.13
	15:11	18:48	15:47
	00:30	00:30	00:30
	15:40	19:17	16:16
$conc_{lean}$ [wt%]	24.20	25.69	24.95
$conc_{rich}$ [wt%]	24.08	25.51	25.57
QIR-pH 1.1 [-]	8.46	8.50	8.35
QIR-pH 2.1 [-]	8.80	8.61	8.57
QIR-pH 3.1 [-]	10.76	10.06	9.85
α_{rich} [mol_{CO_2}/$mol_{equ. amine}$]	0.48	0.49	0.46
α_{lean} [mol_{CO_2}/$mol_{equ. amine}$]	0.22	0.22	0.20
QIR 1.2 [vol%$_{CO_2}$ (dry)]	12.77	13.20	12.98
QIR 2.1 [vol%$_{CO_2}$ (dry)]	1.21	1.30	1.21
FIRC 1.1 [m³/h]	49.98	50.04	49.93
FIR 2.1 [m³/h]	49.84	50.88	44.84
FIR 3.1 [m³/h]	3.44	5.00	3.23
FIR 2.2 [l/h]	353.53	348.71	325.97
FIRC 3.2 [l/h]	345.77	345.81	345.80
PIRC 2.1 [mbar]	40.08	45.33	43.22
PIRC 2.2 [mbar]	7.13	10.02	10.27
PIR 2.3 [mbar]	3.14	3.24	2.79
PIR 2.4 [mbar]	2.25	2.36	2.15
PIR 3.1 [bar$_{rel}$]	1.01	1.02	1.00
PIR 3.2 [bar$_{rel}$]	0.94	0.96	0.94
PIRC 3.3 [bar$_{rel}$]	1.00	1.00	1.00
LIR 3.1 [cm]	36.52	41.35	37.02
TIRC 1.1 [°C]	41.39	41.74	43.46
TIRC 1.2 [°C]	39.64	39.82	40.64
TIR 2.1 [°C]	39.09	51.32	-32.43
TIR 2.2 [°C]	37.72	60.67	60.06
TIR 2.3 [°C]	37.61	63.27	62.77
TIR 2.4 [°C]	37.34	66.37	66.04
TIR 2.5 [°C]	36.86	68.04	67.63
TIR 2.6 [°C]	35.91	69.53	69.33
TIR 2.7 [°C]	34.06	72.09	72.05
TIR 2.8 [°C]	31.47	73.90	73.87
TIR 2.9 [°C]	28.90	76.09	76.28
TIR 2.10 [°C]	25.55	78.30	78.50
TIR 2.11 [°C]	23.13	79.84	80.30
TIR 2.12 [°C]	21.33	76.96	80.91
TIR 2.12.1 [°C]	20.26	41.13	68.98
TIR 2.13 [°C]	34.64	39.88	16.55
TIR 2.14 [°C]	38.12	51.86	51.69
TIR 2.15 [°C]	115.01	116.71	117.26
TIR 2.16 [°C]	112.11	112.94	113.34
TIR 3.1 [°C]	123.79	124.30	124.12
TIR 3.2 [°C]	107.54	106.58	108.15
TIR 3.3 [°C]	10.56	54.27	10.93
TIR 3.4 [°C]	123.66	124.19	123.95
TIR 3.5 [°C]	44.16	56.73	57.48
TIR 3.6 [°C]	**19.67**	**40.02**	**56.84**
ϑ_{out} [°C]	4.04	1.27	7.84
h_{abs} [m]	12.00	12.00	12.00
NH_3 conc. [ppm]	-	-	-
P_{des} [kW]	16.35	15.00	15.60
Δp_{abs} [mbar]	3.99	6.78	7.48
Δp_{des} [mbar]	64.75	57.07	61.11
L/G-ratio [l/m³]	8.00	8.00	8.01
η_{sep} [%]	90.29	90.08	90.50
q_{reb} [GJ/t$_{CO_2}$]	6.24	5.49	5.81

B.7 - 40 wt% NaGly

	Variation of the L/G-ratio (Section 6.3)				Variation in absorber heights (Section 6.7)	
	04.12.13	04.12.13	04.12.13	04.12.13	04.12.13	04.12.13
	17:22	13:42	09:14	11:22	19:03	20:50
	00:30	00:30	00:30	00:30	00:30	00:30
	17:51	14:11	09:43	11:51	19:32	21:19
$conc_{lean}$ [wt%]	40.43	40.22	40.33	40.02	40.33	39.71
$conc_{rich}$ [wt%]	39.60	38.97	39.08	39.39	39.18	39.08
QIR-pH 1.1 [-]	6.90	7.37	7.69	7.55	6.54	4.96
QIR-pH 2.1 [-]	8.90	8.88	8.89	8.94	8.89	9.08
QIR-pH 3.1 [-]	10.71	10.57	10.50	10.39	10.49	10.58
α_{rich} [$mol_{CO_2}/mol_{equ. amine}$]	0.48	0.46	0.46	0.46	0.47	0.44
α_{lean} [$mol_{CO_2}/mol_{equ. amine}$]	0.28	0.29	0.36	0.33	0.30	0.30
QIR 1.2 [$vol\%_{CO_2}$ (dry)]	12.91	12.78	13.02	12.82	12.97	12.94
QIR 2.1 [$vol\%_{CO_2}$ (dry)]	1.27	1.27	1.32	1.12	1.30	1.24
FIRC 1.1 [m³/h]	50.02	49.95	50.03	50.02	50.05	50.00
FIR 2.1 [m³/h]	48.97	52.80	49.27	53.02	49.59	51.89
FIR 3.1 [m³/h]	3.33	3.28	3.29	3.28	3.26	3.28
FIR 2.2 [l/h]	253.30	299.74	344.96	408.67	344.99	346.29
FIRC 3.2 [l/h]	259.58	302.73	345.82	409.12	345.78	345.80
PIRC 2.1 [mbar]	21.39	22.01	19.60	19.81	19.75	19.00
PIRC 2.2 [mbar]	9.62	10.25	7.83	8.04	7.97	7.23
PIR 2.3 [mbar]	3.08	3.40	3.18	3.37	3.20	3.32
PIR 2.4 [mbar]	2.25	2.41	2.27	2.38	2.30	2.33
PIR 3.1 [bar_{rel}]	1.00	1.00	0.99	0.99	1.00	1.01
PIR 3.2 [bar_{rel}]	0.94	0.94	0.95	0.95	0.94	0.95
PIRC 3.3 [bar_{rel}]	1.00	1.00	1.00	1.00	1.00	1.01
LIR 3.1 [cm]	37.23	40.95	33.77	33.43	33.74	39.61
TIRC 1.1 [°C]	42.25	42.08	42.55	42.13	42.72	42.54
TIRC 1.2 [°C]	40.00	40.04	40.34	40.03	40.20	40.34
TIR 2.1 [°C]	50.97	52.69	53.38	51.81	53.74	54.16
TIR 2.2 [°C]	60.51	63.32	62.45	57.21	63.22	63.70
TIR 2.3 [°C]	63.13	66.31	63.87	56.60	64.88	63.26
TIR 2.4 [°C]	67.24	70.25	63.08	54.53	64.61	55.55
TIR 2.5 [°C]	69.49	72.46	60.34	52.43	61.54	50.82
TIR 2.6 [°C]	71.63	74.34	56.57	50.53	57.17	47.35
TIR 2.7 [°C]	74.93	77.14	52.57	48.23	52.78	43.98
TIR 2.8 [°C]	76.87	78.70	48.90	45.76	48.95	42.28
TIR 2.9 [°C]	79.05	80.41	46.60	44.52	46.72	41.56
TIR 2.10 [°C]	80.48	81.39	43.99	42.62	43.87	39.97
TIR 2.11 [°C]	81.83	82.19	42.19	41.59	42.31	40.20
TIR 2.12 [°C]	80.29	75.48	40.92	40.56	40.97	39.75
TIR 2.12.1 [°C]	48.80	42.38	35.80	39.24	38.56	37.47
TIR 2.13 [°C]	32.19	43.18	37.46	42.95	38.48	41.70
TIR 2.14 [°C]	51.88	53.85	54.40	52.42	54.87	55.02
TIR 2.15 [°C]	119.74	119.16	119.26	118.41	119.19	119.61
TIR 2.16 [°C]	115.78	116.19	117.17	117.18	116.99	118.76
TIR 3.1 [°C]	128.18	127.18	127.28	126.34	127.00	127.59
TIR 3.2 [°C]	108.32	105.51	105.29	105.16	103.83	108.10
TIR 3.3 [°C]	11.84	11.15	6.96	-5.17	10.54	10.65
TIR 3.4 [°C]	127.90	127.05	127.13	126.26	126.88	127.37
TIR 3.5 [°C]	57.24	58.89	59.52	57.90	60.03	60.19
TIR 3.6 [°C]	40.00	40.00	39.99	40.00	39.98	40.05
ϑ_{out} [°C]	1.26	4.40	0.63	3.72	2.73	3.41
h_{abs} [m]	12.00	12.00	12.00	12.00	**12.00**	**9.00**
NH_3 conc. [ppm]	-	-	-	-	-	-
P_{des} [kW]	17.40	15.00	15.00	15.31	15.00	18.00
Δp_{abs} [mbar]	6.54	6.85	4.65	4.67	4.77	3.90
Δp_{des} [mbar]	56.70	50.62	48.20	48.88	51.93	57.24
L/G-ratio [l/m³]	**6.00**	**7.01**	**7.99**	**9.47**	8.00	8.01
η_{sep} [%]	89.96	89.82	89.85	91.00	90.05	90.22
q_{reb} [GJ/t_{CO_2}]	6.57	5.73	5.65	5.77	5.65	6.81

187

B.8 - 40 wt% KGly

			Variation of the L/G-ratio (Section 6.3)			
	26.11.14	26.11.14	27.11.14	26.11.14	27.11.14	27.11.14
	14:39	17:34	10:44	21:50	13:02	15:05
	00:30	00:30	00:30	00:30	00:30	00:30
	15:08	18:03	11:13	22:19	13:31	15:34
$conc_{lean}$ [wt%]	41.35	41.23	39.51	40.50	39.02	39.76
$conc_{rich}$ [wt%]	41.59	41.23	38.77	39.89	38.64	38.27
QIR-pH 1.1 [-]	7.60	7.25	8.49	4.92	8.41	8.34
QIR-pH 2.1 [-]	8.76	8.78	8.78	8.81	8.75	8.76
QIR-pH 3.1 [-]	10.88	10.74	10.64	10.66	10.48	10.41
α_{rich} [mol_{CO_2}/$mol_{equ. amine}$]	0.44	0.45	0.46	0.45	0.43	0.42
α_{lean} [mol_{CO_2}/$mol_{equ. amine}$]	0.22	0.24	0.26	0.26	0.28	0.28
QIR 1.2 [$vol\%_{CO_2}$ (dry)]	13.18	13.09	12.92	12.76	12.77	12.85
QIR 2.1 [$vol\%_{CO_2}$ (dry)]	1.28	1.29	1.34	1.15	1.41	1.21
FIRC 1.1 [m³/h]	49.98	49.99	50.01	50.01	50.02	50.06
FIR 2.1 [m³/h]	51.35	51.02	48.31	49.36	47.99	47.99
FIR 3.1 [m³/h]	3.43	3.41	4.00	3.55	3.93	4.15
FIR 2.2 [l/h]	262.11	306.53	349.34	350.80	393.31	436.13
FIRC 3.2 [l/h]	259.65	302.71	345.74	345.79	388.85	431.62
PIRC 2.1 [mbar]	20.15	20.47	15.14	15.26	13.72	13.60
PIRC 2.2 [mbar]	9.36	9.68	9.74	9.87	8.33	8.21
PIR 2.3 [mbar]	3.25	3.17	3.07	3.14	3.02	3.02
PIR 2.4 [mbar]	2.29	2.26	2.20	2.23	2.17	2.18
PIR 3.1 [bar_{rel}]	0.93	0.94	0.91	0.94	0.91	0.91
PIR 3.2 [bar_{rel}]	0.95	0.95	0.94	0.95	0.95	0.95
PIRC 3.3 [bar_{rel}]	1.00	1.00	1.00	1.00	1.00	1.00
LIR 3.1 [cm]	28.54	27.99	33.23	30.55	34.08	35.28
TIRC 1.1 [°C]	41.98	42.63	41.92	42.52	41.83	42.54
TIRC 1.2 [°C]	39.47	39.90	39.93	39.88	39.82	40.11
TIR 2.1 [°C]	48.99	51.11	52.38	52.59	51.96	51.47
TIR 2.2 [°C]	56.64	60.06	61.87	62.56	59.94	57.22
TIR 2.3 [°C]	58.89	62.20	64.49	64.92	61.08	57.65
TIR 2.4 [°C]	62.29	65.57	67.95	68.39	61.75	57.57
TIR 2.5 [°C]	64.05	67.46	69.69	70.28	61.40	57.09
TIR 2.6 [°C]	65.90	69.34	71.47	72.07	60.67	56.62
TIR 2.7 [°C]	68.67	72.09	73.93	74.65	59.90	56.23
TIR 2.8 [°C]	70.67	74.04	75.56	76.29	58.55	54.98
TIR 2.9 [°C]	73.80	76.69	77.72	78.62	55.83	52.57
TIR 2.10 [°C]	77.25	79.24	79.80	80.40	51.19	48.33
TIR 2.11 [°C]	80.18	81.30	81.21	81.68	46.64	45.18
TIR 2.12 [°C]	80.97	79.46	73.85	72.01	43.08	42.52
TIR 2.12.1 [°C]	54.79	49.71	40.61	40.01	36.87	36.79
TIR 2.13 [°C]	40.05	39.96	35.42	36.07	32.23	32.80
TIR 2.14 [°C]	49.77	52.01	53.53	53.84	52.95	51.90
TIR 2.15 [°C]	118.23	119.26	119.31	119.82	118.58	118.08
TIR 2.16 [°C]	114.73	115.41	115.62	115.94	115.00	114.95
TIR 3.1 [°C]	129.00	128.44	127.25	127.79	126.15	125.43
TIR 3.2 [°C]	108.68	104.09	102.70	103.45	101.03	101.48
TIR 3.3 [°C]	4.82	-4.32	13.18	8.69	9.07	9.08
TIR 3.4 [°C]	128.66	128.17	127.12	127.50	125.97	125.30
TIR 3.5 [°C]	54.48	56.69	58.09	58.40	57.59	56.80
TIR 3.6 [°C]	39.93	40.02	40.02	40.03	39.96	39.94
ϑ_{out} [°C]	6.26	5.38	4.81	4.97	5.26	4.54
h_{abs} [m]	12.00	12.00	12.00	12.00	12.00	12.00
NH_3 conc. [ppm]	95.40	122.53	191.47	248.95	182.85	233.47
P_{des} [kW]	17.70	15.30	15.00	14.70	14.10	14.70
Δp_{abs} [mbar]	6.11	6.51	6.67	6.73	5.30	5.19
Δp_{des} [mbar]	-21.96	-11.96	-29.12	-9.19	-35.87	-39.52
L/G-ratio [l/m³]	**6.00**	**7.00**	**8.00**	**8.00**	**9.00**	**9.98**
η_{sep} [%]	90.17	90.06	89.76	90.96	88.95	90.56
q_{reb} [GJ/t_{CO_2}]	6.85	5.99	5.74	5.60	5.51	5.62

Appendix C

List of publications

International peer-reviewed journals

- Rabensteiner, M., Kinger, G., Koller, M., Gronald, G., Hochenauer, C., 2014. Pilot plant study of ethylenediamine as a solvent for post combustion carbon dioxide capture and comparison to monoethanolamine. Int. J. Greenhouse Gas Control 27, 1-14.

- Rabensteiner, M., Kinger, G., Koller, M., Gronald, G., Hochenauer, C., 2015. Investigation of carbon dioxide capture with aqueous piperazine on a post combustion pilot plant – Part I: Energetic review of the process. Int. J. Greenhouse Gas Control 39, 79-90.

- Rabensteiner, M., Kinger, G., Koller, M., Gronald, G., Hochenauer, C., 2015. Investigation of carbon dioxide capture with aqueous piperazine on a post combustion pilot plant – Part II: Parameter study and emission measurement. Int. J. Greenhouse Gas Control 37, 471-480.

- Rabensteiner, M., Kinger, G., Koller, M., Gronald, G., Unterberger, S., Hochenauer, C., 2014. Investigation of the suitability of aqueous sodium glycinate as a solvent for post combustion carbon dioxide capture on the basis of pilot plant studies and screening methods. Int. J. Greenhouse Gas Control 29, 1-15.

- Rabensteiner, M., Kinger, G., Koller, M., Hochenauer, C., 2014. Pilot plant studies of the CO_2 post-combustion process at the Dürnrohr power plant. VGB PowerTech 10, 61-66.

- Rabensteiner, M., Kinger, G., Koller, M., Hochenauer, C., 2015. CO_2 post combustion pilot plant tests at the Dürnrohr power plant with amino acids. VGB PowerTech 11, 47-53.

- Rabensteiner, M., Kinger, G., Koller, M., Hochenauer, C., 2015. PCC pilot plant studies with aqueous potassium glycinate. Int. J. Greenhouse Gas Control 42, 562-570.

- Rabensteiner, M., Kinger, G., Koller, M., Hochenauer, C., 2016. New insights in CO_2 post-combustion in Dürnrohr – An important step towards full-scale plants. VGB PowerTech 1-2, 61-66.

International conferences

- Rabensteiner, M., Kinger, G., Koller, M., Hochenauer, C., 2015. PCC-pilot plant tests with aqueous piperazine. Proceedings of 8th Trondheim Conference on CO_2 Capture, Transport and Storage, Trondheim, Norway, 17 – 18 June 2015.

- Rabensteiner, M., Kinger, G., Koller, M., Hochenauer, C., 2014. Three years of working experience with different solvents at a realistic post combustion capture pilot plant. International Conference on Greenhouse Gas Technologies, Austin, USA, 5 – 9 October 2014, Energy Procedia 63, 1578-1584.

- Rabensteiner, M., Kinger, G., Koller, M., 2013. Pilot plant for CO_2 capture at the power plant Dürnrohr – More than two years of working experience. Fachtagung Gasreinigung, Graz, Austria, 12 – 13 September 2013, Book of Abstracts, 24-25.

- Rabensteiner, M., Koller, M., 2013. Aufbau und Betrieb der CO_2-Abscheideanlage "CO_2SEPPL" am KW Dürnrohr. 9th Minisymposium for Chemical Engineering, Leoben, Austria, 17 – 18 April 2013, Book of Abstracts, 43-47.

Appendix D

Curriculum vitae

Markus Rabensteiner

CV – January 26, 2016

Sandgasse 43/3
A – 8010 Graz
☎ +43 (0)650 8108232
✉ markus-rabensteiner@gmx.at

Personal Information

Date and place of birth	January 25, 1987, Wolfsberg
Nationality	Austria
Marital status	Single

Studies

Ph.D. in mechanical engineering

01/2013 – present	Graz University of Technology (A)
	Ph.D. dissertation (in English)
Issue	*Evaluation of CO_2 absorption solvents for post-combustion capture on the basis of pilot plant studies on a hard coal-fired power plant*
Supervisor	Univ. Prof. DI Dr.techn Christoph Hochenauer

Master's degree in mechanical engineering and economic sciences with a focus on energy technology

10/2010 – 11/2012	Graz University of Technology (A)
11/2012	Master's thesis (in German)
Title	*Alternative Arbeitsstoffgemische für Kompressions/Absorptions-Wärmepumpen für die Anwendung im Hochtemperaturbereich*
Supervisor	Ao. Univ. Prof. DI Dr.techn. René Rieberer

Bachelor´s degree in mechanical engineering and economic sciences

10/2007 - 10/2010	Graz University of Technology (A)
10/2010	Bachelor's thesis (in German)
Title	*Auslegung und Konstruktion eines Rauchgaskühlers*

Professional experience

01/2013 – 03/2016	Project assistant Graz University of Technology (A)
	Institute of Thermal Engineering
	Post-combustion CO_2 Separation from Coal-fired flue gases
10/2010 – 06/2011	Teaching assistant Graz University of Technology (A)
	Institute of Thermal Engineering
07/2003 – 09/2009	Mondi Frantschach GmbH (A)
	Practices in the amount of 20 months

School education

09/2001 – 06/2006	Higher technical school Wolfsberg (A)
	A-level examination passed with distinction
09/1997 – 06/2001	Secondary modern school St. Gertraud (A)
09/1993 – 06/1997	Primary school St. Gertraud (A)

Awards

2015	VGB Innovation Award
	For the investigation of CO_2 solvents at the post-combustion capture test facility on the Dürnrohr hard coal power plant

Skills

Languages	German (native), English (business fluent)
Peer reviewing	International Journal of Industrial Chemistry
Programming	LabVIEW, C++, Visual Basis, Aspen Plus Plus®, Matlab, EES
CAD-software	Pro Engineer 2001i² or Wildfire, CATIA V5, Auto CAD

Selected extra-curricular experience

Driving license	B/F
Military service	Fulfilled (11/2006 - 05/2007)
Sports	Cycling, Climbing, Swimming